THE EFFECT OF TEMPERATURE AND PRESSURE ON LABORATORY OXIDIZED ASPHALT FILMS WITH COMPARISON TO FIELD AGING

Volume I

A Dissertation

by

KEVIN MICHAEL LUNSFORD

Submitted to the Office of Graduate Studies of
Texas A&M University
in partial fulfillment of the requirements for the degree of

DOCTOR OF PHILOSOPHY

May 1994

Major Subject: Chemical Engineering

THE EFFECT OF TEMPERATURE AND PRESSURE ON LABORATORY OXIDIZED ASPHALT FILMS WITH COMPARISON TO FIELD AGING

Volume I

A Dissertation

by

KEVIN MICHAEL LUNSFORD

Submitted to the Office of Graduate Studies of
Texas A&M University
in partial fulfillment of the requirements for the degree of

DOCTOR OF PHILOSOPHY

Approved as to style and content by:

Charles J. Glover
(Chair of Committee)

Richard R. Davison
(Member)

Alan Letton
(Member)

Jerry A. Bullin
(Member)

Kenneth R. Hall
(Interim Department Head)

May 1994

Major Subject: Chemical Engineering

ABSTRACT

The Effect of Temperature and Pressure on
Laboratory Oxidized Asphalt Films with
Comparison to Field Aging. (May 1994)
Kevin Michael Lunsford, B.S., Texas A&M University
Chair of Advisory Committee: Dr. Charles Glover

Two aging models, the asphalt-aging model and the highway-pavement aging model, are developed to describe oxidative aging in asphalt. The first model is based on first principles accounting for carbonyl formation and unsteady-state variable diffusivity oxygen diffusion and reaction. The second model relates measurable properties of pavements to fundamental quantities in the asphalt-aging model.

The long-term constant rate of carbonyl formation at isobaric and isothermal conditions is a function of both temperature and oxygen pressure. An Arrhenius equation models the temperature dependence, and these model parameters are functions of asphalt composition. Activation energies range from 66.7 to 80.5 kJ/gmol. The order of reaction with respect to oxygen pressure is 0.27 and independent of asphalt composition. Laboratory experiments at a single elevated oxygen pressure can be reliably extrapolated; however, multiple laboratory experiments at different elevated temperatures are required to estimate rate of carbonyl formation at highway conditions. Because of an initial non-linearity, the integration constant in the carbonyl formation equation can not be determined from neat material. The integration constant is a function of oxygen pressure; the model parameters are dependent on asphalt composition. Therefore, a single laboratory experiment at the highway pressure is

required to determine the integration constant.

Oxygen diffusivity in asphalt is estimated from laboratory data together with the asphalt-aging model. Oxygen diffusivity is a function of asphalt viscosity; the model parameters are independent of asphalt composition and temperature. Oxygen diffusivity in asphalt is approximately 1×10^{-12} m^2 / s for viscosity of 10,000 poise. Physicochemical models relating viscosity, carbonyl content, temperature, and molecule weight for oxidative aging in asphalts are developed. The model parameters in these equations are functions of initial asphalt composition.

Field- and laboratory-aged asphalt are compared with physicochemical properties and the asphalt-aging model. Laboratory aging at relatively low temperature and high pressure simulates field aging based on the agreement between physicochemical properties. Comparisons between field data and values calculated from the asphalt-aging model are the foundation for the highway-pavement aging model. Hypothesized models relating oxygen pressure and film thickness in the asphalt-aging model to percent air voids, asphalt content, and time are developed.

ACKNOWLEDGEMENTS

This work would not be possible without the extensive help and encouragement of many people. The following is a note of appreciation recognizing all they have done. First, my family, Ron, Joyce, Rhonda, Kenny, and Robyn who provided love and support through the years. Second, my co-workers, Moon-Sun Lin, Meng Liu, Ann Ferry, Penny Bartnicki, Stephen Smiley, Jay Chaffin, and Travis Billiter, who assisted in data collection, data analysis, and proof reading. Third, my advisors, Dr. Charles Glover, Dr. Richard Davison, Dr. Jerry Bullin, and Dr. Alan Letton, who gave me the opportunity and motivation to study such an interesting project. Fourth, the Asphalt Group's administrative assistant, Dorothy Jordan, who made sure all of the bills were paid. Finally, my friends, Wesley, Wendy, Walter and Jane Wills, Tommy Toles, and Lance Ferry, who were always there offering support and understanding.

This work is dedicated to my Mother and Father, Joyce and Ron Lunsford for their Love and Understanding.

TABLE OF CONTENTS

Volume I

Page

ABSTRACT iii

ACKNOWLEDGEMENTS v

TABLE OF CONTENTS vi

LIST OF TABLES ix

LIST OF FIGURES xii

CHAPTER

I INTRODUCTION 1

Objectives 2
Asphalt Aging 3
Oxygen Transport in Asphalt Films 15
Field Aging 18
Summary 22

II AGING MODEL DEVELOPMENT 24

Asphalt-Aging Model 26
Comparing Laboratory and Field Aging 40
Highway-Pavement Aging Model 41

III EXPERIMENTAL METHODS AND MATERIALS 47

Asphalts 47
Oxidative Aging 47
Analytical Procedures 59

IV CARBONYL FORMATION IN ASPHALT 72

Experimental Design 73
Possible Changes in Oxidation Mechanism 74
Order of Reaction 76
Activation Energies and Arrhenius Constants 87
Multi-Variable Parameter Estimation 99
Comparison of E_A with Literature Values 103

CHAPTER Page

Extrapolation of r_{CA} to Lower Temperatures 104
Hypothesized Model for CA_o as a Function of Observable Variables 106
Error Analysis 111
Solubility of Oxygen in Asphalt 113
Summary 114

V OXYGEN DIFFUSIVITY IN ASPHALT FILMS 116

Relationship between r_{O_2} and r_{CA} 117
Relationship between HS and m at Different Temperatures 120
Determination of P_{SI} from r_{CA} 127
Estimation of Oxygen Diffusivity 145
Diffusion and Reaction in Asphalt Aging Tests 205
Oxygen Solubility 208
Summary 210

VI COMPARISON BETWEEN LABORATORY AND FIELD AGING 214

Materials and Laboratory Experimental Design 215
POV- and Field-Aging Comparisons by Physicochemical Properties 218
POV- and Field-Aging Comparisons with the Asphalt-Aging Model 258
Summary 277

VII SHORT-TERM AGING 280

Experimental Design 281
Aging Kinetics for ST 281
Comparing Arrhenius Parameters for ST and LT Aging 291
Physicochemical Relationships 295
Summary 307

VIII CONCLUSIONS 309

IX RECOMMENDATIONS 316

Apparatus 316
Carbonyl Formation Kinetics 316
Oxygen Consumption Rates and Carbonyl Formation Rates 317
Carbonyl-Viscosity Relationships at Different Temperatures 317

Page

Oxygen Diffusion and Reaction in an Asphalt Film 318
Comparison of Laboratory Aging and Field Aging-Properties 318
Comparison of Laboratory Aging and Field Aging-Kinetics 319
Short-Term Aging 319
Overall 320

NOTATION 321

LITERATURE CITED 326

Volume II

APPENDIX

A NEAT DATA 331

B CARBONYL FORMATION DATA 333

C OXYGEN DIFFUSION DATA 372

D OXYGEN DIFFUSION PROGRAMS 437

E LABORATORY AND FIELD DATA 498

F LABORATORY AND FIELD COMPARISON PROGRAMS 593

G SHORT-TERM AGING DATA 608

VITA 659

LIST OF TABLES

Volume I

Table		Page
III-1.	List of Asphalts Studied	48
IV-1.	r_{CA} for All Asphalts and POV Aging Conditions Studied	81
IV-2.	CA_o for All Asphalts and POV Aging Conditions Studied	81
IV-3.	α for All POV-Aged Asphalts Studied	87
IV-4.	E_A for All POV-Aged Asphalts Studied	97
IV-5.	A for All POV-Aged Asphalts Studied	98
IV-6.	Kinetic Model Parameters for All POV-Aged Asphalts Studied	99
IV-7.	r_{CA} and CA_o for All POV-Aged Asphalts at 322.2 K and 20 atm	106
IV-8.	Comparison between Measured r_{CA} at 322.2 K, 20 atm and Extrapolated r_{CA} from Parameters Estimated from 333.3, 344.4, and 355.5 K Data	107
IV-9.	Carbonyl Intercept Model Parameters for All POV-Aged Asphalts Studied	109
V-1.	CA and Wt% O_2 for Neat and POV-Aged SHRP AAA-1 at 344.4 K and 20 atm	119
V-2.	CA and E_V for All Neat, RTFO, and POV-Aged Asphalts Studied	123
V-3.	E_V Model Parameters for All Asphalts Studied	125
V-4.	HS and $\exp(m)$ at 333.3, 344.4, and 355.5 K for All POV-Aged Asphalts Studied	127
V-5.	r_{CA} at the ES and SI for 1 mm Thick Films of All Asphalts and POV-Aging Conditions Studied	138
V-6.	CA_o at the ES and SI for 1 mm Thick Films of All Asphalts and POV-Aging Conditions Studied	138

Table Page

V-7. Estimated P_{SI} Based on r_{CA} for 1 mm Thick Films of All Asphalts and POV-Aging Conditions Studied and Asphalt Specific α 140

V-8. Estimated P_{SI} Based on r_{CA} for 1 mm Thick Films of All Asphalts and POV-Aging Conditions Studied and α of 0.270 140

V-9. Percent Difference in Estimated P_{SI} for Asphalt Specific α and α of 0.270 141

V-10. CA_o Model Parameters from Measured and Estimated P for All POV-Aged Asphalts and Conditions Studied 143

V-11. Estimated $\mathcal{D}_{O_2}$ for Steady-State Constant $\mathcal{D}_{O_2}$ Oxygen Diffusion and Reaction 155

V-12. Estimated $\mathcal{D}_{O_2}$ at ±40% P_{SI} for Steady-State Constant $\mathcal{D}_{O_2}$ Oxygen Diffusion and Reaction 160

V-13. Suspect $\mathcal{D}_{O_2}$ and POV-Aging Conditions for Steady-State Constant $\mathcal{D}_{O_2}$ Oxygen Diffusion and Reaction 161

V-14. Estimated $\mathcal{D}_{O_2}$, Average CA and η_o^*, and POV-Aging Conditions for Steady-State Constant $\mathcal{D}_{O_2}$ Oxygen Diffusion and Reaction 162

V-15. Thiele Modulus, Estimated $\mathcal{D}_{O_2}$ and Average P for All Asphalts and POV-Aging Conditions Studied 166

V-16. Comparisons between Estimated P_{SI} from r_{CA} and Calculated P_{SI} for Steady-State Variable $\mathcal{D}_{O_2}$ Oxygen Diffusion and Reaction for Ampet AC-20, Coastal AC-20, and Cosden AC-20 178

V-17. Comparisons between Estimated P_{SI} from r_{CA} and Calculated P_{SI} for Steady-State Variable $\mathcal{D}_{O_2}$ Oxygen Diffusion and Reaction for Exxon AC-20 and Texaco AC-20 179

V-18. Comparisons between P_{SI} Estimated from r_{CA} and Average P_{SI} Calculated from Unsteady-State Variable $\mathcal{D}_{O_2}$ Oxygen Diffusion and Reaction 200

V-19. Comparisons between Calculated Time to Reach 500 kP η_o^* at 333.3 K, Aging at 322.2 K and P_{ES} of 0.2 atm with and without Diffusion Resistance for Film Thicknesses of 0.8, 1.0, and 1.2 mm 207

Table		Page
VI-1.	Properties of 1987 Samples from Dickens and Pineland Test Sections	217
VI-2.	Model Parameters for All Physicochemical Relationships Based on POV-Aging Data of All Neat Asphalts Studied	242
VI-3.	Comparisons between 1993 and 1987 Properties from Dickens and Pineland Test Sections	257
VI-4.	Arrhenius Parameters of POV- and Field-Aged Asphalts Estimated from POV Data	260
VI-5.	Location and Climatic Data for Dickens, Pineland, and Bryan, Texas	261
VI-6.	Comparisons between t_{act} and t_{theor} for Measured CA of Field-Aged Asphalt	262
VI-7.	Estimated L_{eff} for Dickens and Bryan Asphalts with Constant P_{eff} of 0.2 atm	271
VI-8.	Hypothesized Model between % V and λ	274
VI-9.	Estimated L_{eff} for Dickens, Pineland, and Bryan Asphalts with Variable P_{eff}	275
VII-1.	r_{CA} for Short-Term Aging Studies	284
VII-2.	CA_o for Short-Term Aging Studies	285
VII-3.	Arrhenius Parameters for ST Aging Studies	291
VII-4.	HS and exp(m) at 333.3 K for All ST Aging Studies	299
VII-5.	Comparisons between HS and exp(m) for LT and ST Aging of Different Asphalts	300
VII-6.	RS and $(1 / J'')_o$ at 333.3 K and 10 rad/s for ST Aging Studies of SHRP Asphalts	305
VII-7.	Modified Pal-Rhodes Parameters for ST Aging of Lau *et al.*, (1992) Asphalts	307

LIST OF FIGURES

Volume I

Figure		Page
II-1.	Oxygen concentration profile in an asphalt film	27
II-2.	Highway-pavement cross section	43
III-1.	Pressure Oxygen Vessel, POV, and control panel	50
III-2.	Sample holder for POV apparatus	51
III-3.	Schematic of POV insulation	52
III-4.	POV control panel	54
III-5.	Schematic of Dickens test section on US 82	56
III-6.	Schematic of Pineland test section on US 96	57
III-7.	Schematic of Bryan test section on highway 21	58
III-8.	Infrared spectra of neat and POV-aged Ampet AC-20	61
III-9.	*CA*s of Exxon AC-20 at different positions in a POV	62
III-10.	Technique for measuring IR spectra of the asphalt film exposed surface with one ATR prism	64
III-11.	Comparison between two ATR prisms based on *CA*s of POV-aged asphalt and model compounds	65
III-12.	Technique for measuring IR spectra of the asphalt film substrate interface surface with two ATR prisms	66
III-13.	Calibration curve for GPC analysis based on polystyrene standards	69
IV-1.	IR spectra of neat and POV-aged Ampet AC-20 for 20 days at 344.4 K and 0.2, 2, and 20 atm	75
IV-2.	*CA*s of neat and POV-aged Cosden AC-20 at 333.3 K and 0.2, 2, and 20 atm	77

Figure Page

IV-3. *CA*s of neat and POV-aged Cosden AC-20 at 344.4 K and 0.2, 2, and 20 atm 79

IV-4. *CA*s of neat and POV-aged Cosden AC-20 at 355.5 K and 0.2, 2, and 20 atm 80

IV-5. r_{CA} versus P at 333.3 K for POV-aged Cosden AC-20 83

IV-6. r_{CA} versus P at 333.3 K for all POV-aged asphalts studied 84

IV-7. r_{CA} versus P at 344.4 K for all POV-aged asphalts studied 85

IV-8. r_{CA} versus P at 355.5 K for all POV-aged asphalts studied 86

IV-9. *CA*s of neat and POV-aged Cosden AC-20 at 0.2 atm and 333.3, 344.4, and 355.5 K 89

IV-10. *CA*s of neat and POV-aged Cosden AC-20 at 2 atm and 333.3, 344.4, and 355.5 K 90

IV-11. *CA*s of neat and POV-aged Cosden AC-20 at 20 atm and 333.3, 344.4, and 355.5 K 91

IV-12. r_{CA} versus $(1 / T)$ at 0.2 atm for POV-aged Cosden AC-20 93

IV-13. r_{CA} versus $(1 / T)$ at 0.2 atm for all POV-aged asphalts studied 94

IV-14. r_{CA} versus $(1 / T)$ at 2 atm for all POV-aged asphalts studied 95

IV-15. r_{CA} versus $(1 / T)$ at 20 atm for all POV-aged asphalts studied 96

IV-16. Percent error in predicted r_{CA} for α of 0.27 versus P for all asphalts studied 101

IV-17. Percent error in predicted r_{CA} for α of 0.27 versus T for all asphalts studied 102

IV-18. *CA*s of neat and POV-aged Cosden AC-20 at 322.2 K and 20 atm 105

Figure		Page
IV-19.	CA_o versus POV aging temperature for Cosden AC-20	108
IV-20.	CA_o versus POV aging temperature for all asphalts studied	110
V-1.	Wt% O_2 versus CA for neat and POV-aged SHRP AAA-1	118
V-2.	a_T versus $(1 / T)$ for neat and POV-aged Texaco AC-20 with reference temperature of 273.2 K	122
V-3.	E_V versus CA for neat, RTFO, and POV-aged Texaco AC-20	124
V-4.	E_V versus CA for all RTFO and POV-aged asphalts studied	126
V-5.	CAs of neat and at the ES and SI for 1 mm thick films of POV-aged Coastal AC-20 at 333.3 K and P_{ES} of 0.2 atm	130
V-6.	CAs of neat and at the ES and SI for 1 mm thick films of POV-aged Coastal AC-20 at 333.3 K and P_{ES} of 2 atm	131
V-7.	CAs of neat and at the ES and SI for 1 mm thick films of POV-aged Coastal AC-20 at 344.4 K and P_{ES} of 0.2 atm	132
V-8.	CAs of neat and at the ES and SI for 1 mm thick films of POV-aged Coastal AC-20 at 344.4 K and P_{ES} of 2 atm	133
V-9.	CAs of neat and at the ES and SI for 1 mm thick films of POV-aged Coastal AC-20 at 355.5 K and P_{ES} of 0.2 atm	134
V-10.	CAs of neat and at the ES and SI for 1 mm thick films of POV-aged Coastal AC-20 at 355.5 K and P_{ES} of 2 atm	135
V-11.	CA_o versus measured and estimated P for all POV-aged asphalts studied	144
V-12.	Schematic of oxygen pressure profile in an asphalt film	148
V-13.	Schematic of oxygen pressure profile in an asphalt film with transformation of variables at x_f	151
V-14.	Calculated oxygen pressure profiles in 1 mm thick film Ampet AC-20 at 333.3, 344.4, and 355.5 K with P_{ES} of 0.2 atm for estimated $\mathcal{D}_{O_2}$ from steady-state constant $\mathcal{D}_{O_2}$ oxygen diffusion and reaction	156

Figure Page

V-15. Calculated oxygen pressure profiles in 1 mm thick film Cosden AC-20 at 333.3, 344.4, and 355.5 K with P_{ES} of 2 atm for estimated $\mathcal{D}_{O_2}$ from steady-state constant $\mathcal{D}_{O_2}$ oxygen diffusion and reaction 158

V-16. Estimated $\mathcal{D}_{O_2}$ versus average η_o^* of all 1 mm thick film POV-aged asphalts and conditions studied 164

V-17. Calculated oxygen pressure profiles in 1 mm thick film Ampet AC-20 at 333.3 K and P_{ES} of 0.2 atm for estimated D_o from steady-state variable $\mathcal{D}_{O_2}$ oxygen diffusion and reaction 170

V-18. Calculated oxygen pressure profiles in 1 mm thick film Ampet AC-20 at 344.4 K and P_{ES} of 0.2 atm for estimated D_o from steady-state variable $\mathcal{D}_{O_2}$ oxygen diffusion and reaction 171

V-19. Calculated oxygen pressure profiles in 1 mm thick film Ampet AC-20 at 355.5 K and P_{ES} of 0.2 atm for estimated D_o from steady-state variable $\mathcal{D}_{O_2}$ oxygen diffusion and reaction 172

V-20. Calculated oxygen pressure profiles in 1 mm thick film Ampet AC-20 at 333.3 K and P_{ES} of 0.2 atm for estimated P_{SI} from steady-state variable $\mathcal{D}_{O_2}$ oxygen diffusion and reaction 174

V-21. Calculated oxygen pressure profiles in 1 mm thick film Ampet AC-20 at 344.4 K and P_{ES} of 0.2 atm for estimated P_{SI} from steady-state variable $\mathcal{D}_{O_2}$ oxygen diffusion and reaction 175

V-22. Calculated oxygen pressure profiles in 1 mm thick film Ampet AC-20 at 355.5 K and P_{ES} of 0.2 atm for estimated P_{SI} from steady-state variable $\mathcal{D}_{O_2}$ oxygen diffusion and reaction 176

V-23. ξ versus position in 1 mm thick film Ampet AC-20 at 333.3 K and P_{ES} of 0.2 atm for estimated P_{SI} from steady-state variable $\mathcal{D}_{O_2}$ oxygen diffusion and reaction 183

V-24. ξ versus position in 1 mm thick film Ampet AC-20 at 344.4 K and P_{ES} of 0.2 atm for estimated P_{SI} from steady-state variable $\mathcal{D}_{O_2}$ oxygen diffusion and reaction 184

V-25. ξ versus position in 1 mm thick film Ampet AC-20 at 355.5 K and P_{ES} of 0.2 atm for estimated P_{SI} from steady-state variable $\mathcal{D}_{O_2}$ oxygen diffusion and reaction 185

Figure Page

V-26. Comparisons between measured and calculated *CA* at the *ES* and *SI* of 1 mm thick film POV-aged Texaco AC-20 at 333.3 K and P_{ES} of 0.2 atm 192

V-27. Comparisons between measured and calculated *CA* at the *ES* and *SI* of 1 mm thick film POV-aged Texaco AC-20 at 333.3 K and P_{ES} of 2 atm 193

V-28. Comparisons between measured and calculated *CA* at the *ES* and *SI* of 1 mm thick film POV-aged Texaco AC-20 at 344.4 K and P_{ES} of 0.2 atm 194

V-29. Comparisons between measured and calculated *CA* at the *ES* and *SI* of 1 mm thick film POV-aged Texaco AC-20 at 344.4 K and P_{ES} of 2 atm 195

V-30. Comparisons between measured and calculated *CA* at the *ES* and *SI* of 1 mm thick film POV-aged Texaco AC-20 at 355.5 K and P_{ES} of 0.2 atm 196

V-31. Comparisons between measured and calculated *CA* at the *ES* and *SI* of 1 mm thick film POV-aged Texaco AC-20 at 355.5 K and P_{ES} of 2 atm 197

V-32. Calculated oxygen pressure profiles in 1 mm thick film Texaco AC-20 at 333.3 K and P_{ES} of 0.2 atm from unsteady-state variable $\mathcal{D}_{O_2}$ oxygen diffusion and reaction 201

V-33. Calculated *CA* profiles in 1 mm thick film Texaco AC-20 at 344.4 K and P_{ES} of 0.2 atm from unsteady-state variable $\mathcal{D}_{O_2}$ oxygen diffusion and reaction 202

V-34. Calculated η_o^* profiles in 1 mm thick film Texaco AC-20 at 355.5 K and P_{ES} of 0.2 atm from unsteady-state variable $\mathcal{D}_{O_2}$ oxygen diffusion and reaction 203

V-35. Calculated $\mathcal{D}_{O_2}$ profiles in 1 mm thick film Texaco AC-20 at 355.5 K and P_{ES} of 0.2 atm from unsteady-state variable $\mathcal{D}_{O_2}$ oxygen diffusion and reaction 204

VI-1. GPCs of field-aged Dickens Cosden AC-10 extracted asphalt from #550+00. Cored February, 1993 219

Figure		Page
VI-2.	GPCs of neat and POV-aged Dickens Cosden AC-10 at 355.5 K and 20 atm	221
VI-3.	Comparisons between GPCs from POV (355.5 K, 20 atm) and field-aged (#550+00, February 1993) Dickens Cosden AC-10	223
VI-4.	Comparisons between GPCs from POV (355.5 K, 20 atm) and field-aged (#458+00, February 1993) Dickens Diamond Shamrock AC-20	224
VI-5.	Comparisons between GPCs from POV (355.5 K, 20 atm) and field-aged (#391+00, February 1993) Dickens Dorchester AC-20	225
VI-6.	Comparison between η_o^* at 333.3 K and *CA* of neat, POV- (355.5 K, 20 atm), and field-aged (#599+00, February 1993) Dickens Cosden AC-10	228
VI-7.	Comparisons between η_o^* at 333.3 K and *CA* of neat, POV- (355.5 K, 20 atm), and field-aged (#550+00, February 1993) Dickens Cosden AC-20	229
VI-8.	Comparisons between η_o^* at 333.3 K and *CA* of neat, POV- (355.5 K, 20 atm), and field-aged (#322+00, February 1993) Dickens Exxon AC-20	230
VI-9.	Comparisons between η_o^* at 333.3 K and *CA* of neat, POV- (355.5 K, 20 atm) and field-aged (#270+00, February 1993) Dickens MacMillan AC-20	231
VI-10.	Comparisons between η_o^* at 333.3 K and *CA* of neat, POV- (355.5 K, 20 atm), and field-aged (#458+00, February 1993) Dickens Diamond Shamrock AC-20	232
VI-11.	Comparisons between η_o^* at 333.3 K and *CA* of neat, POV- (355.5 K, 20 atm), and field-aged (#391+00, February 1993) Dickens Dorchester AC-20	233
VI-12.	Comparisons between η_o^* at 333.3 K and *CA* of neat, POV- (333.3 K, 20 atm), and field-aged (#590+00, March 1993) Pineland Cosden AC-20	235

Figure Page

VI-13. Comparisons between η_o^* at 333.3 K and *CA* of neat, POV- (333.3 K, 20 atm), and field-aged (#510+00, March 1993) Pineland Dorchester AC-20 236

VI-14. Comparisons between η_o^* at 333.3 K and *CA* of neat, POV- (333.3 K, 20 atm), and field-aged (#640+00, March 1993) Pineland Exxon AC-20 237

VI-15. Comparisons between η_o^* at 333.3 K and *CA* of neat, POV- (333.3 K, 20 atm), and field-aged (#557+00, March 1993) Pineland MacMillan AC-20 238

VI-16. Comparisons between η_o^* at 333.3 K and *CA* of neat, POV- (333.3 K, 20 atm), and field-aged (#285+00, March 1993) Pineland Texaco AC-20 239

VI-17. Comparisons between η_o^* at 333.3 K and *CA* of neat, RTFO, POV- (344.4 K, 20 atm), and field-aged Bryan Exxon AC-20 241

VI-18. Comparisons between $(1 / J'')$ at 333.3 K, 10 rad/s and *CA* of neat, POV- (355.5 K, 20 atm), and field-aged (#599+00, February 1993) Dickens Cosden AC-10 245

VI-19. Comparisons between η_o^* at 333.3 K and *MW* of neat, POV- (355.5 K, 20 atm), and field-aged (#599+00, February 1993) Dickens Cosden AC-10 247

VI-20. Comparisons between η_o^* at 333.3 K and *MW* of neat, POV- (333.3 K, 20 atm) and field-aged (#285+00, March 1993) Pineland Texaco AC-20 249

VI-21. IR spectra of field-aged Dickens Cosden AC-10 extracted asphalt from #550+00. Cored February, 1993 251

VI-22. IR spectra of neat and POV-aged Dickens Cosden AC-10 at 355.5 K and 20 atm 252

VI-23. IR spectra of field-aged Dickens Exxon AC-20 extracted asphalt from #322+00. Cored February, 1993 253

VI-24. IR spectra of neat and POV-aged Dickens Exxon AC-20 at 355.5 K and 20 atm 254

Figure Page

VI-25. The effect of cyclical temperature on calculated oxygen pressure profiles in 1 mm thick Ampet AC-20 for unsteady-state variable $\mathcal{D}_{O_2}$ oxygen diffusion and reaction 265

VI-26. The effect of cyclical temperature on calculated CA profiles in 1 mm thick Ampet AC-20 for unsteady-state variable $\mathcal{D}_{O_2}$ oxygen diffusion and reaction 267

VI-27. The effect of cyclical temperature on calculated CA_{avg} in 1 mm thick Ampet AC-20 for unsteady-state variable $\mathcal{D}_{O_2}$ oxygen diffusion and reaction 268

VI-28. Hypothesized relationship between P_{eff} time constant λ and percent air voids 273

VI-29. Hypothesized relationship between L_{eff} and percent asphalt 276

VII-1. CAs of neat, RTFO, and POV-aged Lau *et al.*, (1992) Exxon AC-20 at 322.2, 333.3, 344.4, 355.5, and 366.6 K at 20 atm from 1 to 5 days 282

VII-2. r_{CA} versus $(1 / T)$ at 20 atm for all short term POV-aged Lau *et al.*, (1992) asphalts studied 286

VII-3. r_{CA} versus $(1 / T)$ at 20 atm for all short term POV-aged Jemison *et al.*, (1992b) asphalts studied and Dickens Diamond Shamrock AC-20 287

VII-4. r_{CA} versus $(1 / T)$ at 20 atm for all short term POV-aged SHRP asphalts studied 288

VII-5. Comparisons between E_A for all short term and long term POV-aged asphalts studied 293

VII-6. Comparisons between A for all short term and long term POV-aged asphalts studied 294

VII-7. η_o^* at 333.3 K and CA of neat, RTFO, and all short term POV-aging conditions studied for Lau *et al.*, (1992) Coastal AC-20 297

Figure Page

VII-8. η_o^* at 333.3 K and *CA* of neat, RTFO, and all short term POV-aging conditions studied for Lau *et al.*, (1992) Cosden AC-20 298

VII-9. $(1 / J'')$ at 333.3 K, 10 rad/s and *CA* of all short term POV-aging conditions studied for SHRP AAC-1 303

VII-10. $(1 / J'')$ at 333.3 K, 10 rad/s and *CA* of all short term POV-aging conditions studied for SHRP AAA-1 304

VII-11. η_o^* at 333.3 K and % hexane asphaltenes of neat, RTFO, and all short term POV-aging conditions studied for Lau *et al.*, (1992) Ampet AC-20 306

CHAPTER I
INTRODUCTION

Billions of dollars are spent annually constructing and repairing asphalt-pavement highways. Despite this large expenditure, relatively little is known about the chemical composition and physical properties of the asphalt binder. A further complicating factor is that the properties of the asphalt change as a result of oxidative aging and specifications designed for neat asphalt do not necessarily correspond or predict the extent and speed of the changes in the physical and chemical properties due to oxidative aging.

Chemically, asphalt is a complex mixture of hydrocarbons derived from crude petroleum. Because asphalt is a complex mixture, the composition has been defined both in terms of elemental analysis and generic fractions based on solubility and polarity in organic solvents.

Asphalt is not inert and, during service life, oxidizes over time. The primary result of this oxidation is a hardening characterized by an increase in viscosity and decrease in ductility. The actual oxidative aging and resulting hardening of asphalt in the field occurs in a two-step process. The first occurs at high temperatures, 436.1 K, for a short time period during hot-mix processing. The second occurs at low temperatures, 333.2 K or below, for long time periods.

Standard procedures have been designed to simulate hot-mix processing. The most widely accepted are the Thin Film Oven Test, TFOT, ASTM D-1754 (1984) and the Rolling Thin Film Oven Test, RTFOT, ASTM D-2872. Jemison *et al.*,

---

This dissertation conforms to the style and format of the *AIChE Journal.*

(1991) compared the two laboratory procedures to each other and to hot-mix samples. When compared to each other, both laboratory tests produced the same changes in chemical and physical properties. However, neither laboratory test produced the same chemical changes as measured by Fourier Transform Infrared Spectroscopy, FTIR, when compared with hot-mix.

Unfortunately, an accurate, reliable, and practical laboratory procedure that simulates long-term, low-temperature field aging has not been developed. Ideally, this test would evaluate the ability of an asphalt to resist field aging. Since there is no test, both inferior and superior asphalt binders are used in highway construction.

Objectives

The ultimate objective of this work is to elevate the understanding of oxidative aging in asphalts to a point such that field aging is not only simulated but also predicted. For both field and laboratory aging, the primary variables are temperature, pressure, and asphalt composition. A laboratory aging test is designed to last several days for practical reasons. The rate of change of the physical and chemical properties are greatly accelerated by increasing temperature, pressure, or both. In contrast, field aging results after many years. However, if the results of these accelerated tests do not show similar changes in chemical composition and physical properties when compared to field-aged material, the laboratory aging procedure has failed.

The specific goals of this research include the following:

1) To develop kinetic equations for carbonyl formation that include the effect of both temperature and oxygen pressure.

2) To investigate the impact of the physical properties on oxygen diffusion through an asphalt film during aging and develop an oxygen diffusion and reaction model in an asphalt film.
3) To establish physicochemical relationships for asphalt oxidation.
4) To relate laboratory aging of asphalt to field aging.

The literature review for asphalt aging is divided into three major sections, asphalt aging, oxygen transport properties, and field aging. The first describes changes in chemical and physical properties due to aging both in the field and laboratory, the development of laboratory aging test and models to describe the aging, and discovery of physicochemical relationships for oxidative aging of asphalts. The second details measurements and determinations of oxygen diffusivity, permeability, and absorption in asphalts. The last section discusses field aging with respect to the comparison with laboratory data, the climatic conditions, the presence of aggregate, and measurable core properties.

Asphalt Aging

An excellent review of the changes in chemical composition, material properties, and measured physical properties resulting from aging are given by Petersen (1984). In summary, oxidative aging in both field and laboratory increases carbonyl content, viscosity, and asphaltene content and decreases penetration and ductility. Overall, aging results in a harder, more brittle binder. Ultimately, these changes in physical properties cause eventual failure.

In order to understand and begin to model a complex process such as highway aging, observations of the actual phenomenon are critical. Previous researchers have analyzed many field-aged samples. Brown *et al.*, (1957) measured softening points,

penetrations, and ductilities of field-aged specimens. The maximum age of the samples was nine years. Brown proposed an empirical hyperbolic model given in equation I – 1 to represent the field data.

$$\Delta y = \frac{t}{a_h + b_h t} \qquad (I-1)$$

The change in property as a result of aging is Δy, and aging time is t. Both a_h and b_h are model parameters estimated from experimental data. The limiting value of the aged property is given by the parameter $1 / b_h$. Way *et al.*, (1959) measured penetrations and asphaltene contents of field-aged samples with a maximum age of four years. Using test sections with a maximum age of ten years, Kandhal and Koehler (1984) reported penetration, percent air voids, log viscosity, and ductility. Using coal-tar pitch thin films and aging outside for a maximum of 24 hours, Ruede (1979) measured carbonyl content as a function of aging time. All of the field-aged data could be represented by this hyperbolic model. Unfortunately, none of the researchers attempted to estimate the model parameters from laboratory data and then use those estimated parameters to successfully predict field aging. Because equation I – 1 does not predict field aging based on model parameters estimated from laboratory data, more fundamental models and laboratory tests have been studied.

Early development of an asphalt aging test evaluating long-term durability has been extensive. Strieter and Snoke (1936) aged 0.635 mm thick asphalt films using a cyclic exposure to light, heat, refrigeration, and forceful spraying of water. Anderson *et al.*, (1942) aged asphalt in benzene solutions at 6.8 atm pure oxygen at 323.2 K for 40 hours. Chemical oxidation using potassium permanganate on asphalt films at 333.3 K has also been studied (Ebberts, 1942). Griffin *et al.*, (1955) developed a micro durability test aging 5 micron thick asphalt films at 380 K for two hours.

However, in the development of these informative and inventive tests, the researchers neglected to include a fundamental aging model or show how the test data relate to the model. Furthermore, comparisons between laboratory data and field observations only yielded more empirical models.

Ideally, a long-term aging test and model should include the same variables affecting the material in the field. Long-term aging occurs at temperatures of 333.3 K or below and at oxygen partial pressures of 0.2 atm. Krchma *et al.*, (1960) suggest using a temperature as close to field aging as possible. Unfortunately, a laboratory test at these conditions is impractical. One promising procedure designs laboratory experiments at elevated temperatures and pressures and uses those results to extrapolate to road aging conditions. However, to be valid, elevated temperatures and pressures should only accelerate the rate at which products are formed and not change the mechanism. Changing mechanism usually results in the formation of different products and, if this happens, conclusions drawn from high temperature data would not be valid at road conditions.

In 1954, the Road Research Laboratory in England designed a Pressure Oxygen Vessel, POV, to age 7 mm thick asphalt films at 20 atm oxygen and 338.2 K for 64 hours (Lee and Dickinson, 1954). This test has the advantage of accelerating the aging with high pressure oxygen, at relatively low temperatures. The Frass brittle temperature was measured before and after POV aging. Laboratory- and field-aged samples were compared. However, this group also did not include an aging model.

Improving the POV test, Lee (1968) used TFOT residue of 3.2 mm thickness at 338.9 K under 20 atm pure oxygen for 10 days. Measured properties before and after aging were penetration, log viscosity, and asphaltene content. Equation I – 1 modeled all of the measured properties. Oxidation results at lower pressures were

also reported. For equal aging times and temperatures, the viscosity increased two to five times by raising the aging pressure from 1 to 20 atm. This suggests that the oxygen pressure of the test affects the results. However, Lee did not discuss how the pressure relates to an aging model in terms of its effect on the oxidation kinetics or the oxygen transport in the asphalt film. Lee (1973) compared field data at two years with laboratory aging and concluded that 46 hours of aging at 338.9 K under 20 atm oxygen was equivalent to 60 months of service life. This conclusion was based on the set of experimental data and an empirical correlation. However, he did not report that these laboratory tests and the empirical correlation successfully predicted field aging. In another paper, Lee and Huang (1973) measured carbonyl content for aging 3.2 mm thick films at 338.9 K and 20 atm oxygen for 1000 hours. The hyperbolic model also described carbonyl content.

Researchers are continuing to make modifications to the POV procedure and the oven tests in an attempt to simulate field aging. The Strategic Highway Research Program, SHRP, has modified the POV using air at 20 atm. TFOT residue is aged for 24 hours at a given single temperature depending on climatic regions. The aging temperatures are 363.2, 373.2, and 383.2 K (SHRP, 1992).

Still other researchers have studied extending the high temperature oven tests in an effort to simulate long-term field aging. Petersen (1989) developed the Thin Film Accelerated Aging Test, TFAAT. Four grams of RTFO residue are aged at 386.2 K for three days. When the laboratory data were compared with field data, the most dominating variable was the void content of the mix. One critical element missing in all of these aging test developments is a fundamental aging model.

Comparisons of laboratory- and field-aged materials have been inconclusive. Some researchers have concluded that laboratory tests do not simulate field aging. Jamieson and Hattingh (1970) used the Road Research Laboratory method to age asphalt films. By comparing rheological properties, the authors concluded that the laboratory simulation did not agree with field-aged data. Vallerga and Halstead (1971) compared field- and oven-aged materials and concluded that different chemical changes occurred. Other researchers have attempted to compare laboratory aging with field aging with limited success. Kim *et al.*, (1984) aged cores at 6.8 atm oxygen and 333.3 K for up to five days. The laboratory aged cores were compared with field cores based on the resilient modulus and the Corbett analysis of the extracted asphalt. In two of three cases there was generally fair agreement. However, the authors indicate that a diffusion problem did exist in the cores. They did not attempt to separate the diffusion and kinetic effects. The lack of agreement between laboratory- and field-aged samples is probably due to incomplete extraction of the field-aged sample (Burr *et al.*, 1990) or the fact that the laboratory tests were at too high a temperature.

All of the previous methods described specify experiments at only one elevated temperature. Many are designed for only one time period. Furthermore, and most important, no fundamental aging model is developed. The main focus has been on developing empirical relationships between field- and laboratory-aged materials, such as equation I – 1, which have no predictive capability. In an attempt to make the evaluations or tests quick and efficient, these methods fail to yield any fundamental information about asphalt oxidation. Furthermore, past comparisons between laboratory- and field-aged materials have not been accurate because of poor extraction and recovery of the asphalt (Burr *et al.*, 1990; Burr *et al.*, 1991) or uncontrolled variables relating to the construction of the highway and not the binder itself (Davison *et*

al., 1989). Comparing laboratory tests at elevated temperatures to field aging at low temperatures has been suspect, causing erroneous conclusions about the durability of an asphalt. In other words, the previously determined empirical relationships between field- and laboratory-aged materials may not be accurate.

The most interesting and fundamentally important work in recent years in terms of developing an aging model has been done by Lau *et al.*, (1992). Asphalt films, one mm thick, were aged at 333.3, 344.4, 355.5, and 366.7 K in a POV at 20 atm oxygen. Thin films were used in an attempt to diminish the oxygen diffusion problem. They measured carbonyl content and viscosity to monitor the aging. For isothermal and isobaric conditions, the long-term carbonyl formation and log viscosity increase are described by equation I – 2.

$$\Delta y = a_l + b_l t \qquad (\text{I} - 2)$$

Both a_l and b_l are model parameters. This linear model is believed to be valid because diffusion was diminished by high pressure and thin films. However, this linear model does not have a zero intercept because of an initial non-linearity, resulting from a small concentration of activated compounds. Using POV- and TFAAT- aged materials, Petersen *et al.*, (1993) also conclude that the initial non-linearity is due to a small population of reactive components. After this initial step, the rate of aging is constant. Careful review of the data (Lau, 1991) shows a hyperbolic function at the lower aging temperatures of 333.3 and 344.4 K, suggesting that a diffusion problem may still exist. No field data were compared to these samples.

Lau *et al.*, (1992) also discovered that the rate of carbonyl formation, r_{CA}, and log viscosity increase are functions of temperature and were successfully modeled

using an Arrhenius relationship (Froment and Bischoff, 1979) given in equation I – 3.

$$r_{CA} = A \exp\left(\frac{-E_A}{RT}\right) \qquad (I-3)$$

A is the Arrhenius constant; E_A is the activation energy; R is the universal gas constant, and T is the absolute aging temperature. E_A and A varied from asphalt to asphalt. As a result, a ranking of different asphalts based on r_{CA} is a function of aging temperature. Petersen *et al.*, (1993) confirm this result with aging under air at temperatures ranging from 338.2 to 403.2 K. Button *et al.*, (1993) also verify this with Pressure Air Vessel, PAV, aging from 327.2 to 350.2 K for aging times up to 144 hours. These studies show that the oxidation resistance of an asphalt at a single elevated temperature may not reflect its true resistance to aging at road conditions. Therefore, even with a fundamental aging model, a single elevated temperature test does not provide enough information.

Using the Arrhenius relationship and the estimated parameters from elevated multiple temperature data, Davison *et al.*, (1992) suggest that the actual aging rates at road temperature can be calculated. However, only qualitative evaluation and rankings of the asphalt binders were achieved. The effect of aging pressure on the reaction rate and diffusion was not included, and the fact that the laboratory tests were conducted at 20 atm oxygen and the road conditions are at 0.2 atm oxygen was not sufficiently addressed.

Verhasselt and Choquet (1991) report on an accelerated aging test using oxygen similar to the RTFOT. The asphalt film thickness was 2 mm, and the temperatures ranged from 343.2 to 383.2 K. The authors measured and correlated changes in asphaltene content, ring and ball softening point, reciprocal of the penetration, and the infrared absorption at 1700 cm^{-1}. The authors state that the data follow the

empirical kinetic equation I – 4.

$$(\Delta y)^2 = kt \qquad (I-4)$$

k is the overall reaction constant for each property. This empirical equation supposedly includes the effect of oxygen diffusion in the film. However, the equation does not account for the fact that the diffusivity may vary with time since the physical properties of the asphalt change as a result of oxidation. The Arrhenius relationship modeled the temperature effect on k. Furthermore, E_A varied from 66.9 to 87.1 kJ/gmol for different asphalts. Using the Arrhenius relationship, the researchers could extrapolate rates of aging to road conditions.

Finally, a more complete model for asphalt oxidation is given by Dickinson and Nicholas (1949). These researchers measured oxygen absorption in asphalt films at temperatures ranging from 338.2 to 392.2 K and oxygen pressures from 1 to 0.2 atm. The experimental conditions were such that oxygen diffusion resistance was minimized. They proposed a model with two simultaneous reactions. The first reaction is essentially constant; however, the second is very fast and is complete after approximately 100 hours. The kinetic model is given in equation I – 5.

$$\Delta y = kt + a_n\left[1 - \exp(-b_n t)\right] \qquad (I-5)$$

The rate of the first reaction is k and the model parameters for the second reaction are a_n and b_n. The authors report that k is very sensitive to temperature and is modeled with an Arrhenius relationship. E_A was 29.3 kJ/gmol. However, b_n is insensitive to changes in temperature. a_n increases with increasing temperature. Furthermore, the authors noted that increases in pressure were linearly related to increases in a_n. b_n decreased with increasing pressure. In equation I – 5 the overall effect of oxygen transport and reaction is included in the model parameters. The authors did not

attempt to separate the reaction and transport effects. For conditions where diffusion is minimized this model appears to account for the initial non-linearity in the data of Lau *et al.*, (1992) and Petersen *et al.*, (1993).

Overall, equations I – 2, I – 3, and I – 5 represent the most fundamental kinetic models providing the basis for an asphalt-aging model. The effect of temperature on the kinetic parameters has been studied; however, the effect of pressure on these model parameters is not sufficiently understood. Lau *et al.*, (1992) showed that aging at a single elevated temperature may not relate to aging at road conditions because of asphalt specific E_A and A. Lee (1968) showed that for POV aging, the hardening rate increased with pressure. He did not attempt to separate the effect of oxygen pressure on diffusion and the reaction rate. Button *et al.*, (1993) aged asphalt films of 1.6, 3.2, and 6.4 mm thickness in a PAV at 20 atm and 344.2 K for 144 hours. Based on viscosity measured at 333.3 K, the increase in film thickness was inversely proportional to the viscosity. Furthermore, the proportionality constant was dependent on the asphalt. The authors did not discuss diffusion and reaction in the asphalt film.

In the area of polymer oxidation, research has shown the pressure effect can be substantial especially in the area of free radical formation. At high oxygen pressures, the concentration of radicals are so low compared to that of oxygen that the termination and propagation steps show only one mechanism. At low oxygen pressure (0.132 atm), the concentration of oxygen approaches that of the radicals and the termination steps produce different products (Bolland, 1949; Bateman, 1954). This is not suggesting that asphalt oxidation occurs by a free radical mechanism. However, the oxygen concentration affects the rate of carbonyl formation, and possibly, at low oxygen concentrations, even changes the oxidation products. With a substantial

amount of data generated using the high-pressure POV method, no data has shown that aging at high oxygen pressure also reliably extrapolates to field aging pressures.

The performance and durability of an asphalt binder is directly related to its physical properties. Thus, relationships between physical and chemical properties provide a way to estimate physical properties and ultimately performance by measurements of chemical properties. Furthermore, these physicochemical relationships may, in and of themselves, be used to characterize and rank asphalts. Lee *et al.*, (1973) first quantified the linear relationship between the ratio of the aged and neat viscosity and the increase in the carbonyl absorption band for POV- and field-aged asphalts. The model parameters were crude-source dependent. Similar linear relationships between asphaltene content and carbonyl were given. Comparisons between field aging for 48 months with laboratory simulation at 338.9 K and 20 atm for up to 40 days were excellent. Martin *et al.*, (1990) also showed the viscosity and carbonyl content increase for field aging, and the viscosity increase was independent of sulfoxide content. They defined the *Hardening Susceptibility*, *HS*, as the change in log-viscosity with respect to the change in carbonyl content, *CA*. The relationship between viscosity, η_o^*, and *CA* is given in equation I – 6.

$$\eta_o^* = \exp\Big\{ HS \cdot CA + m \Big\} \qquad \text{(I – 6)}$$

m is the log-viscosity intercept. *HS* and m are estimated parameters based on experimental data and were asphalt dependent. Furthermore, *HS* is a measure of the asphalt's tendency to harden due to a given carbonyl formation as a result of oxidative aging. Lau *et al.*, (1992) showed that the relationship between η_o^*, the zero-shear limiting complex viscosity, and *CA* for asphalts was independent of aging temperatures from 333.3 to 366.7 K, time, and the presence of aggregate. This

work is important since it shows that physicochemical relationships may be studied independent of the reaction kinetics or aging model. Jemison *et al.*, (1992b) reported that the η-CA relationship not only existed for asphalts but also for supercritically fractionated components of asphalt. Petersen *et al.*, (1993) aged asphalt films in a POV at 20 atm oxygen and the TFAAT at atmospheric air and concluded that the η-CA relationship was independent of aging pressure.

Since the asphalt performance is ultimately related to its rheological properties and CA directly relates to a rheological property, monitoring and modeling CA is equivalent to modeling changes in rheological properties as a result of oxidative aging. Since CA correlates with rheological properties, it appears that changes in the rest of the IR spectrum can be discounted. Furthermore, the η-CA relationship appears to be independent of the kinetic or aging model. This is a truly remarkable discovery. In the efforts to develop a reliable and accurate laboratory long-term aging simulation, comparisons between field- and laboratory-aged materials have not been favorable, primarily because the researchers imposed an empirical kinetic model. However, agreement between the physicochemical properties, which are independent of a kinetic model, of field- and laboratory-aged samples should provide sufficient evidence that the laboratory simulation is accurate. Unfortunately, the researchers only report the η-CA model parameters for viscosity measured at 333.3 K. The effect of temperature on HS and m needs to be further understood, if this physicochemical relationship is used in an asphalt-aging model.

Other physicochemical relationships for asphalt oxidation have been discovered. Lin *et al.*, (1993) POV aged SHRP asphalts at 333.3, 344.4, 355.5, and 366.7 K at 20 atm oxygen. The percent hexane asphaltenes, % A, and η_o^* at 333.3 K, and $(1 \,/\, J'')$ and 333.3 K and 10 rad/s were measured. They used a modified Pal-Rhodes model

to describe η_o^* dependence on % A, as given in equation I – 7.

$$\eta_o^* = \eta_M(1 - K' \cdot \%\ A)^{-\nu} \qquad (I-7)$$

η_M is the viscosity of the maltene. K' and ν are estimated free parameters. All of the asphalts studied showed unique values of the model parameters. Furthermore, these model parameters were independent of kinetics, and surprisingly, only dependent on the composition of the neat maltene. These researchers also showed that the rheological property $(1 / J'')$ at 333.3 K and 10 rad/s also correlates with % A. This is important since SHRP researchers showed that $(1 / J'')$ correlates with the rate of rut depth in pavement mixes (SHRP, 1992). Thus, Lin *et al.*, (1993) have successfully shown that changes in asphalt performance due to oxidative aging are directly related to changes in measurable chemical properties.

A review of the literature has shown that no fundamental asphalt-aging models describing both the effect of temperature and pressure have been developed. In recent years, researchers have studied the effect of temperature on the reaction kinetics concluding that multiple temperature tests along with extrapolation to road conditions gives a more realistic measure of an asphalt's resistance to oxidative aging. Unfortunately, since POV aging tests are run at elevated oxygen partial pressures, it is not known whether the kinetic information at high pressure is truly representative of the actual kinetics at road pressure. The discovery of a physicochemical relationship between η and CA for asphalt oxidation has been a tremendous advancement in characterizing asphalts. This relationship is independent of the kinetic model and provides a better way of comparing laboratory- and field-aged materials to confirm that the simulation is accurate. However, the effect of temperature on the physicochemical model parameters is not known. Other physicochemical relationships have

been discovered relating η and $(1 / J'')$ to % A formation from oxidation. These relationships were also independent of the kinetics. The discovery of even more physicochemical relationships may lead to a more complete understanding of asphalts.

Oxygen Transport in Asphalt Films

The literature is limited with regard to oxygen transport properties in asphalt. The fundamental transport property for is diffusivity, $\mathcal{D}_{O_2}$. Other transport properties, such as permeability and oxygen absorption, used primarily to characterize non-homogenous matrices have also been studied. The difficulty in performing these experiments and analyzing the data is separating the transport from the reaction effect. Anderson and Wright (1941) measured both the permeability of oxygen and water vapor in an asphalt film. Based on the permeability data, the researchers concluded that water diffuses much faster than oxygen through asphalt films. Krchma *et al.*, (1960) measured oxygen absorption at 333.3 K for 48 hrs and 372.2 K for 8 hrs. They concluded that for different asphalts there was no relationship between the amount of absorbed oxygen and the degree of hardening. Knoterus (1972) reported on oxygen absorption experiments with asphalt toluene solutions. He reports that an organic solution was used to minimize the diffusion effect.

Even less work has been attempted in the theoretical development of aging models for asphalt films including both reaction and diffusion of oxygen. The combined effects of diffusion and reaction of oxygen in an asphalt film are described by Van Oort (1956). By starting from fundamental transport and reaction equations, a theoretical model was proposed. Assumptions in this model include a first order

reaction in oxygen concentration and $\mathcal{D}_{O_2}$ varies through the film by equation I – 8.

$$\mathcal{D}_{O_2} = D_o\left(1 - \frac{g}{G_o}\right) \qquad (I-8)$$

D_o is the oxygen diffusivity of the neat material; g is the concentration of chemically bound oxygen, and G_o is the theoretical maximum concentration of chemically bound oxygen. Experimental observations based on oxygen absorption were used to confirm the theory. Actual determinations of G_o were achieved after 100 hours of aging. Based on the model, the layer of exposed asphalt film near the surface forms a skin of high viscosity and retards the aging of the asphalt below the skin. He reported a $\mathcal{D}_{O_2}$ of 8.6×10^{-16} m^2 / s in a neat asphalt film at 323.2 K. Although theoretically sound, the values of G_o for different asphalts are not known and cannot be measured.

Measuring oxygen absorption and asphalt viscosity, Blokker and Van Hoorn (1959) confirmed a skin formation but stated that the order of reaction in terms of oxygen concentration was 0.6. The depth of bound oxygen penetration was 2.5 mm for 10 days aging at 323.2 K, 1 atm pure oxygen. Comparisons between field-aged samples led to the conclusion that aging at 20 atm oxygen, 323.2 K for one day is equivalent to 1/2 year of actual service. They report a $\mathcal{D}_{O_2}$ of 12×10^{-11} m^2 / s in neat asphalt films at 323.2 K. The authors argue that $\mathcal{D}_{O_2}$ in the film is not really changing. The reactivity of the components in the asphalt decreases with time. The values reported by Blokker and van Hoorn are four orders of magnitude higher than that reported by Van Oort. In terms of model development, these works are significant, and little model development has occurred since then. However, using these procedures in a laboratory simulation are not practical.

Dickinson *et al.*, (1958) studied the absorption of oxygen in asphalt films. They used a model with first order reaction and constant $\mathcal{D}_{O_2}$. They concluded that at highway-pavement conditions, the process was diffusion controlled. Furthermore, the rate of oxygen absorption decreased with increasing viscosity and film thickness. The rate increased with temperature and the activation energy for the process is 42 kJ/gmol. However, their model is only valid for the initial rate of absorption because the properties of the asphalt change as a result of oxidation. Lee and Dickinson (1962) also concluded that the absorption of oxygen was continuously modified by high viscosity skin formation. For aging at 303.2 K under atmospheric pressure, the absorption of oxygen was diffusion controlled. Unfortunately, actual experimental measurements of the surface of the films were never reported.

Equation I – 4, as given by Verhasselt and Choquet, supposedly includes the effect of oxygen transport. However, the equation does not account for changes in $\mathcal{D}_{O_2}$ as a function of CA in the film. Comparison with field aging for two asphalts was not very good. Furthermore, equation I – 4 is not a realistic model for field aging. It predicts an infinite change in the measured property as aging time goes to infinity. Actual field aging is asymptotic or diffusion limited.

Only two literature sources report $\mathcal{D}_{O_2}$ in asphalts at one temperature, 323.2 K. More importantly no quantitative model relating $\mathcal{D}_{O_2}$ to other measurable properties such as temperature, η, or CA exists. Since research has shown that field aging is diffusion limited, only a fundamental aging model containing both oxygen diffusion and reaction has any attempt of providing accurate predictions of field aging.

Field Aging

During laboratory aging, the materials, temperature, oxygen pressure, and film thickness can be accurately monitored and controlled. In the field, these values can only be estimated. Furthermore, the presence of aggregate in contact with the asphalt may also result in different mechanisms and different oxidation products. For modeling field aging, climatic conditions and measurable core properties must be included. These measurable core properties then must be related to the fundamental quantities in an asphalt-aging model.

The study of asphalt oxidation in the presence of different aggregates has led to many different conclusions. Petersen *et al.*, (1974) studied asphalt oxidation on mineral surfaces with inverse gas liquid chromatography. They concluded that a majority of the oxidation catalysis resulted from components naturally present in the asphalt. By comparison, the catalytic effect of the aggregate is significantly reduced. Plancher *et al.*, (1976) concluded that hydrated lime decreases the rate of asphalt hardening. Edler *et al.*, (1985) confirm this result using lime-treatment and Extended RTFOT and POV aging. These last two studies suggest that the kinetics of oxidation may be affected by the type of aggregate. With limited data, Lau *et al.*, (1992) concluded that the physicochemical relationships were independent of aggregate type by comparing POV-aged materials. This suggests that the products formed as a result of oxidation and their effect on physical properties is independent of aggregate. However, this says nothing of the nature of the kinetics.

Highway-pavement temperature is a very significant factor in field aging (Kemp and Predoehl, 1981). This affects both the rate of reaction and the rate of oxygen transport. The estimation of the maximum surface temperature, T_{sur}, based on ambient temperatures, T_{air} and latitude, ψ, is given by Solaimanian and Kennedy

(1993). Based on field measurements and the conservation of energy for steady-state heat flow at the asphalt surface, the difference between the maximum T_{sur} and T_{air} is a quadratic function of ψ given in equation I – 9.

$$(T_{sur} - T_{air})_{max} = -0.01113\psi^2 + 0.41202\psi + 43.877 \qquad (I-9)$$

For equation I – 9 the temperatures are in units of °F. The temperature of the pavement below the surface is also important. By comparing measured and estimated temperatures, the top 20.3 cm (8 inches) of the pavement are within 2.8 to 3.3 K of the surface temperature. At greater depths, the temperature difference increases. Using ambient temperature data from different locations and equation I–9 the annual temperature cycle of the pavement can be estimated. Verhasselt and Choquet (1993) discuss an interesting approach of including the annual temperature variation in the reaction kinetics. Integrating the Arrhenius equation over the annual temperature profile they calculate a kinetic mean temperature. However, they do not discuss the fact that the kinetic mean temperature is not only a function of location but also asphalt, since the Arrhenius parameters are asphalt dependent.

The measurable core properties of percent voids, % V, asphalt content, % Asp, and aggregate gradation affect the rate of oxidation and hardening in the field. For field aging, Davison *et al.*, (1989) provides an exhaustive literature review showing the % V is the single most dominating factor in the rate of asphalt oxidation and hardening. This work shows that the effect of air voids is greater than the difference in asphalt compositions. Heithaus and Johnson (1958) concluded that a linear relationship existed between % V and binder hardening rate based on measured viscosity.

A study of the effect of voids, air permeability, asphalt content, and aggregate gradations on oven aging of asphalts using molded test specimens was done by Goode and Lufsey (1965). For a given gradation, aging and permeability increased with voids. At high void content, the permeability was affected more than the aging. They found that aging increased as asphalt film thickness decreased. At fairly low voids, all gradations could be correlated with the ratio of voids to averaged film thickness. This ratio, called the voids-bitumen index, was suggested as a possible design parameter, permitting a range of air voids depending on the aggregate. Halstead (1963) noted the tendency for lower hardening with higher asphalt content based on the Zaca-Wigmore test sections.

In terms of oxidative aging in the field, permeability is critical but at low void levels becomes very difficult to measure (Chipperfield *et al.*, 1970). Permeability is very low at the top of the pavement from compaction due to traffic. Yet, oxidative aging is much greater at the top of the pavement relative positions below the surface primarily due to elevated surface temperatures. At this position in the pavement with such low permeability, oxygen transport occurs primarily from diffusion. Goode and Lufsey (1965) found that air permeability was a function of aggregate gradation as well as % V. At high air voids, the effect of gradation was more pronounced than at low air voids. At void levels of 4-5%, the measured values of air permeability were very low and independent of aggregate gradation.

Based on experience, Campen *et al.*, (1959) stated that asphalt film thickness of 6 to 8 microns are most desirable for pavement mixtures. This film thickness provides a thick asphalt film and at the same time the desired void content and stability. Kumar and Goetz (1977) report on a study of aging as a function of permeability and film thickness. Laboratory compacted cores were prepared with graded and ungraded

aggregate at varying asphalt content and compaction levels. The cores were aged by passing 333.3 K air through the cores. The aging was monitored periodically by a non-destructive creep test. For the single size mixtures, the best correlation was the ratio of asphalt film thickness to permeability and permeability alone. The ratio of film thickness to voids did not correlate well, even though there was a strong correlation between voids and permeability. Surprisingly, for graded mixtures, everything correlated. The authors admitted that this is not very logical. Based on microscopic studies, they decided the idea of film thickness is not applicable to graded mixtures, and correlations were made only with permeability and voids. They discuss dividing the total air voids into two groups, accessible voids and non-accessible voids. Neither of these studies provide a fundamental model for calculating film thickness. Instead, film thickness is determined from empirical models based on % *Asp*. The authors did not provide any relation between the total voids, permeability, and non-accessible voids. Furthermore, the authors did not discuss the relationship of the permeability and void levels to the oxygen pressure in the air voids as a function of aging time.

There are few systematic and successful attempts to include other variables such as percent asphalt or aggregate gradation in correlations of road aging. Krchma and Groening (1959) in analyzing data of Pauls and Halstead (1958) showed that both percent asphalt and voids affect the asphalt hardening. As mentioned earlier, Kumar and Goetz (1977) correlated aging of lab samples in terms of film thickness but obtained poor results for dense mixtures. Goode and Lufsey (1965) used asphalt content to calculate a bitumen index that also included aggregate gradation and is supposedly a measure of film thickness. The best correlation was with percent air voids divided by the bitumen index. They also showed a relation between percent voids, asphalt gradation and permeability.

Similar to the laboratory aging tests, the main focus has been on the attempt to develop empirical correlations between measured core properties and degree of aging. No researcher has successfully used any of these models to predict field aging based solely on the current laboratory tests and empirical correlations. Unfortunately, these empirical models do not contain sufficient information to accurately predict field aging based on the measured core properties at some initial time. A more fundamental approach is to relate the measured core properties to fundamental quantities in an asphalt-aging model. Then, in the context of the model, accurate predictions of field aging based on initial measured core properties are possible.

Summary

The effect of temperature and pressure on the rate of asphalt aging has not been satisfactorily determined. Some theoretical and experimental work has been accomplished for diffusion and reaction of pure oxygen in an asphalt film; however, models relating oxygen diffusivity to measurable changes in an asphalt film have not been studied. The development of an asphalt-aging model including both oxygen diffusion and reaction has not been attempted. Furthermore, comparisons between POV- and field-aged materials have not conclusively shown that POV aging simulates field aging. Finally, a highway-pavement aging model including climatic conditions, and measurable core properties has not been investigated. With the development of an accurate asphalt-aging model and implementation of laboratory tests designed to estimate the model parameters, researchers will then be able to reliably predict highway aging, potentially saving millions of dollars.

To elevate the understanding of asphalt oxidation to a point such that field aging can not only be simulated but also predicted requires accurate kinetic equations including both effects of temperature and pressure, estimations of oxygen diffusivity in asphalt as a function of asphalt material properties or extent of aging, developments of additional physicochemical properties, and successful comparisons between field- and laboratory-aged materials.

CHAPTER II
AGING MODEL DEVELOPMENT

As stated in Chapter I, the ultimate objective of this work is to elevate the understanding of asphalt aging to a level that would enable predictions of pavement life. Modeling the changes in chemical and physical properties as a result of oxidative aging are fundamental in reaching this objective. Furthermore, changes in chemical and physical properties are expressed by two separate methods. The first method uses rate equations where the dependent variables are functions of time. With accurate rate equations, simulation and prediction of highway-pavement aging is possible. The second method uses physicochemical relationships. These expressions have no predictive capability like the rate equations; however, they do provide information about the oxidative characteristics of different asphalts. Furthermore, the physicochemical relationships decrease the number of measurable variables and allow the researcher to calculate properties that would otherwise be difficult or impossible to measure. For example, with equation I – 6 and the known model parameters for a given asphalt, η_o^* at the surface of an asphalt film can be estimated from a CA measurement at the surface.

The chemical changes resulting from oxidation are expressed in terms of observable variables through a kinetic equation (Froment and Bischoff, 1979). For oxidation in asphalt to occur, both oxygen and an active site on the asphalt molecule must be present. Therefore, the ability to transport oxygen in an asphalt film of finite thickness affects the oxidative aging characteristics. The $\mathcal{D}_{O_2}$ is a measure of the oxygen transport in an asphalt film.

To simplify the picture, first a model is developed for laboratory aging of asphalt films. In laboratory experiments, film thickness, temperature, and oxygen pressure can be carefully controlled and monitored. Included in this development is a kinetic expression relating changes in chemical properties to observable variables. To estimate the parameters, the explicit assumption in this model is that the oxygen concentration is known. This work is focused on developing kinetic expressions for *CA*. Researchers have shown that *CA* and changes in the physical properties due to oxidative aging are correlated (Martin *et al.*, 1990; Lau *et al.*, 1992; Petersen *et al.*, 1993). Thus, deriving kinetic expressions for *CA* is equivalent to deriving kinetic expressions for the physical properties. Applying this kinetic model, an oxygen diffusion and reaction model is formulated. The oxygen diffusion and reaction model requires that the kinetic parameters from the first model be known in order to estimate $\mathcal{D}_{O_2}$. Furthermore, models relating $\mathcal{D}_{O_2}$ to asphalt η_o^* and *CA* are also studied. The kinetic model and the oxygen diffusion and reaction model collectively are the asphalt-aging model.

With accurate kinetic and oxygen diffusion models, including estimates of model parameters based on laboratory data, a highway-pavement aging model is proposed. In field aging, temperature, oxygen pressure and film thickness are not necessarily known. These quantities must be estimated from measurable properties such as air temperature, percent asphalt, aggregate gradation, and percent air voids. The objective of this study is to relate the measurable core properties to fundamental quantities in the asphalt-aging model. With these relationships and an estimation of the temperature of the highway, the asphalt-aging model can provide accurate simulations and predictions of field aging.

Asphalt-Aging Model

In an asphalt, carbonyl forms only in the presence of oxygen. Since the asphalt film is a finite thickness, both diffusion and reaction of oxygen must be taken into consideration. Figure II-1 shows a cross section of an asphalt film during the aging process. At the exposed surface, ES, the oxygen concentration or pressure is a function of the state of the system. For a dilute solution of oxygen in the asphalt, the oxygen concentration at the surface is proportional to the oxygen concentration in the gas. For the most simple assumption, the oxygen concentration at the surface is equal to the oxygen concentration in the gas. In the film, for the case where oxygen consumption rates are much greater than oxygen diffusion rates, an oxygen concentration gradient is established. At the impermeable boundary or substrate interface, SI, the oxygen concentration gradient is zero. Since the oxygen transport properties are functions of composition and physical properties, the oxygen concentration profile, as shown in the figure, is a function of time.

Because of the complexity of the aging process, the explanation of the asphalt-aging model is further divided in four subsections. The first describes the rate of formation of carbonyl compounds in terms of temperature aned oxygen concentration. The second relates the carbonyl production rate to the rate of oxygen consumption. The third section describes relationships between η_o^* and CA. The fourth section uses the reaction kinetics in the development of an oxygen diffusion and reaction model.

Carbonyl formation in asphalts

It is hypothesized that at any point in an asphalt, CA changes only due to reaction; there is no bulk flow or diffusion of CA. Thus, an accounting of CA at any

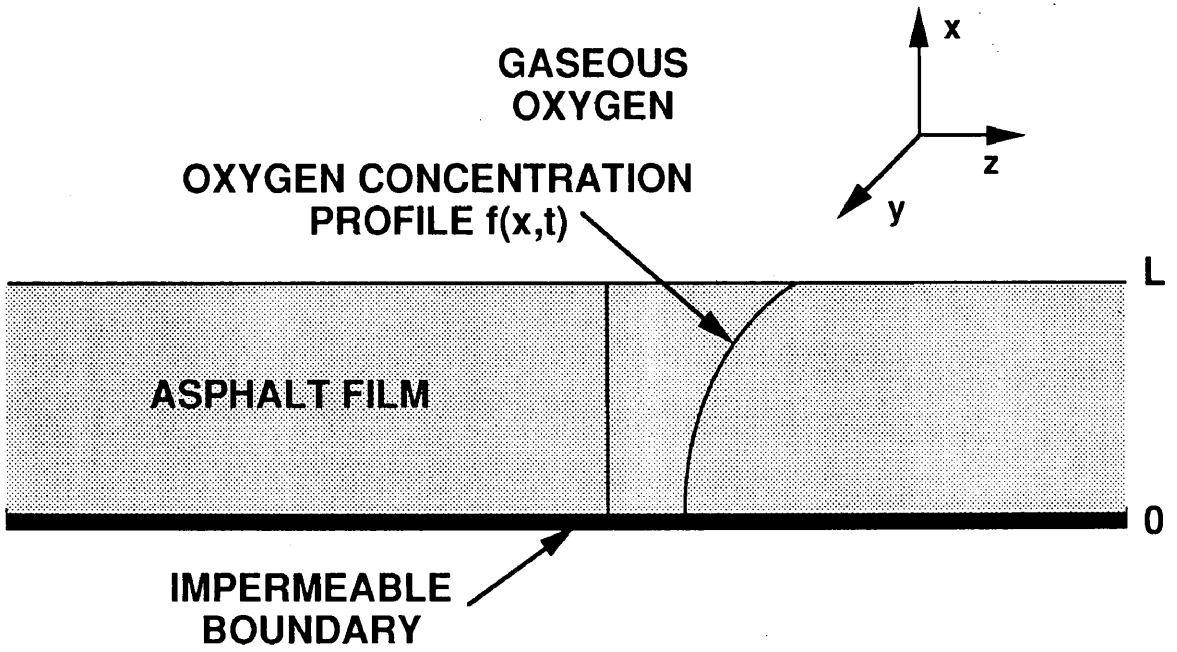

Figure II-1. Oxygen concentration profile in an asphalt film.

point in an asphalt is given by equation II – 1.

$$\left(\frac{\partial CA}{\partial t}\right) = r_{CA} \qquad \text{(II – 1)}$$

The integrated form gives the magnitude of carbonyl at any time t.

$$CA(t) = \int_0^t r_{CA}\, d\theta + CA_o \qquad \text{(II – 2)}$$

θ is a dummy variable of integration. Since CA correlates with physical properties such as η_o^* from equation I – 6 and the physical properties dictate the performance of the asphalt, the ability to calculate CA based on observable variables is extremely important. Even with an accurate model for r_{CA}, the integration constant, CA_o, must be determined from experimental data.

For equations II – 1 and II – 2 to be useful, r_{CA} and CA_o must be expressed in terms of observable variables. Based on previous work, the most logical variables are the aging temperature, T, oxygen concentration, C_{O_2}, or pressure, P, and the particular asphalt. For r_{CA} this is given in equation II – 3.

$$r_{CA} = f(T, C_{O_2}, C_{A+}) \qquad \text{(II – 3)}$$

C_{A+} is the concentration of active components in the asphalt. Based on the work of Lau *et al.*, (1992) at 20 atm oxygen for long-term aging, the r_{CA} is independent of C_{A+}. Dickinson and Nicholas (1949) also conclude that the long-term aging rate is constant for oxygen absorption measurements. In other words, the C_{A+} in the asphalt is so great, those active compounds that form CA as a result of oxidation do not affect the overall C_{A+}.

A simplified rate expression is given in equation II – 4 including only T and C_{O_2}.

$$r_{CA} = k_C(T) C_{O_2}^{\alpha} \qquad \text{(II – 4)}$$

k_C is the rate constant in terms of concentration as a function of T, and α is the order of reaction with respect to oxygen concentration. By eliminating C_{A+}, the characteristics of a particular asphalt have not been removed but appear in the model parameters, k_C and α (Lau *et al.*, 1992).

Expressing C_{O_2} in terms of partial pressures by an equation of state is given in equation II – 5.

$$r_{CA} = k_P(T) P^{\alpha} \qquad \text{(II – 5)}$$

The subscript O_2 has been removed since only one component, oxygen, is included in the kinetic expression.

An Arrhenius relationship describes the temperature dependence on the rate constant k_P (Lau *et al.*, 1992).

$$k_P = A \exp\left(\frac{-E_A}{RT}\right) \qquad \text{(II – 6)}$$

A is the Arrhenius constant; E_A is the activation energy, and R is the universal gas constant. Lau discovered that both A and E_A were dependent on asphalt composition. Substituting equation II – 6 into equation II – 5 gives:

$$r_{CA} = A \exp\left(\frac{-E_A}{RT}\right) P^{\alpha} \qquad \text{(II – 7)}$$

This equation contains three adjustable parameters A, E_A, and α describing r_{CA}. The parameters may be determined from experimental data as described in Chapter IV. Furthermore, the experimental data must be such that P is known. The pressure

of the gas is measured; however, the oxygen pressure at the surface should be proportional to the pressure in the gas. For lack of accurate oxygen solubility data, in this study, the proportionality constant is assumed to be unity. For aging asphalts in thin films, the only place P is known or a function of thermodynamic variables, is at the *ES* in Figure II-1. Unfortunately, P in the film is not known because of diffusion and reaction.

Another important point needs to be stressed. The experimental data are discrete values of CA and t at various isothermal and isobaric conditions. Independent of II – 5, a mathematical relationship between CA and t must be developed based on the data in order to estimate $\left(\frac{\partial CA}{\partial t}\right)$. The two most fundamental relationships are equations I – 2 of Lau *et al.*, (1992), and I – 5 of Dickinson and Nicholas (1949). In this study, equation I – 2 is used exclusively.

To calculate CA, the integration constant, CA_o, in equation II – 2 must be also be determined. Based on Lau *et al.*, (1992) for aging at 20 atm oxygen pressure, the initial conditions of the neat asphalt did not correspond to the long-term aging characteristics because of an initial non-linearity. Petersen *et al.*, (1993) also reports this initial non-linearity with POV and TFAAT aging. Fortunately, equation II – 1 suggests that CA_o may be of the following form.

$$CA_o = f(T, P) \qquad \text{(II – 8)}$$

Only through experimental data can the exact nature and functionality and the model parameters in equation II – 8 be determined. The model of Dickinson and Nicholas (1949) accounts for the initial non-linearity; therefore, with this model, the value of CA_o could be determined from neat asphalt. Furthermore, the discussion by Dickinson and Nicholas for oxygen absorption measurements suggest a linear model

in pressure from 0.2 to 1 atm for equation II – 8. The authors reported that increases in temperature would also increase CA_o; however, no model was provided.

r_{O_2} versus r_{CA}

In the proposed experiments, the rate of oxygen consumption, r_{O_2}, is not measured; however, r_{CA} is. To estimate $\mathcal{D}_{O_2}$, the r_{O_2} is required. From the conservation of mass, r_{O_2} is equal to the rate of production of all oxygen-containing compounds as a result of oxidation.

$$r_{O_2} = n_{CA} r_{CA} + n_{SO} r_{SO} + \cdots \qquad (II - 9)$$

The rate of sulfoxide formation is r_{SO}. n_{CA} and n_{SO} are required stoichiometric coefficients to satisfy conservation of elemental oxgyen. The dots symbolize all of the other oxygen reactions in the asphalt. The formation of sulfoxides as measured by FTIR did not increase after an initial growth for long-term (Lau *et al.*, 1992) and highway-pavement (Martin *et al.*, 1990) aging. In other words, r_{SO} for long-term aging is approximately zero. However, CA continued to increase. From this information, long-term r_{O_2} is approximated as being proportional to the r_{CA}.

$$r_{O_2} = c r_{CA} \qquad (II - 10)$$

c is an experimentally determined parameter accounting for the differences in the FTIR measurement for CA and the true mass of oxygen. For aged aspahlts, CA is compared with oxygen content as determined from elemental analysis to determine c in equation II – 10.

Relationships between η_o^* and CA for multiple temperatures

Lau *et al.*, (1992) showed that for long-term oxidative aging η_o^* and CA are related by equation I – 6.

$$\eta_o^* = \exp\Big\{ HS \cdot CA + m \Big\} \qquad (\text{I} - 6)$$

However, only estimated parameters for η_o^* at 333.3 K were provided. The parameter m does not necessarily correspond to the neat η_o^*. Furthermore, the authors suggest that the HS is independent of temperature.

A model is developed, relating the parameters HS and m to measurement temperature. At the reference temperature, T_o, and any other temperature, T, η_o^* as a function of CA is given in equation II – 11.

$$\begin{aligned} \ln\Big(\eta_o^*(T_o)\Big) &= HS(T_o) \cdot CA + m(T_o) \\ \ln\Big(\eta_o^*(T)\Big) &= HS(T) \cdot CA + m(T) \end{aligned} \qquad (\text{II} - 11)$$

Jemison (1992) measured η_o^* from 273.15 to 333.3 K. He used the Andrade equation (Andrade, 1930) to model η_o^* as a function of temperature as given in equation II – 12.

$$\ln\left(\frac{\eta_o^*(T)}{\eta_o^*(T_o)}\right) = E_V\left(\frac{1}{T} - \frac{1}{T_o}\right) \qquad (\text{II} - 12)$$

E_V is the viscosity activation energy divided by the universal gas constant, and is also called the Andrade parameter. By comparing equations II – 11 and II – 12:

$$E_V\left(\frac{1}{T} - \frac{1}{T_o}\right) = \Big(HS(T) - HS(T_o)\Big)CA + \Big(m(T) - m(T_o)\Big) \qquad (\text{II} - 13)$$

E_V must be a linear function of CA.

$$E_V = \gamma CA + \delta \qquad (\text{II} - 14)$$

This contradicts the findings of Lau *et al.*, (1992) in which the authors suggested a constant HS independent of temperature.

From equation II–14, with known model parameters, γ, δ, $HS(T_o)$, and $m(T_o)$, HS and m at other temperatures can be determined.

$$\begin{aligned} HS(T) &= HS(T_o) + \gamma\left(\frac{1}{T} - \frac{1}{T_o}\right) \\ m(T) &= m(T_o) + \delta\left(\frac{1}{T} - \frac{1}{T_o}\right) \end{aligned} \qquad (\text{II} - 15)$$

For linear visco-elastic behavior, values of η_o^* are not required at other temperatures in order to estimate the model parameters γ and δ. Ferry (1985) describes time-temperature superposition where the horizontal shift factor, a_T, relates the response time and frequency to temperature by equation II – 16.

$$a_T = \frac{t_T}{t_{T_o}} = \frac{\omega_{T_o}}{\omega_T} \qquad (\text{II} - 16)$$

T and T_o represent any temperature and the reference temperature, respectively.

The complex viscosity, η^*, at the reference temperature is defined by equation II – 17 in terms of the storage, G', and loss, G'', moduli. η_o^* is defined when G' is negligible compared with G''.

$$\eta^*_{T_o} = \frac{1}{\omega_{T_o}}\sqrt{(G')^2 + (G'')^2} \qquad (\text{II} - 17)$$

For any temperature, T, η^* is given by II – 18.

$$\eta^*_T = \frac{1}{\omega_T}\sqrt{(G')^2 + (G'')^2} \qquad (\text{II} - 18)$$

Substituting equation II – 16 into equation II – 18 yields:

$$\eta^*_T = \frac{a_T}{\omega_{T_o}}\sqrt{(G')^2 + (G'')^2} \qquad (\text{II} - 19)$$

Since the moduli are the same at the two different temperatures because of the horizontal shift only, the ratio of η^* at T to η^* at T_o is a function of a_T only.

$$\frac{\eta^*_T}{\eta^*_{T_o}} = a_T \qquad (\text{II} - 20)$$

Comparing equation II – 12 and II – 20, a_T must have the same temperature dependence as η^* as given in equation II – 21.

$$\ln a_T = E_V\left(\frac{1}{T} - \frac{1}{T_o}\right) \qquad (\text{II} - 21)$$

For asphalts at different degrees of aging or CA, the dynamic mechanical properties are measured at different temperatures. Shift factors, a_T, are determined as functions of T, and E_V is calculated at different degrees of aging. The model parameters, γ and δ, are estimated by comparing E_V and CA through equation II – 14. From these results, η^*_o at any CA and T can be calculated from the reference temperature HS and m and the E_V model parameters, γ and δ. Extending the η^*_o-CA relationships to multiple temperatures is required to formulate an asphalt oxygen diffusion and reaction model. Furthermore, this development is needed to apply the physicochemical property relationships to highway-pavement aging.

Oxygen diffusion and reaction

With a known kinetic expression and a relationship between r_{CA} and r_{O_2}, an asphalt oxygen diffusion and reaction model is described. Bird *et al.*, (1960) provide a mathematical model accounting for oxygen in a differential volume.

$$\left(\frac{\partial C_{O_2}}{\partial t}\right) = -\nabla \cdot \mathbf{N}_{O_2} - r_{O_2} \qquad (\text{II} - 22)$$

$\mathbf{N}_{O_2}$ is the molar flux of oxygen. In an asphalt, there is no bulk flow of oxygen and the molar flux is expressed by Fick's law of diffusion as given in equation II – 23.

$$\mathbf{N}_{O_2} = -\mathcal{D}_{O_2}\nabla C_{O_2} \qquad (\text{II} - 23)$$

Substituting back into equation II – 22 gives equation II – 24.

$$\left(\frac{\partial C_{O_2}}{\partial t}\right) = -\nabla \cdot (-\mathcal{D}_{O_2} \nabla C_{O_2}) - r_{O_2} \qquad \text{(II – 24)}$$

Equation II – 24 is expanded for variable $\mathcal{D}_{O_2}$.

$$\left(\frac{\partial C_{O_2}}{\partial t}\right) = \nabla \mathcal{D}_{O_2} \cdot \nabla C_{O_2} + \mathcal{D}_{O_2} \nabla^2 C_{O_2} - r_{O_2} \qquad \text{(II – 25)}$$

Equation II – 25 accounts for changes in $\mathcal{D}_{O_2}$ in the film as a result of changes in physical properties due to oxidation. Unfortunately, it is not known how significant these changes are to oxygen transport in asphalt. Obviously, changes in $\mathcal{D}_{O_2}$ as a function of position in the film further affect the oxygen concentration profile.

The asphalt film shown in Figure II-1 extends infinitely wide and deep. Furthermore, for laboratory aging, the oxygen transport in the asphalt film is assumed to occur in only one direction based on the experimental procedures described in Chapter III. Hence, the three-dimensional model of equation II – 25 reduces to a one-dimensional model as given in equation II – 26.

$$\left(\frac{\partial C_{O_2}}{\partial t}\right) = \left(\frac{\partial \mathcal{D}_{O_2}}{\partial x}\right)\left(\frac{\partial C_{O_2}}{\partial x}\right) + \mathcal{D}_{O_2}\left(\frac{\partial^2 C_{O_2}}{\partial x^2}\right) - r_{O_2} \qquad \text{(II – 26)}$$

x is the spatial variable. Using equation II – 26 along with experimental data from laboratory aging, an estimation of $\mathcal{D}_{O_2}$ in an asphalt film is possible. For constant $\mathcal{D}_{O_2}$, this is a one parameter estimation. For variable $\mathcal{D}_{O_2}$, the estimation is more complex depending on the relationship between $\mathcal{D}_{O_2}$ and the asphalt properties in the film.

Since the measurable variables in the laboratory experiments are temperature and pressure and the experiments are designed at low oxygen pressure, the ideal gas law converts C_{O_2} to terms of T and P.

$$C_{O_2} = h\left(\frac{P_{O_2}}{RT}\right) \qquad \text{(II – 27)}$$

h is the Henry's law constant, relating the oxygen pressure to the concentration of oxygen in the asphalt. In terms of P, the accounting of oxygen in the asphalt film is:

$$\frac{h}{RT}\left(\frac{\partial P}{\partial t}\right) = \frac{h}{RT}\left(\frac{\partial \mathcal{D}_{O_2}}{\partial x}\right)\left(\frac{\partial P}{\partial x}\right) + \frac{h}{RT}\mathcal{D}_{O_2}\left(\frac{\partial^2 P}{\partial x^2}\right) - r_{O_2} \qquad (II-28)$$

The subscript O_2 has been dropped from P in equation II – 28 since pure oxygen gas is used in the experiments. The subscript has been retained on the diffusivity since this is the component that is diffusing. Rearranging equation II – 28 gives:

$$\left(\frac{\partial P}{\partial t}\right) = \left(\frac{\partial \mathcal{D}_{O_2}}{\partial x}\right)\left(\frac{\partial P}{\partial x}\right) + \mathcal{D}_{O_2}\left(\frac{\partial^2 P}{\partial x^2}\right) - \left(\frac{RT}{h}\right) r_{O_2} \qquad (II-29)$$

Since r_{CA} is determined from experimental data, equation II – 10 is substituted into II – 29 giving equation II – 30.

$$\left(\frac{\partial P}{\partial t}\right) = \left(\frac{\partial \mathcal{D}_{O_2}}{\partial x}\right)\left(\frac{\partial P}{\partial x}\right) + \mathcal{D}_{O_2}\left(\frac{\partial^2 P}{\partial x^2}\right) - \left(\frac{cRT}{h}\right) r_{CA} \qquad (II-30)$$

For this final form, the boundary conditions and initial conditions are specified.

$\left(\frac{\partial P}{\partial x}\right) = 0$	at	$x = 0$	Substrate interface
$P = P_{\text{gas}}$	at	$x = L$	Exposed surface
$P = 0$	at	$t = 0$	Initial condition

$\mathcal{D}_{O_2}$ in equation II – 30 is not known and must be estimated. An infinite number of values of $\mathcal{D}_{O_2}$ satsify the initial and boundary conditions. Unfortunately, a unique determination of $\mathcal{D}_{O_2}$ is not possible based on the initial and boundary conditions. An additional specification, either P at the substrate interface, SI, or the pressure gradient at the exposed surface, ES, is required. In this study the additional specification is P_{SI}.

Before proceeding further, a description of the experimental procedure is given in an attempt to estimate P_{SI}. Asphalt films of known thickness, L, are laboratory-aged at different oxygen pressures, temperatures, and time periods. CA_{ES} and CA_{SI} are measured. Since r_{CA} is a function of T and P, an estimation of P can be made from measured r_{CA} and T, provided the model parameters are known. For isothermal aging in the film, the difference in $(r_{CA})_{SI}$ compared to $(r_{CA})_{ES}$ provides a measure of the difference in P_{SI} and P_{ES}. Furthermore, since P_{ES} is assumed to be known from the measurements, P_{SI} is calculated from equation II – 7 with the known kinetic parameters. The required additional specification to estimate a unique $\mathcal{D}_{O_2}$ from equation II – 30 is based solely on the reaction kinetics.

A parameter estimation of $\mathcal{D}_{O_2}$ or $\mathcal{D}_{O_2}$ as a function of physical properties in the asphalt film using equation II – 30 is not possible without a model relating $\mathcal{D}_{O_2}$ to physical properties. Even with a model relating $\mathcal{D}_{O_2}$ to physical properties, estimation of the parameters with unknown initial guesses is difficult. Preliminary estimates for the parameters are made by simplifying equation II – 30. The most significant simplifying assumption is pseudo-steady state for P in the film. This reduces equation II – 30 to:

$$0 = \left(\frac{d\mathcal{D}_{O_2}}{dx}\right)\left(\frac{dP}{dx}\right) + \mathcal{D}_{O_2}\left(\frac{d^2P}{dx^2}\right) - \left(\frac{cRT}{h}\right)r_{CA} \qquad \text{(II – 31)}$$

This assumption reduces the complexity of the parameter estimation; the partial differential equation becomes an ordinary differential equation. A further assumption of constant $\mathcal{D}_{O_2}$ reduces equation II – 31 to:

$$0 = \mathcal{D}_{O_2}\left(\frac{d^2P}{dx^2}\right) - \left(\frac{cRT}{h}\right)r_{CA} \qquad \text{(II – 32)}$$

Although equations II – 31 and II – 32 are approximations, estimated $\mathcal{D}_{O_2}$ obtained

from these reduced equations can be used as initial guesses in the more complicated unsteady-state expression, equation II – 30.

To account for changes in $\mathcal{D}_{O_2}$ as a result of *CA* due to reaction and η_o^* increase by *HS*, a mathematical relationship between $\mathcal{D}_{O_2}$ and the amount of aging must be developed. Only with such a function can equations II – 30 and II – 31 be numerically integrated. Reid *et al.*, (1983) provide models relating diffusivity to viscosity and temperature as given in equation II – 33.

$$\mathcal{D}_{O_2} = f(\eta_o^*, T) \qquad \text{(II – 33)}$$

In the literature, for isothermal conditions, the diffusivity of oxygen in liquids is dependent on the viscosity of the liquid by equation II – 34.

$$\mathcal{D}_{O_2} = D_o(\eta_o^*)^B \qquad \text{(II – 34)}$$

B ranges from -1 to -0.5 for organic liquids (Reid *et al.*, 1983). The values for B in the literature are based on diffusion measurements of carbon dioxide in various organic solvents and n-hexane in hydrocarbons. The viscosity of the solvents ranged from 0.5 to 5000 cP in the later case. Although the viscosity of asphalt is much higher, in the neighborhood of 2000 P at 333.3 K for neat material, this model provides a reasonable starting point. For the asphalts studied, D_o and B are the estimated parameters.

The temperature dependence of the diffusivity is expressed by two different models (Reid *et al.*, 1983). The first model relates the diffusivity and temperature:

$$\mathcal{D} \propto T \qquad \text{(II – 35)}$$

while the second model relates the log of diffusivity to reciprocal temperature.

$$\ln \mathcal{D} \propto \frac{1}{T} \qquad (\text{II}-36)$$

Since η_o^* of asphalt is such a strong function of temperature, equation II – 34 may be sufficient to describe $\mathcal{D}_{O_2}$ as a function of asphalt material properties.

η_o^* is related to CA by HS and m.

$$\eta_o^* = \exp\Big\{ HS \cdot CA + m \Big\} \qquad (\text{I}-6)$$

HS and m are functions of temperature. CA is calculated as a function of aging temperature, oxygen pressure, and time.

$$CA(t) = \int_0^t r_{CA}\, d\theta + CA_o \qquad (\text{II}-2)$$

This calculation of CA in an asphalt is an accumulation of all of the aging history at a position x and over a time period t. This represents the amount of aging. Substituting equations II – 2 and I – 6 into equation II – 34.

$$\mathcal{D}_{O_2}(t,x) = D_o \left[\exp\Big\{ HS\Big[T(t,x)\Big] \Big(\int_0^t r_{CA}\Big[T(\theta,x), P(\theta,x)\Big] d\theta + CA_o \Big) + m\Big[T(t,x)\Big] \Big\} \right]^B \qquad (\text{II}-37)$$

Equation II – 37 relates $\mathcal{D}_{O_2}$ to the current temperature, position, and all of the aging history.

For variable $\mathcal{D}_{O_2}$, the derivative of $\mathcal{D}_{O_2}$ with respect to x is required in equations II – 30 and II – 31. This derivative is calculated by the chain rule in equation II – 38.

$$\left(\frac{\partial \mathcal{D}_{O_2}}{\partial x}\right) = \left(\frac{\partial \mathcal{D}_{O_2}}{\partial P}\right)\left(\frac{\partial P}{\partial x}\right) \qquad (\text{II}-38)$$

The partial of $\mathcal{D}_{O_2}$ with respect to P is given in equation II – 39.

$$\left(\frac{\partial \mathcal{D}_{O_2}}{\partial P}\right) = B \cdot HS \cdot \mathcal{D}_{O_2} \cdot \int_0^t \left(\frac{\partial r_{CA}}{\partial P}\right) d\theta \qquad (\text{II}-39)$$

Substituting equation II – 38 into II – 30 gives equation II – 40.

$$\left(\frac{\partial P}{\partial t}\right) = \left(\frac{\partial \mathcal{D}_{O_2}}{\partial P}\right)\left(\frac{\partial P}{\partial x}\right)^2 + \mathcal{D}_{O_2}\left(\frac{\partial^2 P}{\partial x^2}\right) - \left(\frac{cRT}{h}\right) r_{CA} \qquad \text{(II – 40)}$$

For isothermal conditions, all of the other variables are only functions of t, and x. Furthermore, $\mathcal{D}_{O_2}$ is not only a function of the present state of the system but also the accumulated aging history as given by equation II – 37. In this form, the diffusivity model parameters, D_o and B, can be estimated. However, this estimation requires numerically integrating equations II – 30, II – 31, or II – 32 such that the boundary conditions and the additional specified condition, P_{SI} at the given temperatures and time periods, are satisfied. A trial and error procedure must be performed. Initial guesses are obtained from $\mathcal{D}_{O_2}$ calculated from the simplified equations, II – 31 and II – 32. With the optimized parameters, P, CA, η_o^*, and $\mathcal{D}_{O_2}$ profiles in the asphalt film are correct to the extent that the model and the estimated parameters from experimental measurements are accurate.

Comparing Laboratory and Field Aging

Before a highway-pavement aging model that uses laboratory-determined parameters is proposed, it must be confirmed that laboratory aging simulates field aging. In other words, it must determined that the same reaction mechanisms are occurring in the laboratory and field, with the laboratory aging occuring at an accelerated rate. One way to determine if the same reaction mechanisms are occurring in the field and laboratory is to compare physicochemical properties of oxidized asphalts such as HS and m. These properties are independent of any hypothesized kinetic models or reaction rates provided the mechanisms are the same.

Neat asphalts from selected test sections are laboratory aged. After aging, the chemical and physical properties are measured. Likewise, highway-pavement cores from the test sections are extracted and recovered, and the chemical and physical properties are measured. By comparing the laboratory-aged physicochemical relationships for a given asphalt and the field-aged data, conclusions can be made about the ability of the laboratory experiments to simulate field aging. If the physicochemical properties are the same, it can be concluded that the same oxidation products are being formed and the same mechanism occurs in both laboratory and field aging.

Highway-Pavement Aging Model

Based on laboratory experiments, the aging characteristics of an asphalt binder can be determined. These aging characteristics include the carbonyl formation kinetics and the oxygen diffusion in the asphalt film. Both of these characteristics are expressed as functions of measurable variables, T and P, and together, these form an asphalt-aging model.

In a highway-pavement aging model, the exact nature of the asphalt film and oxygen pressure at the air void/asphalt film interface are unknown. Using laboratory-determined asphalt-aging model parameters and climatic data accounting for variable temperature in the pavement, field-aged asphalt data are compared to calculated changes in properties from integrating equations II – 40 and II – 1. Based on these comparisons, models relating measured core properties of percent air voids, % V, and asphalt content, % Asp, to an effective asphalt film thickness, L_{eff}, for oxygen diffusion and an effective pressure at the air void/asphalt-film interface, P_{eff}, are developed.

Figure II-2 gives a simplified picture of a highway-pavement cross section. The pavement is composed of three components; aggregate, asphalt, and air voids. The asphalt only represents 5% by volume of the highway pavement. The void content ranges from 2 to 15% depending on the construction procedures but ideally is about 5%. The aggregate represents the balance. For air voids higher then 10%, the pavement structure is probably porous enough to continually cycle air and oxygen with the daily thermal cycling. However, with low voids, a continuing renewal of oxygen for P_{eff} may not be possible, and with time, the oxygen concentration in the void decreases.

The measurable core properties of percent asphalt, and % V should provide some measure of L_{eff} and P_{eff} in the voids. P_{eff} in the voids is a function of void content through permeability and aging time on the road. At low void levels, the oxygen pressure in the void decreases and is not replenished.

$$P_{\text{eff}} = f(\%\ V, t) \qquad (\text{II}-41)$$

A hypothesized model for L_{eff} is given in equation II$-$42 in terms of % Asp and % V.

$$L_{\text{eff}} = f(\%\ Asp, \%\ V) \qquad (\text{II}-42)$$

The exact nature of these functions given by equations II $-$ 41 and II $-$ 42 cannot be determined from fundamental principles. Only with experimental data can these correlations be determined.

To accurately evaluate the reaction kinetics and oxygen diffusion rates, the temperature in the pavement as a function of time and position must be known. However, without this information, approximations are proposed. A crude model of the ambient temperature is a sinusoidal function with a period of one year and

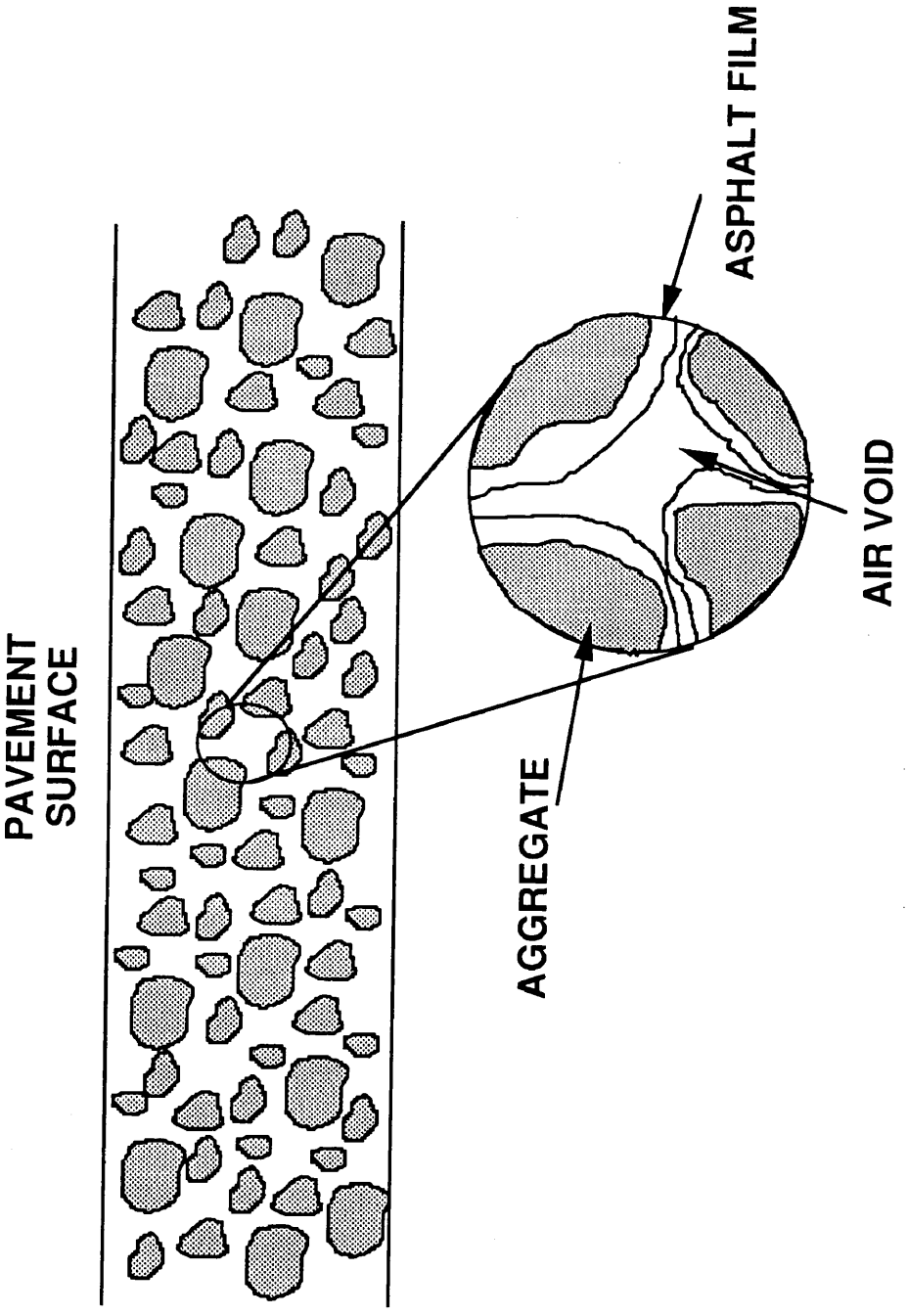

Figure II-2. Highway-pavement cross section.

an amplitude ranging from T_{max} in the middle of summer to T_{min} in the middle of winter. Since most highway construction is during the summer months, equation II – 43 gives an approximate ambient temperature as a function of time.

$$T(t)_{sur} = T_{avg} + (T_{max} - T_{avg})\cos(\omega t) \qquad (II - 43)$$

The average temperature, T_{avg}, is an arithmetic average of the maximum and minimum temperatures. The frequency is ω. From local climate data, T_{max} is approximated as the maximum monthly average air temperature for the year. T_{min} is approximated as the minimum monthly average air temperature of the year.

Now that a model for the ambient temperature is given, the surface temperature of the pavement is determined from equation I – 9 (Solaimanian and Kennedy, 1993).

$$(T_{sur} - T_{air})_{max} = -0.01113\psi^2 + 0.41202\psi + 43.877 \qquad (I - 9)$$

In equation I – 9, T is in °F, and ψ is the latitude. $(T_{sur})_{min}$ is assumed to be equal to T_{min}. Although the temperature in the pavement does vary as a function of depth, Solaimanian and Kennedy (1993) concluded that within the top 20.3 cm (8 inches) of the pavement the difference between the surface temperature and the bulk temperature is within 2.8 to 3.3 K. For this work, the variation of temperature with pavement depth is not included in the calculations.

As a first calculation of using the laboratory-determined kinetics to predict field aging, the film thickness is assumed to be small enough such that diffusion resistance is negligible. From the climatic conditions and location, pavement temperature as a function of time is determined from equations II – 43 and I – 9. Equation II – 1 is integrated from the initial time to the time the core was taken from the road. The calculated changes in physical and chemical properties in this case represent the

worst case aging. Actual aging for that given time period should be less because of diffusion resistance in the film. However, comparisons with field aging give a first approximation of how core properties relate to diffusion resistance and P_{eff} and L_{eff}.

To include diffusion resistance and a finite film thickness, equations II – 40 and II – 1 are integrated simultaneously from the time of placement to coring. The effect of diffusion of oxygen gas through nitrogen in air is also assumed to be negligible. In the absence of experimental data, P_{eff} at the void/asphalt interface in the core is assumed to be the partial pressure of oxygen in air. For high void content, this is probably a valid assumption; however, for low void contents, P_{eff} at the void/asphalt interface should decrease with time due to oxygen diffusion and reaction in the asphalt film. To begin the integration, L_{eff} is assumed. Equation II – 40 is integrated for the known time period of aging. The integral-averaged changes in CA at the end of the time period are calculated by equation II – 44.

$$CA_{\text{avg}} = \frac{1}{L_{\text{eff}}} \int^{L_{\text{eff}}} CA(x)\,dx \qquad \text{(II – 44)}$$

Measured CA from field-aged asphalt after extraction and recovery are compared to calculated CA_{avg}. To the extent that the values differ, L_{eff} is modified and the estimation is repeated. When L_{eff} gives the same changes in CA_{avg} as that measured from the field data within a specified tolerance, L_{eff} is determined.

If the assumption of constant P_{eff} leads to unrealistic values of L_{eff} that satisfies the conditions that CA_{avg} and CA_{mea} are within a specified tolerance, P_{eff} must be a function of time. This condition most likely occurs for field aging locations of low void content. The exact nature of this function is unknown, and a proposed model is given in equation II – 41. Only by comparing field data to the calculated properties can the form of this model be deduced.

After comparing the field-aged core properties including % V and % Asp with the optimized P_{eff} and L_{eff}, the relationships given in equations II – 41 and II – 42 can be determined.

Field aging predictions

With an asphalt-aging model based on laboratory-determined data, a highway-pavement aging model that provides relationships between measurable core properties and L_{eff} and P_{eff}, and historical climatic data, reliable predictions of asphalt pavement aging are possible. This means that the life of new and existing highways could potentially be predicted, provided the neat asphalt is available to perform the laboratory experiments.

CHAPTER III
EXPERIMENTAL METHODS AND MATERIALS

A description of the asphalts studied, the two aging procedures both laboratory and field, and the analytical methods of measuring changes in chemical, rheological, and compositional properties are given. The determination of void content in the field-aged cores and extraction and recovery of the field-aged asphalt are also explained.

Asphalts

Many different asphalts were analyzed for this study, and all of the asphalts are given in Table III-1. The asphalts are grouped according to previous publications as noted in the table. Even though the asphalts may have the same name and be from the same refinery, the year and crude source may be different. Accordingly, asphalts with the same name but different groupings are considered to be different asphalts. For the field-aged samples, the location is given in the table and explained in the section on field aging.

Oxidative Aging

Two different modes of aging were examined. The first was a laboratory simulation in a pressure oxidation vessel, POV. The second was field data from highway test sections.

Table III-1. List of Asphalts Studied[a]

Experiment	Location	Asphalts
Long Term Aging		Ampet, Coastal, Cosden, Exxon, Texaco[b]
Field Aging Comparison		
	Dickens[c]	Cosden 10, Cosden 20, Diamond Shamrock, Dorchester, Exxon, MacMillan
	Pineland[c]	Cosden, Dorchester, Exxon, MacMillan, Texaco
	Bryan[d]	Exxon #8, #15, #16, #18, #19, #1B
Short Term Aging		Ampet, Coastal, Cosden, Exxon, Texaco[b] AAA-1, AAC-1, AAD-1, AAG-1, AAK-2, AAM-1[e] Coastal, Fina, Texaco[f] Dickens, Diamond Shamrock[c]

[a] Asphalts are AC-20 grade unless noted in the table.
[b] From Lau *et al.*, (1992)
[c] From Adams and Holmgreen (1986)
[d] From Davison *et al.*, (1989)
[e] From SHRP (1990)
[f] From Jemison *et al.*, (1992b)

Pressure oxidation vessel

For laboratory aging studies, the POV described by Lau *et al.*, (1992) was modified and improved. Four additional vessels were constructed so that aging studies at several temperatures and pressures could be performed in a reasonable amount of time. Figure III-1 shows one of the POVs and the corresponding features on the control panel. The asphalt samples are weighed into aluminum trays, distributed evenly to a 1 mm thickness, and placed in the sample rack as shown in Figure III-2.

The modifications to the vessels and control panel are described. Two heating tapes in series now supply the energy to the vessels. The additional heating tape was added to the bottom of the vessel to reduce a temperature gradient. A temperature probe, inserted in the bottom of the vessel, monitors the temperature. An on/off controller along with a variable transformer to supply the electrical energy controls the POV temperature. For best control, the variable transformer is set such that the controller is on 90% of the time for the desired temperature setting. As shown in Figure III-3, the POVs are insulated with a combination of fiberglass and block insulation further reducing the temperature gradient and covering the exposed heating tapes from possible operator contact. The insulation covers both bottom and top of the vessels. Furthermore, to obtain POV-aged asphalt samples, the top insulation is designed to be easily removed during operation. The diameter of the stainless steel rupture disk on the cover flange is 38.1 mm (1.5 inches), and the disk is rated at 30 atm (450 psi) at 366.7 K. Since the vessels are evacuated during the experimental procedures, the rupture disk is also vacuum supported. Ashcroft compound test gauges, with an operating range from 0.03 (29 inches Hg vacuum) to 27.2 (400 psi) atm and specially cleaned for oxygen service, monitor the pressure in the vessel. These compound gauges extend the operating range of the POVs to pressures below

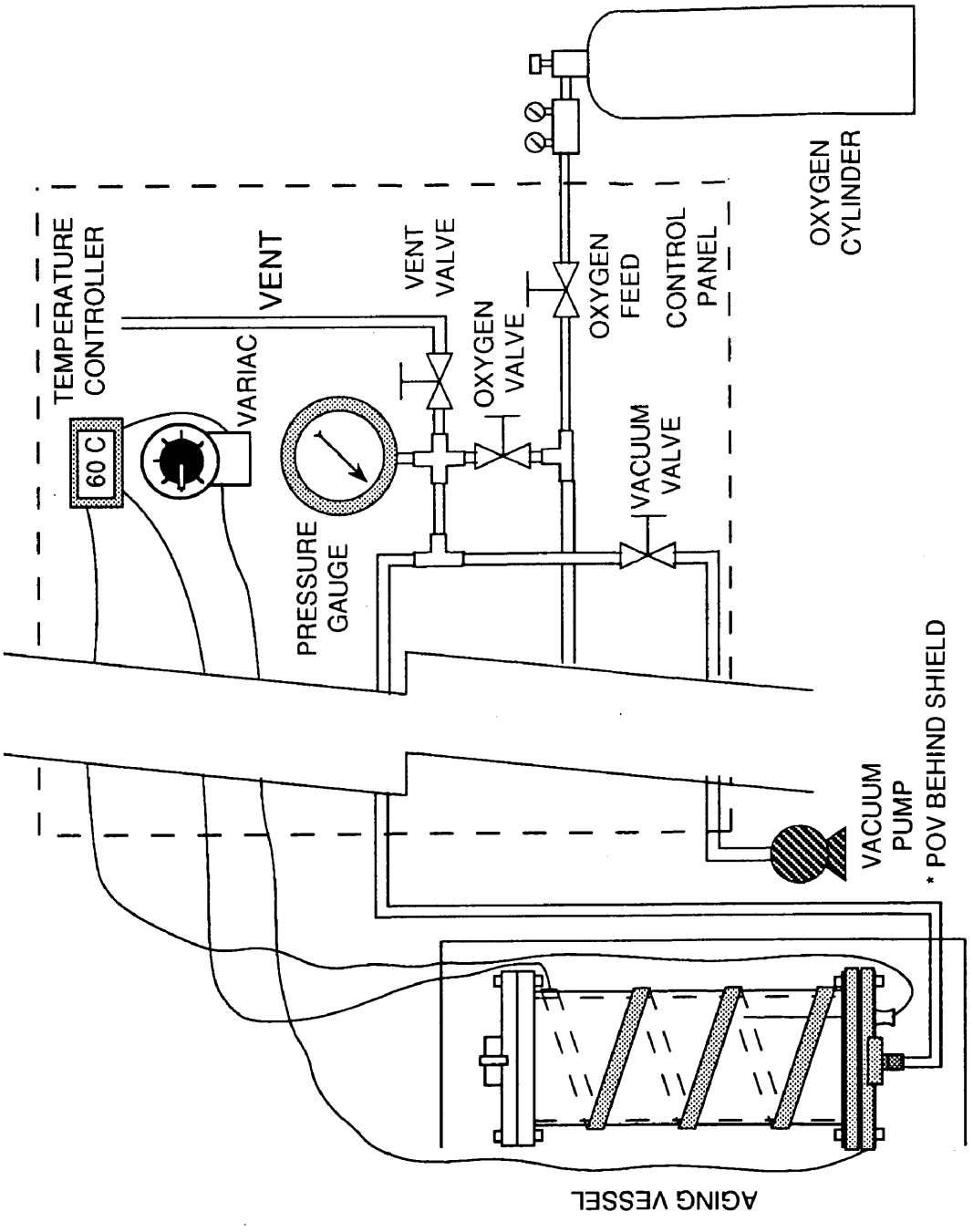

Figure III-1. Pressure Oxygen Vessel, POV, and control panel.

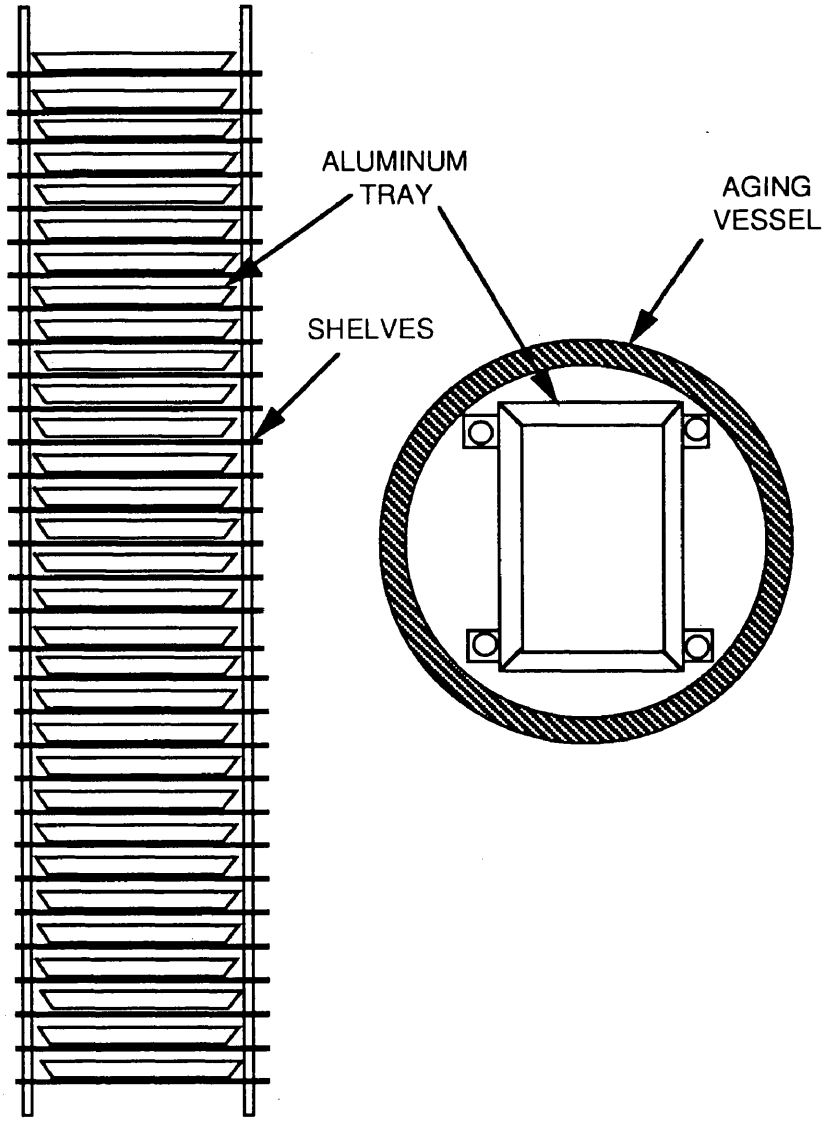

Figure III-2. Sample holder for POV apparatus.

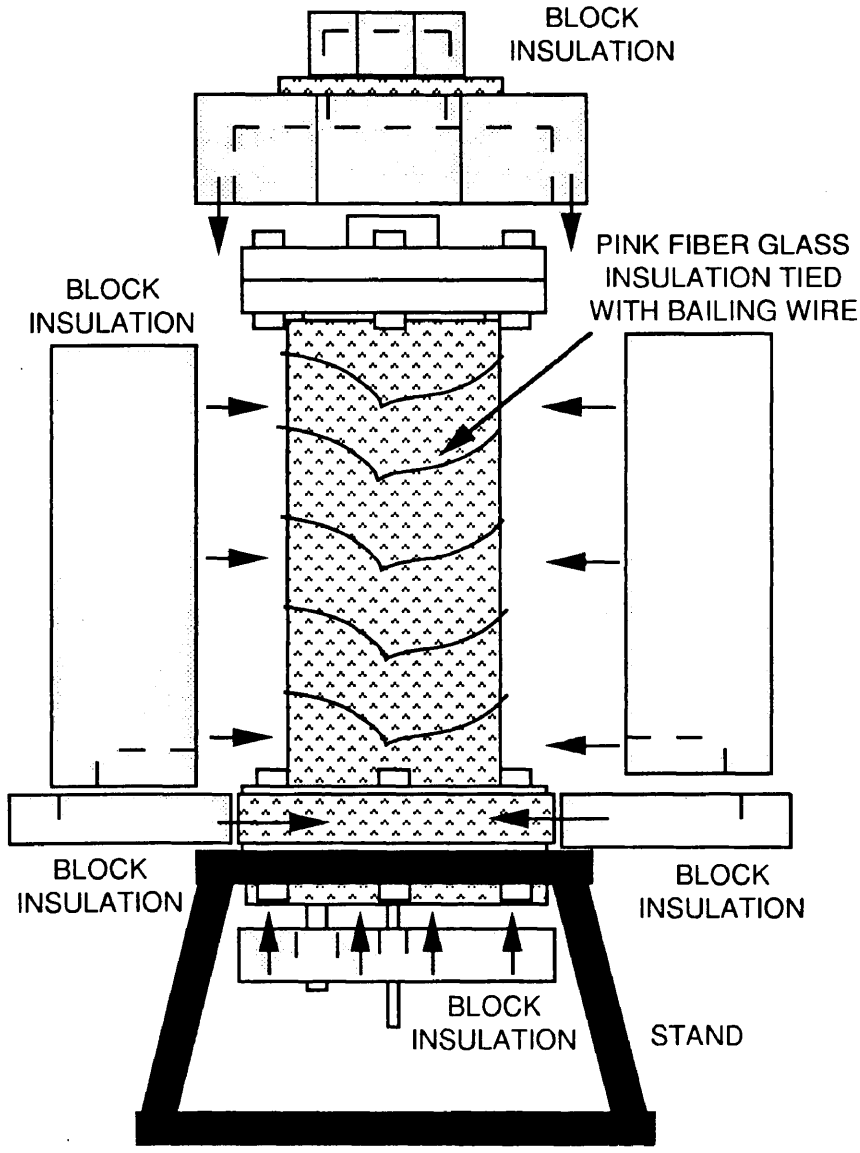

Figure III-3. Schematic of POV insulation.

atmospheric. Finally, a new control panel, shown in Figure III-4, allows independent operation and monitoring of the five vessels by the operator.

Although a detailed description of the POV operation and sample collection is provided by Lau *et al.*, (1992), a short review is given to account for the changes made to the apparatus and operating procedures. Asphalt samples of 2.4 grams are prepared in aluminum trays. The dimensions of the tray are 7.0 cm by 3.5 cm. When the asphalt is evenly distributed by slightly heating, the effective film thickness is 1 mm. After preparing the asphalt samples, loading the sample rack, and allowing the temperature in the POV to reach equilibrium, the operator places the rack inside the POV and bolts the cover flange to the top. The vent valves, oxygen feed valves, and vacuum valves are closed. A vacuum pump evacuates the air in the vessel to a pressure of 0.03 atm absolute. The vessels are slowly pressurized to the desired level by manipulating the oxygen cylinder regulator and oxygen feed valves. Once the desired oxygen pressure is reached, the cylinder, regulators, and feed valves are closed. The vessel is isolated for the experimental time period.

During the experiment, samples are periodically removed. To obtain samples, the pressure in the vessel is decreased by slowly venting off the oxygen to the atmosphere until the pressure gauge reads zero. The operator removes the top insulation, unbolts the cover flange, and collects the samples. Samples to be aged further are loaded back into the vessel, and the process is repeated. The aged samples are saved for chemical and physical analysis.

To obtain the necessary data for kinetic and diffusion studies, POV experiments ranged in oxygen pressure from 0.2 to 20 atm and temperatures from 322.2 to 366.7 K. Time periods for the aging experiments ranged from 1 to 80 days depending on the temperature of the experiment. For the most part, lower aging temperatures required

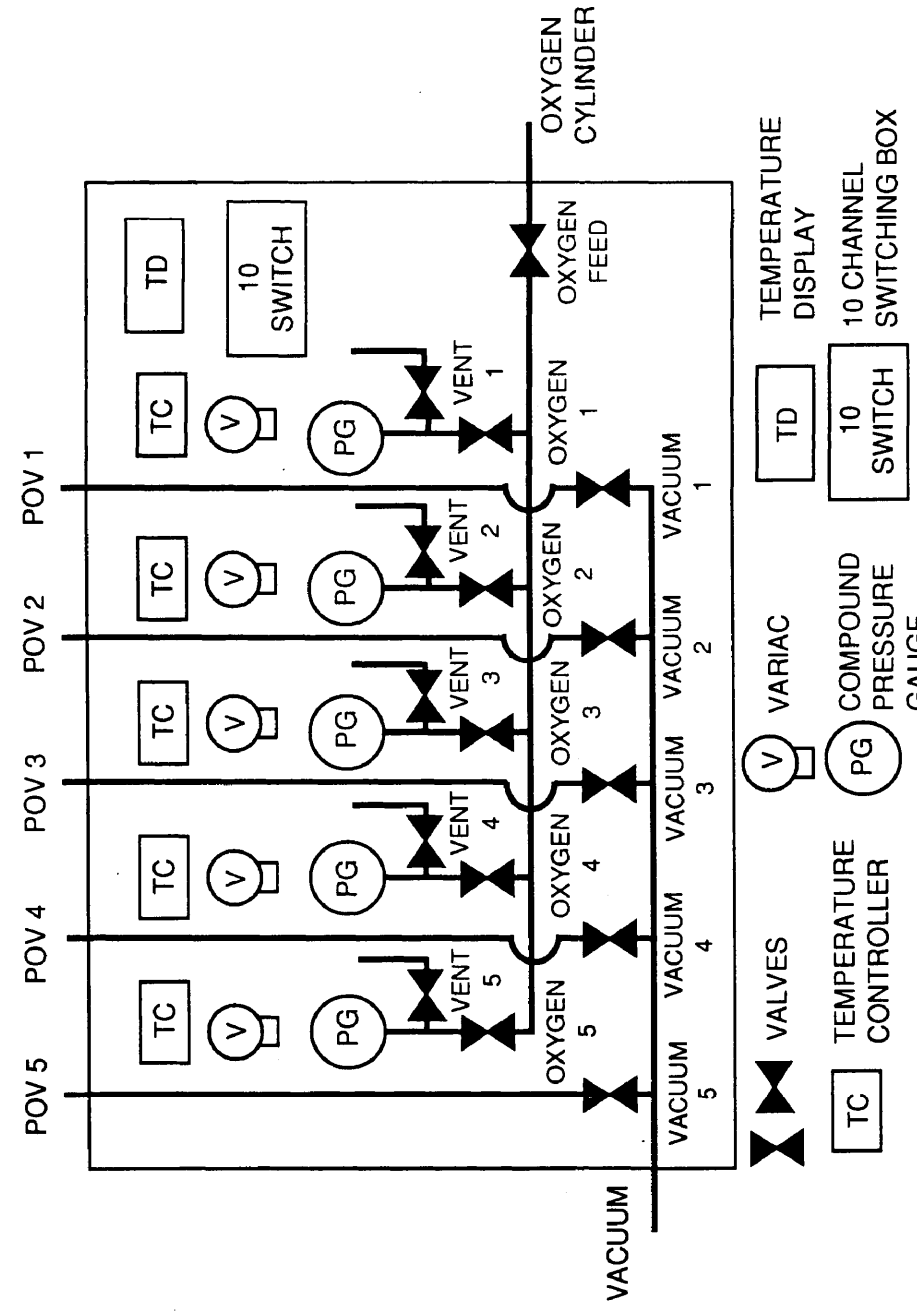

Figure III-4. POV control panel.

longer time periods.

Highway-pavement test sections

To compare POV-aged materials with field data, three test sections in the state of Texas were located and analyzed. The test sections are located in Dickens, Pineland, and Bryan, Texas.

The Dickens and Pineland test sections have been documented in previous reports (Adams and Holmgreen, 1986; Martin *et al.*, 1990). These sections are valuable for comparing asphalts since each test section is comprised of several different asphalts. The Dickens test section is located seven miles east of Dickens on US 82 in the west-bound driving lane. This section was originally constructed in 1982 and contains six different asphalts: Cosden AC-10, Cosden AC-20, Diamond Shamrock AC-20, Dorchester AC-20, Exxon AC-20, and MacMillan AC-20. Figure III-5 shows a schematic of the test section and the start/stop location for each asphalt. The Pineland test section is located 3 miles south of Pineland on US 96 in the north-bound lane. Unlike the Dickens test section, this test section is an overlay. It was placed in 1983 and contains five different asphalts: Cosden AC-20, Dorchester AC-20, Exxon AC-20, MacMillan AC-20, and Texaco AC-20. Figure III-6 shows a schematic of the Pineland test section and the start/stop locations.

The third test section is located six miles west of Bryan on Highway 21 in the west-bound lane. Figure III-7 shows a schematic of this test section. This section was placed in 1987 and is documented in an FHWA report (Davison *et al.*, 1989). Only one asphalt, Exxon AC-20, is used in this test section.

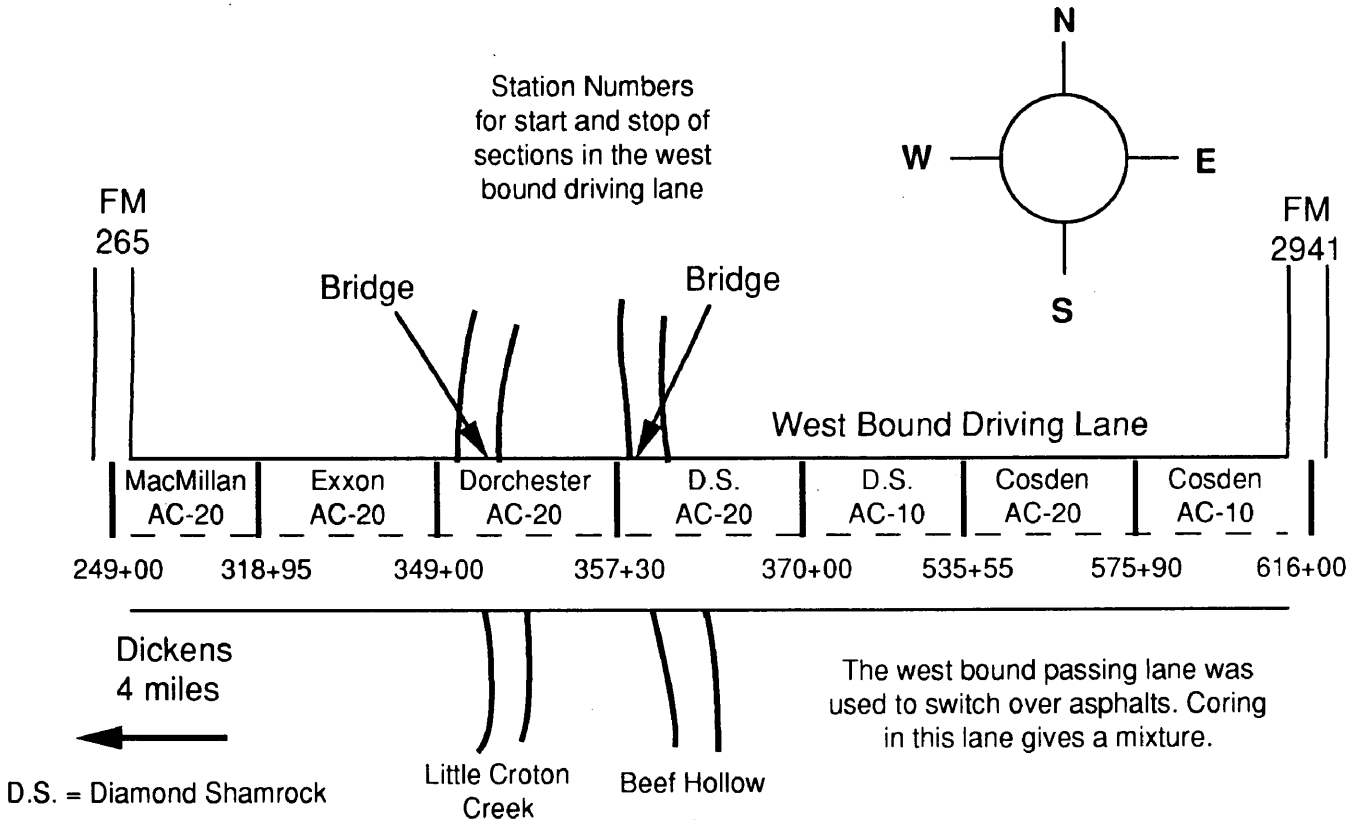

Figure III-5. Schematic of Dickens test section on US 82.

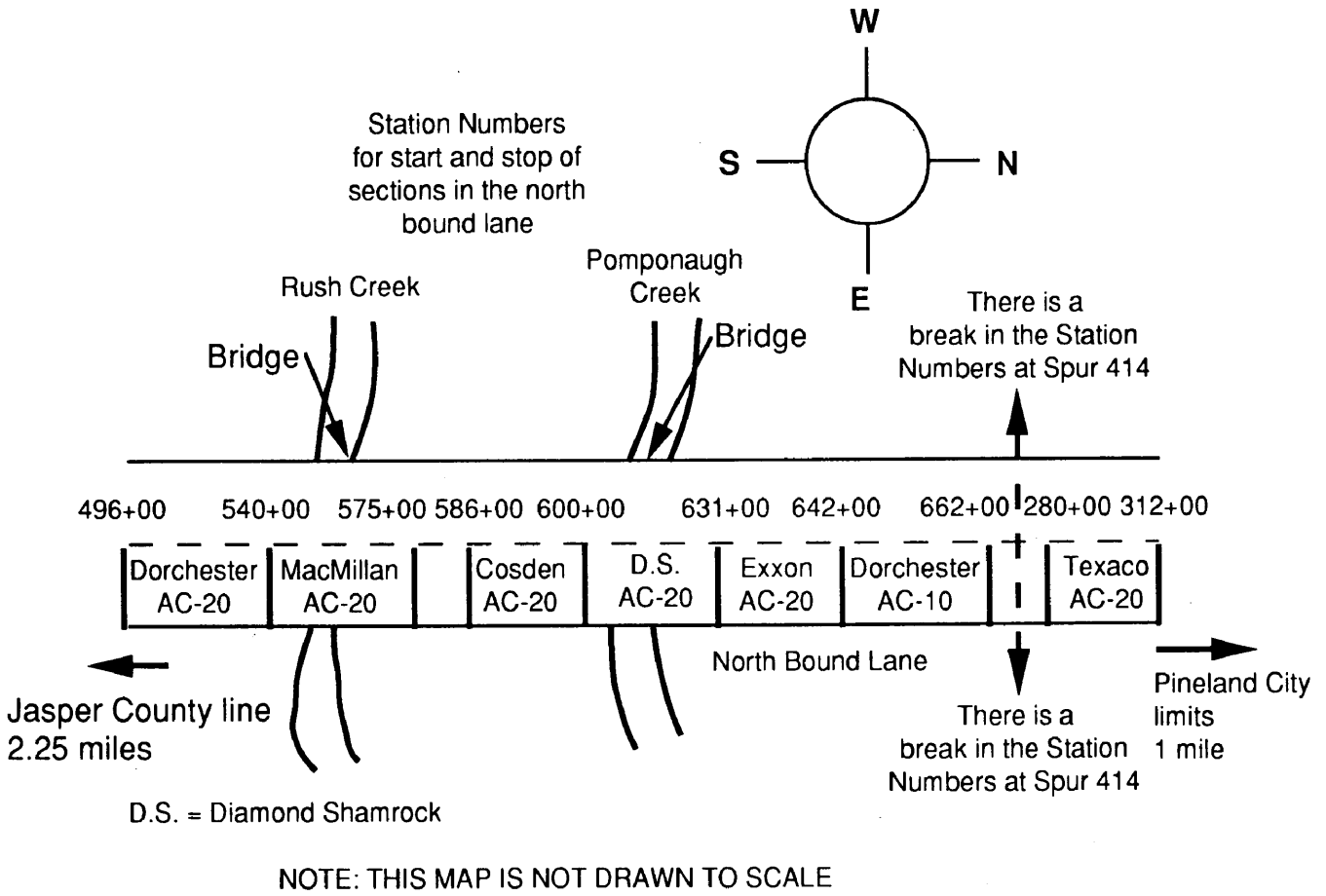

Figure III-6. Schematic of Pineland test section on US 96.

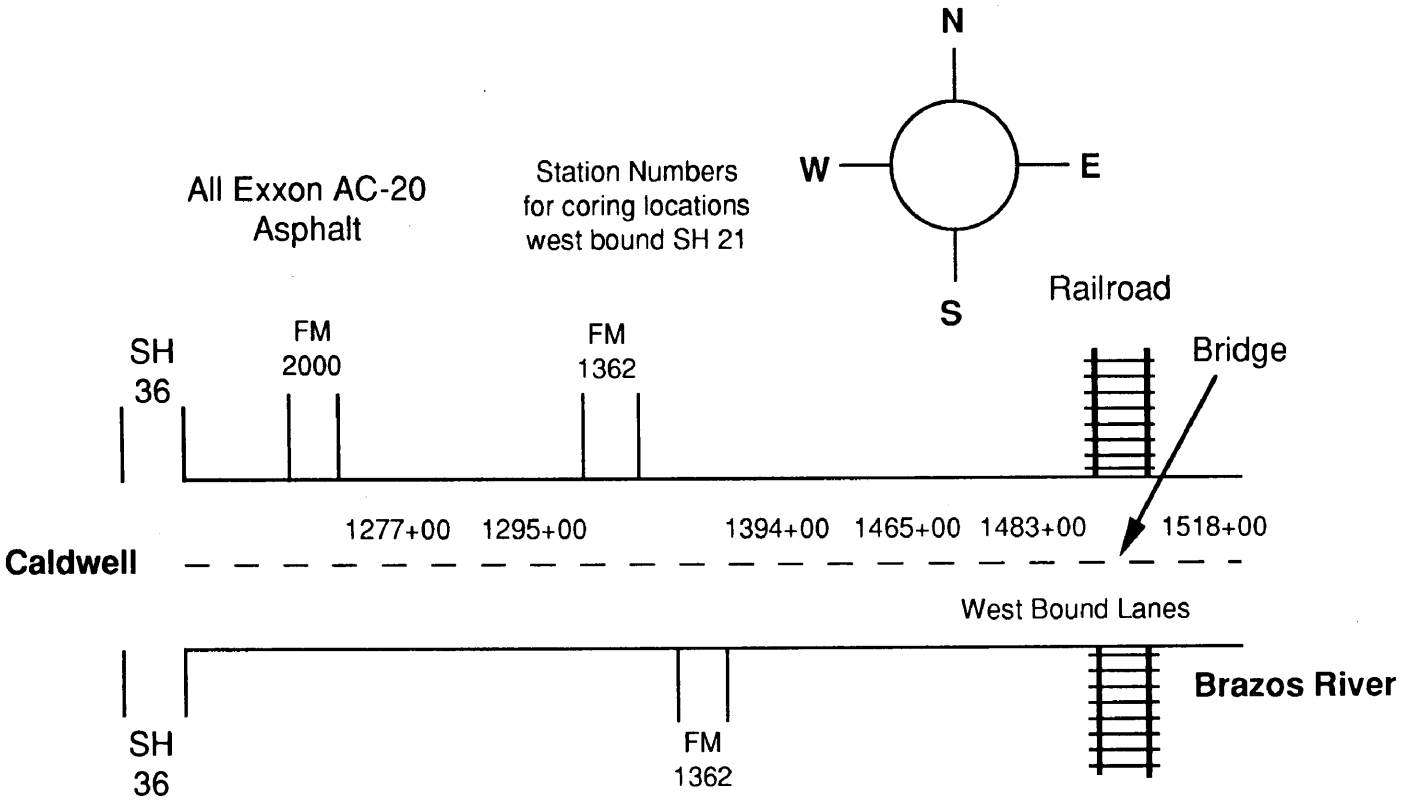

NOTE: THIS MAP IS NOT DRAWN TO SCALE

Figure III-7. Schematic of Bryan test section on highway 21.

Analytical Procedures

Because aging of asphalt is a complex phenomenon, several analytical tools were used. Changes in chemical, rheological, and compositional properties as a result of aging were measured by Fourier Transform Infrared Spectroscopy, FTIR, Dynamic Mechanical Analysis, DMA, and asphaltene precipitation, % A. Further analyses were performed on the highway-pavement samples to determine core properties. In particular, the void content, % V, was measured, and the asphalt was extracted and recovered. Gel permeation chromatography, GPC, was also used to determine the molecular weight distribution of the asphalt and to detect for trace amounts of solvent after extraction and recovery.

Fourier transform infrared spectroscopy

A Mattson Galaxy series 5020 Spectrometer at 4 cm^{-1} resolution and 64 scans measured the infrared absorbance spectra of the samples. Because oxidation at the surface of the asphalt film was being studied, the Attenuated Total Reflectance, ATR, method with a Zinc Selenide prism was used. Even though ATR spectra differ from the traditional transmission spectra at low wave numbers as a result of changes in the refractive index (Jemison *et al.*, 1992a), the changes in ATR spectra due to oxidative aging can be quantified.

The process of analyzing an asphalt sample by FTIR is described. To begin, the presence of water vapor and carbon dioxide in the sample compartment poses significant problems in analyzing a spectrum of asphalt. In particular, water vapor absorbs energy in the same infrared region as carbonyl compounds. To minimize the effects of carbon dioxide and water vapor, the sample compartment is purged with nitrogen. The ATR prism is placed in the holder and analyzed. This spectrum is

the background. To subtract the carbon dioxide and water vapor effects, the sample compartment is again analyzed. This spectrum is the purge reference. Next, the asphalt sample is applied to the prism face either with a Teflon spatula for bulk analysis or by placing a surface on the prism for surface analysis. The asphalt spectrum is collected. A ratio of the asphalt spectrum and the background spectrum removes any artifacts of the prism. The carbon dioxide and water vapor noise are subtracted out with the purge reference leaving the asphalt spectrum. When an acceptable spectrum is acquired, the prism is removed from the sample compartment, cleaned of asphalt residue with dichloromethane, and dried with a heater gun to remove trace amounts of solvents. For more consistent results, two or more spectra were collected from each sample and averaged.

Examples of FTIR spectra from neat and POV-aged Ampet AC-20 for 20 days at 344.4 K and 20 atm oxygen are shown in Figure III-8. To quantify the changes in the spectra, the carbonyl content is defined as the integrated absorbance from 1820 to 1650 cm^{-1} with respect to the baseline at the absorbance of 1820 cm^{-1}. This area is called the *Carbonyl Area* or *CA*. The range of wave numbers includes the following carbonyl compounds: esters, ketones, aldehydes, and carboxylic acids. The primary absorbance peak for the oxidized asphalt is located at 1700 cm^{-1} and corresponds to ketone formation.

To confirm that a temperature gradient in the vessel was removed, one asphalt was placed at different positions in the vessel and aged at a known temperature and time period. The FTIR spectra of the aged material were collected and analyzed. Figure III-9 shows *CA* as a function of vessel position for aging at 355.5 K and 20 atm oxygen for 4 days. Based on this data, only the top five and bottom five positions in the sample rack have a lower temperature compared with the rest of the vessel.

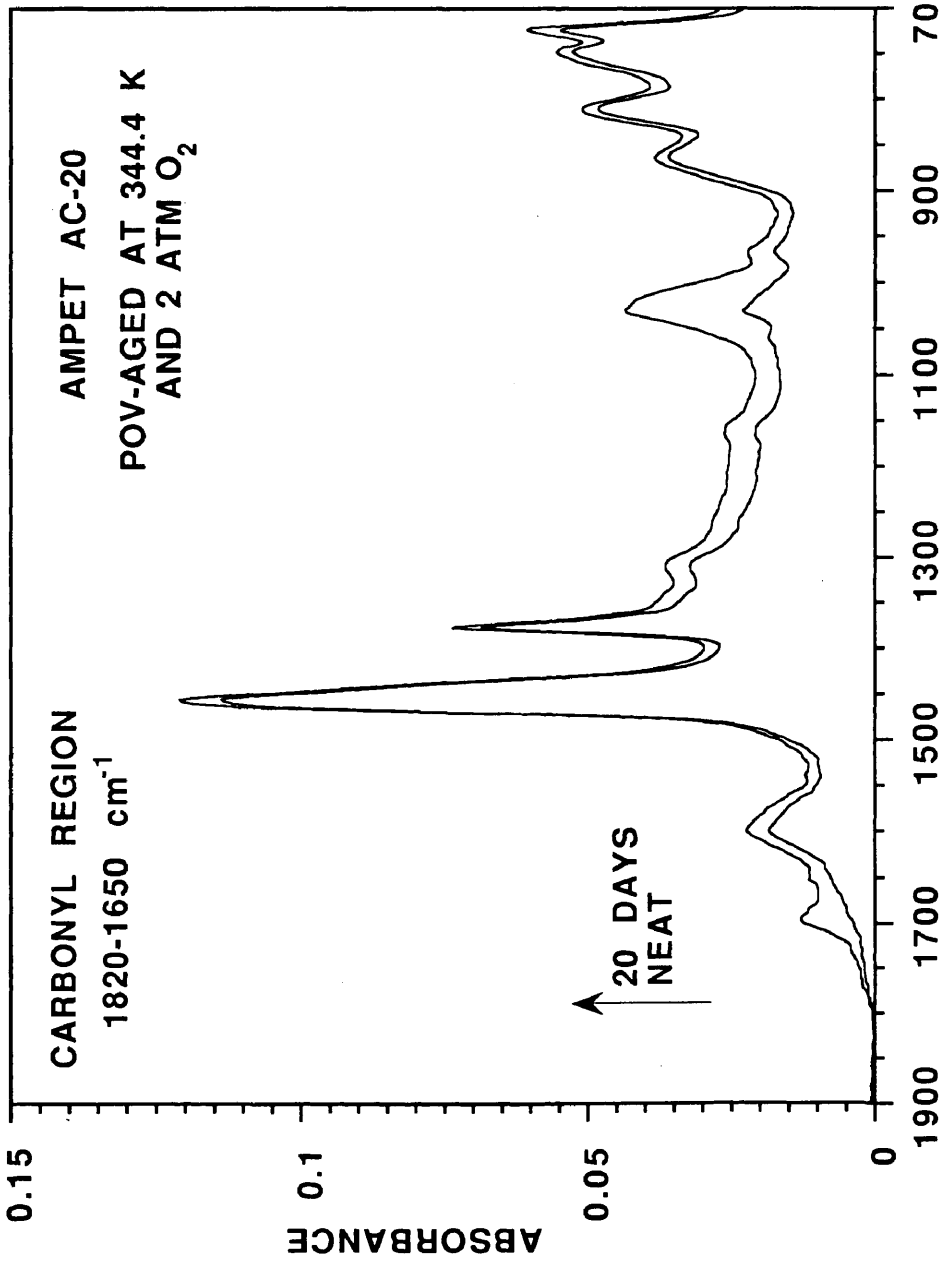

Figure III-8. Infrared spectra of neat and POV-aged Ampet AC-20.

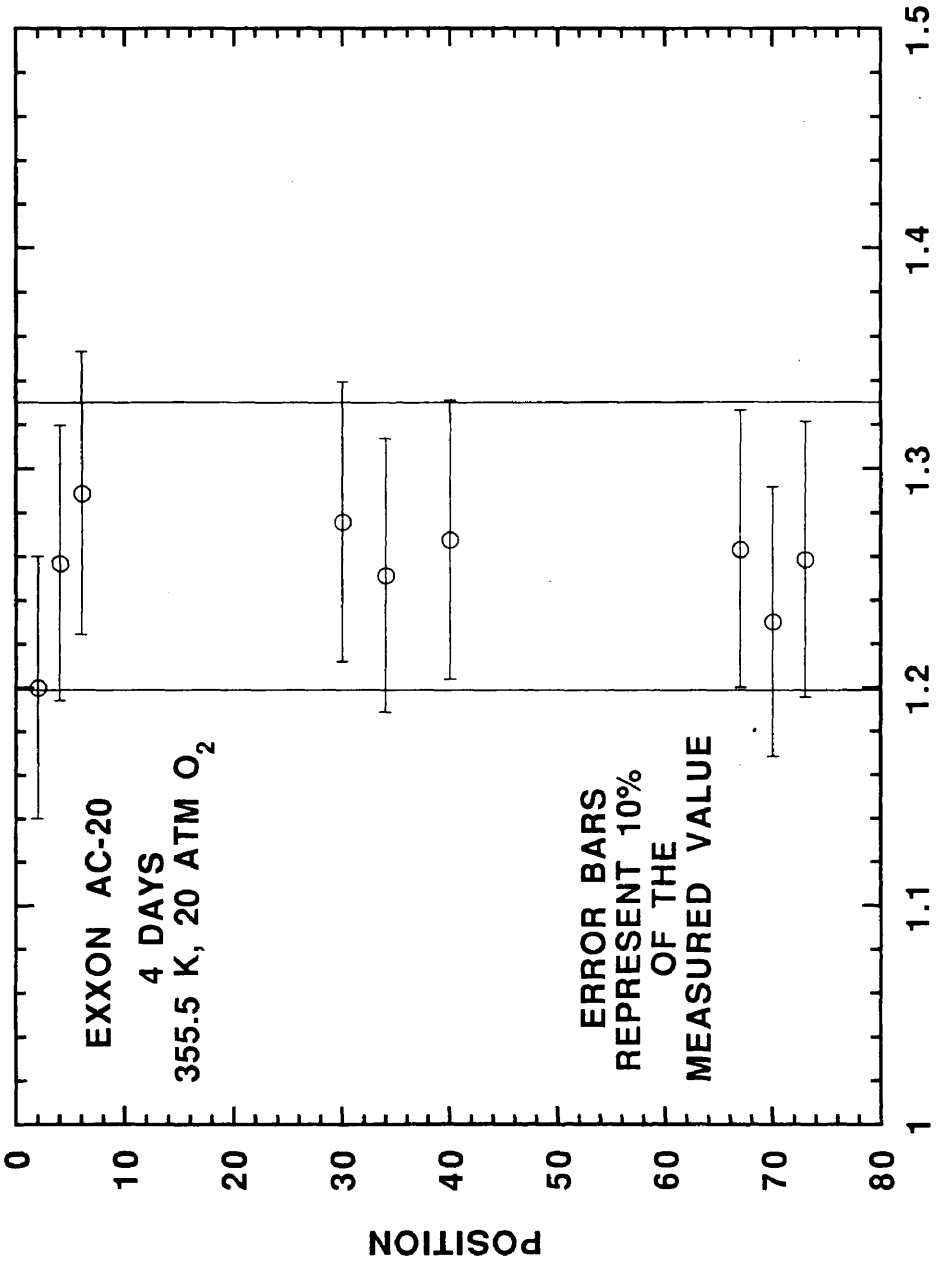

Figure III-9. CAs of Exxon AC-20 at different positions in a POV.

Based on this data, trays of asphalt samples were only placed in the locations starting five positions from the top and stopping five positions from the bottom. Furthermore, the samples were shuffled during the aging experiments to further decrease the effect of a temperature gradient.

At low aging pressures of 2 and 0.2 atm oxygen, an oxygen diffusion problem may be significant. To partially eliminate this diffusion problem, only the exposed surface, *ES*, of the film was analyzed for kinetic data. The depth of penetration of the IR beam for the ATR prism was 1 micron. For analysis, a quarter of the aluminum tray was removed and the *ES* placed on the prism face as shown in Figure III-10. To insure good contact at the sample/prism interface, the sample was compressed. Heating of the sample was avoided if possible.

For oxygen diffusion determinations in the asphalt film, it was required to measure FTIR spectra at both the *ES* and the substrate interface, *SI*. This procedure required two ATR prisms. Spectra of POV-aged asphalts and model compounds containing carbonyl groups were analyzed with both prisms. *CA* for the different compounds and aged asphalt from each prism are compared in Figure III-11. The agreement in the two ATR prisms is within 2% based on *CA* determinations, and it was concluded that the two prisms are equivalent.

The actual procedure for measuring the *ES* and *SI* spectra with the two ATR prisms is explained. First, the *ES* spectrum is measured as shown in Figure III-10 with one of the ATR prisms. The second prism is placed in the sample compartment and the required backgrounds and purge references are collected. The aluminum is removed, and the *SI* surface is ready for analysis. The second prism face is placed on the *SI* surface as shown in Figure III-12 creating a sandwich configuration with the asphalt film. Good surface contact between the second prism and the *SI* surface was

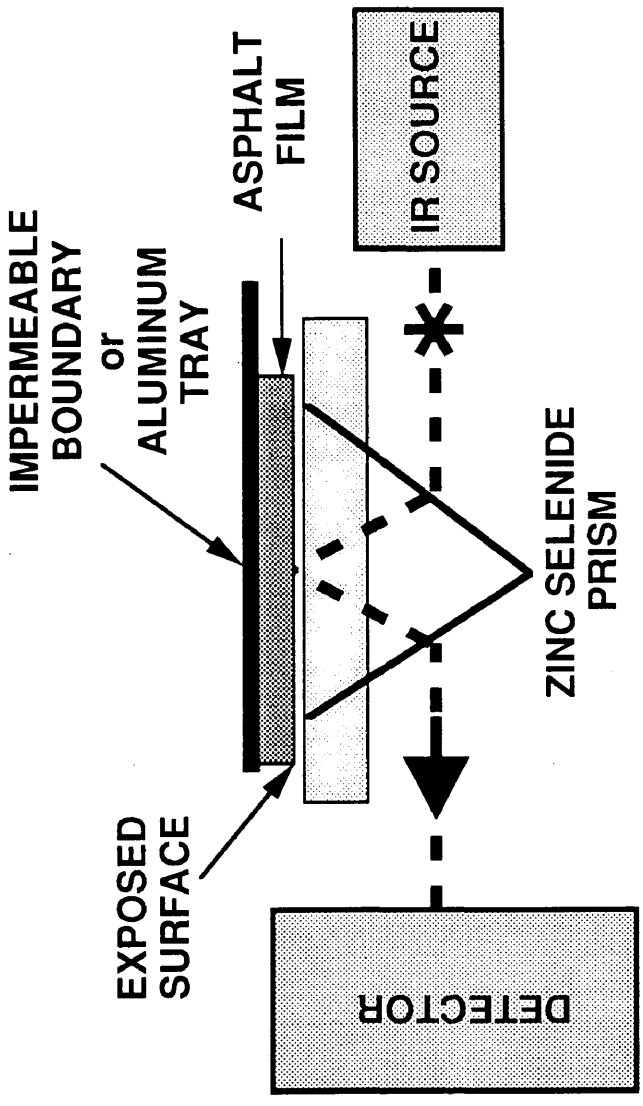

Figure III-10. Technique for measuring IR spectra of the asphalt film exposed surface with one ATR prism.

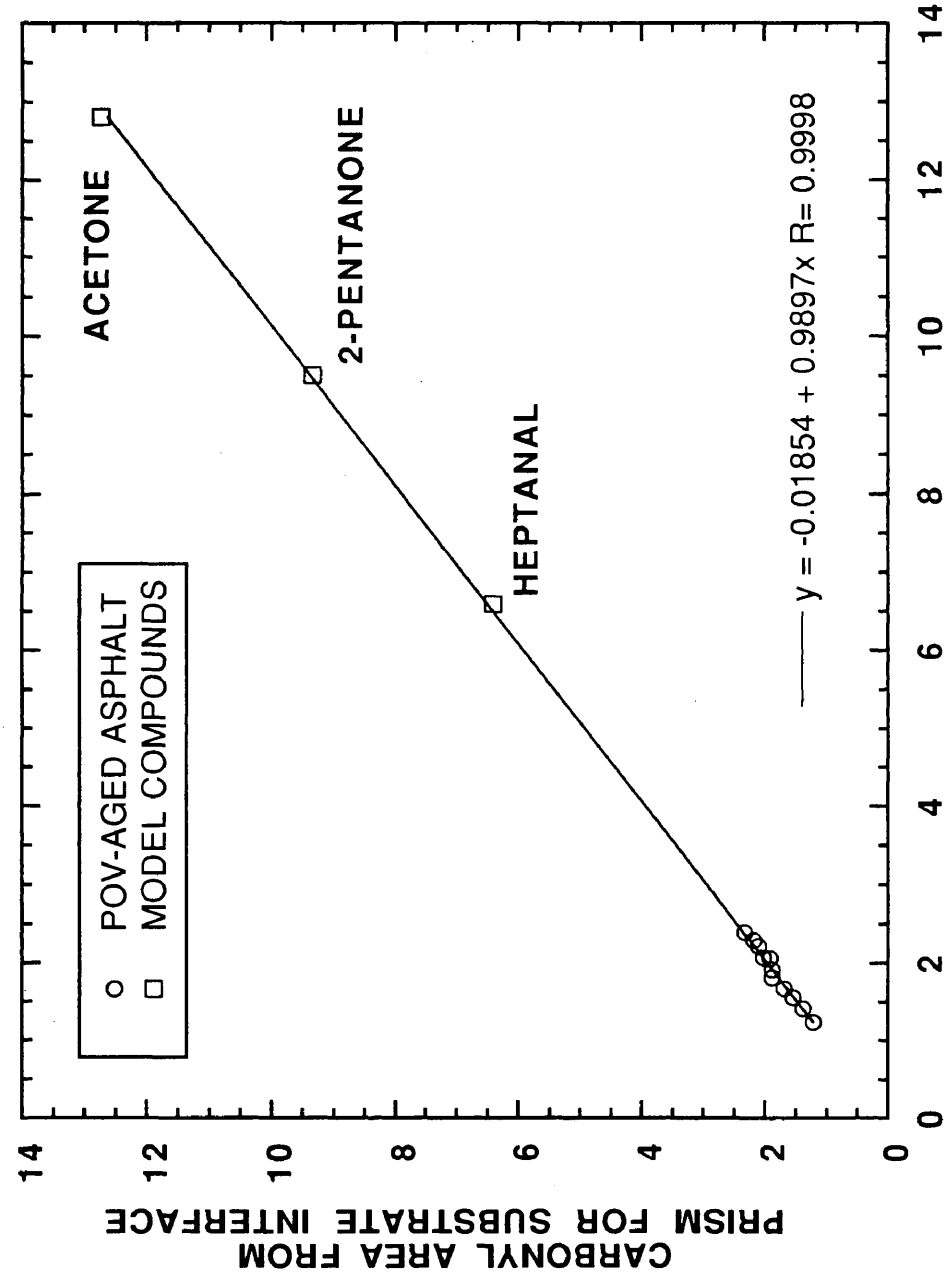

Figure III-11. Comparison between two ATR prisms based on CAs of POV-aged asphalt and model compounds.

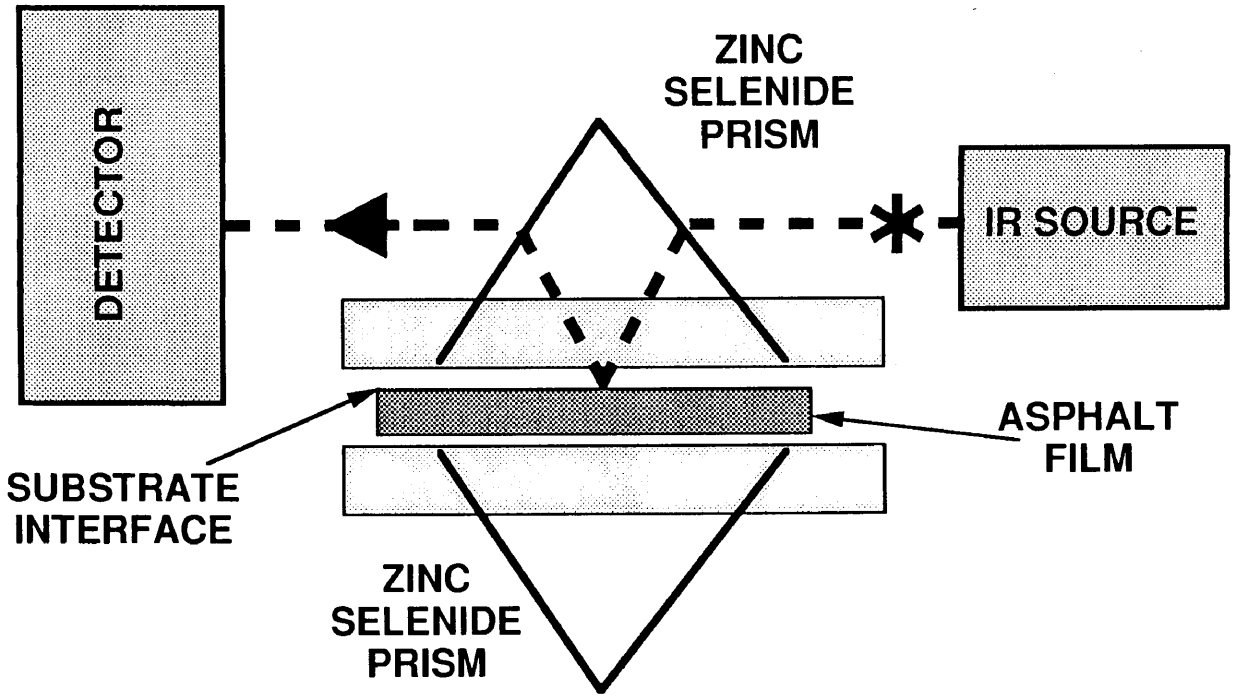

Figure III-12. Technique for measuring IR spectra of the asphalt film substrate interface surface with two ATR prisms.

sometimes difficult to achieve since heating the samples was avoided and excessive compression would damage the prism. When sufficient contact was achieved, the prism configuration was placed in the sample compartment, and the *SI* spectrum was collected. Again several spectra were collected and averaged to obtain more consistent results. Finally, when both sides of the asphalt film were analyzed, both ATR prisms were cleaned with dichloromethane, completely removing the asphalt.

Dynamic mechanical analysis

The rheological properties of neat and aged asphalt were measured on a Carri-Med 500 Controlled Stress Rheometer. The specific properties used to characterize the asphalts were the limiting zero shear complex viscosity, η_o^*, and the reciprocal of the loss compliance, $(1 / J'')$. Both properties were measured at a temperature of 333.3 K and values of $(1 / J'')$ are reported at a frequency of 10 rad/s. The value of η_o^* is independent of frequency or shear rate (Lau *et al.*, 1992). The geometry consisted of a 2.5 cm parallel plate with a 0.5 mm gap. Torque levels were such that the behavior of the asphalt was linear visco-elastic in the frequency range of 100 to 0.1 rad/s. η_o^* was not measurable at 333.3 K and 0.1 rad/s on samples with viscosity higher than 200,000 poise. For these hard samples, rheological measurements were performed at both 333.3 and 363.2 K. The moduli curves were superimposed at 333.3 K using time-temperature superposition (Ferry, 1985) and η_o^* was calculated.

Only field- and POV-aged samples at 20 atm were analyzed with DMA. At low pressure, the oxygen diffusion problem in the film results in non-uniform samples. No rheological properties were measured for low-pressure aging.

Hexane asphaltene determination

Asphaltenes, % A, are the insoluble portion of the asphalt in a paraffinic solvent. The hexane % A of neat and aged asphalts were precipitated as described by Pearson *et al.*, (1986). Solutions of 0.2 grams of asphalt in 20 mL of hexane were made, sonicated for 30 minutes, and precipitated for 12 hours. The solutions were filtered through pre-weighed 0.4 micron membranes. After drying for approximately three days, the membranes were post weighed. The difference in the weight of the membrane relative to the sample weight multiplied by 100 is the % A.

Gel permeation chromatography

A WATERS GPC 600E system was used to determine the molecular weight, MW, distributions of asphalts and detect for trace amounts of solvent after extraction and recovery (Burr *et al.*, 1991). Three columns in series of decreasing pore size of 1000, 100, and 50 Å separated the sample based on molecular size or hydrodynamic volume. The first two columns were 305 mm long and were obtained from WATERS. The final column, from PLGel, was 610 mm long. Solvent detection after extraction and recovery required this final column (Burr *et al.*, 1991). The mobile phase was tetrahydrofuran, THF, at a flow rate of 1 mL/min. The injection volume was 100 μL. A Differential Refractive Index detector, RI, monitored the elution of the sample through system. Isothermal operation of the columns and detectors was at 313.2 K.

The system was calibrated with a known set of polystyrene, PS, standards at a concentration of 0.025 g/mL. Based on the retention time or elution volume of the PS and the known MW, a calibration curve was constructed as shown in Figure III-13. A high order polynomial was used to fit the data points providing a smooth function through the data. Furthermore, the retention times for the asphalt samples

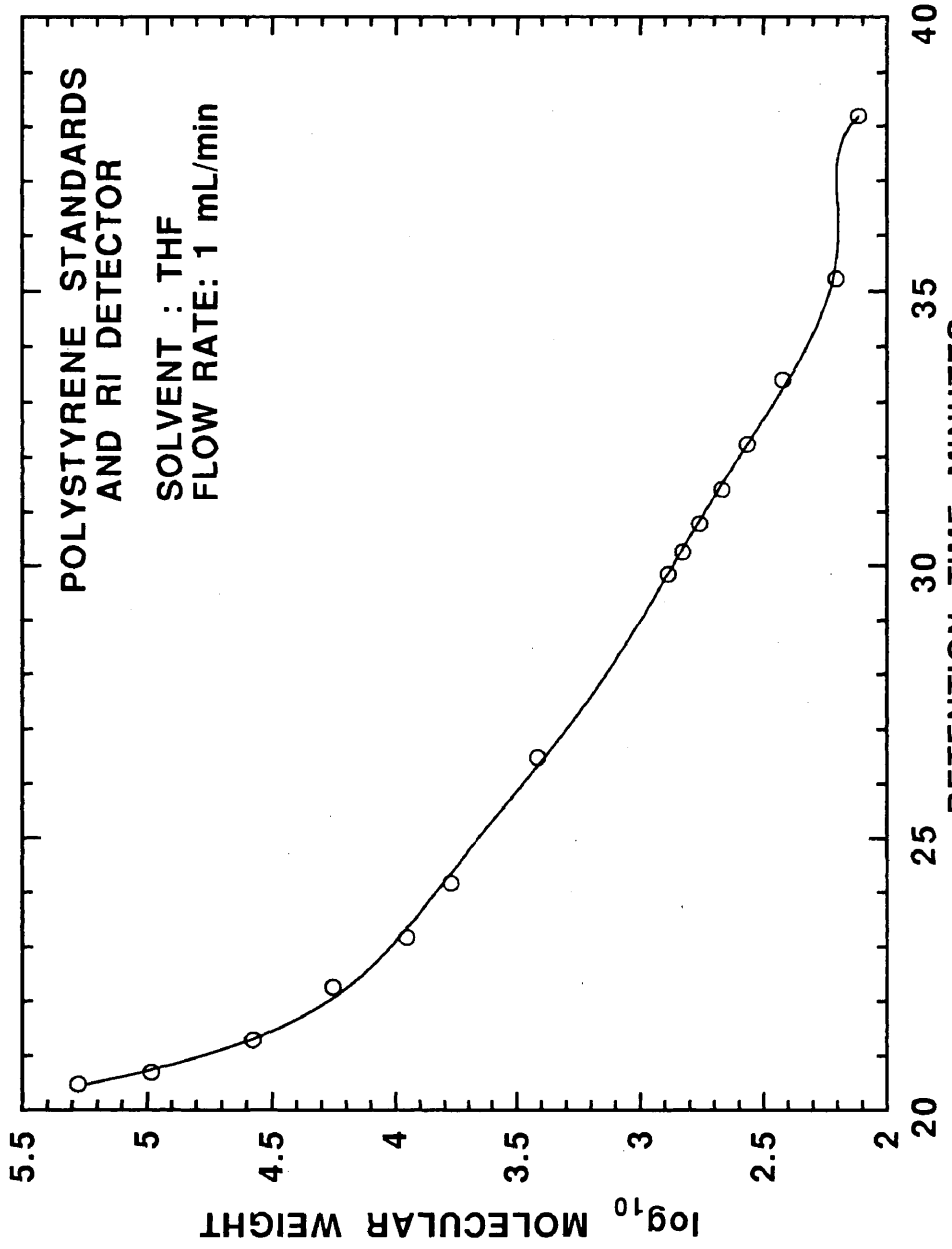

Figure III-13. Calibration curve for GPC analysis based on polystyrene standards.

were in the range of the PS standards. Errors introduced from extrapolation of the polynomial outside of the retention time range were eliminated since this calibration curve was not used for retention times outside the calibration range.

After calibration, samples were prepared at a concentration of 0.020 g/mL. The samples were sonicated for 30 minutes and filtered through 0.4 micron membranes, removing insoluble particles that could damage the GPC columns. Samples are analyzed within 2 days of preparation decreasing the effect of solvent aging (Burr *et al.*, 1991). The weight average molecule weight based on RI MW was calculated from the measured chromatogram and calibration curve.

For convenience, the neat CA, η_0^* at 333.3 K, $(1 \,/\, J'')$ at 333.3 K and 10 rad/s, % A, and MW are presented in Table A-1 in Appendix A. The – notation in the table signifies that the property was not measured.

Void content of field-aged cores

Percent air voids, % V, was the only core property measured. This procedure is designated ASTM D 3203-83, a combination of measuring the bulk specific gravity of the core, D 2726-83, and the theoretical maximum specific gravity, D 2041-78.

Extraction and recovery of field-aged asphalt

After measuring the % V of the cores, the asphalt was extracted. Two different procedures were used. The extracting solvent for both procedures was the same, a mixture of 15% ethanol and 85% TCE by volume. The first procedure is an automated system that continuously feeds and removes solvent (Burr, 1993). The second procedure is a manual method, extracting the asphalt with discrete volumes of solvent. The manual or micro method is similar to ASTM D 2172-81 Method A.

In both procedures, a rotary evaporator recovered the asphalt from the extraction solution. To minimize the solvent effects on the asphalt during recovery, the asphalt concentrations were kept as high as possible, and the oil bath temperature was maintained at 388.9 K. For final recovery, the temperature was increased to 444.4 K. To insure sufficient solvent removal, the final recovery process was extended 30 minutes beyond the detection of the last drop of solvent in the collection flask. To detect for incomplete solvent removal, all of the extracted asphalts were analyzed with GPC (Burr *et al.*, 1991).

For the Dickens and Pineland samples, the percent asphalt was determined by comparing the amount of asphalt recovered to the initial amount of aggregate/asphalt mixture used. No aggregate properties were measured. After extraction and confirmation of sufficient solvent removal, the field-aged asphalts were analyzed with FTIR and DMA.

CHAPTER IV

CARBONYL FORMATION IN ASPHALT

Several authors have reported that the carbonyl content, CA, in an asphalt as a result of oxidative aging changes the physical properties of the asphalt in a predictable way (Lee and Huang, 1972; Martin *et al.*, 1990; Lau *et al.*, 1992; and Petersen *et al.*, 1993). An integrated form of the rate equation calculates CA at any time t as given in equation II – 2.

$$CA(t) = \int_0^t r_{CA}\, d\theta + CA_o \qquad \text{(II – 2)}$$

A preliminary kinetic model with an Arrhenius form was presented (Lau *et al.*, 1992).

$$r_{CA} = A \exp\left(\frac{-E_A}{RT}\right) \qquad \text{(I – 3)}$$

Although equation I – 3 describes the effect of T on r_{CA}, this model neglects any oxygen concentration or pressure effects. An improved model, accounting for both T and P, was discussed in Chapter II and given in equation II – 7.

$$r_{CA} = A \exp\left(\frac{-E_A}{RT}\right) P^{\alpha} \qquad \text{(II – 7)}$$

If one uses the linear model, equation I – 2, to estimate r_{CA} formation from experimental data, an initial non-linearity must be accounted for (Lau *et al.*, 1992). CA_o is not measured from neat material but must be estimated from observable variables.

$$CA_o = f(T, P) \qquad \text{(II – 8)}$$

However, if one uses the model of Dickinson and Nicholas (1949), the initial non-linearity is taken into account. CA_o for this model could be measured from neat

material. In this work, only the linear model, equation I – 2, is used to estimate r_{CA}. Therefore, an attempt is made to model CA_o as a function of T and P.

Experimental data are required to estimate the model parameters describing the r_{CA} and CA_o. With these parameters determined, CA at any time t can be calculated if $T(\theta)$ and $P(\theta)$ are known. Furthermore, physical properties can also be determined from the value of CA provided accurate physicochemical relationships exist. These physical properties are ultimately related to the performance of the asphalt binder. Therefore, the ability to predict CA in asphalt as a result of oxidative aging is a fundamental step toward predicting asphalt performance.

Experimental Design

A series of aging experiments at different temperatures, oxygen pressures, and asphalts, is described. These experiments provide the necessary data to estimate the model parameters in equation II – 7. Because of simultaneous diffusion and reaction of oxygen in the asphalt film, the method of data collection and analysis is critical. If steps are not taken to minimize the effect of oxygen diffusion in the data collection, the conclusions may be erroneous. Oxygen diffusion and reaction varies the oxygen concentration or pressure through the asphalt film. For high oxygen pressures and thin films, the diffusion problem is decreased. However, for low oxygen pressures, the diffusion problem may be significant. In an asphalt film, Figure II-1, the exposed surface, ES, is the only location the oxygen pressure is known. To partially eliminate the diffusion effects at low aging pressures, only the asphalt film ES was analyzed.

To evaluate the effects of both T and P on r_{CA} in asphalt, five AC-20 grade asphalts were aged in the POV. These asphalts correspond to those studied by Lau *et al.*, (1992) as shown in Table II-1. The experimental design included aging at

pressures of 20, 2, and 0.2 atm pure oxygen. Air was not used because complications due to oxygen diffusion through the nitrogen gas film at the asphalt *ES* would have to be considered in the analysis of the data. Aging temperatures were 333.3, 344.4, and 355.5 K, and aging times ranged from 2 to 80 days depending on the aging temperatures. The changes in the chemical properties of the POV-aged asphalt were analyzed by FTIR. For aging at 0.2 and 2 atm the *CA* at the *ES* of the asphalt film was measured. At 20 atm, the bulk *CA* was analyzed since the top surface and bulk showed the same degree of carbonyl formation. Tables B-1 through B-5 show the *CA*s for the aging conditions and asphalts studied. To evaluate the model's ability to extrapolate to highway-pavement conditions (low temperatures) from parameters determined at elevated temperatures, a separate experiment was designed, POV aging the asphalts at 322.2 K and 20 atm for 80 days.

Possible Changes in Oxidation Mechanism

Low oxygen concentrations can change the reaction mechanism and final products during the oxidation of olefins (Bateman, 1949). For free-radical oxidation at low oxygen concentration, the termination step in olefins is different. Because of this observation, the possibility that different mechanisms and oxidation products may result from aging asphalts at low oxygen pressure was studied. If different products were formed at low oxygen pressure, these products should show characteristic IR peaks. A comparison of IR spectra of POV-aged Ampet AC-20 at 344.4 K for 20 days at 0.2, 2, and 20 atm is illustrated in Figure IV-1. The carbonyl absorption is located between 1820 and 1650 cm^{-1}. For the range of 1900 to 700 cm^{-1} the relative peak heights and shapes are the same. Only the peak height is increasing, and this growth is directly related to the increasing oxygen pressure at isothermal

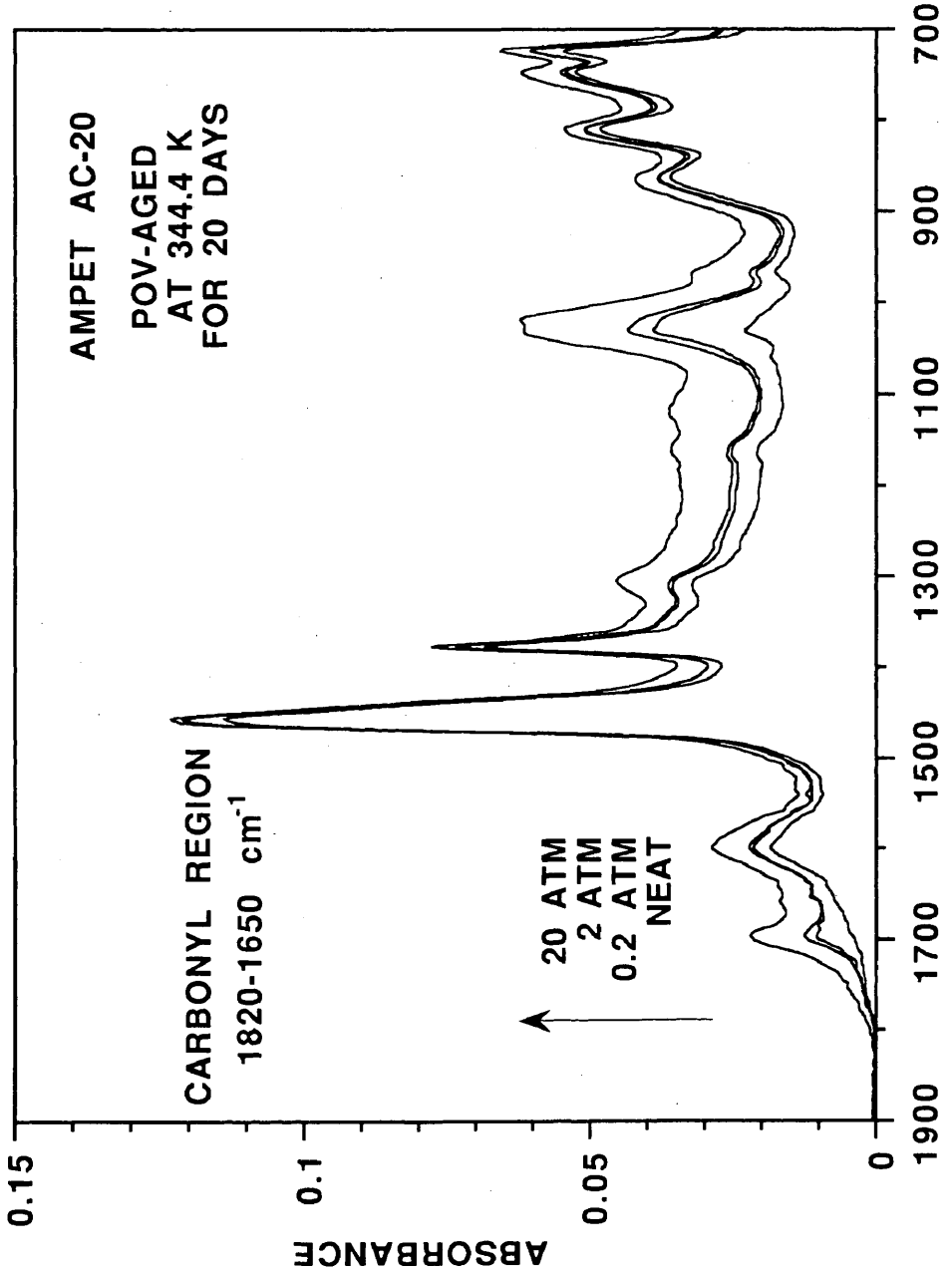

Figure IV-1. IR spectra of neat and POV-aged Ampet AC-20 for 20 days at 344.4 K and 0.2, 2, and 20 atm.

conditions. These data suggest that the oxidation mechanism and resulting products are equivalent for aging pressures ranging from 20 to 0.2 atm.

Order of Reaction

At isothermal aging conditions, a measure of how the change in oxygen pressure affects the change in r_{CA} is defined as the order of reaction. Ideally, the order of reaction should be independent of temperature; however, for the complex reactions of carbonyl formation in asphalts, equation II – 7 may be too simplistic to completely separate the pressure and temperature effects. For asphalts, the order of reaction in terms of oxygen pressure is α. Low values of α suggest that pressure has little effect on r_{CA}; high values of α suggest P has significant effects. α was determined for isothermal aging at 333.3, 344.4, and 355.5 K for the asphalts studied. The process of determining α for one of the asphalts studied is described below.

A model describing the r_{CA} in terms of experimental data must be determined. Figure IV-2 shows CA at 0.2, 2, and 20 atm oxygen for Cosden AC-20 at 333.3 K. Aging times ranged from 0 to 80 days. The neat CA is depicted by the filled circle; the open circle, square, and diamond represent 0.2, 2, and 20 atm oxygen respectively. Initially, there is a non-linearity from the neat CA to the first recorded POV-aged sample at eight days. After that initial jump, CA increases linearly with aging time at isothermal and isobaric conditions. Furthermore, the data show that r_{CA} increases with oxygen pressure. To quantify r_{CA} and CA_o, a linear model, equation I – 2, is used to represent the data, and the estimated parameters are shown on the figure. At low pressures, 0.2 and 2 atm, the linear model provides an excellent representation of the data. However, the linear model does not describe the 20 atm data as well. This discrepancy is probably due to the fact that bulk CA was measured at 20 atm,

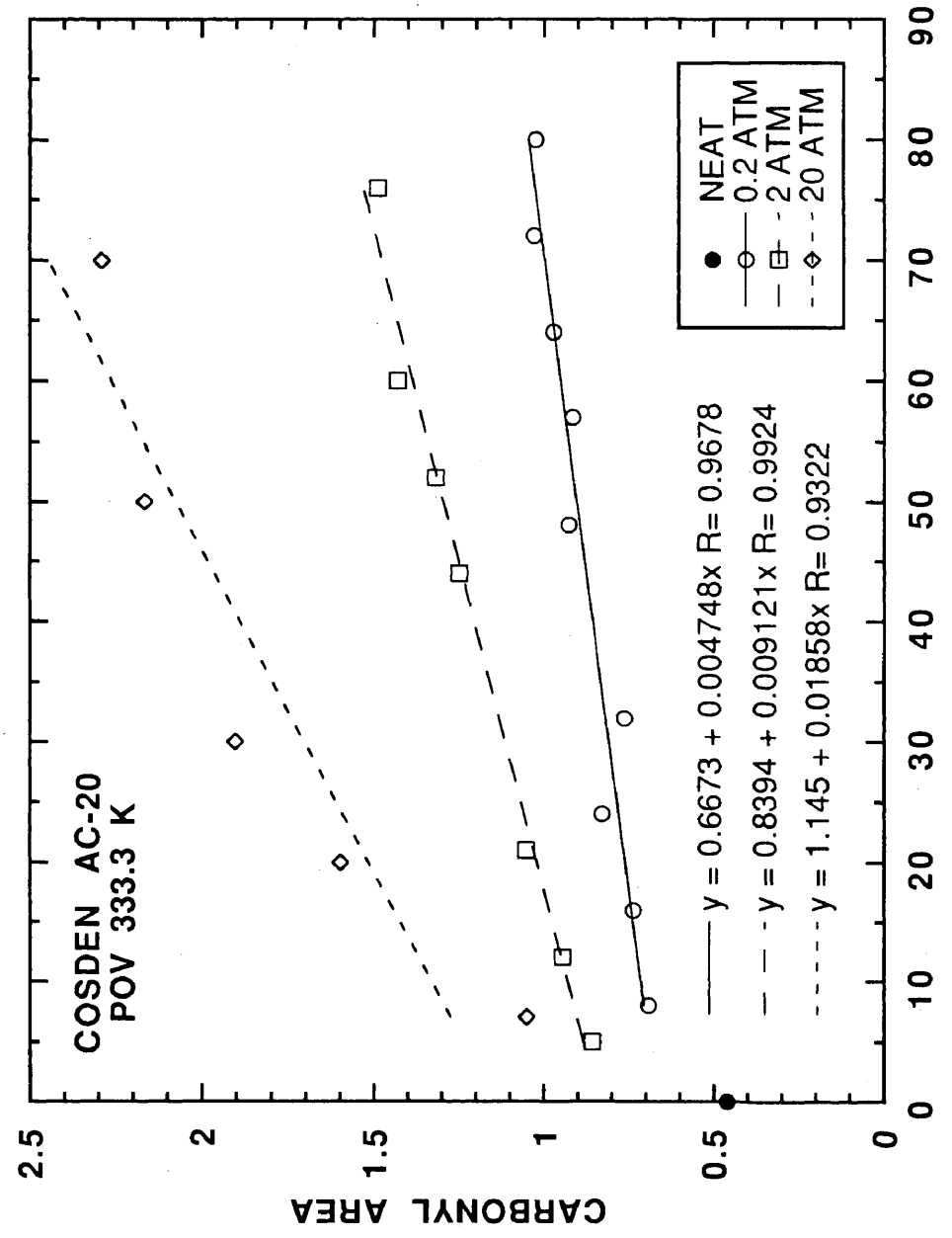

Figure IV-2. CAs of neat and POV-aged Cosden AC-20 at 333.3 K and 0.2, 2, and 20 atm.

compared to the *CA* at the *ES* for the lower pressures. The non-linear behavior for long term aging at 333.3 K and 20 atm oxygen is probably due to diffusion effects. Figures IV-3 and IV-4 show *CA* for Cosden AC-20 at aging temperatures of 344.4 and 355.5 K. Again the initial non-linearity exists followed by a constant r_{CA} at all oxygen pressures studied. The linear model shows good agreement with the data for the long-term, constant-aging region. Data at 20 atm and higher temperatures show better linearity relative to data at 333.3 K. Since bulk *CA* was measured at 20 atm aging, this suggests that the diffusion problem diminishes with increasing temperature. With *CA* measured at the *ES*, all temperatures show excellent agreement with the linear model.

From Figures IV-2, IV-3, and IV-4, the linear model is used to estimate *CA* as a function of time for long-term aging. Furthermore, this linear model implies a constant r_{CA} at isothermal and isobaric conditions. The data show that, at isothermal conditions, increasing the pressure results in higher r_{CA} and intercept. These intercepts provide an initial estimate of CA_o. At isobaric conditions, increasing aging temperature increases r_{CA} but appears to have little effect on estimated CA_o. The same conclusions may be drawn from on Figures B-1 through B-12 in Appendix B for the other asphalts studied.

Table IV-1 shows r_{CA} at 0.2, 2, and 20 atm oxygen and 333.3, 344.4, and 355.5 K for all asphalts studied. r_{CA} increases with increasing pressure at isothermal conditions and increasing temperature at isobaric conditions for a given asphalt. Table IV-2 shows CA_o for all asphalts and aging conditions studied. CA_o increases with pressure at isothermal conditions but appears to be independent of temperature over the range of 333.3 to 355.5 K for a given asphalt.

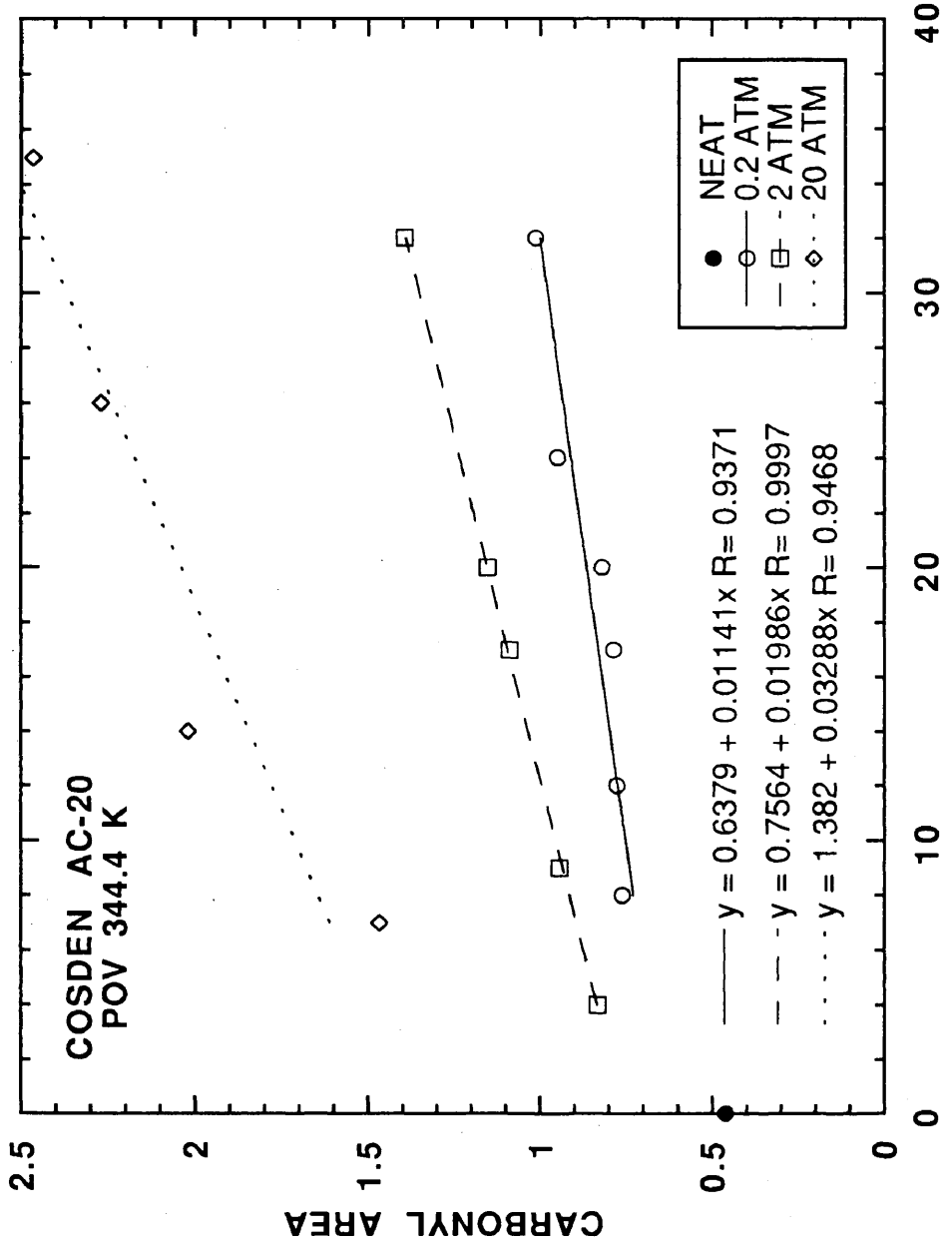

Figure IV-3. *CA*s of neat and POV-aged Cosden AC-20 at 344.4 K and 0.2, 2, and 20 atm.

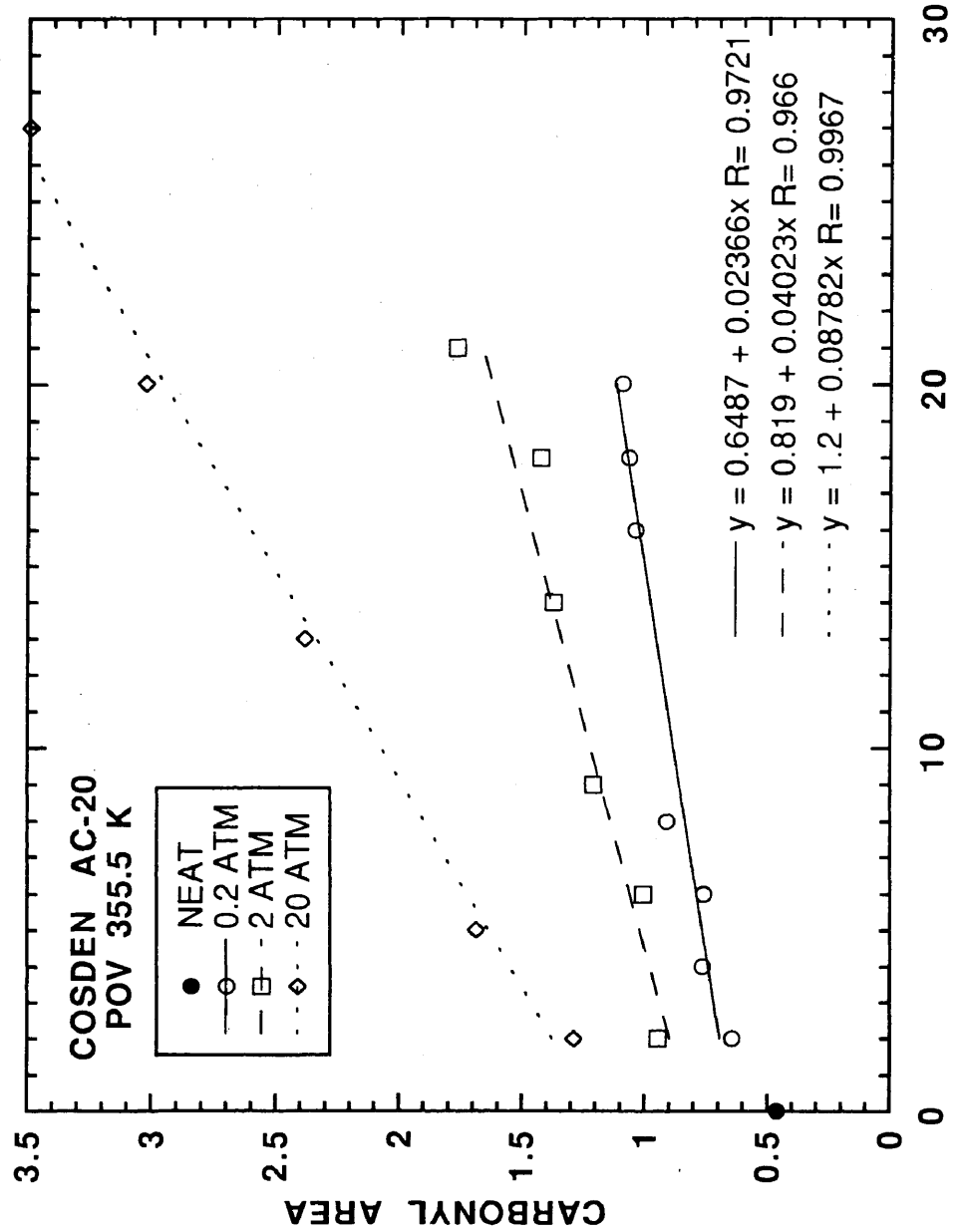

Figure IV-4. CAs of neat and POV-aged Cosden AC-20 at 355.5 K and 0.2, 2, and 20 atm.

Table IV-1. r_{CA} for All Asphalts and POV Aging Conditions Studied

Asphalt	$r_{CA} \times 10^3$ at 0.2 atm			$r_{CA} \times 10^3$ at 2 atm			$r_{CA} \times 10^3$ at 20 atm		
	333.3 K CA/day	344.4 K CA/day	355.5 K CA/day	333.3 K CA/day	344.4 K CA/day	355.5 K CA/day	333.3 K CA/day	344.4 K CA/day	355.5 K CA/day
Ampet AC-20	3.24	6.85	18.66	6.79	14.55	34.50	12.34	25.55	67.02
Coastal AC-20	3.73	8.91	21.32	6.36	15.74	37.92	11.46	31.19	78.21
Cosden AC-20	4.75	11.41	23.66	9.12	19.86	40.23	18.58	32.88	87.82
Exxon AC-20	4.19	7.87	19.73	8.10	13.92	32.47	12.40	29.43	60.18
Texaco AC-20	3.66	7.78	18.62	6.04	14.80	28.63	10.95	26.96	56.64

Table IV-2. CA_o for All Asphalts and POV-Aging Conditions Studied

Asphalt	CA_o at 0.2 atm			CA_o at 2 atm			CA_o at 20 atm		
	333.3 K CA	344.4 K CA	355.5 K CA	333.3 K CA	344.4 K CA	355.5 K CA	333.3 K CA	344.4 K CA	355.5 K CA
Ampet AC-20	0.669	0.654	0.605	0.730	0.672	0.747	0.705	0.890	0.704
Coastal AC-20	0.618	0.641	0.575	0.795	0.761	0.737	0.959	1.009	0.838
Cosden AC-20	0.667	0.638	0.649	0.839	0.756	0.819	1.145	1.382	1.200
Exxon AC-20	0.698	0.721	0.770	0.863	0.781	0.802	1.020	1.066	0.969
Texaco AC-20	0.542	0.580	0.560	0.698	0.665	0.728	0.791	0.814	0.850

For isothermal aging, r_{CA} versus P should produce a straight line when plotted on a log-log scale, equation II – 7. The slope of this line is α. For Cosden AC-20 at 333.3 K, Figure IV-5 shows the log of r_{CA} versus log P. Although there are only three data points, the data suggest a linear model, and the estimated parameters are given. The order of reaction for Cosden AC-20 at 333.3 K is 0.296. A comparison of the effect of P on r_{CA} at 333.3 K for all five asphalts studied is shown in Figure IV-6. The asphalts appear to fall into two groups: Ampet AC-20 and Cosden AC-20 with α of 0.29 in one group and Coastal AC-20, and Exxon AC-20 , and Texaco AC-20 with α of 0.24 in another. However, a comparison at 344.4 K in Figure IV-7 shows that the groups change. All asphalts except for Cosden AC-20 have an α of 0.27; α for Cosden AC-20 is 0.23. Finally, at 355.5 K, Figure IV-8 suggest yet another grouping of Ampet AC-20, Coastal AC-20, and Cosden AC-20 with α of 0.28, and Exxon AC-20 and Texaco AC-20 with α of 0.24.

From Figures IV-5, IV-6, IV-7, and IV-8, the kinetic model in equation II – 7 describes the pressure dependence on the r_{CA} for a given asphalt and temperature. Furthermore, the magnitude of α is small, suggesting that the effect on r_{CA} is minimal. From preliminary comparisons, it appears that α may not only a function of temperature, but also a function of the asphalt composition. A more complete comparison is discussed in order to determine if α is actually independent of temperature and composition, and the variability simply due to the experimental error.

Table IV-3 gives α for all asphalts studied at 333.3, 344.4, and 355.5 K. There appears to be no correlation between T and α for a given asphalt. For example, Ampet AC-20 shows decreasing α with increasing T, Coastal AC-20 shows increasing α with increasing T, and Cosden AC-20, Exxon AC-20, and Texaco AC-20 show no recognizable trend. Although there is significant scatter, the lack of correlation

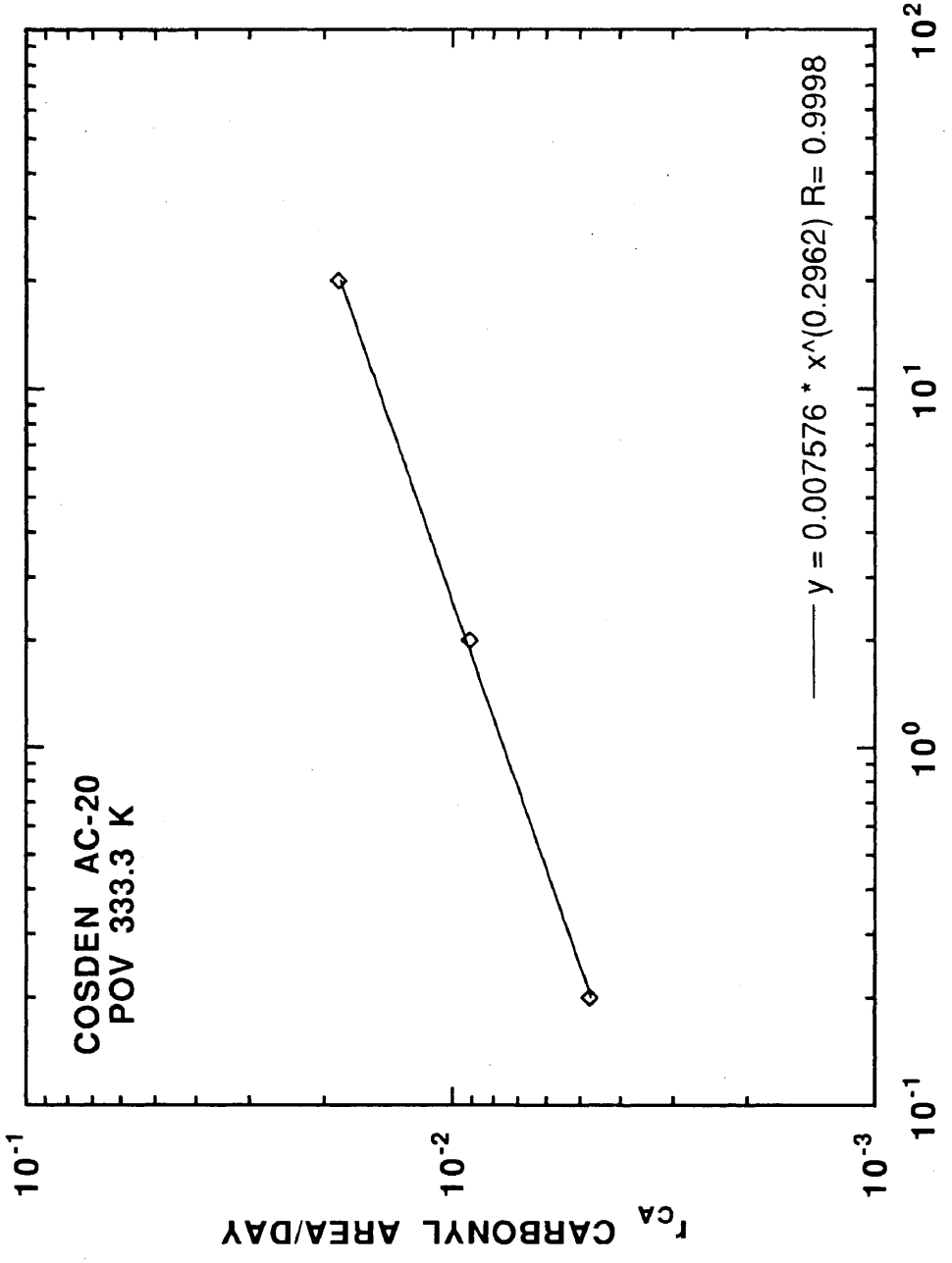

Figure IV-5. r_{CA} versus P at 333.3 K for POV-aged Cosden AC-20.

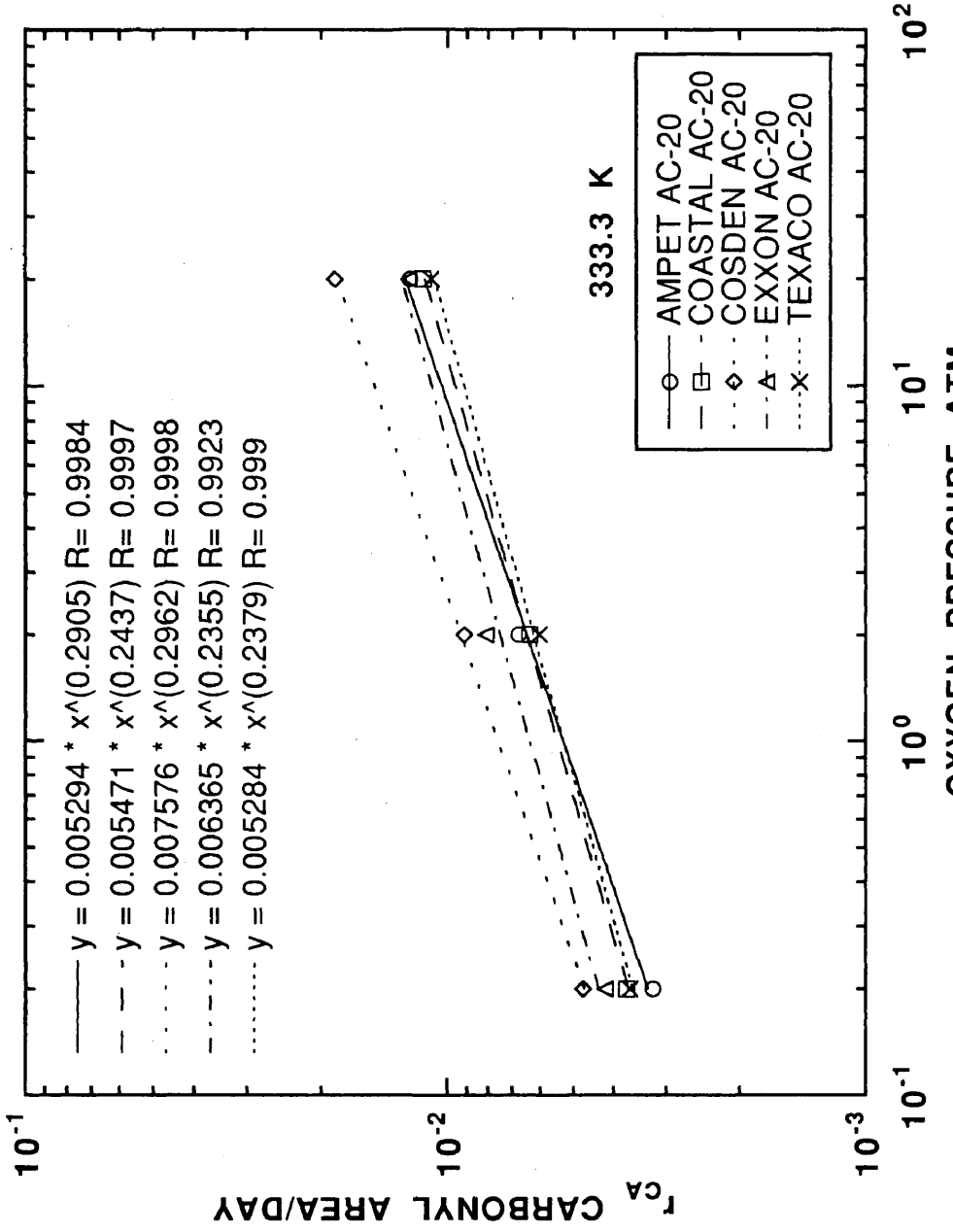

Figure IV-6. r_{CA} versus P at 333.3 K for all POV-aged asphalts studied.

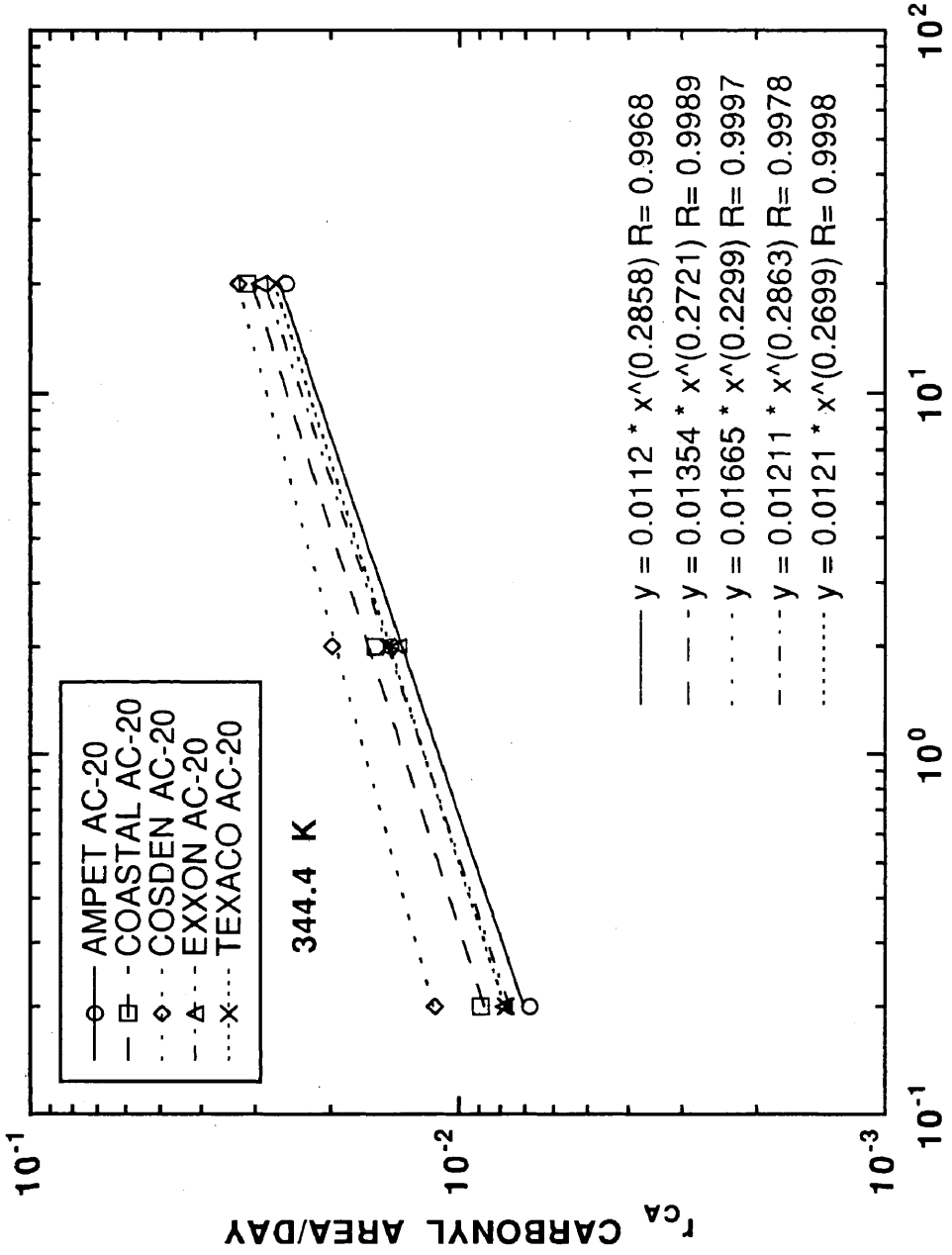

Figure IV-7. r_{CA} versus P at 344.4 K for all POV-aged asphalts studied.

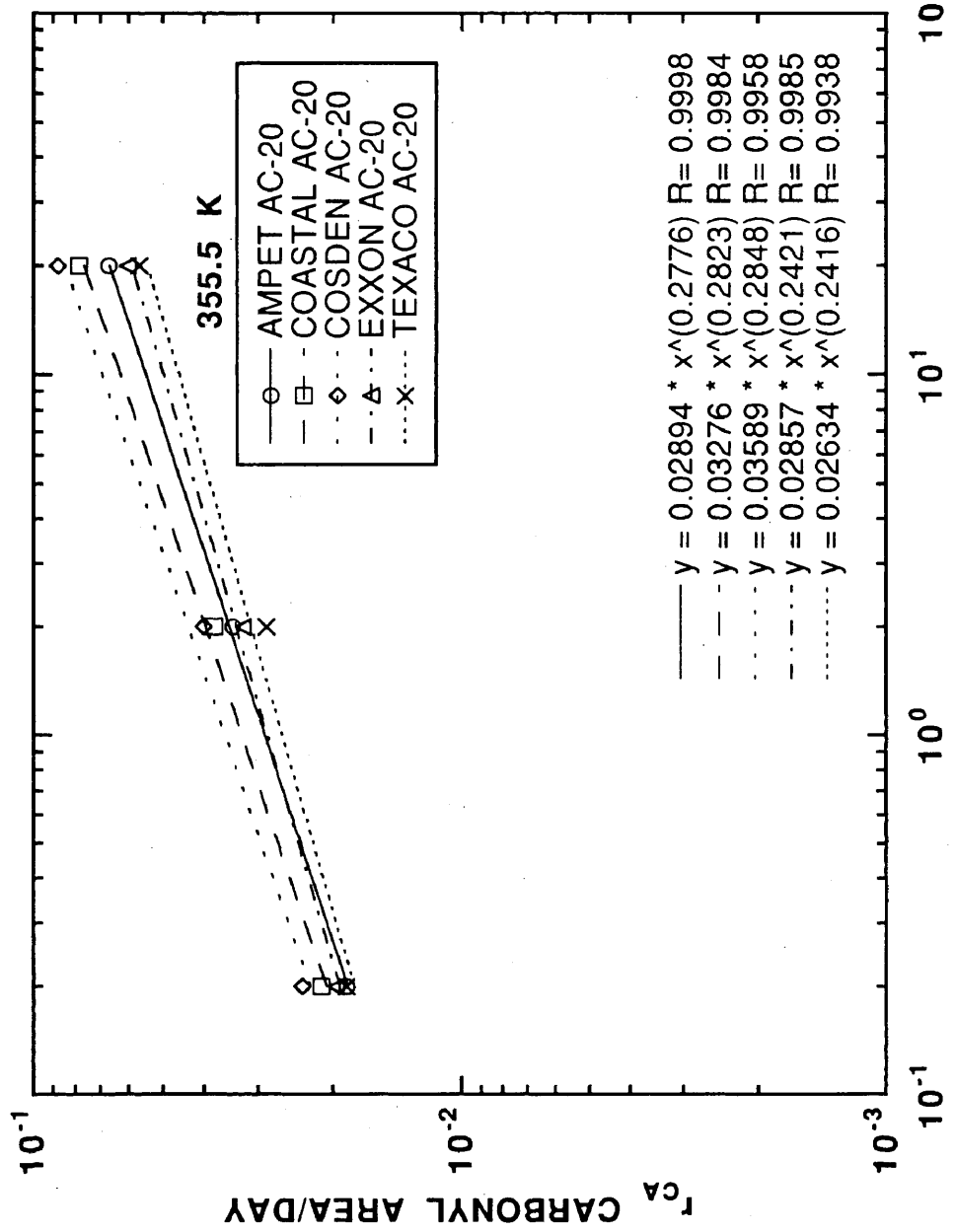

Figure IV-8. r_{CA} versus P at 355.5 K for all POV-aged asphalts studied.

Table IV-3. α for All POV-Aged Asphalts Studied[a]

Asphalt	α		
	333.3 K	344.4 K	355.5 K
Ampet AC-20	0.290	0.286	0.278
Coastal AC-20	0.244	0.272	0.282
Cosden AC-20	0.296	0.230	0.285
Exxon AC-20	0.236	0.286	0.242
Texaco AC-20	0.238	0.270	0.242

[a] Oxygen pressures from 0.2 to 20 atm.

between α and T suggests that α is independent of T. Furthermore, at a given aging temperature, the values of α are somewhat independent of asphalt. Except for Ampet AC-20, which tends to be higher than the other asphalts at all temperatures, no other asphalts show a recognizable trend. The range of α for all asphalts and temperatures is 0.296 to 0.230 representing about 25% difference. Even with significant scatter, all of the data suggests a constant α, independent of aging temperature and crude source. The different groupings as a function of T and shown in Figures IV-6, IV-7, and IV-8 probably result from experimental error and the fact that only three aging pressures were used to estimate α. Finally, α is small and changes of an order of magnitude in pressure only result in doubling r_{CA}. This effect is small when compared to aging temperature (Lau *et al.*, 1992).

Activation Energies and Arrhenius Constants

The effect of T on r_{CA} is expressed in terms of an Arrhenius relationship having two estimated parameters, the Arrhenius constant A and activation energy E_A.

$$r_{CA} = A \exp\left(\frac{-E_A}{RT}\right) P^{\alpha} \qquad (\text{II} - 7)$$

R is 8.314 J/gmol. At 20 atm, this model described asphalt oxidation (Lau *et al.*, 1992). However, at lower oxygen pressures the Arrhenius relationship needs to be confirmed. For the asphalts studied, the parameters A and E_A were determined for isobaric aging at 0.2, 2.0, and 20.0 atm oxygen. The process of determining A and E_A for one of the asphalts studied is described below. Similar to the determination of α, a model describing CA as a function of t is determined to estimate r_{CA}.

Figure IV-9 shows CA at 333.3, 344.4 and 355.5 K for Cosden AC-20 at isobaric conditions of 0.2 atm. The solid circle represents the neat CA, and the hollow circle, square, and diamond represent the 333.3, 344.4, and 355.5 K aging temperatures, respectively. As discussed in Figures IV-2, IV-3, and IV-4, there is an initial non-linearity followed by constant r_{CA} for isothermal and isobaric aging. The linear model and estimated parameters are shown on the figure. The linear model represents the data for all temperatures; however, there is some scatter. The scatter appears to be independent of T at 0.2 atm. Figures IV-10 and IV-11 show CA as a function of t for isobaric aging of Cosden AC-20 at 2 and 20 atm, respectively. Again the linear model represents the data very well. Furthermore, the degree of scatter decreases with increasing pressure. CAs in Figure IV-11 are bulk measurements. At 333.3 K it appears that there is a diffusion problem compared with 344.4 and 355.5 K bulk CA. When CA at the ES are used, Figures IV-9 and IV-10, the scatter increases but the linear relationship between CA and t for long-term aging is undeniable.

From the data in Figures IV-9, IV-10, and IV-11 for isobaric aging, r_{CA} increases with isothermal aging temperature. However, for isobaric aging, all of the regression lines tend to intersect. This suggest that the intercept, CA_o, is independent of aging temperature. From Figures B-13 through B-24 for the other asphalts studied, similar conclusions about isobaric POV aging of asphalts are reached.

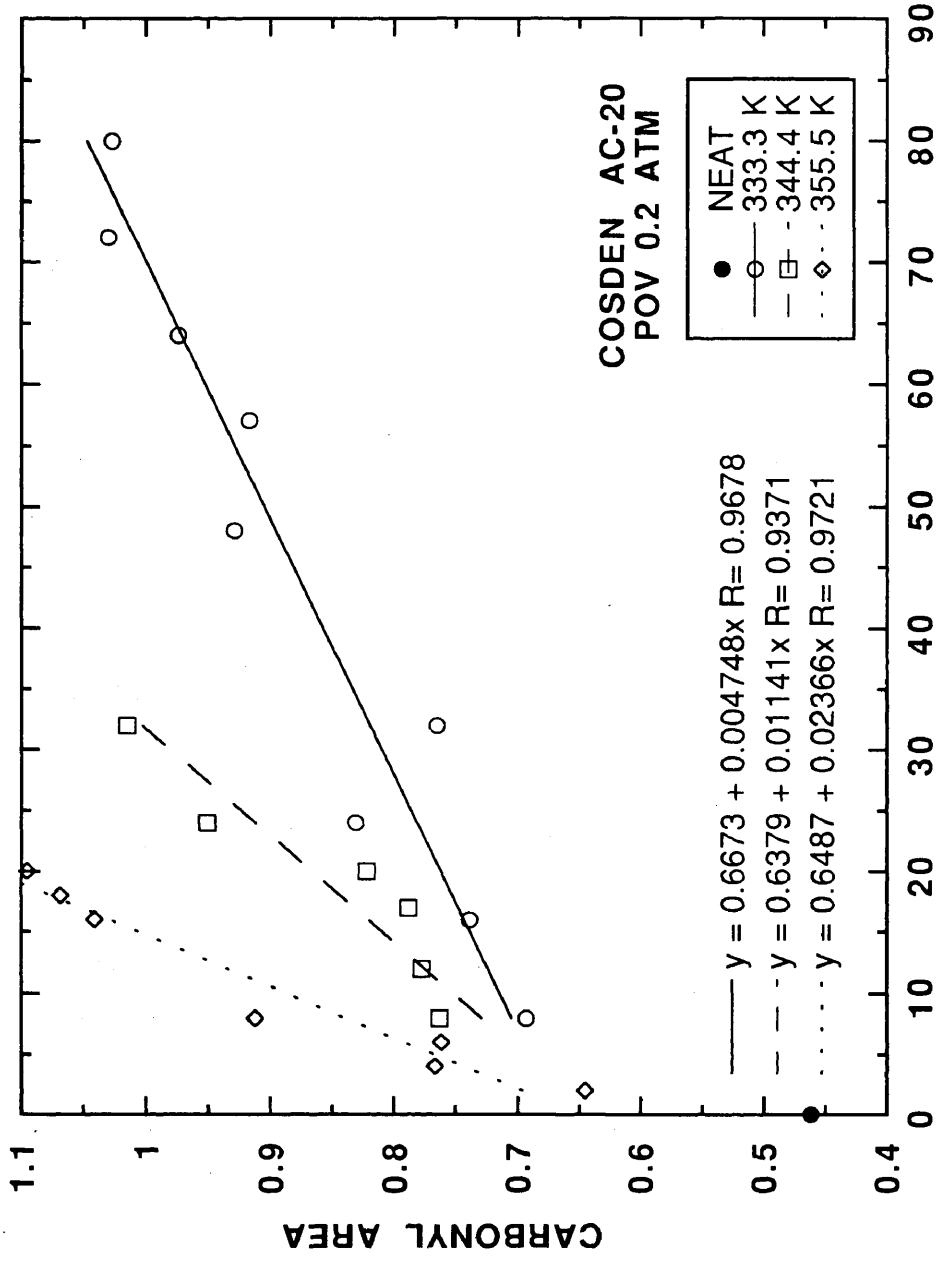

Figure IV-9. *CA*s of neat and POV-aged Cosden AC-20 at 0.2 atm and 333.3, 344.4, and 355.5 K.

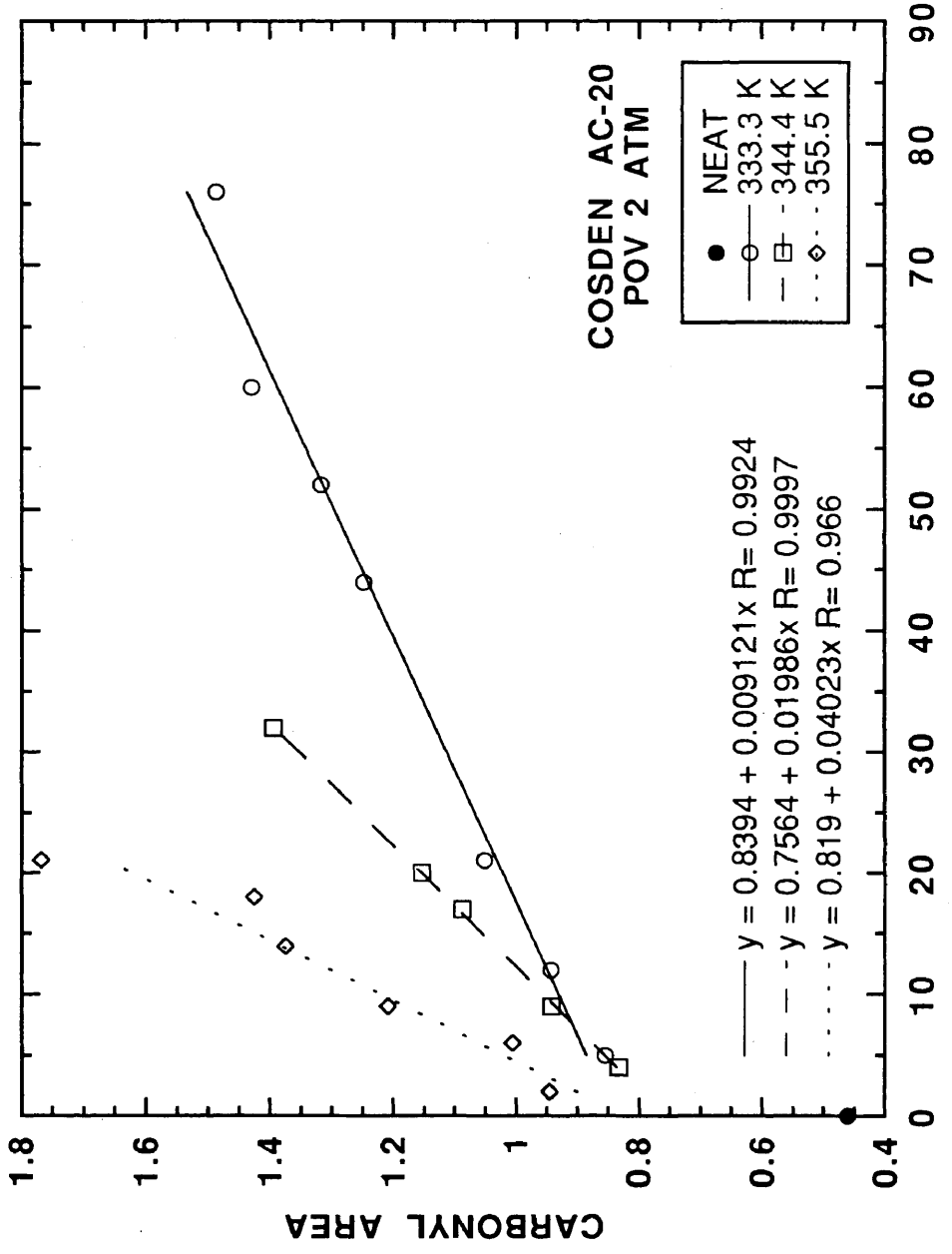

Figure IV-10. *CA*s of neat and POV-aged Cosden AC-20 at 2 atm and 333.3, 344.4, and 355.5 K.

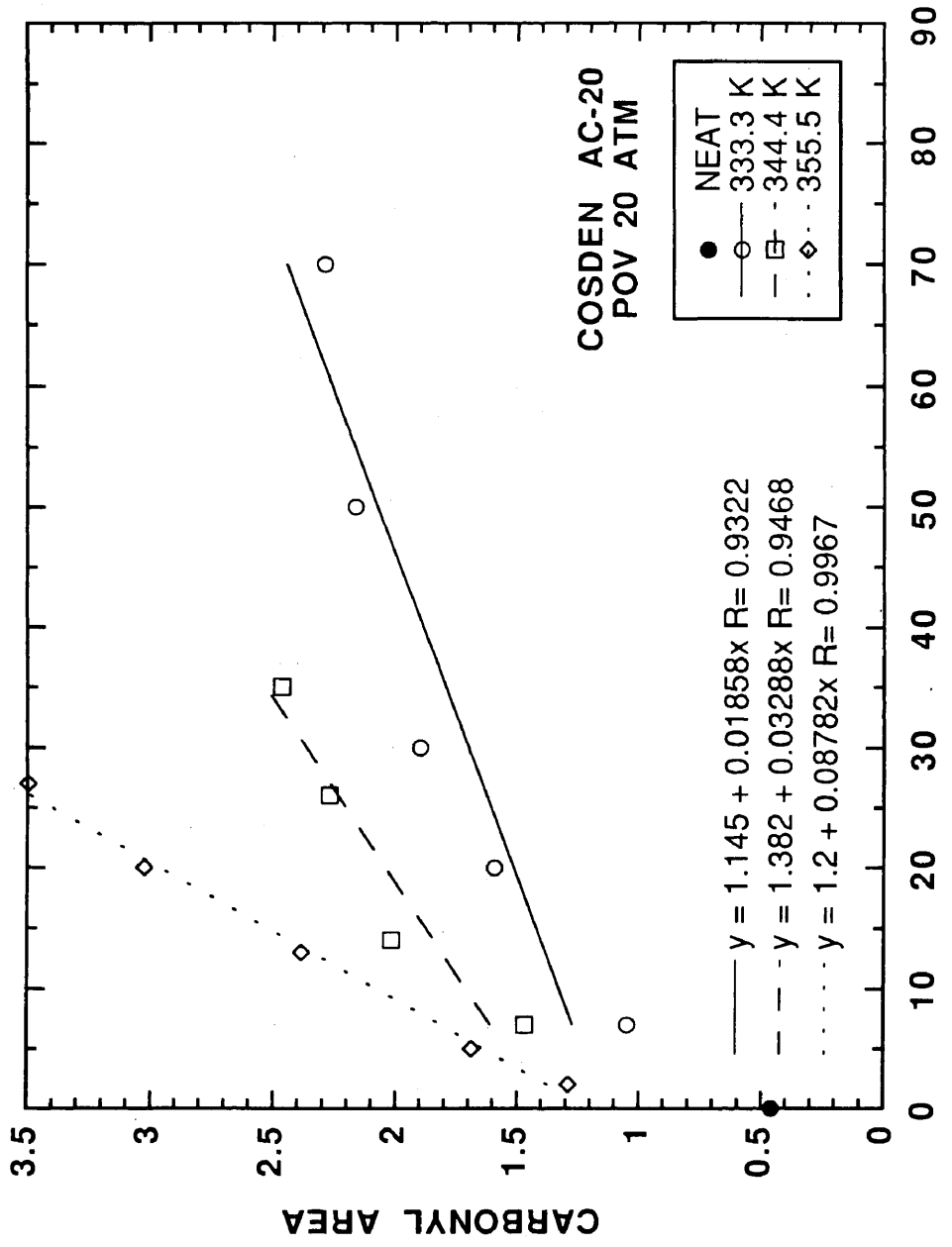

Figure IV-11. CAs of neat and POV-aged Cosden AC-20 at 20 atm and 333.3, 344.4, and 355.5 K.

For isobaric conditions, a linear relationship must exist between the log of r_{CA} and the reciprocal of the absolute aging temperature, (1 / T), for the Arrhenius relationship to be valid. From the linearity shown in Figure IV-12 for POV-aged Cosden AC-20 at 0.2 atm, the Arrhenius relationship is successful, modeling the effect of T on r_{CA} at low aging pressures. Both the Arrhenius constant, A, and the slope are reported on the figure. The slope of the line is the negative of the activation energy divided by the universal gas constant.

Previous research has shown that E_A depends on asphalt composition or crude source for POV aging at 20 atm (Lau *et al.*, 1992). A comparison of the asphalts studied for isobaric POV aging at 0.2 atm is shown in Figure IV-13. At this low oxygen pressure, it is difficult to conclude if the E_As or slopes are different. Only Exxon AC-20, represented by the hollow triangle symbol, has a markedly different slope. The estimated slopes, also shown on the figure, range from -9330 to -8240 K, only a 13% difference. At aging pressures of 2 atm, Figure IV-14 compares the temperature dependence on the r_{CA} of the asphalts studied. In this case, the differences in the slopes are more apparent. Slope parameters range from -9520 K for Coastal AC-20, hollow square, to -7380 K for Exxon AC-20. The percent difference is 30. At 20 atm shown in Figure IV-15, the slopes range between -10200 K for Coastal AC-20 and -8250 K for Cosden AC-20, a 24% difference.

The Arrhenius model accurately describes the temperature dependence on r_{CA} at all pressures and for all asphalts studied. The effect of composition or crude source on E_A is more apparent as a result of POV aging at higher oxygen pressures. This is probably a result of the measurement of CA and the experimental designed time periods for low pressures. At low P, CA changes very little for isothermal aging at 333.3, 344.4, and 355.5 K. Values of CA ranged from 0.7 to 1.1 for Cosden AC-20, Figure

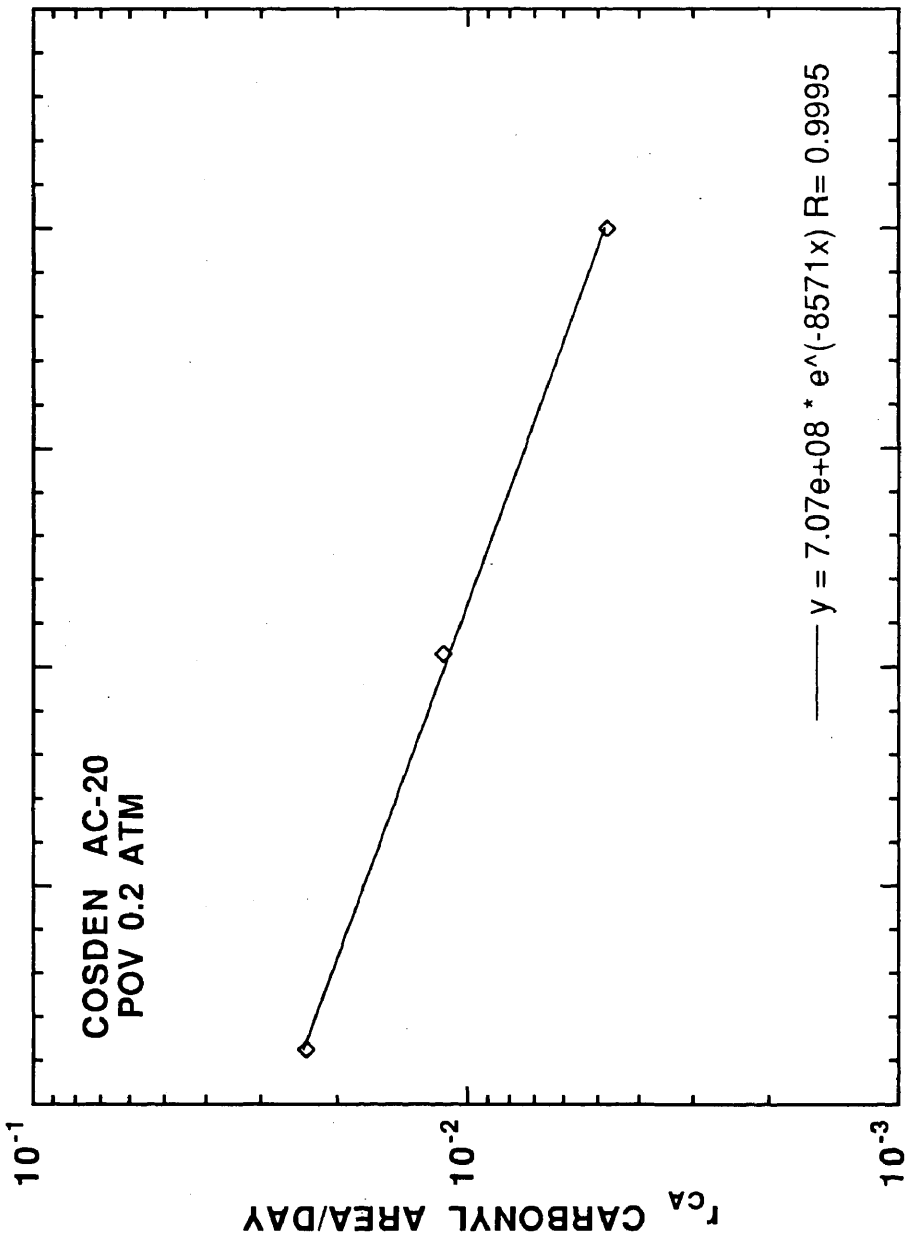

Figure IV-12. r_{CA} versus $(1/T)$ at 0.2 atm for POV-aged Cosden AC-20.

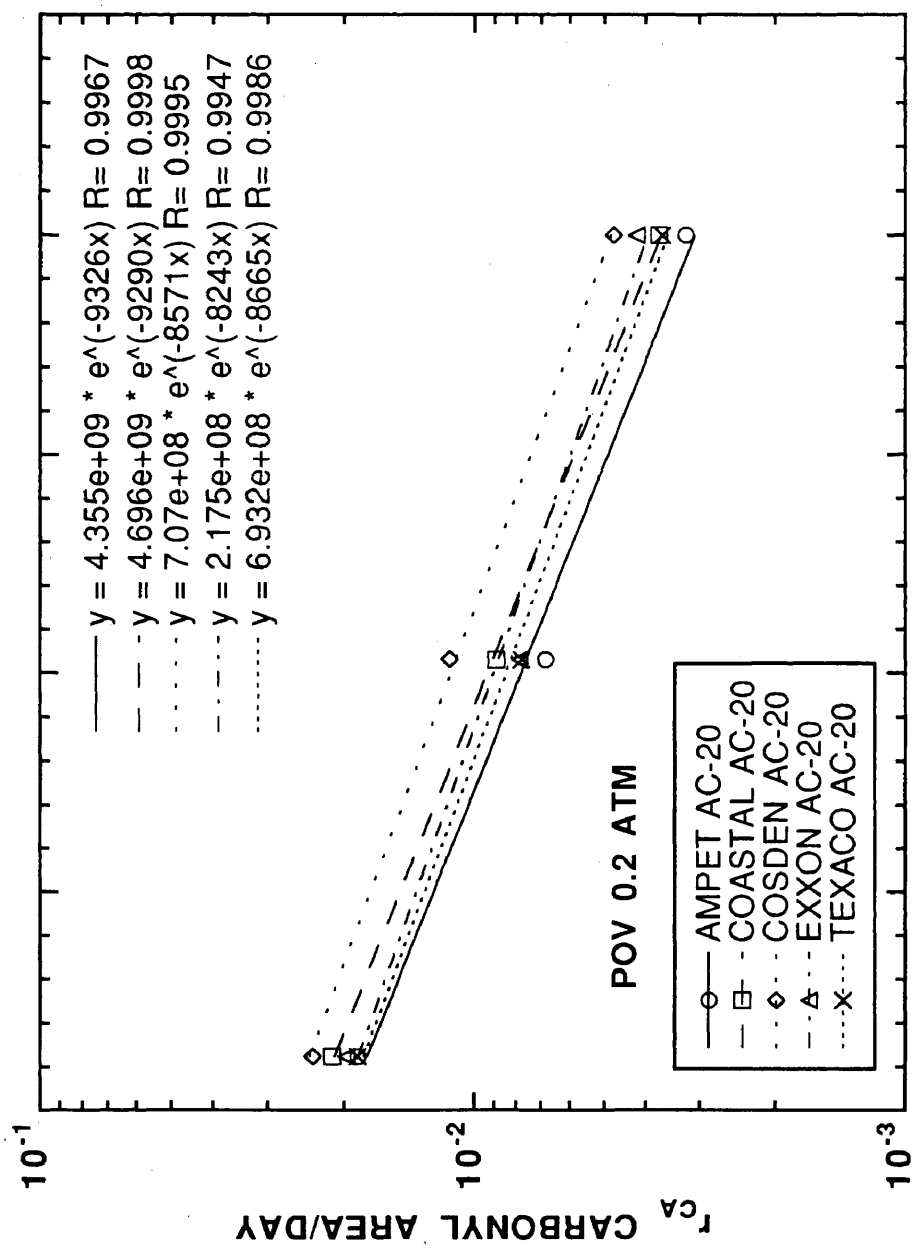

Figure IV-13. r_{CA} versus $(1 / T)$ at 0.2 atm for all POV-aged asphalts studied.

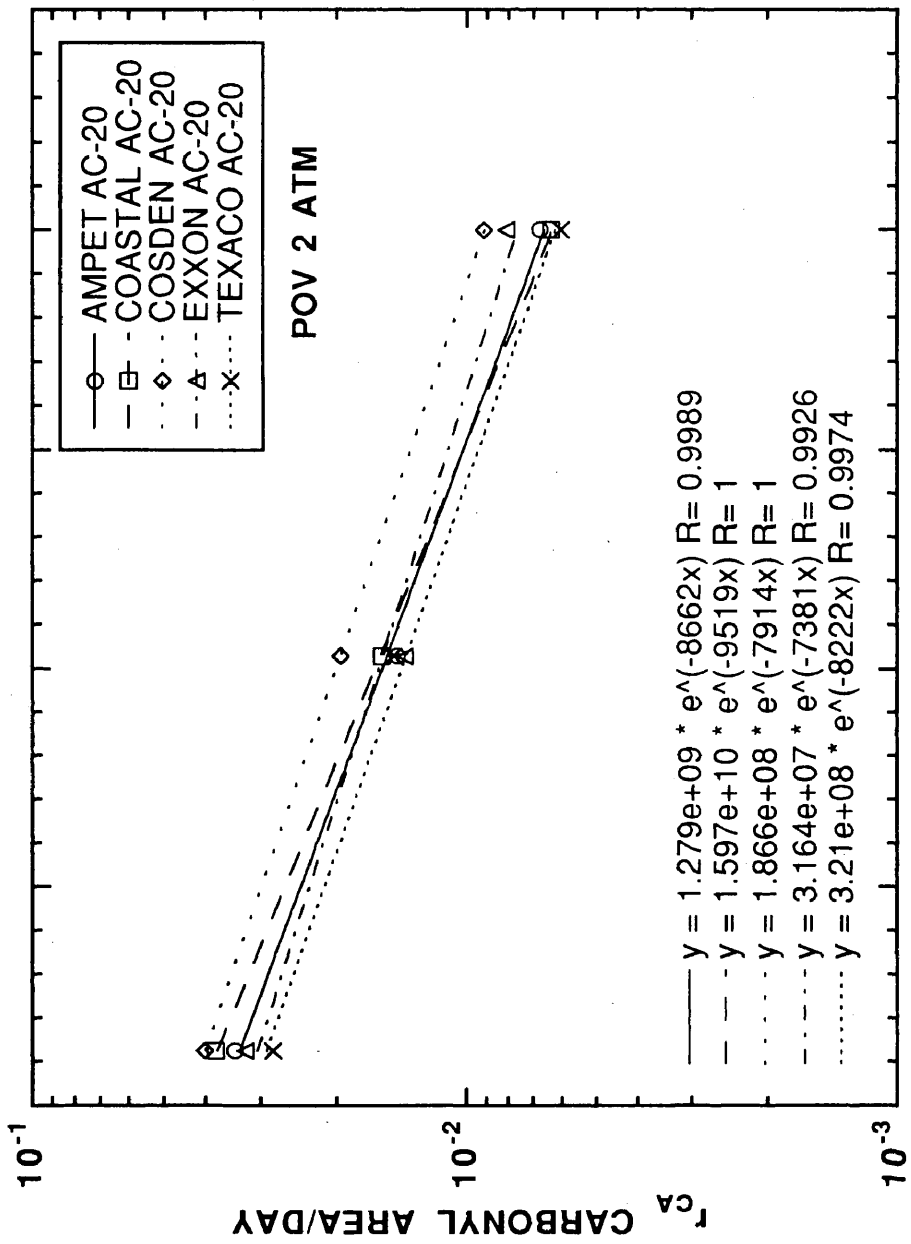

Figure IV-14. r_{CA} versus $(1 / T)$ at 2 atm for all POV-aged asphalts studied.

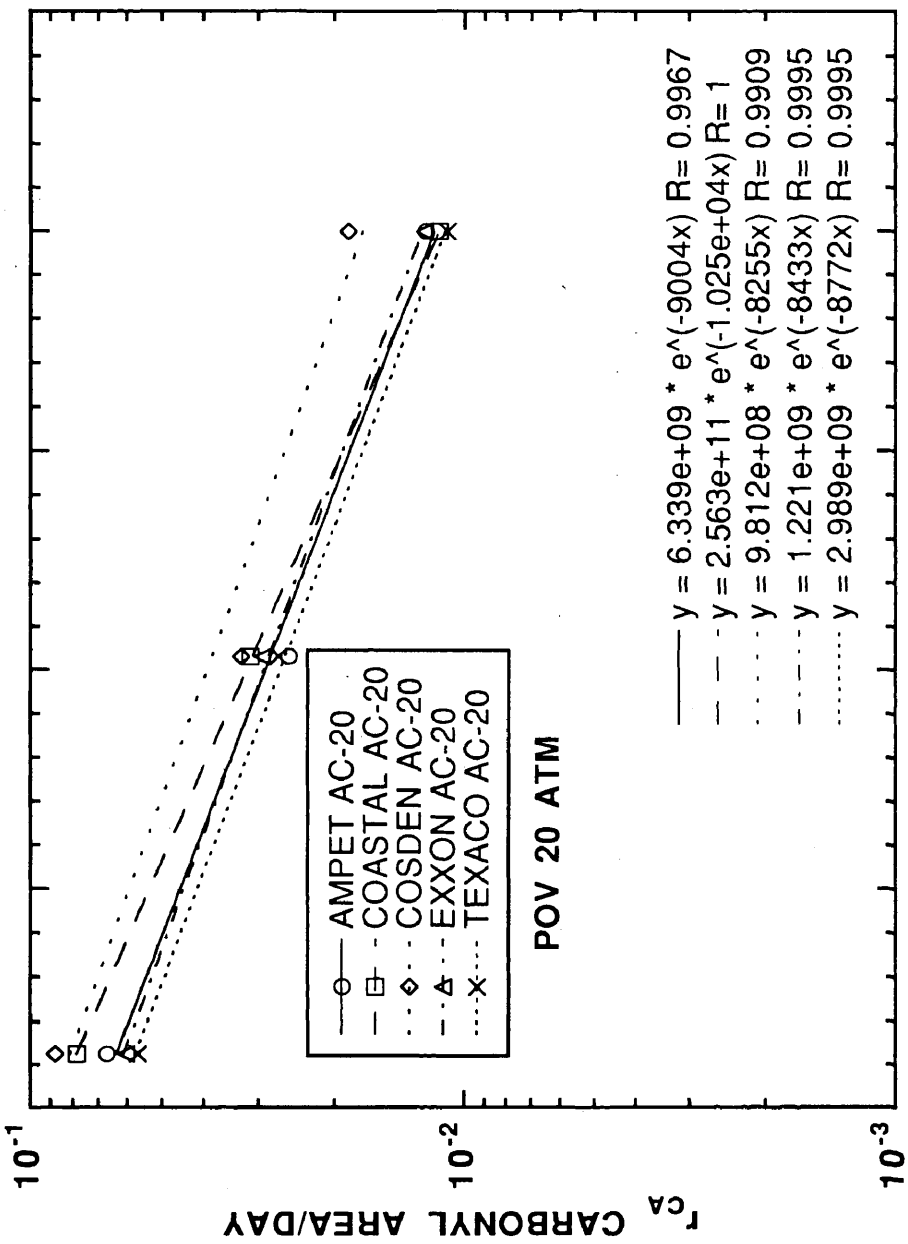

Figure IV-15. r_{CA} versus $(1\ /\ T)$ at 20 atm for all POV-aged asphalts studied.

IV-9. For Cosden AC-20 at 20 atm, CA ranged from 1.0 to 3.5 by comparison, Figure IV-11. These ranges are representative of all of the asphalts studied by reviewing Figures B-1 through B-24. As a consequence, at low aging pressures, the ability to discriminate different asphalts by r_{CA} at different temperatures is diminished. Thus, there is only a 13% difference in E_A at 0.2 atm and higher percent differences at the higher aging pressures.

E_A is calculated by multiplying the slope by the universal gas constant, R. Table IV-4 shows E_As of the asphalts studied at 0.2, 2, and 20 atm. Ideally, E_A should be independent of P, and from the table, there appears to be no correlation between E_A and aging pressures. For example, Coastal AC-20 shows increasing E_A with increasing P; however, the lowest E_A is at the aging pressure of 2 atm for the other asphalts. From the data, it appears that E_A is independent of aging pressure for a given asphalt. The magnitude of E_A for the asphalts studied indicates that the temperature effect on the r_{CA} is significant compared with the pressure effect. At constant pressure, an increase of 5.5 K roughly doubles r_{CA}; however, at constant temperature, an order of magnitude change in pressure doubles r_{CA}.

Table IV-4. E_A for All POV-Aged Asphalts Studied[a]

Asphalt	E_A kJ/gmol		
	0.2 atm	2 atm	20 atm
Ampet AC-20	77.5	72.0	74.8
Coastal AC-20	77.2	79.1	85.1
Cosden AC-20	71.2	65.8	68.6
Exxon AC-20	68.5	61.4	70.1
Texaco AC-20	72.0	68.3	72.9

[a] Aging temperatures from 333.3 to 355.5 K

Figures IV-13, IV-14, and IV-15 also show that the asphalts have different pre-exponential factors or Arrhenius constants, A. For example, the lines in Figure IV-13 are off-set vertically as a result of the different values of A for each asphalt. A represents the rate or frequency of collisions between the active sites in the asphalt and the oxygen molecules. Overall, a broad trend of increasing A with increasing P is reached by overlaying Figure IV-13, IV-14, and IV-15 for the asphalts studied. From the parameters shown in Table IV-5, only Coastal AC-20 shows a monotonic increase in A with P. The other asphalts show a decrease in A from 0.2 to 2 atm followed by an increase in A from 2 to 20 atm over and above the value of A at 0.2 atm. Since no pressure dependency was included in the Arrhenius parameters analysis, these reported values of A contain some pressure information. Furthermore, the large variations of several orders of magnitude in A is a direct result of the exponential relationship between the temperature dependence and the r_{CA}. Values of $\ln(A)$ obviously show significantly less variability as shown in the next section.

Table IV-5. A for All POV-Aged Asphalts Studied[a]

Asphalt	$A \times 10^{-8}$ CA / day		
	0.2 atm	2 atm	20 atm
Ampet AC-20	43.5	12.8	63.4
Coastal AC-20	47.0	160.	2560.
Cosden AC-20	7.07	1.87	9.81
Exxon AC-20	2.18	0.316	12.2
Texaco AC-20	6.93	3.21	29.9

[a] Aging temperatures from 333.3 to 355.5 K

Multi-Variable Parameter Estimation

For POV aging of asphalts, the effects of P and T were analyzed independently, confirming that the kinetic model, equation II – 7, was valid. With this confirmation, a multi-variable regression of r_{CA} as a function of T and P was performed. The estimated parameters are shown in Table IV-6. For each of the parameters, a 95% confidence limit is also shown. In this table, $\ln(A)$ is given and not the value of A. Reporting $\ln(A)$ provides a better comparison between asphalts and is required because the model must be linear in the parameters to provide the 95% confidence limits. The error of the estimated r_{CA} from the model parameters versus the measured r_{CA} is also given. The percent errors are all under 10%.

Table IV-6. Kinetic Model Parameters for All POV-Aged Asphalts Studied[a]

Asphalt	$\ln(A)$ $\ln(CA$ / day atm$^{\alpha})$	E_A kJ/gmol	α	% Error[b]
Ampet AC-20	21.71 ± 2.95	74.8 ± 8.2	0.285 ± 0.042	7
Coastal AC-20	23.83 ± 4.40	80.5 ± 12.3	0.266 ± 0.062	4
Cosden AC-20	19.86 ± 3.10	68.6 ± 8.7	0.270 ± 0.044	7
Exxon AC-20	19.86 ± 3.39	66.7 ± 9.5	0.255 ± 0.048	8
Texaco AC-20	20.42 ± 2.02	71.1 ± 5.6	0.250 ± 0.028	5
All	20.95 ± 1.72	72.3 ± 4.9	0.270 ± 0.024	14

[a] Model: $r_{CA} = A\exp(-E_A / RT)P^{\alpha}$
Aging temperatures from 333.3 to 355.5 K
and pressures from 0.2 to 20 atm

[b] % Error $= 100(1 / n)\sqrt{\sum\left(\frac{\text{mea} - \text{cal}}{\text{mea}}\right)^2}$

A 95% confidence limit is roughly 15% of the value of the parameter. The confidence limit for Coastal AC-20 is broadest indicating that there is more variability in this set of data. The data with the least variability is Texaco AC-20. Unfortunately,

the size of the confidence limit is such that it is difficult to conclude if the parameters are dependent on the asphalt source. Since the Arrhenius parameters describe the temperature dependence and this is the most significant factor affecting the determination of r_{CA}, it is concluded that the Arrhenius parameters are composition dependent. However, pressure dependence is far less significant than temperature and α is concluded to be independent of asphalt composition.

All of the r_{CA} data for the asphalts were grouped together, and the parameters were estimated again. These parameters are given on the bottom line of the table. The percent error increased with the grouping of the data, as expected, and the value is 15%. However, the 95% confidence limit for the averaged parameters decreased by roughly a factor of 2. This is a direct result of the increased number of observations in the data set. From the over all parameter estimation, the composition-independent α for the asphalts studied is 0.27.

A series of calculations comparing the measured r_{CA} with the predicted r_{CA} using the particular Arrhenius parameters in Table IV-6 and the constant value of 0.27 for α were performed. The percent errors in the estimated r_{CA} and the measured r_{CA} are shown in Figures IV-16 as a function of P and Figure IV-17 as a function T. In Figure IV-16, the maximum error is 15%, and results for Ampet AC-20, Cosden AC-20, and Exxon AC-20. A majority of the errors lie within a band of plus or minus 10% and are random with respect to P. Figure IV-17 shows that the maximum error of 15% occurs only at the aging temperature of 344.4 K. Furthermore, the errors are not random and appear parabolic. These parabolic residuals may be due to the fact that only three different aging temperatures were used in the analysis. Obviously, more aging temperatures would result in a larger data set and better parameter estimation. Aside from the 15% error that occurred for one temperature and three

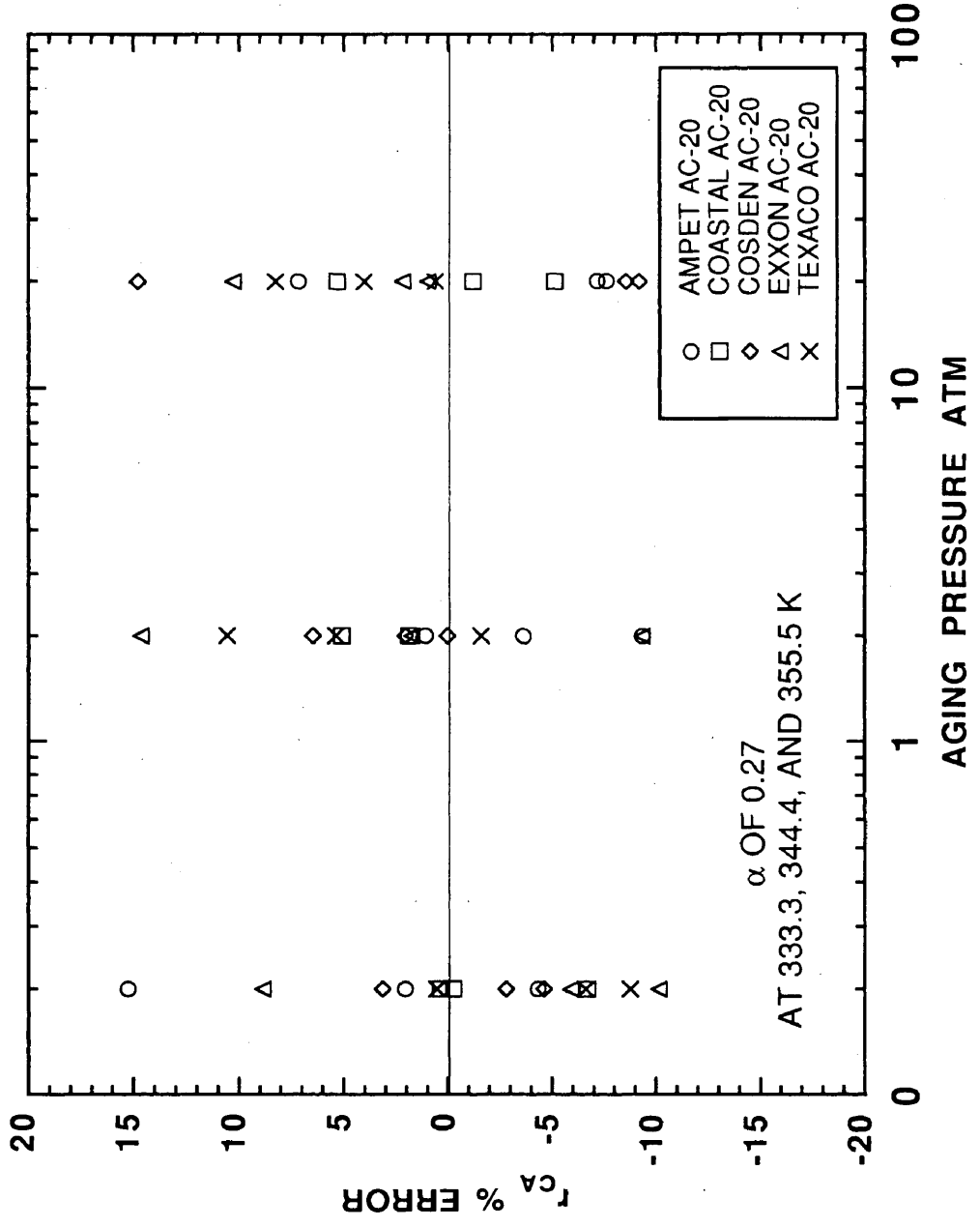

Figure IV-16. Percent error in predicted r_{CA} for α of 0.27 versus P for all asphalts studied.

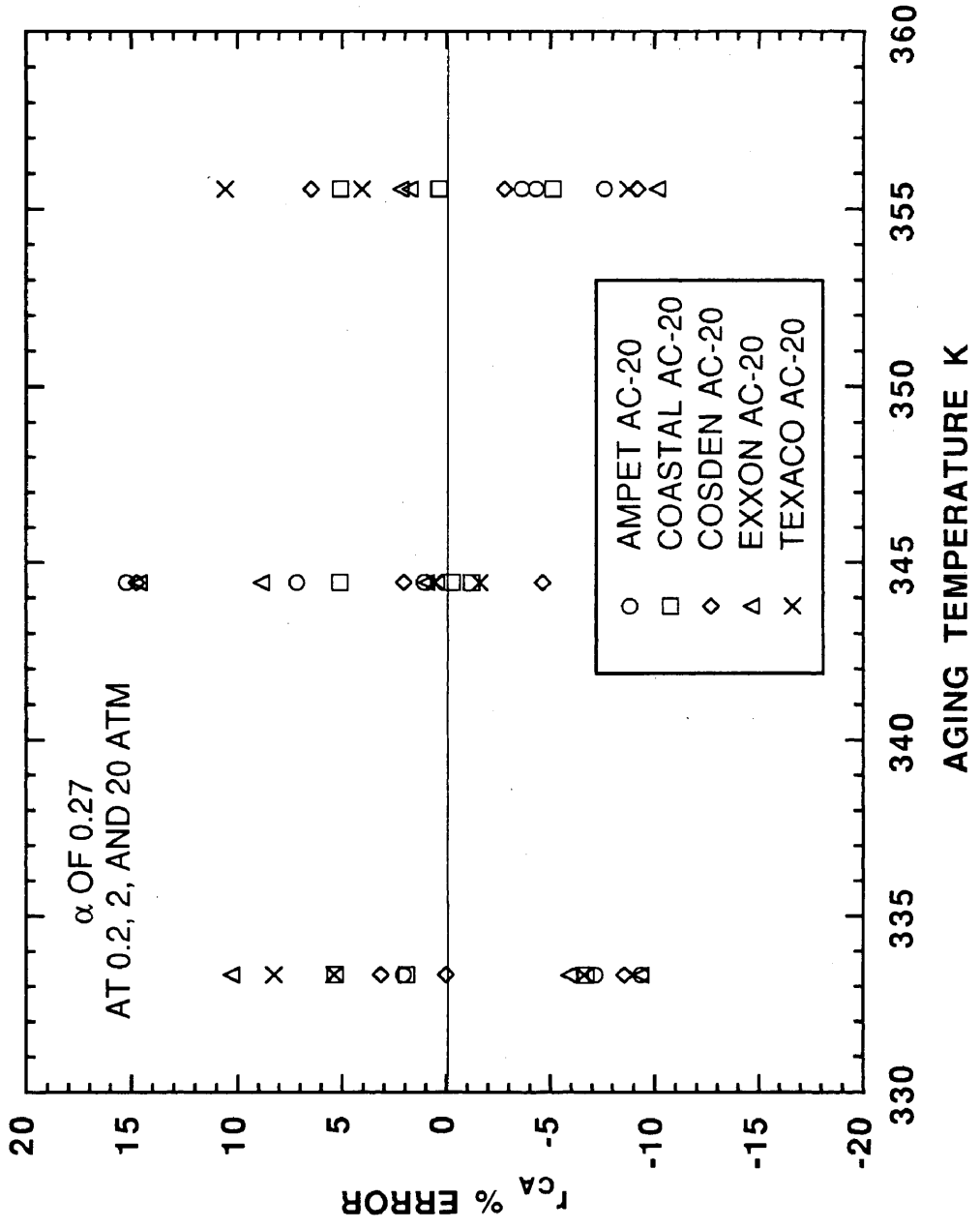

Figure IV-17. Percent error in predicted r_{CA} for α of 0.27 versus T for all asphalts studied.

asphalts, using a constant α for all asphalts only contributes about 10% error in the r_{CA} for the asphalts studied.

Comparison of E_A with Literature Values

The calculated E_A of the asphalts studied are compared with literature values. For asphalt oxidation, only a few sources report values of E_A. Van Oort (1956) measured oxygen absorption in asphalts and reports an E_A of 100 kJ/gmol. Verhasselt and Choquet (1991) report E_As between 66.9 and 87.1 kJ/gmol for aging at 343.2 and 373.2 K. The measured properties were percent asphaltenes, ring and ball softening points, penetrations and IR absorption in the carbonyl region. Verhasselt and Choquet used equation I – 4 to analyze their data. Values of E_A in this study are about 25% lower than those of Van Oort but show excellent agreement with Verhasselt and Choquet. These differences may result from the fact that only carbonyl formation is being accounted for in this study while all oxygen reactions are accounted for in Van Oort's study. Two sources (Bateman, 1954; Bolland, 1949) give values of E_A of 41.8 kJ/gmol for olefin oxidation. Values of E_A in this study are twice those reported for olefin oxidation, resulting because the model compound reaction characteristics do not reflect those found in the asphalt.

Measuring oxygen absorption at different temperatures, two papers report activation energies of 29.3 and 41.7 kJ/gmol (Dickinson and Nicholas, 1949; Dickinson *et al.*, 1958). The authors conclude that the activation energies are not really E_A for the chemical reaction; however, the activation energy does provide a measure of the rate of acceleration of the complex aging process of diffusion and reaction. E_A in this work is twice as great as those reported for oxygen absorption measurements. Dickinson and Nicholas (1949) attempted to minimize diffusion resistance; however,

they used equation I – 5 to analyze their data. Van Oort (1956) also measured oxygen absorption, but he attempted to separate reaction and diffusion and account for variable diffusivity in his model. He reports E_A of 100 kJ/gmol. From these comparisons with literature values, researchers that attempted to minimize diffusion resistance or account for variable diffusivity in the analysis report higher E_A than those that did not. Overall, E_A values in this study lie in the range given by all the literature sources and are essentially identical to those reported by Verhasselt and Choquet.

Extrapolation of r_{CA} to Lower Temperatures

For an effective model, the accurate prediction of low temperature r_{CA} is critical. To test this, the asphalts studied were aged at 322.2 K and 20 atm from 7 to 80 days. *CA*s are given in Table B-6 in Appendix B. Figure IV-18 shows *CA* as a function of aging time for Cosden AC-20 at 322.2 K and 20 atm. Figures B-25 through B-28 show *CA* versus time at 322.2 K and 20 atm for the other asphalts studied. The observations of an initial non-linearity followed by a constant r_{CA} for aging at 333.3, 344.4, and 355.5 K also exists at 322.2 K. Consequently, a linear model was used to represent the long-term aging characteristics. From the linear model, r_{CA} from the measured data were determined and are given in Table IV-7. CA_o are also reported in the table.

From data at 333.3, 344.4, and 355.5 K and estimated parameters, Table IV-4 with constant α of 0.27, r_{CA} at 322.2 K was determined by extrapolation. A comparison between measured and calculated r_{CA} from extrapolation of high temperature data are given in Table IV-8. The predicted and measured values agree within 5% for Coastal AC-20, Exxon AC-20, and Texaco AC-20. However, for Ampet

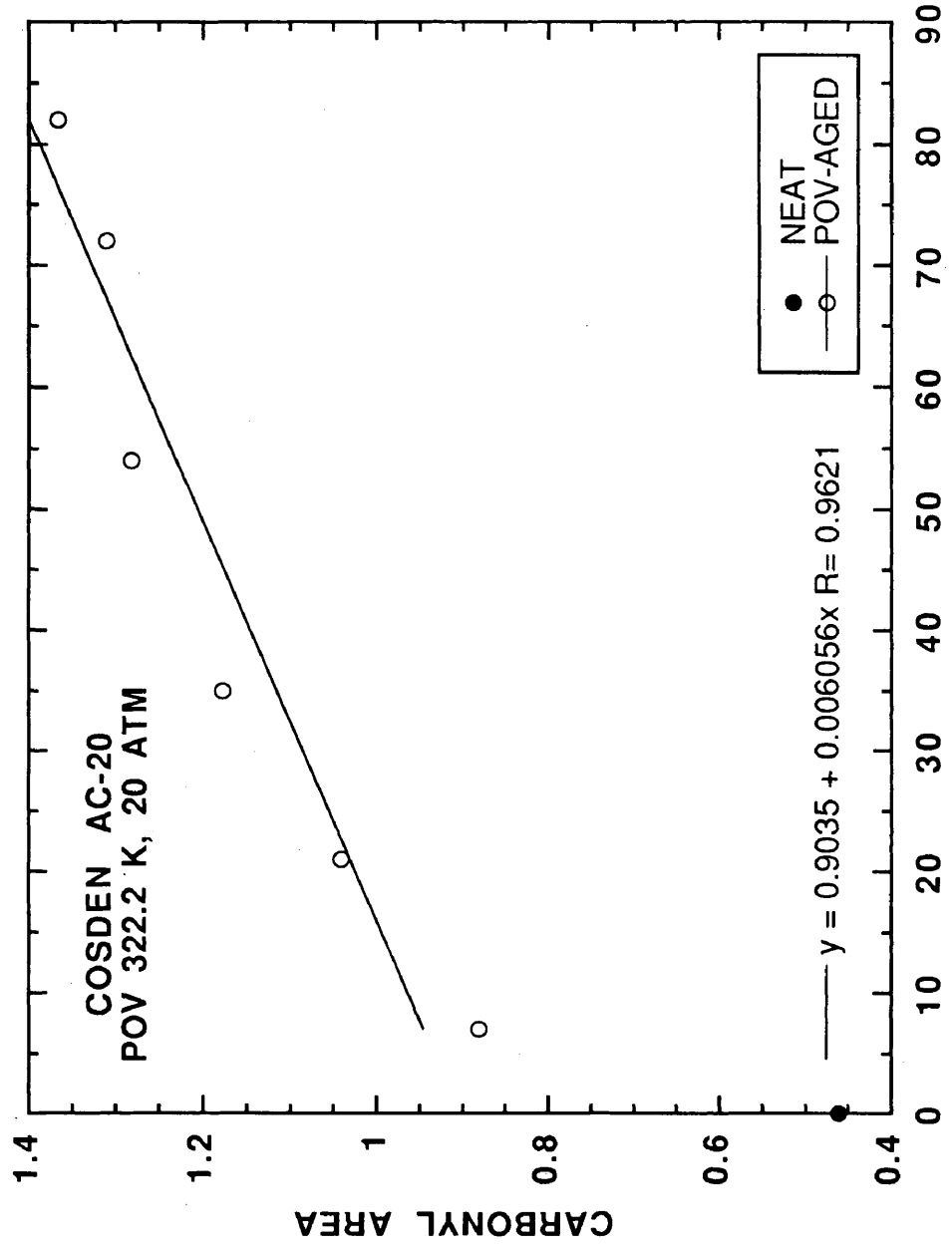

Figure IV-18. CAs of neat and POV-aged Cosden AC-20 at 322.2 and 20 atm.

Table IV-7. r_{CA} and CA_o for All POV-Aged Asphalts at 322.2 K and 20 atm[a]

Asphalt	$r_{CA} \times 10^3$ CA / day	CA_o CA
Ampet AC-20	5.07	0.759
Coastal AC-20	4.41	0.761
Cosden AC-20	6.06	0.903
Exxon AC-20	5.97	0.843
Texaco AC-20	4.78	0.681

AC-20 and Cosden AC-20, the percent error is about 15% with Ampet AC-20 under predicting r_{CA} and Cosden AC-20 over predicting. These errors are probably due to the fact that only three temperatures were used in the experimental design and subsequent parameter estimation. Overall, the agreement between the calculated and the measured r_{CA} is excellent suggesting that the model with constant α of 0.270 is reliable for predicting pavement-temperature r_{CA}.

Hypothesized Model for CA_o as a Function of Observable Variables

Since the magnitude of CA relates to the physical properties and ultimately to the performance of the asphalt, knowing the r_{CA} as a function of observable variables is not enough. A method to estimate the integration constant, CA_o, must also be developed. Long-term linear aging characteristics do not start from the neat material because of an initial non-linearity. Using neat asphalt CA as CA_o would result in low predictions of actual CA. For highway-pavement aging, the hot-mix process causes carbonyl formation (Jemison *et al.*, 1991) and represents a more realistic initial condition for modeling. However, in the absence of hot-mix processed asphalt and from the standpoint of a pure laboratory test, the initial condition, CA_o, is estimated

Table IV-8. Comparison between Measured r_{CA} at 322.2 K, 20 atm and Extrapolated r_{CA} from Parameters Estimated from 333.3, 344.4, and 355.5 K Data

Asphalt	$r_{CA} \times 10^3$		% Error[b]
	Measured CA / day	Extrapolated[a] CA / day	
Ampet AC-20	5.07	4.41	13.0
Coastal AC-20	4.41	4.39	0.4
Cosden AC-20	6.06	7.03	-16.0
Exxon AC-20	5.97	5.80	2.8
Texaco AC-20	4.78	4.82	-0.7

[a] Model: $r_{CA} = A\exp(-E_A / RT)P^{\alpha}$ with α of 0.27. A and E_A are from Table IV-5 for each asphalt

[b] % Error $= 100\left(\frac{\text{mea} - \text{ext}}{\text{mea}}\right)$

from the linear model for long-term aging.

CA_o appears to be only a function of aging pressure from experimental data. Figure IV-19 shows the intercepts for Cosden AC-20 at all aging pressures and 333.3, 344.4, and 355.5 K. Figures B-29 through B-32 show the other asphalts studied. These figures show that the intercept is only a function of aging pressure, and equation II–8 reduces to:

$$CA_o = f(P) \qquad \text{(IV - 1)}$$

The arithmetic average value of CA_o for each asphalt at 0.2, 2, and 20 atm were determined. Dickinson and Nicholas (1949) suggest a linear relationship between CA_o and P for aging conditions from 0.2 to 1 atm. However, the data in this study span pressures from 0.2 to 20 atm. Figure IV-20 shows all of the asphalt arithmetic averaged CA_o versus aging P on a log-log plot. Since no fundamental theory exists

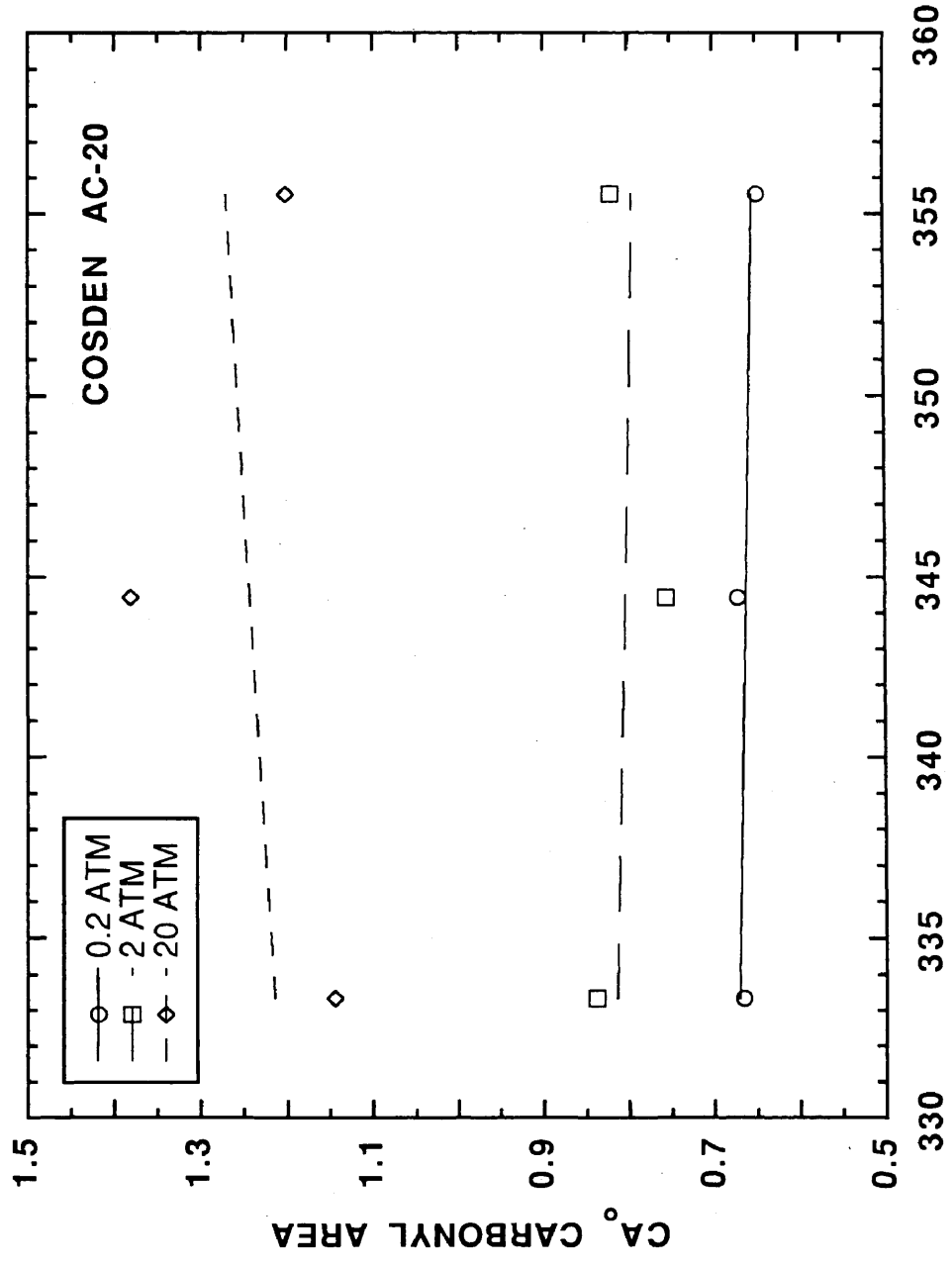

Figure IV-19. CA_o versus POV aging temperature for Cosden AC-20.

for the development of a model, an empirical model of the form

$$CA_o = sP^{\beta} \qquad (IV-2)$$

was selected. This model provided the best fit for the asphalts studied, and the model parameters are given in Table IV-9.

There appears to be three distinct groups with regard to the parameter β. β for Coastal AC-20, Exxon AC-20, and Texaco AC-20 is close to 0.8. However, β for Ampet AC-20 and Cosden AC-20 are 0.04 and 0.14, respectively. With the limited data set and the empirical nature, it is concluded that the parameters are composition dependent. Unfortunately, one aging experiment at 0.2 atm is required to estimate CA_o for asphalt aging at highway conditions. Clearly, more asphalts, pressures, and models need to be considered to understand the pressure dependence on CA_o. The first model to assess for extending this work is that proposed by Dickinson and Nicholas (1949).

Table IV-9. Carbonyl Intercept Model Parameters for All POV-Aged Asphalts Studied[a]

Asphalt	s CA / atm$^{\beta}$	β
Ampet AC-20	0.688	0.038
Coastal AC-20	0.712	0.092
Cosden AC-20	0.786	0.140
Exxon AC-20	0.803	0.073
Texaco AC-20	0.646	0.082

[a] Model: $CA_o = sP^{\beta}$
Oxygen pressures from 0.2 to 20 atm

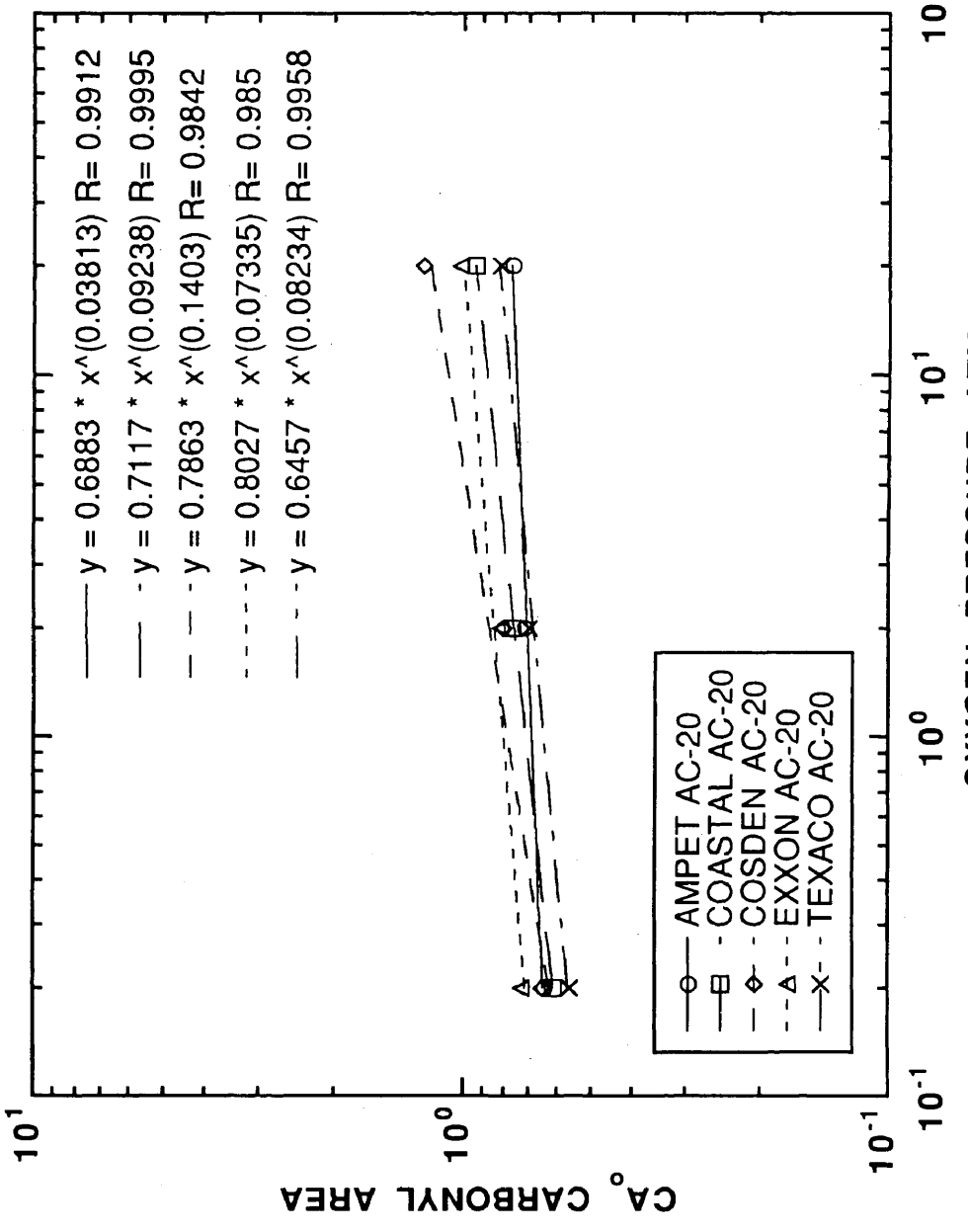

Figure IV-20. CA_o versus POV aging temperature for all asphalts studied.

The model parameters for r_{CA} and CA_o were obtained from physical situations that attempted to minimize oxygen diffusion problems in the asphalt film. At low oxygen pressures, only the ES of the aged sample was analyzed. Even though the parameters were estimated from data at the ES, the r_{CA} and CA_o models as functions of aging T and P are valid anywhere in the asphalt film. Unfortunately, unless the diffusion of oxygen is taken into account, the oxygen pressure at points in the film are not accurately known.

Error Analysis

With the model parameters for r_{CA} and CA_o determined, the sensitivity of these determinations with respect to the controlled variables, T and P, is analyzed. This gives a measure of how precise the determinations of r_{CA} and CA_o should be with all other measurement errors being zero. This assumes that there is no uncertainty in the measurement of CA from FTIR.

Since r_{CA} is a function of T and P, the total differential is given in equation IV – 3.

$$dr_{CA} = \left(\frac{\partial r_{CA}}{\partial T}\right) dT + \left(\frac{\partial r_{CA}}{\partial P}\right) dP \qquad \text{(IV – 3)}$$

The two partial derivatives are given in equation IV – 4 and IV – 5, respectively.

$$\left(\frac{\partial r_{CA}}{\partial T}\right) = r_{CA}\left(\frac{E_A}{RT^2}\right) \qquad \text{(IV – 4)}$$

$$\left(\frac{\partial r_{CA}}{\partial P}\right) = r_{CA}\left(\frac{\alpha}{P}\right) \qquad \text{(IV – 5)}$$

Substituting equations IV – 4 and IV – 5 into IV – 3 and dividing by r_{CA} gives:

$$\frac{dr_{CA}}{r_{CA}} = \frac{E_A}{RT}\left(\frac{dT}{T}\right) + \alpha\left(\frac{dP}{P}\right) \qquad \text{(IV – 6)}$$

The precision of r_{CA} decreases for decreasing pressure and decreasing temperature from equation IV – 6. Furthermore, asphalts with higher E_A show increasing uncertainty in r_{CA}.

Sample calculations of the worst and best case give a range of precision for r_{CA}. The precision of the pressure and temperature measurements were 0.136 atm (2 psi) for positive pressure and 0.007 atm (5 mm Hg) under vacuum and 1.11 K (2 °F), respectively. An arithmetic average of E_A from Table IV-5 for all asphalts studied yields a value of 72.5 kJ/gmol. The value of R is 8.314 J/gmol K, and α is 0.27. Since the precision in pressure measurement under vacuum is significantly lower when compared to positive pressure measurements, the worst case pressure is 2 atm. At a temperature of 333.3 K and pressure of 2 atm, the percent error in r_{CA} is:

$$T = 333.3 \text{ K} \qquad P = 0.2 \text{ atm} \qquad \frac{dr_{CA}}{r_{CA}} = 0.087 + 0.018 = 0.105 \qquad \text{(IV – 7)}$$

For the best case, a temperature 355.5 K and pressure of 20 atm is used. The percent error in r_{CA} is:

$$T = 333.3 \text{ K} \qquad P = 0.2 \text{ atm} \qquad \frac{dr_{CA}}{r_{CA}} = 0.077 + 0.002 = 0.079 \qquad \text{(IV – 8)}$$

The range of worst and best case analysis is 0.105 and 0.079 which is very small. Over 80% of the uncertainty in r_{CA} results from uncertainty in temperature measurements. From the controlled experimental variables, the precision of all r_{CA} is within 10%.

For CA_o, a function of only one variable, P, the total differential is given in equation IV – 9

$$dCA_o = \left(\frac{\partial CA_o}{\partial P}\right) dP \qquad \text{(IV – 9)}$$

The partial derivative is given in equation IV – 10.

$$\left(\frac{\partial CA_o}{\partial P}\right) = CA_o\left(\frac{\beta}{P}\right) \qquad \text{(IV – 10)}$$

Substituting equation IV – 10 into IV – 9 and dividing by CA_o gives

$$\frac{dCA_o}{CA_o} = \beta\left(\frac{dP}{P}\right) \qquad \text{(IV – 11)}$$

The highest β is 0.140 from Table IV-9, and the worst case percent error in CA_o is at 2 atm.

$$\frac{dCA_o}{CA_o} = 0.010 \qquad \text{(IV – 12)}$$

The uncertainty of CA_o from the model given in equation IV – 2 is 1%.

Solubility of Oxygen in Asphalt

It was assumed that the oxygen concentration in the film at the *ES* was equal to the oxygen pressure of the gas in the previous discussion.

$$P_{ES} = P = P_{\text{gas}} \qquad \text{(IV – 13)}$$

This is not precisely true. The concentration at the *ES* may be a function of equilibrium conditions between the gas and semi-solid, viscous-liquid, asphalt. For very low concentrations of oxygen in the asphalt, a Henry's law behavior is assumed.

$$P_{ES} = P = hP_{\text{gas}} \qquad \text{(IV – 14)}$$

h is the Henry's law constant. Unfortunately, values of h for asphalts in the literature are scarce. Baldwin and Daniel (1953) report values of h at approximately 0.1 for oils with viscosity of 100 cP at 373.2 K. However, measurement of the true solubility of oxygen in asphalt is very difficult since reaction is occurring. Therefore, errors in h might be significant.

r_{CA} is the same regardless of which reference frame the observer is using. Thus, with respect to the true oxygen concentration in the film, parameter A is adjusted by the Henry's law constant.

$$A_{\text{true}} = \frac{A_{\text{gas}}}{h^{\alpha}} \qquad \text{(IV - 15)}$$

With respect to the measured P in the gas, the parameter A needs no adjusting. In either case, E_A is not effected.

Summary

The carbonyl formation in asphalt is expressed as an explicit function of observable variables, aging temperature T, oxygen pressure P, and time t.

$$CA\Big[t, P(t_o)\Big] = \int_0^t r_{CA}\Big[T(\theta), P(\theta)\Big]\, d\theta + CA_o\Big[P(t_o)\Big] \qquad \text{(IV - 16)}$$

r_{CA} is a given as a function of T and P by equation II – 7.

$$r_{CA} = A \exp(-E_A / RT) P^{\alpha} \qquad \text{(II - 7)}$$

Each asphalt has a unique E_A and A, and the temperature effect is significant in calculating r_{CA}. To obtain E_A and A, laboratory experiments at several temperatures are required. The order of reaction, α, is 0.27 and independent of the asphalts studied. The pressure effect is not as significant as the temperature effect on r_{CA}. Laboratory experiments to determine r_{CA} at elevated pressures can be reliably extrapolated to low pressure with constant α. The ability of the model to extrapolate to highway aging temperatures was confirmed. A comparison between measured r_{CA} at 322.2 K and extrapolated r_{CA} from high temperature data and estimated model parameters was successful. Comparison of E_A with literature values was favorable with those researchers who attempted to minimize diffusion resistance or account for variable diffusivity in the analysis.

Because of the initial non-linearity, an initial condition, CA_o, was defined from the long-term constant-rate aging data. CA_o was only a function of oxygen pressure as given in equation IV – 2.

$$CA_o = sP^{\beta} \qquad \text{(IV – 2)}$$

It appeared that the parameters, s and β, varied for the asphalts studied. One laboratory aging experiment at highway oxygen levels is required to determine CA_o at highway-pavement conditions. However, using a more sophisticated model similar to that proposed by Dickinson and Nicholas (1949) to analyze the data should incorporate the initial non-linearity into the reaction kinetics. In this case, the integration constant, CA_o, could be measured from neat asphalt. The uncertainty in r_{CA} is within 10% and CA_o is within 1% from the precision of the controlled variables during POV aging, the models as given in equations II – 7 and IV – 2, and the estimated model parameters. This error analysis did not account for uncertainties in the measurement of CA from FTIR. If the solubility of oxygen in the asphalt film is accounted for by a Henry's law model, the kinetic parameter, A, requires modification to calculate r_{CA} with respect to the true oxygen pressure. E_A needs no adjustment.

CHAPTER V
OXYGEN DIFFUSIVITY IN ASPHALT FILMS

With a model describing carbonyl formation in asphalt as a function of aging temperature and pressure, the next aspect is the estimation of oxygen diffusivity, $\mathcal{D}_{O_2}$, in asphalt. Equation II – 30 accounts for changes in oxygen pressure in a differential volume of asphalt for one-dimensional oxygen transport.

$$\left(\frac{\partial P}{\partial t}\right) = \left(\frac{\partial \mathcal{D}_{O_2}}{\partial x}\right)\left(\frac{\partial P}{\partial x}\right) + \mathcal{D}_{O_2}\left(\frac{\partial^2 P}{\partial x^2}\right) - \left(\frac{cRT}{h}\right) r_{CA} \qquad \text{(II – 30)}$$

In this equation, $\mathcal{D}_{O_2}$ is unknown. As described in Chapter II, the parameter estimation is simplified for steady-state constant $\mathcal{D}_{O_2}$ oxygen diffusion and reaction, equation II–32. Equation II–31 accounts for changes in $\mathcal{D}_{O_2}$ as a function of position for steady-state oxygen diffusion and reaction. Unfortunately, it is not known how significant these changes are with respect to the overall oxygen transport through the film.

Because the estimation of $\mathcal{D}_{O_2}$ required several different experiments and studies, this chapter is divided into several sections. The first section discusses the relationship between measured r_{CA} and r_{O_2}, since r_{O_2} is required to estimate $\mathcal{D}_{O_2}$. The second section extends the η_0^*-CA relationship to other temperatures since laboratory experiments were conducted at several elevated temperatures. For highway-pavement simulation at variable temperatures, changes in rheological properties as a result of aging over the range of service temperatures must be predictable. The third section details the POV experiments with known asphalt film thickness. From the data, it was possible to estimate the oxygen partial pressure at the substrate interface, SI, based on measured r_{CA} and the kinetic parameters from Chapter IV. The fourth

section explains the estimation of $\mathcal{D}_{O_2}$ or the parameters relating $\mathcal{D}_{O_2}$ to η_o^* and temperature. These parameter estimations involved numerical integration techniques along with trial and error root finding methods. The estimated $\mathcal{D}_{O_2}$ parameters are used to calculate *CA* and oxygen profiles in the film. *CA* profiles are compared with measured *CA* at the *ES* and *SI*. Including oxygen diffusion and reaction in an asphalt aging test is also studied. Finally, the effect of solubility of oxygen in asphalt on estimated parameters is discussed.

Relationship between r_{O_2} and r_{CA}

An estimation of the r_{O_2} in terms of r_{CA} is required to estimate $\mathcal{D}_{O_2}$ in an asphalt. For the initial non-linearity, both the carbonyl and sulfoxide regions grow with aging as shown by infrared analysis; however, only carbonyl continues to grow for long-term aging (Martin *et al.*, 1989; Lau *et al.*, 1992, Petersen *et al.*, 1993). Equation II – 10 is a simple linear model relating r_{O_2} to r_{CA}.

$$r_{O_2} = c r_{CA} \qquad \text{(II – 10)}$$

The parameter c is determined from experimental data.

A simple POV aging experiment with one asphalt, SHRP AAA-1, at 344.4 K and 20 atm for 4 and 12 days was designed to obtain the necessary information to estimate c. Neat and aged *CA* and wt% O_2 were measured. Elemental oxygen determinations were performed by LECO and FISON. *CA* and wt% O_2 are given in Table V-1. Figure V-1 shows wt% O_2 from both companies plotted versus *CA*. Although there is a difference in the magnitude of wt% O_2, the change in wt% O_2 for given change in *CA* is the same. This off set is probably due to inaccurate calibration. The slope and the required conversion factors defines the proportionality constant, c.

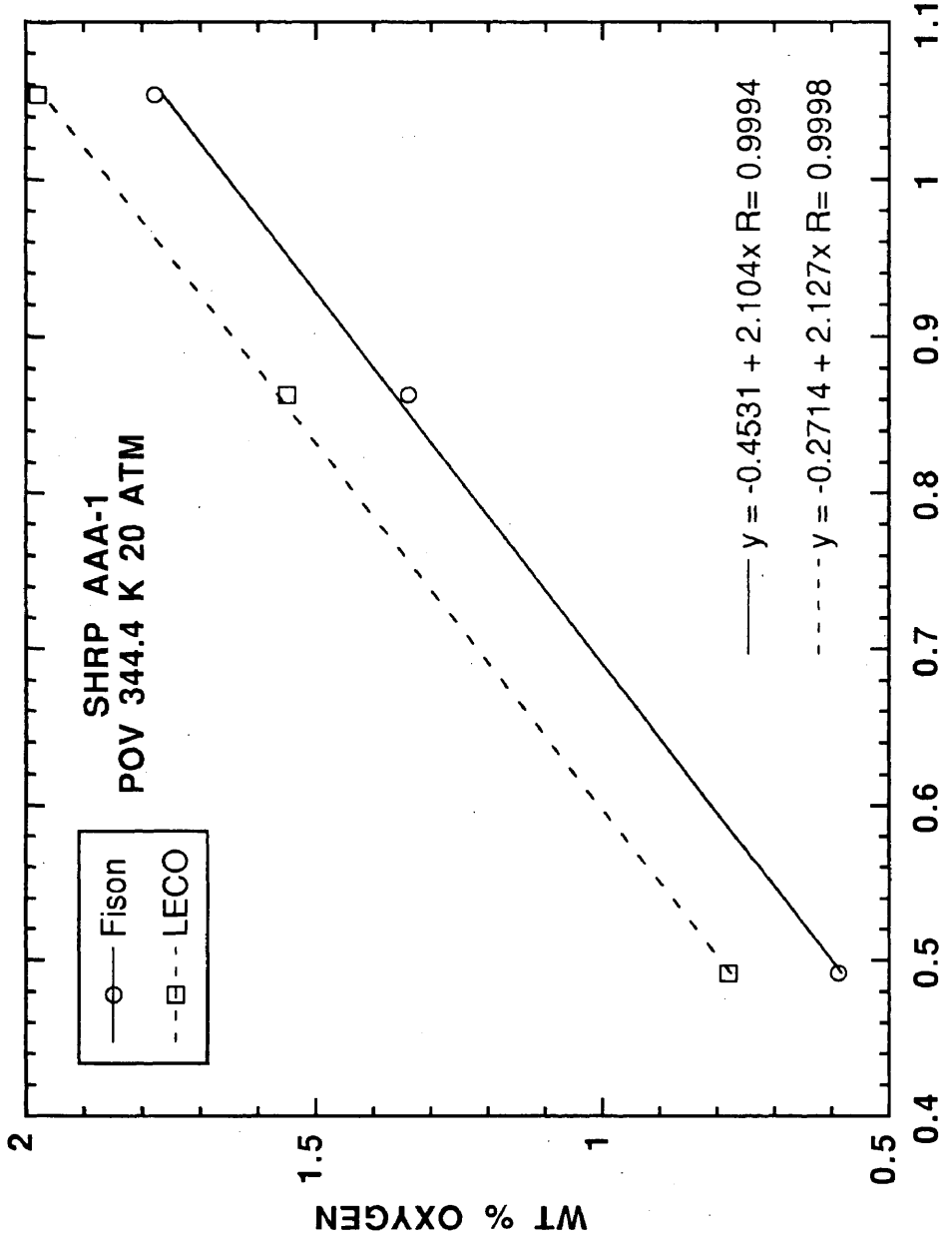

Figure V-1. Wt% O_2 versus CA for neat and POV-aged SHRP AAA-1.

This calculation is given in equation V – 1.

$$c = \left(\frac{d \text{ wt\% } O_2}{d\ CA}\right)\left(\frac{\rho_{\text{Asph}}}{100(MW)_{O_2}}\right) \qquad \text{(V – 1)}$$

where:

$$\rho_{\text{Asph}} = 1.0 \text{ g / mL}$$

$$(MW)_{O_2} = 32 \text{ g / gmol}$$

$$\left(\frac{d \text{ wt\% } O_2}{d\ CA}\right) = 2.1 \text{ g } O_2 \text{ / g Asph } CA$$

Substituting into equation V – 1 gives:

$$c = 6.56 \times 10^{-4} \text{ gmol } O_2 \text{ / mL } CA \qquad \text{(V – 2)}$$

c was determined for only one asphalt. In the present study, the relationship is assumed to be independent of the asphalts studied.

Table V-1. *CA* and Wt% O_2 for Neat and POV-Aged SHRP AAA-1 at 344.4 K and 20 atm

Time days	*CA*	wt%O_2 FISON	wt%O_2 LECO
0	0.492	0.59	0.78
4	0.863	1.34	1.55
12	1.054	1.78	1.98

Since neat material was used in Figure V-1, the *CA*-wt% O_2 relationship does not exhibit an initial non-linearity. This indicates that only a small amount of oxidation may occur with the sulfur compounds. IR absorbance is greater for sulfoxide than carbonyl; however, this is not a measure of the number of chemical bonds present. Sulfoxide may have a higher absorptivity than carbonyl for the same number of bonds accounting for the higher absorption. These conclusions were made on a very limited

set of data. More asphalts need to be studied to further understand the CA-wt% O_2 relationship.

Relationship between HS and m at Different Temperatures

Physicochemical relationships provide a powerful way to characterize asphalts. With these relationships determined for an asphalt, the number of independent measurable properties is decreased. One of the most important physicochemical relationships discovered for asphalt oxidation is given in equation I – 6.

$$\eta_o^* = \exp\Big\{ HS \cdot CA + m \Big\} \qquad (\text{I} - 6)$$

This model was developed from both POV- and field-aged samples for η_o^* measured at 333.3 K, and was independent of the kinetics for POV aging temperatures ranging from 333.3 to 366.7 K. Including both T and CA on η_o^*, equation II–15 was described in Chapter II.

$$\begin{aligned} HS(T) &= HS(T_o) + \gamma\left(\frac{1}{T} - \frac{1}{T_o}\right) \\ m(T) &= m(T_o) + \delta\left(\frac{1}{T} - \frac{1}{T_o}\right) \end{aligned} \qquad (\text{II} - 15)$$

γ and δ are determined from viscosity activation energy, E_V, at given CA. Experimental data are required to estimate the parameters in the model, equation II – 14.

$$E_V = \gamma CA + \delta \qquad (\text{II} - 14)$$

With T_o, $HS(T_o)$, $m(T_o)$, γ, and δ determined, η_o^* at a known CA over a range of temperatures can be calculated.

POV aging of the five neat asphalts of Lau (1992) at 355.5 K and 20 atm for 2, 5, and 13 days produced the required data. RTFO residue was also analyzed. CA and rheological properties of the neat and aged asphalts were measured at 273.2,

283.2, 298.2, and 313.2 K. Since the time-temperature superposition shift factor, a_T, relative to a reference temperature has the same temperature dependence as η_o^* for linear visco-elastic behavior, a_T was calculated from rheological measurements. The reference temperature was 273.2 K for this study. Table C-1 in Appendix C gives CA, a_T relative to 273.2 K, and T for the asphalts studied.

Figure V-2 shows a_T versus $(1\,/\,T)$ with increasing CA for Texaco AC-20. The data suggest that a linear relationship between $\ln a_T$ and $(1/T)$ at given CA, equation II – 21.

$$\ln a_T = E_V\left(\frac{1}{T} - \frac{1}{T_o}\right) \qquad \text{(II – 21)}$$

a_T decreases with increasing T and CA. E_V increases with CA formation. The other asphalts studied support this conclusion from Figures C-1 through C-4 in Appendix C. Neat asphalts with severe hardness problems at low temperature only get worse with aging. However, depending on the E_V-CA relationship, a neat asphalt with superior low temperature properties may actually be far worse than other asphalts after aging. Table V-2 gives E_V and CA for all of the asphalts and aging conditions studied. Although the data in the table show that E_V increases with CA, equation II – 14 further constrains the relationship.

$$E_V = \gamma CA + \delta \qquad \text{(II – 14)}$$

Figure V-3 shows E_V as a function of CA for Texaco AC-20. Symbolized by **X**, the aged data, both RTFO and POV, suggest a linear relationship. Again, an initial non-linearity exists. The neat sample, shown in the solid circle, is significantly lower than the linear estimation from aged data. The RTFO datum is the aged datum with the lowest CA. Also, the model parameters, γ and δ, are shown on the figure. Good estimations exist for Ampet AC-20 and Exxon AC-20. Significant scatter is shown

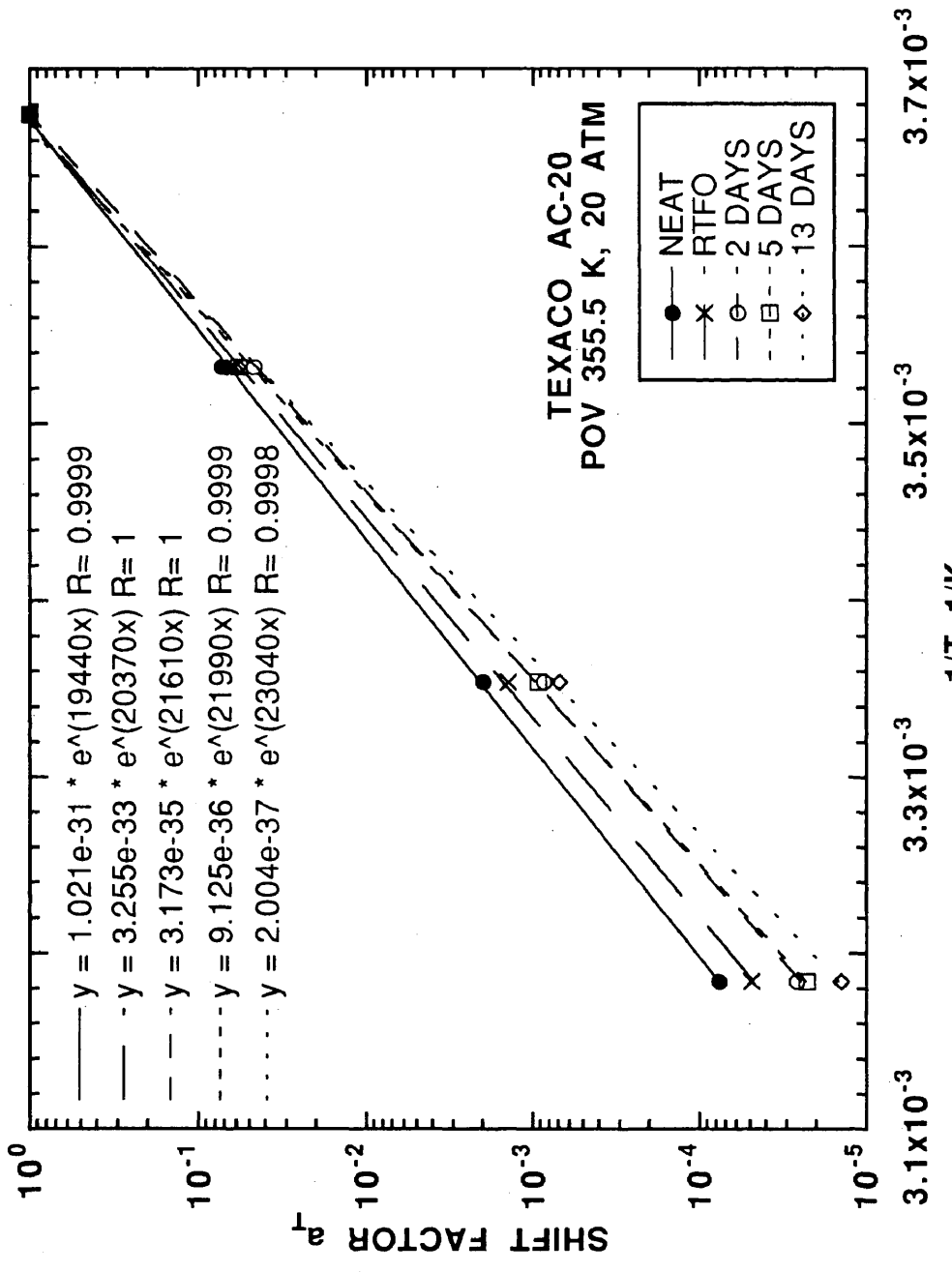

Figure V-2. a_T versus $(1/T)$ for neat and POV-aged Texaco AC-20 with reference temperature of 273.2 K.

Table V-2. CA and E_V for All Neat, RTFO, and POV-Aged Asphalts Studied

Asphalt	Aging	CA	$E_V \times 10^{-3}$ K
Ampet AC-20	Neat	0.452	20.9
	RTFO	0.581	21.4
	2 d[a]	0.890	22.4
	5 d	1.046	22.2
	13 d	1.496	23.3
Coastal AC-20	Neat	0.461	20.7
	RTFO	0.663	21.2
	2 d	1.037	23.1
	5 d	1.224	22.3
	13 d	1.754	23.1
Cosden AC-20	Neat	0.462	21.5
	RTFO	0.637	22.1
	2 d	1.290	21.6
	5 d	1.688	24.8
	13 d	2.385	23.2
Exxon AC-20	Neat	0.450	20.1
	RTFO	0.523	20.9
	2 d	0.953	21.9
	5 d	1.471	22.4
	13 d	1.727	22.5
Texaco AC-20	Neat	0.438	19.4
	RTFO	0.595	20.4
	2 d	0.946	21.6
	5 d	1.130	22.0
	13 d	1.620	23.0

[a] POV at 355.5 K at 20 atm.

for Coastal AC-20 and Cosden AC-20 (Figure V-4), and these asphalts have poor correlation coefficients. In the absence of other experimental data, the parameters will be used in subsequent calculations. Clearly, more data are necessary for better estimates of γ and δ for aged asphalts. Table V-3 summarizes the model parameters for the asphalts studied.

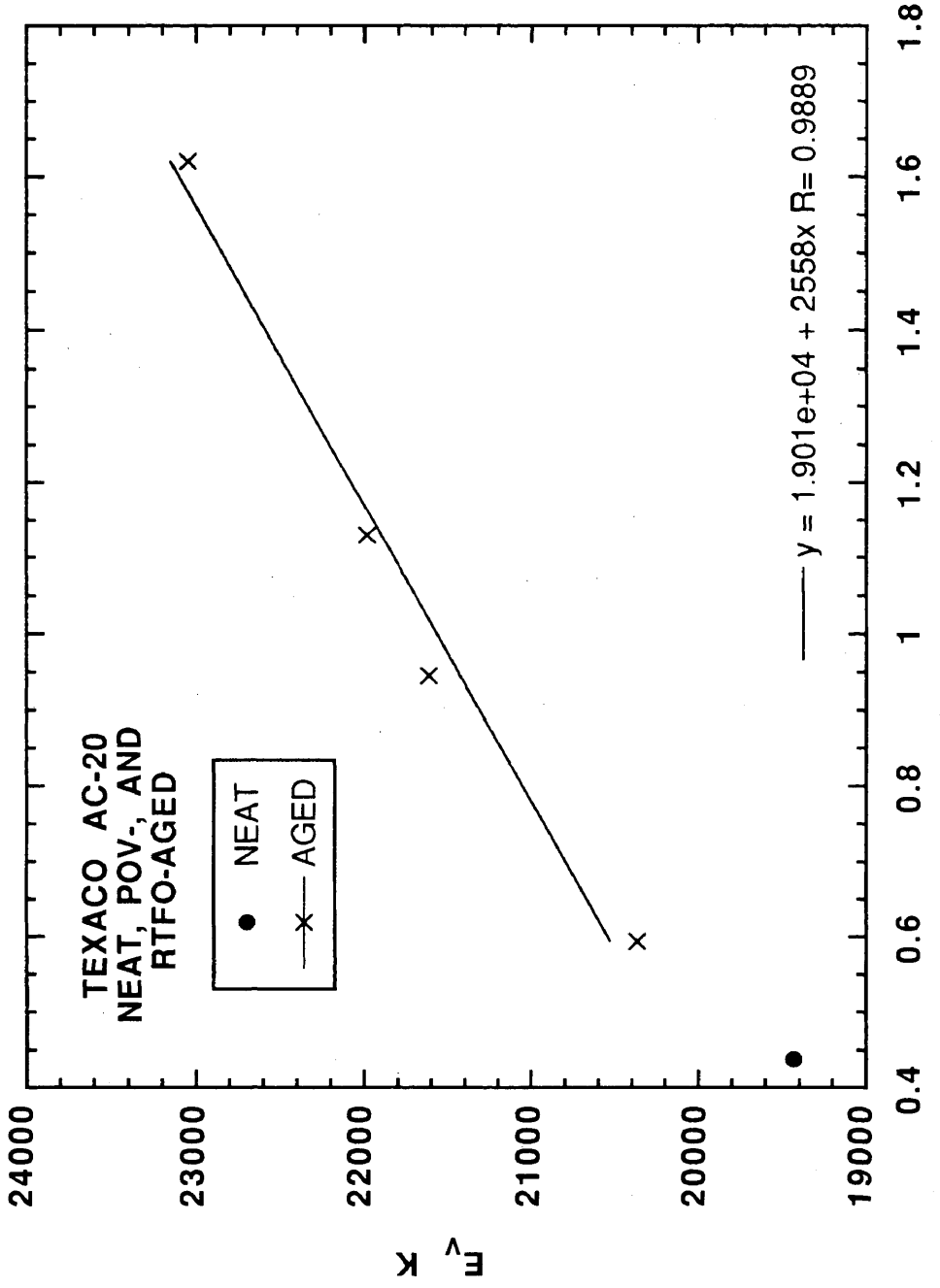

Figure V-3. E_V versus CA for neat, RTFO, and POV-aged Texaco AC-20.

Figure V-4 compares E_V and CA for all of the asphalts studied. Only the aged data are shown, and the neat datum is omitted. E_V for Texaco AC-20 and Ampet AC-20 are most sensitive to CA. Cosden AC-20 is the least sensitive but also has a poor correlation coefficient. For different asphalts, there is over 100% difference in γ compared to only 13% difference in δ. Furthermore, based on the order of magnitude of γ and δ, HS should change very little with temperature compared with m.

Table V-3. E_V Model Parameters for All Asphalts Studied

Asphalt	γ K / CA	δ K
Ampet AC-20	1920	20400
Coastal AC-20	1520	20600
Cosden AC-20	1000	21400
Exxon AC-20	1280	20400
Texaco AC-20	2560	19000

[a] Model: $E_V = \gamma CA + \delta$

With T_o of 333.3 K and $HS(T_o)$ and $m(T_o)$ known from the data of Lau (1991), HS and m at 344.4 and 355.5 K are calculated. These temperatures are outside the range for estimating γ and δ and are extrapolations. POV aging experiments to determine carbonyl formation kinetics and to estimate $\mathcal{D}_{O_2}$ were conducted at these temperatures. The extrapolated HS and $\exp(m)$ are given in Table V-4. As expected, HS is relatively insensitive to changes in temperature compared with $\exp(m)$. Unfortunately, no comparison between measured and extrapolated HS and m was done. Since HS is so insensitive to changes in temperature, Lau *et al.*, (1992) report that HS is independent of temperature from 333.3 K to 298.2 K. A more likely explanation for this conclusion is that η_o^* was not reached in the measurements. The reported η_o^*

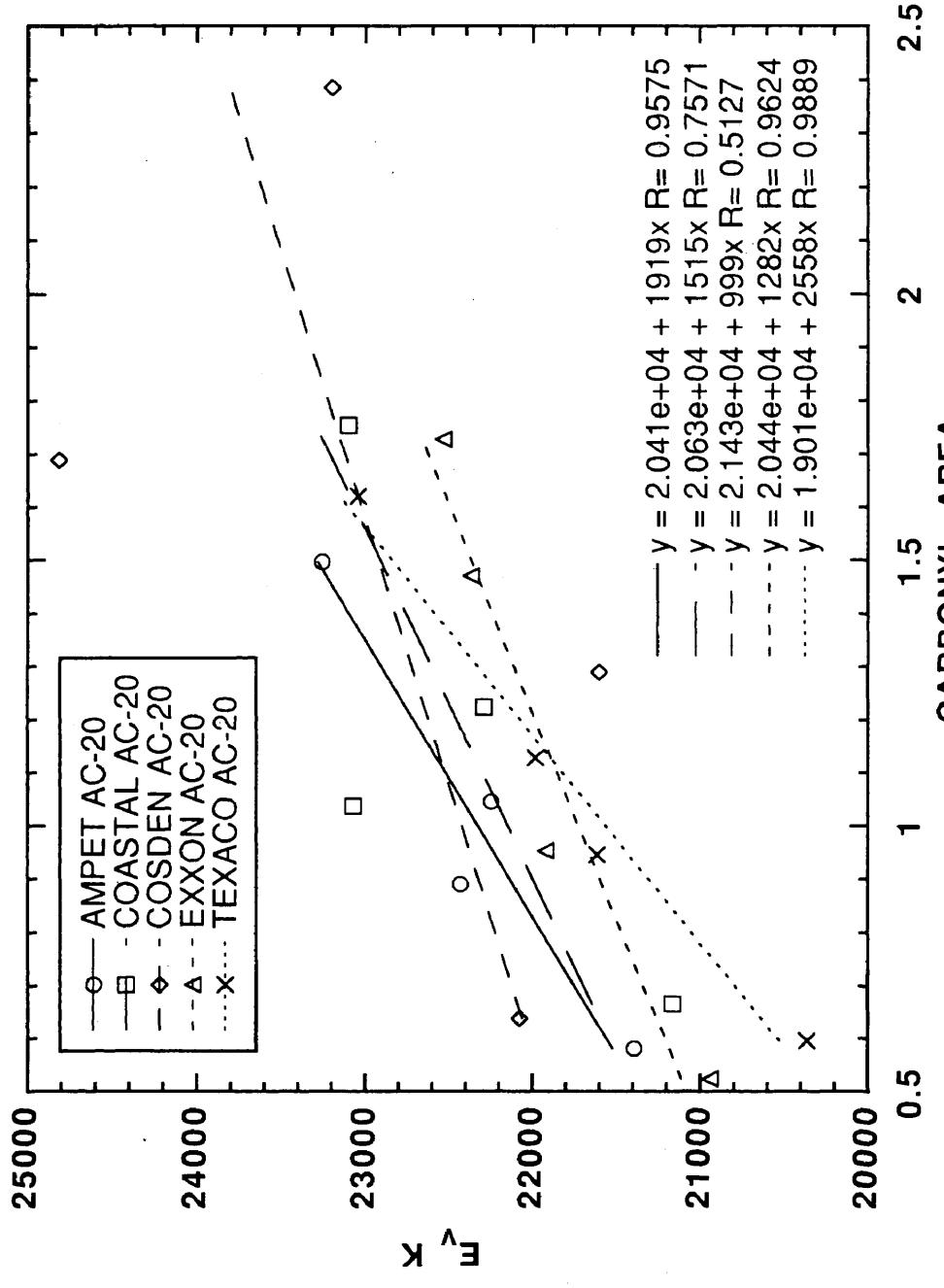

Figure V-4. E_V versus CA for all RTFO and POV-aged asphalts studied.

values at lower temperatures are lower than true η_o^*. The lower reported η_o^* decreases *HS* at the lower temperatures and approaches *HS* at 333.3 K.

Table V-4. *HS* and exp(m) at 333.3, 344.4, and 355.5 K for All POV-Aged Asphalts Studied[a]

Asphalt	333.3 K[b]		344.4 K[c]		355.5 K[c]	
	HS 1 / *CA*	exp(m) p	*HS* 1 / *CA*	exp(m) p	*HS* 1 / *CA*	exp(m) p
Ampet AC-20	3.03	1126	2.84	168.0	2.68	26.8
Coastal AC-20	3.97	655	3.82	95.3	3.69	14.9
Cosden AC-20	2.95	1032	2.85	140.0	2.77	20.4
Exxon AC-20	2.63	1377	2.51	200.0	2.40	31.8
Texaco AC-20	3.39	687	3.14	116.0	2.92	21.0

[a] Model: $\eta_o^* = \exp(m)\exp(HS \cdot CA)$
[b] Measured
[c] Calculated

Similar to *HS* and m, the parameters γ and δ are also physicochemical properties. However, these parameters describe how T and CA affect η_o^* and a_T. This model development was intended to supplement $\mathcal{D}_{O_2}$ estimation, and only preliminary calculations were attempted. A more exhaustive study may lead to asphalt specifications in terms of *HS*, m, γ, and δ.

Determination of P_{SI} from r_{CA}

The boundary conditions for equation II – 30 must be specified to estimate $\mathcal{D}_{O_2}$ in asphalt. At the *ES*, the oxygen pressure is assumed to be equal to that in the gas. At the *SI*, the oxygen pressure gradient is zero since the aluminum tray is assumed to be impermeable to oxygen. In this study, the initial condition specifies zero oxygen pressure in the film. These conditions establish the oxygen pressure profile with a

known $\mathcal{D}_{O_2}$. An infinite number of values of D_{O_2} satisfy the boundary conditions. To estimate a unique $\mathcal{D}_{O_2}$, another condition must be specified. In this study, P_{SI} is the additional constraint. Specifying oxygen pressure as a function of time in addition to the oxygen pressure gradient at the *SI*, yields an initial value problem. A trial and error numerical solution is used to estimate $\mathcal{D}_{O_2}$.

The estimation of P_{SI} required experimental data from POV aging at low oxygen pressure and moderate temperatures. The data set consisted of five AC-20 asphalts of Lau *et al.*, (1992). Three aging temperatures of 333.3, 344.4, and 355.5 K and two oxygen pressures of 0.2 and 2 atm were used. Aging times ranged from 2 to 80 days depending on the aging temperature. These asphalts were studied since kinetic information was already determined in Chapter IV. Pure oxygen was the oxidizer. For air, diffusion of oxygen gas through the nitrogen gas film at the free surface would complicate the analysis. Asphalt films, 1 mm thick, were made by weighing 2.4 grams of material into pre-made aluminum trays as described in Chapter III. For each aging condition, 10 trays per asphalt were used. Carbonyl formation at the *ES* and *SI* of the POV-aged asphalt film was monitored by FTIR. The procedure was described in Chapter III.

The study in Chapter IV showed that equation II – 5 related oxygen pressure and temperature to r_{CA}.

$$r_{CA} = k_P(T)P^{\alpha} \qquad \text{(II – 5)}$$

For isothermal aging and a given asphalt, measured r_{CA} as a function of time can be used to estimate oxygen pressure, P, as a function of time. This idea is applied to the *SI* of the POV-aged asphalt film. P_{SI} is estimated from the difference in the r_{CA} at the *ES* and *SI* through equation II – 5 with pre-determined kinetic parameters.

Tables C-2 through C-11 give *CA* at the *ES* and *SI* for aging pressures of 0.2 and 2 atm and temperatures of 333.3, 344.4 and 355.5 K for all the asphalts studied. Figure V-5 shows *CA* versus aging time for Coastal AC-20 at 333.3 K and 0.2 atm oxygen pressure. *ES*, *SI*, and neat data are designated by hollow circles, hollow squares, and a solid circle, respectively. For both *ES* and *SI*, the data show an initial non-linearity from the neat datum followed by a linear relationship between *CA* and time. The linear model for the *ES* is shown in the solid line. The linear model for the *SI* is shown with the dashed line. Similarly, for Coastal AC-20 at 333.3 K and 2.0 atm, Figure V-6 shows similar phenomena. At higher aging temperatures of 344.4 K, Figures V-7 and V-8 show *CA* versus time for Coastal AC-20 at 0.2 and 2.0 atm, respectively. For the highest experimental aging temperature of 355.5 K, *CA* of Coastal AC-20 at 0.2 and 2.0 atm versus time are given in Figures V-9 and V-10.

The following conclusions are drawn from all these figures. After an initial non-linearity, a linear model, equation I – 2, for long-term aging describes both *ES* and *SI*. Carbonyl content at the *SI* is lower than that at the *ES*, holding all other aging variables constant. From the model parameters reported in the figures, the r_{CA} at the *SI* is less than the r_{CA} at the *ES* for a given aging condition. The conclusion that both *CA* and r_{CA} at the *SI* are lower than that at the *ES* strongly suggests an oxygen pressure gradient in the film. There appears to be quite a bit of scatter in the *CA* measurement for both the *ES* and *SI*. Except for Cosden AC-20 at 0.2 atm, 355.5 K shown in Figure C-13, similar conclusions are drawn from careful review of Figures C-5 through C-28 for the other asphalts studied. In Figure C-13, r_{CA} at the *SI* is higher than that at the *ES*. This anomaly probably resulted from errors in *CA* measurements and was discarded from further analysis.

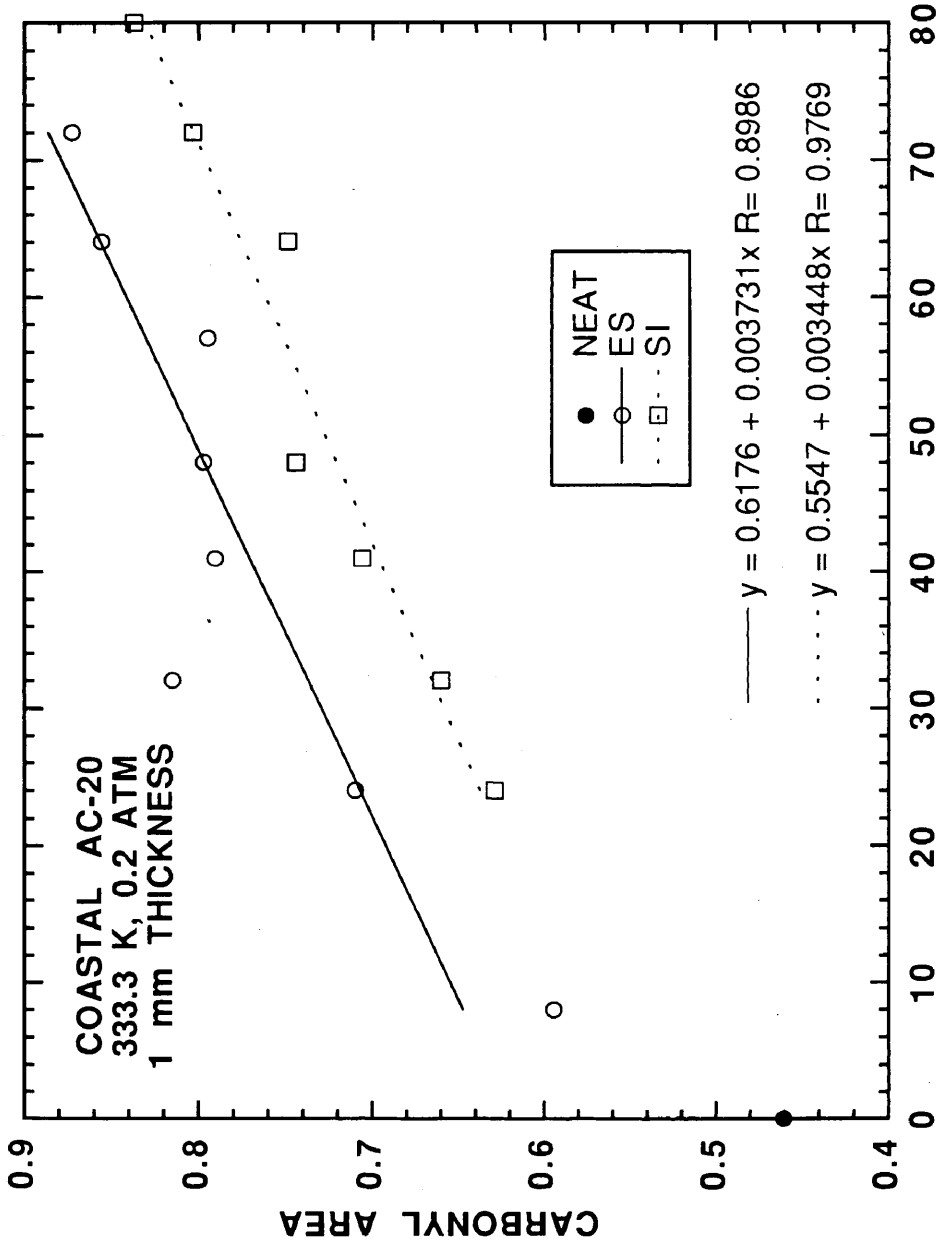

Figure V-5. CAs of neat and at the ES and SI for 1 mm thick films of POV-aged Coastal AC-20 at 333.3 K and P_{ES} of 0.2 atm.

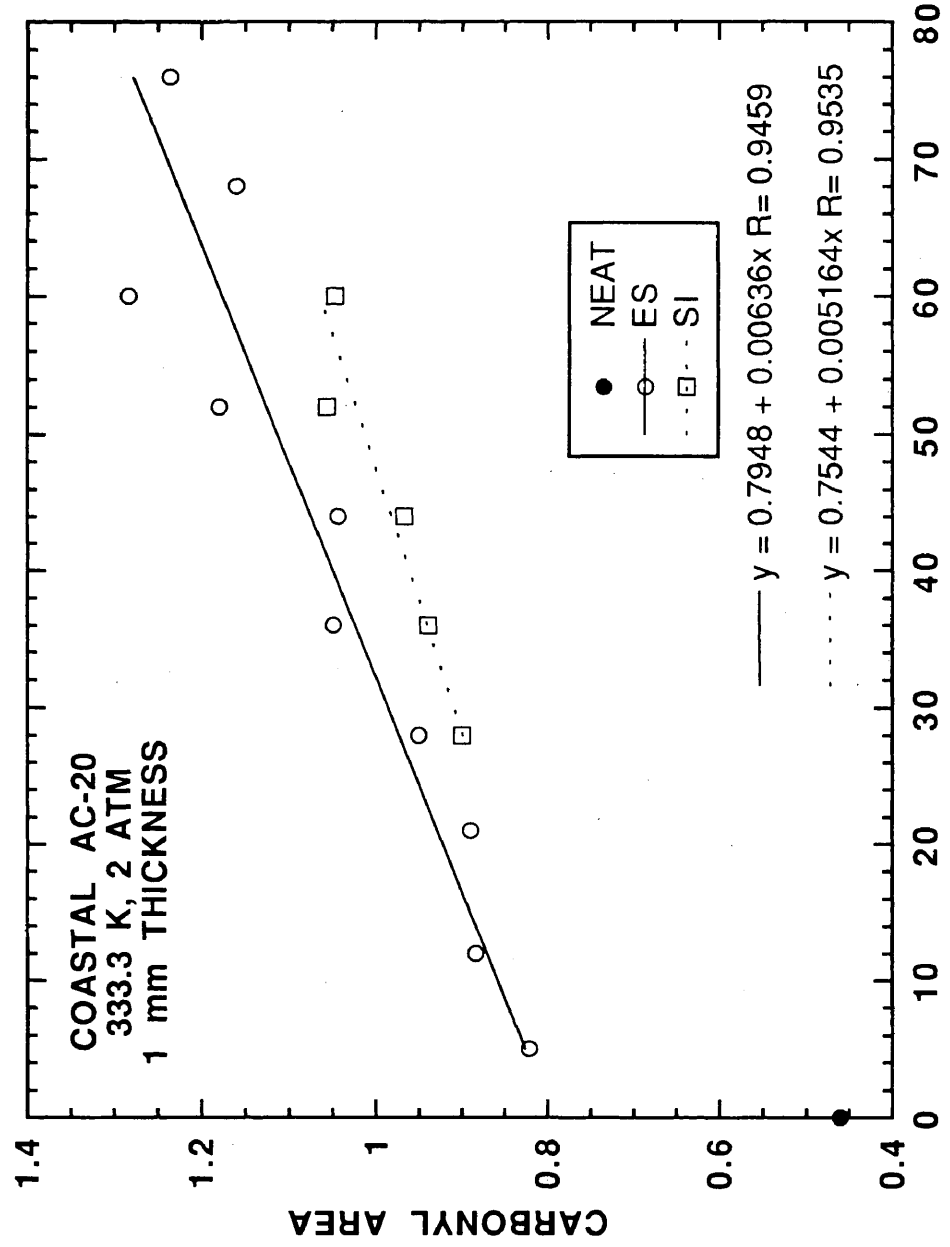

Figure V-6. CAs of neat and at the ES and SI for 1 mm thick films of POV-aged Coastal AC-20 at 333.3 K and P_{ES} of 2 atm.

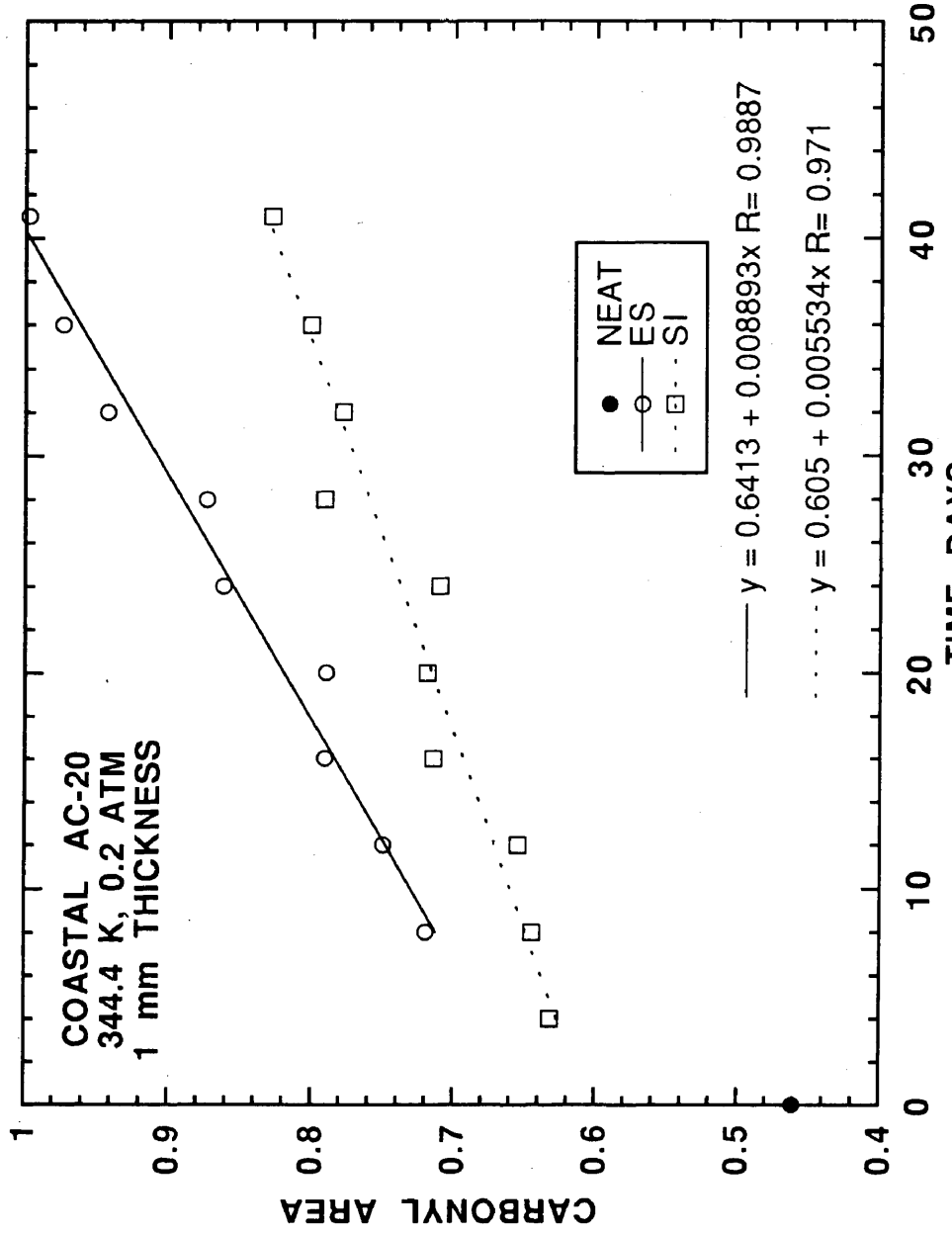

Figure V-7. CAs of neat and at the ES and SI for 1 mm thick films of POV-aged Coastal AC-20 at 344.4 K and P_{ES} of 0.2 atm.

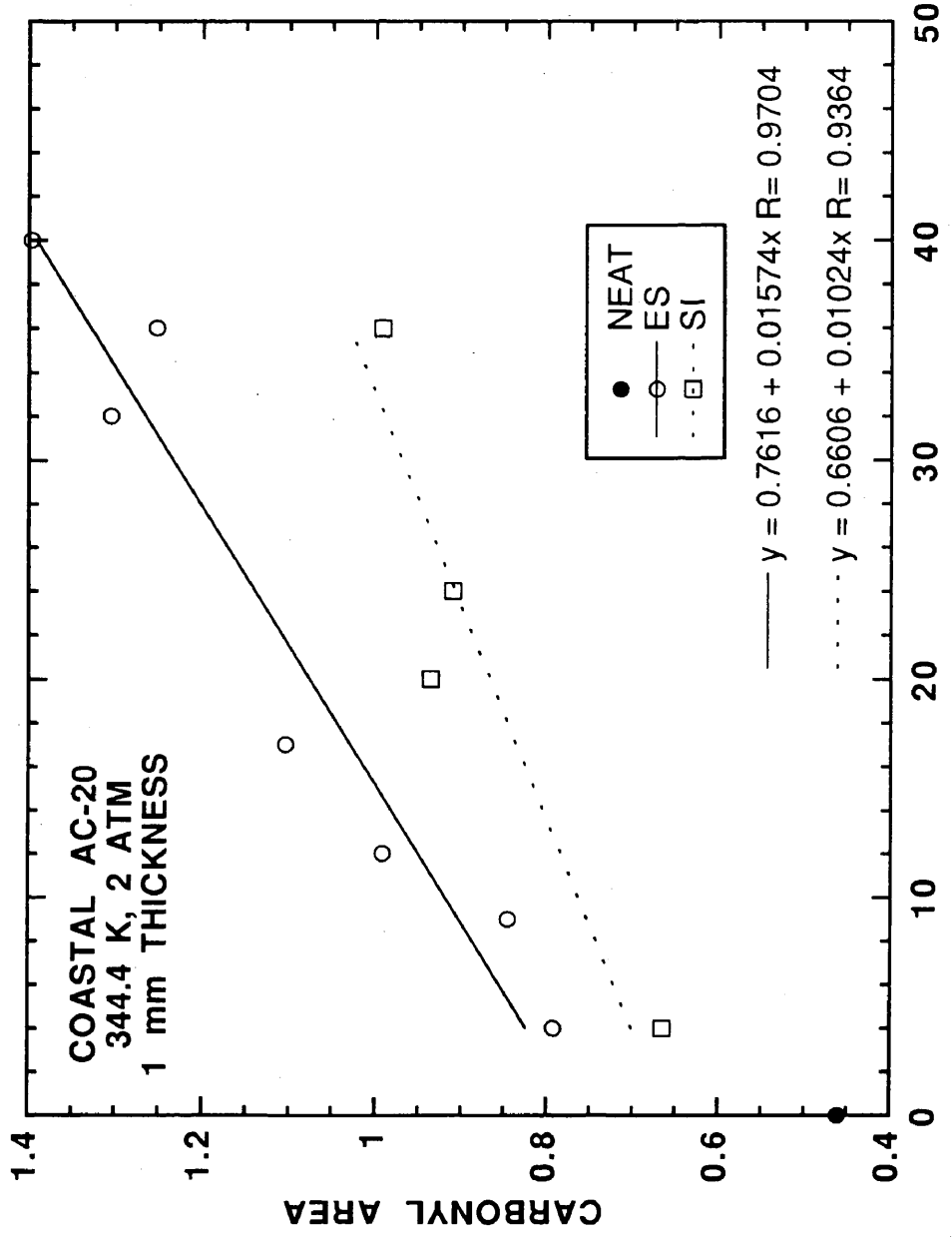

Figure V-8. CAs of neat and at the ES and SI for 1 mm thick films of POV-aged Coastal AC-20 at 344.4 K and P_{ES} of 2 atm.

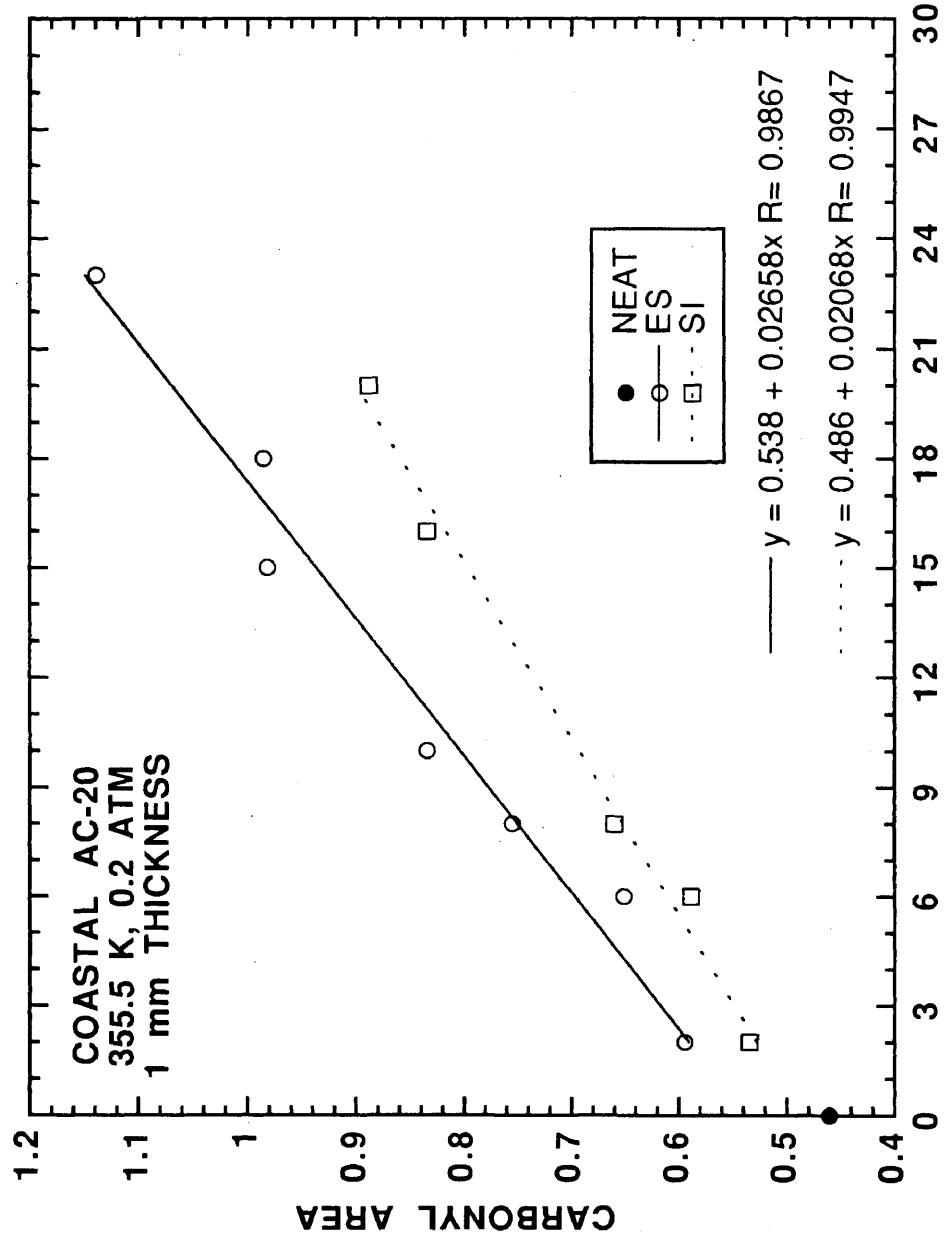

Figure V-9. CAs of neat and at the ES and SI for 1 mm thick films of POV-aged Coastal AC-20 at 355.5 K and P_{ES} of 0.2 atm.

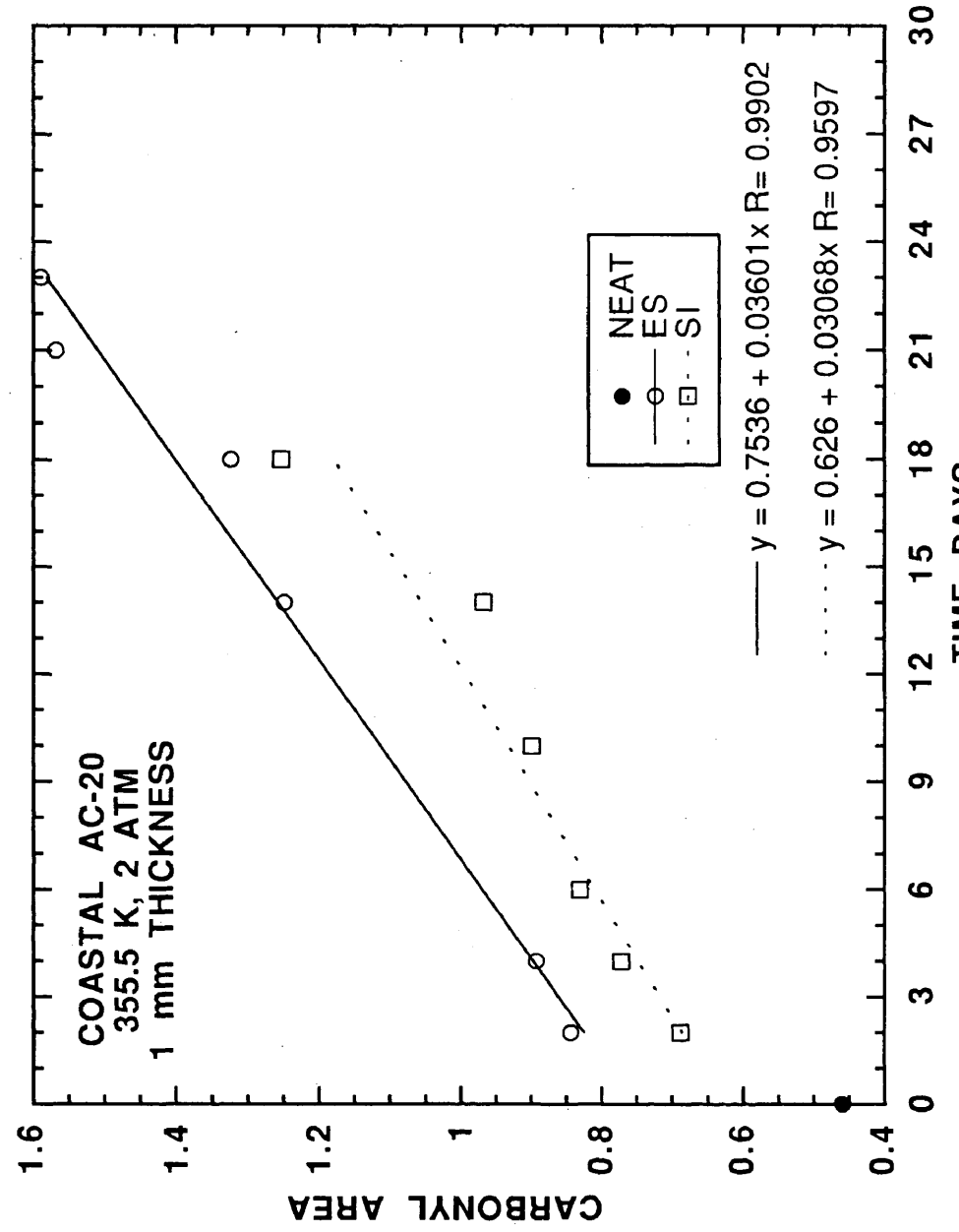

Figure V-10. CAs of neat and at the ES and SI for 1 mm thick films of POV-aged Coastal AC-20 at 355.5 K and P_{ES} of 2 atm.

The conclusion that r_{CA} at both the *ES* and *SI* is constant for long-term isothermal aging, suggests that oxygen pressure at the *ES* and *SI* is also constant reducing equation II – 30 to II – 31.

$$\left(\frac{\partial P}{\partial t}\right) = 0 \qquad \text{(V – 3)}$$

This steady-state assumption is probably valid, at least as a preliminary estimate, for the experimental temperatures and film thicknesses. The degree of scatter in *CA* at the *SI* is such that more complex models, estimating the decrease in r_{CA} with time because of oxygen diffusion limitations, would be impractical. Even equation I – 5 does not account for decreasing r_{CA} with increasing time from diffusion resistance.

There is scatter in both *SI* and *ES* carbonyl measurements. The degree of scatter in *CA* at the *SI* is larger compared to the *ES*. This scatter obviously makes the analysis more difficult, and the measurement technique probably accounts for a significant portion of the error. First, to obtain true *SI* measurements, the aluminum backing must be cleanly removed without any trace of asphalt. This clean removal was not always possible. Trace asphalt remaining on the aluminum tray results in *SI* measurements being closer than 1 mm from the *ES*; therefore, the true difference in *CA* at the *ES* and *SI* may actually be greater than the reported difference. No systematic corrections accounted for how clean the aluminum backing was removed from the film. Second, care was taken not to damage the two prisms during the compression of the asphalt samples. The contact on the second prism in the analysis of the *SI* was not always as precise as desired. Insufficient contact lowers the IR energy absorbed by the asphalt sample producing lower *CA* than actual. The inability to cleanly remove the aluminum backing produces a higher than actual *CA* at the *SI*, and imprecise contact with the prism produces lower than actual *CA* at the *SI*.

From analyzing approximately 10 films per asphalt per aging experiment, these errors should cancel each other. Therefore, the average constant r_{CA} at the *SI* is probably a good estimate, even with the scatter. The *ES* scatter probably results from the displayed range for the data. For example, Figure V-5 shows a *CA* range from 0.4 to 0.9, and one would conclude that there is terrible scatter in the *ES* carbonyl measurement. This same set of data is also used in the kinetic parameter estimations in Figures B-4 and B-16. The scatter in these figures appears less significant since the range of *CA* is from 0.4 to 1.8 and 0.4 to 1.2, respectively.

Tables V-5 and V-6 contain r_{CA} and CA_o at the *ES* and *SI* for all aging conditions and asphalts studied. The tables are not used for comparisons. More importantly, oxygen pressure at the *SI* are estimated from the r_{CA} data. From measured r_{CA} at the *ES* and *SI* and known oxygen pressure at the *ES*, equation II – 5 calculates the average effective oxygen pressure at the *SI*.

$$r_{CA} = k_P(T)P^{\alpha} \qquad \text{(II – 5)}$$

Equation II – 5 is applied at the *ES* and *SI* of an asphalt film.

$$\begin{aligned} &\text{Exposed Surface} && (r_{CA})_{ES} = k_P(P_{ES})^{\alpha} \\ &\text{Substrate Interface} && (r_{CA})_{SI} = k_P(P_{SI})^{\alpha} \end{aligned} \qquad \text{(V – 4)}$$

For isothermal aging in the film and a given asphalt, k_P is constant. Equation V – 4 is combined yielding equation V – 5.

$$\frac{(r_{CA})_{SI}}{(r_{CA})_{ES}} = \left(\frac{P_{SI}}{P_{ES}}\right)^{\alpha} \qquad \text{(V – 5)}$$

Rearranging equation V – 5, P_{SI} is determined from measured r_{CA} at each surface, α, and P_{ES}.

$$P_{SI} = P_{ES}\left(\frac{(r_{CA})_{SI}}{(r_{CA})_{ES}}\right)^{1/\alpha} \qquad \text{(V – 6)}$$

Table V-5. r_{CA} at the *ES* and *SI* for 1 mm Thick Films of All Asphalts and POV-Aging Conditions Studied

	$r_{CA} \times 10^3$ at P_{ES} of 0.2 atm						$r_{CA} \times 10^3$ at P_{ES} of 2 atm					
	333.3 K *CA*/day		344.4 K *CA*/day		355.5 K *CA*/day		333.3 K *CA*/day		344.4 K *CA*/day		355.5 K *CA*/day	
Asphalt	*ES*	*SI*	*ES*	*SI*	*ES*	*SI*	*ES*	*SI*	*ES*	*SI*	*ES*	*SI*
Ampet AC-20	3.234	2.410	7.126	6.138	18.68	17.62	6.790	4.375	14.56	11.58	34.47	33.48
Coastal AC-20	3.373	3.448	8.894	5.534	26.58	20.68	6.360	5.164	15.74	10.24	36.01	30.68
Cosden AC-20	4.746	2.920	11.41	10.15	23.65	28.81	9.122	7.433	19.84	12.51	40.23	37.11
Exxon AC-20	4.191	4.045	7.884	6.669	19.74	15.29	8.110	6.891	13.90	12.02	32.48	31.85
Texaco AC-20	3.653	3.208	7.779	6.681	18.62	17.81	6.035	5.458	14.80	10.55	28.14	24.96

Table V-6. CA_o at the *ES* and *SI* for 1 mm Thick Films of All Asphalts and POV-Aging Conditions Studied

	CA_o at P_{ES} of 0.2 atm						CA_o at P_{ES} of 2 atm					
	333.3 K *CA*		344.4 K *CA*		355.5 K *CA*		333.3 K *CA*		344.4 K *CA*		355.5 K *CA*	
Asphalt	*ES*	*SI*	*ES*	*SI*	*ES*	*SI*	*ES*	*SI*	*ES*	*SI*	*ES*	*SI*
Ampet AC-20	0.669	0.514	0.646	0.576	0.605	0.554	0.730	0.756	0.671	0.686	0.748	0.633
Coastal AC-20	0.618	0.555	0.641	0.605	0.538	0.486	0.795	0.754	0.762	0.661	0.754	0.626
Cosden AC-20	0.667	0.603	0.638	0.518	0.649	0.425	0.839	0.832	0.757	0.759	0.819	0.709
Exxon AC-20	0.699	0.543	0.720	0.606	0.770	0.735	0.863	0.781	0.782	0.786	0.802	0.668
Texaco AC-20	0.542	0.494	0.580	0.504	0.556	0.486	0.698	0.627	0.665	0.671	0.728	0.584

P_{SI} was calculated two different ways using r_{CA} data. For the first calculation, α was different for each asphalt, Table IV-6, and calculated P_{SI} are reported in Table V-7. α was 0.27 in the second calculation for all the asphalts, Table V-8. The percent difference for the two calculations is given in Table V-9. The maximum percent difference is only 10%. From the small difference, P_{SI} for α of 0.27 was used in subsequent calculations.

The $(r_{CA})_{SI}$ precision and how it related to calculated P_{SI} was studied. If P_{ES} and $(r_{CA})_{ES}$ are assumed to have zero variability, the total differential of P_{SI} is given in equation V – 7.

$$dP_{SI} = P_{ES}\left(\frac{1}{\alpha}\right)\left(\frac{(r_{CA})_{SI}}{(r_{CA})_{ES}}\right)^{1/\alpha}\left(\frac{d(r_{CA})_{SI}}{(r_{CA})_{SI}}\right) \qquad (V-7)$$

Substituting equation V – 6, P_{ES} is eliminated yielding equation V – 8.

$$\frac{dP_{SI}}{P_{SI}} = \left(\frac{1}{\alpha}\right)\left(\frac{d(r_{CA})_{SI}}{(r_{CA})_{SI}}\right) \qquad (V-8)$$

With α of 0.27, equation V – 8 shows that small variability in $(r_{CA})_{SI}$ magnifies to large variability in P_{SI}. For example a 10% error in $(r_{CA})_{SI}$ results in a 37% error in P_{SI}. From equation V – 7, very accurate determinations of $(r_{CA})_{SI}$ are required to calculate P_{SI}.

The values of P_{SI} are physically consistent since P_{SI} is less than P_{ES} holding all other aging variables constant. This conclusion does not mean that all the data are correct. For isothermal aging conditions, increasing P_{ES} also increases P_{SI}. For example, Coastal AC-20 at 333.3 K with P_{ES} of 0.2 atm has P_{SI} of 0.149 atm. Increasing P_{ES} to 2 atm at the same temperature yields P_{SI} of 0.925 atm. Increasing P_{ES} appears to suppress the oxygen pressure gradient in the film. This is one of the reasons previous POV research was conducted at 20 atm. Again, one would conclude

Table V-7. Estimated P_{SI} Based on r_{CA} for 1 mm Thick Films of All Asphalts and POV-Aging Conditions Studied and Asphalt Specific α

Asphalt	α	P_{SI} at P_{ES} of 0.2 atm atm			P_{SI} at P_{ES} of 2 atm atm		
		333.3 K	344.4 K	355.5 K	333.3 K	344.4 K	355.5 K
Ampet AC-20	0.285	0.0713	0.118	0.163	0.428	0.896	1.80
Coastal AC-20	0.266	0.149	0.0336	0.0778	0.914	0.398	1.10
Cosden AC-20	0.270	0.0331	0.130	–	0.937	0.363	1.48
Exxon AC-20	0.255	0.174	0.104	0.0734	1.06	1.13	1.85
Texaco AC-20	0.250	0.119	0.118	0.167	1.34	0.516	1.24

Table V-8. Estimated P_{SI} Based on r_{CA} for 1 mm Thick Films of All Asphalts and POV-Aging Conditions Studied and α of 0.270

Asphalt	P_{SI} at P_{ES} of 0.2 atm atm			P_{SI} at P_{ES} of 2 atm atm		
	333.3 K	344.4 K	355.5 K	333.3 K	344.4 K	355.5 K
Ampet AC-20	0.0673	0.115	0.161	0.393	0.857	1.80
Coastal AC-20	0.149	0.0345	0.0789	0.925	0.408	1.105
Cosden AC-20	0.0331	0.130	–	0.937	0.363	1.48
Exxon AC-20	0.175	0.108	0.0775	1.09	1.17	1.86
Texaco AC-20	0.124	0.122	0.170	1.39	0.570	1.28

Table V-9. Percent Difference in Estimated P_{SI} for Asphalt Specific α and α of 0.270[a]

Asphalt	% Diff for P_{ES} at 0.2 atm			% Diff for P_{ES} at 2 atm		
	333.3 K	344.4 K	355.5 K	333.3 K	344.4 K	355.5 K
Ampet AC-20	-5.6	-2.9	-1.1	-8.2	-4.4	-0.57
Coastal AC-20	0.44	2.7	1.4	1.2	2.4	0.90
Exxon AC-20	0.78	3.7	5.7	3.6	3.2	0.43
Texaco AC-20	3.9	4.0	1.3	3.0	10.6	3.6

[a] $\%\ \text{Diff} = 100 \times \left(\frac{P_{SI}(0.270) - P_{SI}(\alpha)}{P_{SI}(\alpha)} \right)$

Cosden AC-20 is not reported since the difference is zero.

that the data are correct. However, for isobaric aging conditions, inconsistencies in the data are more apparent. Consider the data at 2 atm. Coastal AC-20, Cosden AC-20, and Texaco AC-20 have lower P_{SI} at 344.4 than 333.3 K. Both P_{SI} at 344.4 and 355.5 K are lower than P_{SI} at 333.3 K for Texaco AC-20. Consider the data at 0.2 atm. Both Coastal AC-20 and Exxon AC-20 show lower P_{SI} at 344.4 and 355.5 K than at 333.3 K. P_{SI} at 333.3 and 344.4 K is virtually the same for Texaco AC-20. One concludes that diffusion problems are more severe at higher temperature holding all other variables constant from these data. This conclusion is probably incorrect. At this point, none of the calculated P_{SI} are discarded. It is difficult to conclude exactly what data are erroneous because simultaneous diffusion and reaction occurs in the film. All P_{SI} data will be used to estimate $\mathcal{D}_{O_2}$.

In Chapter IV, an attempt to relate CA_o and P led to the development of equation IV – 2.

$$CA_o = sP^{\beta} \qquad \text{(IV – 2)}$$

Surprisingly, this relationship was independent of T. The parameters were dependent on composition as reported in Table IV-9. Incorporating the data at the *SI* from Table V-6 for CA_o and Table V-8 for P_{SI} with the data from the kinetics in Chapter IV produces a larger data set. Using this larger set, the ability of equation IV – 2 to model CA_o as a function of P is studied.

Using $(CA_o)_{SI}$ and P_{SI} in equation IV – 2 is complicated by the oxygen transport problem. Initially, there is a transient period when P_{SI} changes with time. $(CA_o)_{SI}$ does not account for the transient period since the parameter is based on long-term steady-state carbonyl formation. Using all $(CA_o)_{SI}$ data may not give reliable determinations of P_{SI}. From Table V-6, $(CA_o)_{SI}$ is usually lower than

$(CA_o)_{ES}$ because of lower P. However, Ampet AC-20 at P_{ES} of 2 atm and 333.3 and 344.4 K show higher CA_o at the SI than the ES. For P_{ES} of 2 atm, 344.4 K, all of the asphalts except Coastal AC-20 show higher $(CA_o)_{SI}$ than $(CA_o)_{ES}$. This is probably due to the initial transient at the SI.

P_{ES}, P_{SI} for α of 0.27, $(CA_o)_{ES}$, and $(CA_o)_{SI}$ for all of the asphalts studied are given in Table C-12 in Appendix C. $(CA_o)_{SI}$ denoted with an asterisk are unrealistic because of reasons described in the previous paragraph. These were omitted in the parameter estimation. Figure V-11 shows CA_o as a function of P for all asphalts studied. P_{ES} was measured; P_{SI} was calculated. The estimated parameters are given on the figure and in Table V-10.

Table V-10. CA_o Model Parameters from Measured and Estimated P for All POV-Aged Asphalts and Conditions Studied[a]

Asphalt	s CA / atm$^{\beta}$	β
Ampet AC-20	0.652	0.063
Coastal AC-20	0.704	0.113
Cosden AC-20	0.805	0.104
Exxon AC-20	0.740	0.097
Texaco AC-20	0.612	0.098

[a] Model: $CA_o = sP^{\beta}$

The larger data set reduces the differences between asphalts, comparing the estimated parameters in Table IV-9 for P_{ES} and Table V-10 for P_{ES} and P_{SI}. s changed very little from Table IV-9 to V-10. However, β for Ampet AC-20 and Cosden AC-20 changed significantly. β doubled for Ampet AC-20 and decreased by one-third for Cosden AC-20. From Table V-10, there are two distinct groups. Ampet

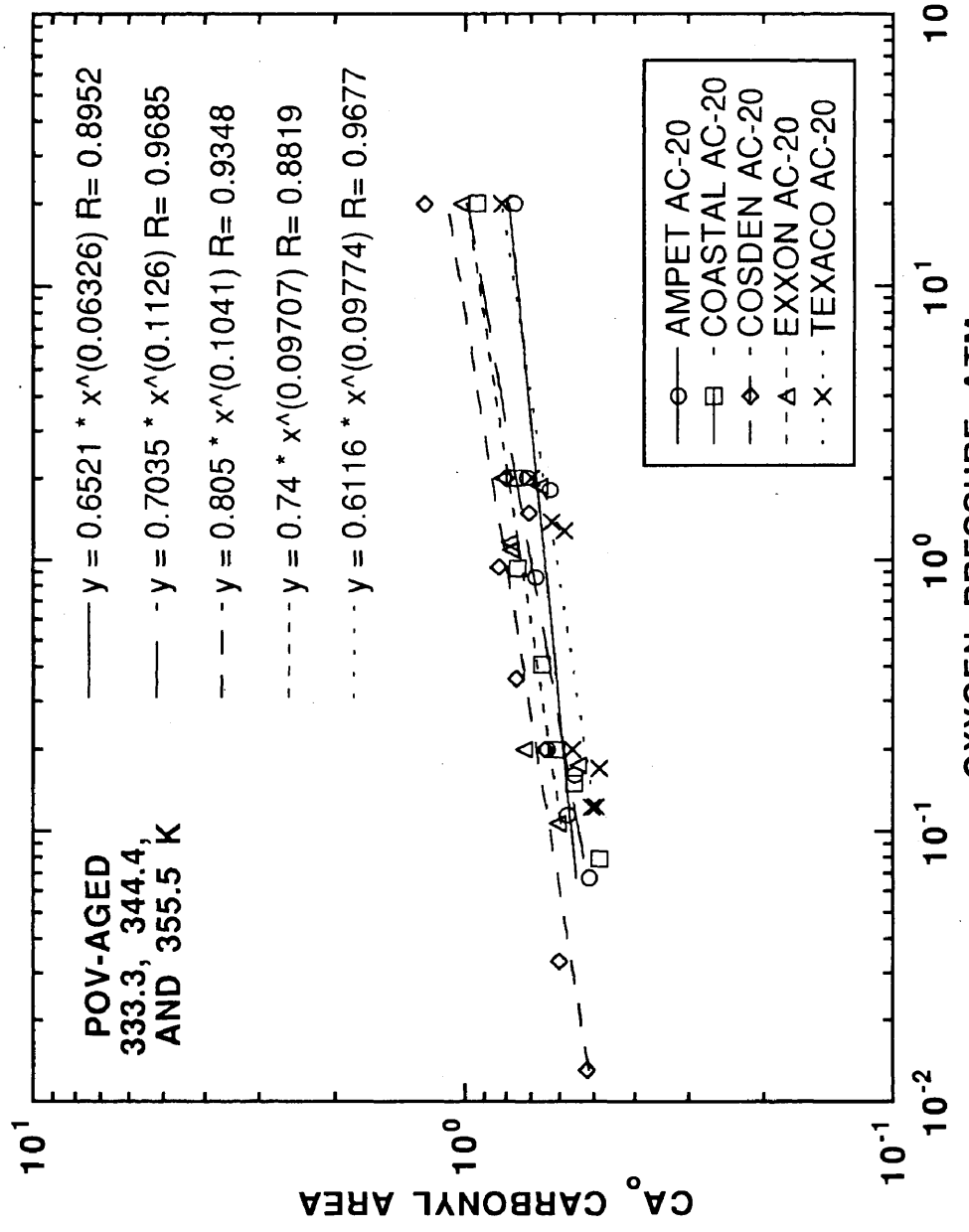

Figure V-11. CA_o versus measured and estimated P for all POV-aged asphalts studied.

AC-20 is one group, and the other asphalts studied is another. The asphalt specific parameters are used in subsequent calculations because equation IV – 2 is empirical. No parameter estimation for the entire data set of all asphalts studied was attempted.

Using r_{CA} at the *ES* and *SI* along with pre-determined kinetic parameters, P_{SI} was estimated. A steady-state assumption for long-term aging was used, and a linear model represented the data. Very precise and accurate r_{CA} were required to determine P_{SI} since α is small. Unfortunately, *CA* data showed significant scatter, and some P_{SI} were physically inconsistent. The difficult technique of measuring *CA* at the *SI* contributed to the scatter. Calculated P_{SI} and $(CA_o)_{SI}$ were used to estimate parameters in equation IV – 2. With these extra data, the model relating CA_o to P appeared to be less sensitive to composition. Determining P_{SI} provides a necessary constraint to estimate a unique $\mathcal{D}_{O_2}$ based on equation II – 30.

Estimation of Oxygen Diffusivity

The previous sections developed relationships between measurable quantities and fundamental variables in an oxygen diffusion and reaction model. For example, r_{O_2} is related to r_{CA} through equation II – 10. η_o^* is expressed as an explicit function of *CA* and T, equations I – 6, II – 14, and II – 15. P_{SI} is estimated from r_{CA} and pre-determined kinetic parameters, equation V – 6, for POV-aged asphalt films. These relationships are required to achieve the main objective, the estimation of $\mathcal{D}_{O_2}$ in asphalt films. From Chapter II, equation II – 30 accounts for oxygen in a differential volume of asphalt for one-dimensional oxygen transport.

$$\left(\frac{\partial P}{\partial t}\right) = \left(\frac{\partial \mathcal{D}_{O_2}}{\partial x}\right)\left(\frac{\partial P}{\partial x}\right) + \mathcal{D}_{O_2}\left(\frac{\partial^2 P}{\partial x^2}\right) - \left(\frac{cRT}{h}\right) r_{CA} \qquad \text{(II – 30)}$$

The boundary conditions are based on the experimental conditions.

$\left(\frac{\partial P}{\partial x}\right) = 0$	at	$x = 0$	Substrate interface
$P = P_{ES}$	at	$x = L$	Exposed surface
$P = 0$	at	$t = 0$	Initial condition

The previous conditions do not provide enough constraints to uniquely determine $\mathcal{D}_{O_2}$. An infinite number of $\mathcal{D}_{O_2}$ values satisfy the conditions. One further constraint, P_{SI}, yields a unique determination of $\mathcal{D}_{O_2}$. In the absence of reliable oxygen solubility data, h is assumed to be unity.

A brief outline of the research strategy is provided. Simplifying assumptions reduce the complexity of equation II–30 for initial estimations of $\mathcal{D}_{O_2}$. First, a steady-state assumption is made. This reduces the partial differential equation, PDE, to an ordinary differential equation, ODE. A detailed discussion of the numerical integration with variable transformation to estimate $\mathcal{D}_{O_2}$ is provided. Along with steady-state, constant $\mathcal{D}_{O_2}$ that is independent of position is assumed. These conditions represent the least complex parameter estimation problem.

Then, a model relating $\mathcal{D}_{O_2}$ to η_o^* is developed from estimations of constant $\mathcal{D}_{O_2}$. This model is used in a steady-state, variable $\mathcal{D}_{O_2}$, oxygen diffusion and reaction model. Pressure profiles in an asphalt film are calculated. Finally, an unsteady-state variable $\mathcal{D}_{O_2}$ oxygen diffusion and reaction model, equation II – 30, is solved. With this numerical solution, calculated CA at the SI and ES are compared to the measured CA. The ability of estimated $\mathcal{D}_{O_2}$ to predict CA formation in the asphalt as a function of position and time is examined. A rigorous parameter estimation based on equation II – 30 is not attempted.

Steady-state assumption

From the experimental data and $(r_{CA})_{SI}$, a steady-state assumption is used.

$$\left(\frac{\partial P}{\partial t}\right) = 0 \qquad (V-3)$$

This assumption reduces equation II – 30 from a parabolic PDE in time and one spatial variable to an ODE in one spatial variable.

$$0 = \left(\frac{d\mathcal{D}_{O_2}}{dx}\right)\left(\frac{dP}{dx}\right) + \mathcal{D}_{O_2}\left(\frac{d^2P}{dx^2}\right) - \left(\frac{cRT}{h}\right)r_{CA} \qquad (II-31)$$

The boundary conditions are:

$\left(\frac{dP}{dx}\right) = 0$	at	$x = 0$	Substrate interface
$P = P_{ES}$	at	$x = L$	Exposed surface

These conditions are not sufficient to estimate a unique $\mathcal{D}_{O_2}$. Specifying P_{SI} provides a necessary constraint. In the absence of reliable oxygen solubility data, h is assumed to be unity.

Many equations describing diffusion and reaction of oxygen in an asphalt film have been given. Figure V-12 shows a qualitative and visual solution of equation II – 31, the oxygen pressure profile in the film. The shape of the profile assumes nothing about the functionality of $\mathcal{D}_{O_2}$. The same general profile results regardless if $\mathcal{D}_{O_2}$ is constant or varies through the film. At the SI, the oxygen pressure gradient is zero since the aluminum tray is assumed to be impermeable. At the ES, the oxygen pressure in the film equals the oxygen pressure in the gas. Providing P_{SI} fixes the profile.

For all x over the range 0 to L, equation II – 31 is expressed as equation V – 9.

$$P'' = f(P, P', x) \qquad (V-9)$$

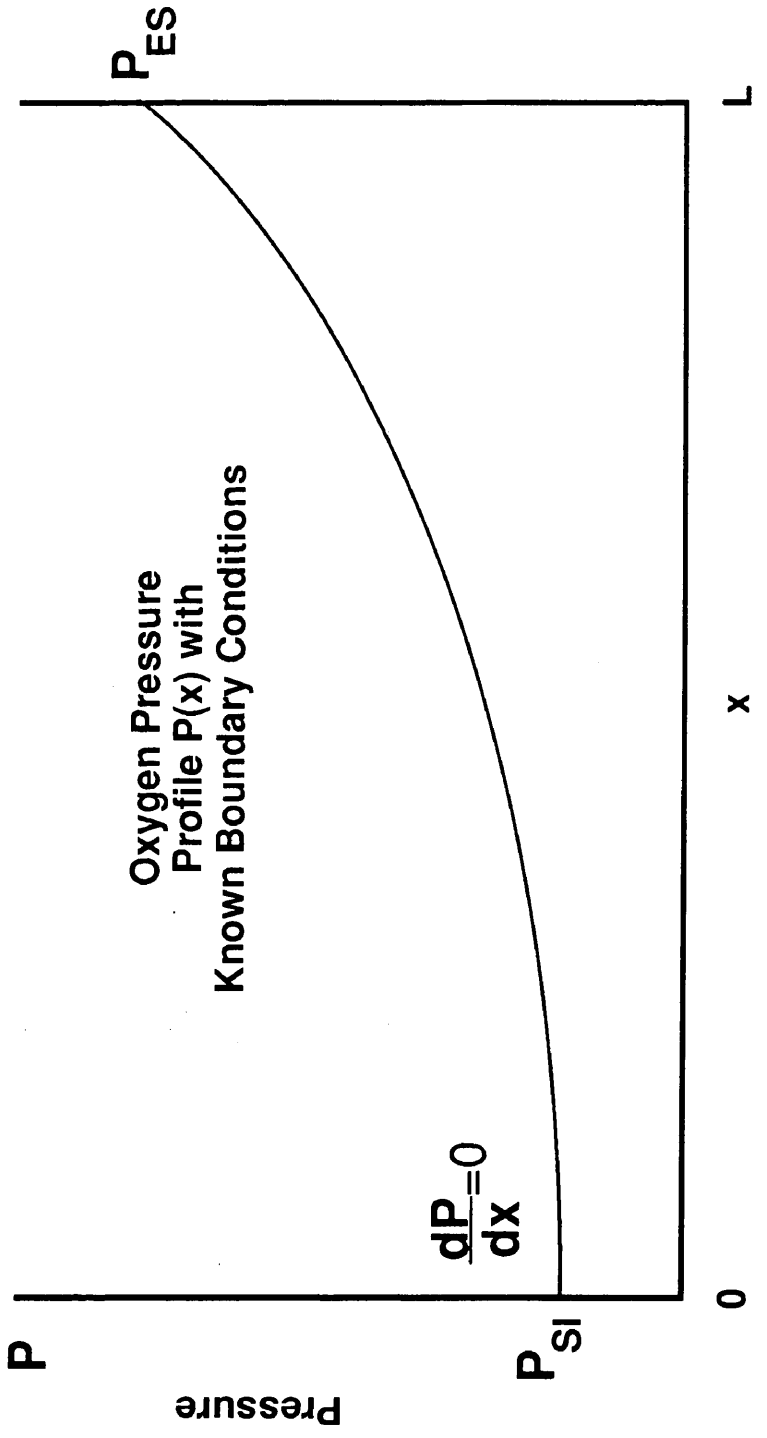

Figure V-12. Schematic of oxygen pressure profile in an asphalt film.

The prime denotes differentiation with respect to position. Initial conditions are based on zero oxygen flux from the experimental design and estimated P_{SI} from kinetics.

$$x = 0 \qquad P' = 0 \qquad P = P_{SI}$$

A $\mathcal{D}_{O_2}$ is assumed, and equation V – 9 is solved by forward integration techniques. To the extent that calculated and measured P_{ES} differ, $\mathcal{D}_{O_2}$ is updated and the process continued. When the difference between calculated and measured P_{ES} is within a given tolerance, the calculation is halted, and $\mathcal{D}_{O_2}$ is determined.

Starting at the SI, the derivatives of P with respect to x increase as the function approaches the ES or L. Since numerical integration techniques are used to determine the oxygen pressure profile, large derivatives as the function approaches the ES introduce numerical errors, cause instability, and require excessive computation time. Fortunately, the derivatives at the ES are not infinite. An infinite derivative at the ES of the asphalt film suggests an explosive reaction. For the experimental conditions, this is not observed. The derivatives at the ES become large for two reasons. First, the parameters describing $\mathcal{D}_{O_2}$ are unknown. An incremental search and final optimization may require numerical integration of equations with large derivatives even though the optimized parameters yield a solution that does not have large derivatives. Second, the magnitudes of r_{O_2} and $\mathcal{D}_{O_2}$ from increasing η_o^* with CA may yield very steep profiles as the function approaches the ES. This results from the formation of a very hard impermeable skin at the ES, severely limiting further oxygen transport.

A transformation of variables eliminates the problem resulting from large derivatives as P approaches the ES. This procedure, developed by co-worker Moon-Sun Lin, transforms P as a function of x to X as a function of P^*. Continuity provides

the necessary constraints to perform the transformation. The derivatives of the transformed function decrease as the *ES* is approached. Therefore, numerical errors are less significant; the numerical solution is more stable, and the calculation is faster.

The values and first derivatives of the original and transformation function are related by equations V – 10 and V – 11 satisfying continuity.

$$X = g(P^*) \qquad \text{at} \qquad P = f(x) \tag{V – 10}$$

$$\frac{dP}{dx} = \frac{1}{dX \,/\, dP^*} \tag{V – 11}$$

By the chain rule, $\frac{d^2P}{dx^2}$ is expressed in terms of the transformation variables, X and P^*, equation V – 12.

$$\frac{d^2P}{dx^2} = -\frac{d^2X \,/\, dP^{*2}}{(dX \,/\, dP^*)^3} \tag{V – 12}$$

Thus, equation V – 9 becomes equation V – 13.

$$X'' = g(X, X', P^*) \tag{V – 13}$$

The initial conditions, defined at the point of transformation, are given in equation V – 14.

$$P^* = 0 \qquad \text{and} \qquad \left.\frac{dP}{dx}\right|_{x=x_f} = \left.\frac{1}{dX \,/\, dP^*}\right|_{P^*=0} \qquad X = x_f \tag{V – 14}$$

P^* is the difference between P and $P(x_f)$ as given in equation V – 15.

$$P^* = P(x) - P(x_f) \tag{V – 15}$$

Figure V-13 shows a schematic of the oxygen pressure profile with variable transformation at x equals x_f. Using numerical integration and variable transformation to estimate $\mathcal{D}_{O_2}$ is described. $\mathcal{D}_{O_2}$ is assumed. Using a forward integration technique,

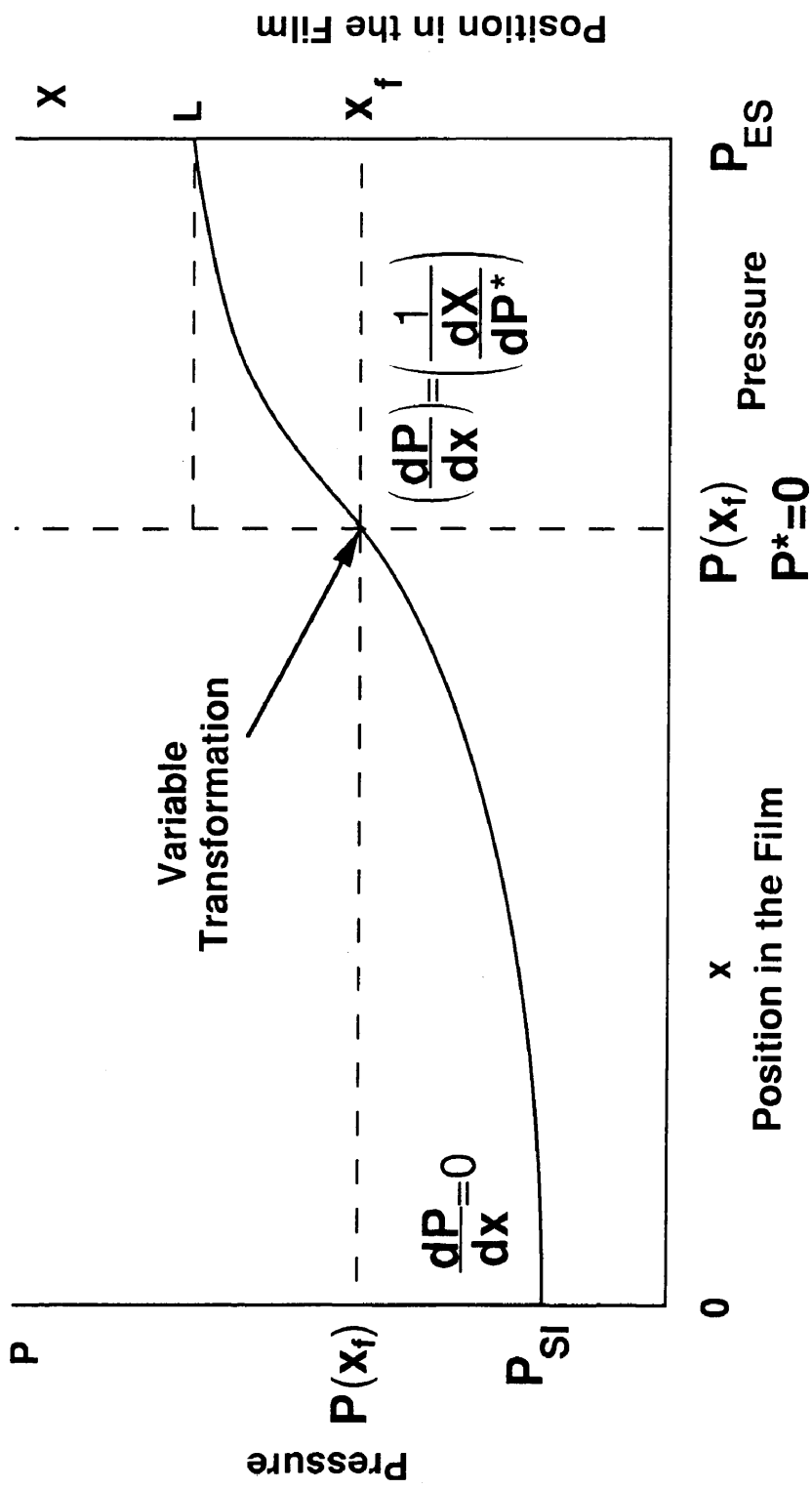

Figure V-13. Schematic of oxygen pressure profile in an asphalt film with transformation of variables at x_f.

equation V – 9 with the specified initial conditions is solved until the magnitude of the first derivative exceeds a pre-defined criterion. At this point, x_f, transformation is performed. Numerical integration proceeds with equation V – 13 until the known P_{ES} is reached. To the extent that calculated and measured L are different, $\mathcal{D}_{O_2}$ is modified and the entire procedure repeated. Calculation is stopped when the difference between calculated and measured L is within a pre-defined tolerance. At this point, $\mathcal{D}_{O_2}$ is determined.

Steady-state constant diffusivity

The previous section described a qualitative understanding of the oxygen pressure profiles in asphalts films and numerical tools. With this knowledge, $\mathcal{D}_{O_2}$ in asphalt films are estimated from experimental data for steady-state constant $\mathcal{D}_{O_2}$ oxygen diffusion and reaction. This reduces equation 11 – 31 to 11 – 32.

$$0 = \mathcal{D}_{O_2}\left(\frac{d^2P}{dx^2}\right) - \left(\frac{cRT}{h}\right)r_{CA} \qquad \text{(II – 32)}$$

Since equation II – 32 is a second order ODE, the boundary conditions are:

$\left(\frac{dP}{dx}\right) = 0$	at	$x = 0$	Substrate interface
$P = P_{ES}$	at	$x = L$	Exposed surface

Specifying P_{SI} insures an estimation of a unique $\mathcal{D}_{O_2}$. In the absence of reliable oxygen solubility data, h is assumed to be unity.

A trial and error parameter estimation procedure is developed since $\mathcal{D}_{O_2}$ is unknown. First, an incremental search is used. $\mathcal{D}_{O_2}$ is assumed to be 1 m^2 / s, and with the known conditions at the SI, equation V – 9 is numerically integrated. If no transformation is required, the objective function is given in equation V – 16.

$$O(\mathcal{D}_{O_2}) = P_{\text{cal}}|_{x=L} - P_{ES} \qquad \text{(V – 16)}$$

If variable transformation is required, the objective function is given in equation V – 17.

$$O(\mathcal{D}_{O_2}) = L - X_{\text{cal}}|_{P=P_{ES}} \qquad \text{(V – 17)}$$

$\mathcal{D}_{O_2}$ is decreased geometrically until the objective function changes sign from the previous trial to the current trial. At this point, the root of the objective function is bound. Further refinement of $\mathcal{D}_{O_2}$ to a pre-defined tolerance is achieved by the method of false-position. With the estimated $\mathcal{D}_{O_2}$, all boundary conditions are satisfied. The FORTRAN source code is given in Appendix D.

To confirm that the numerical integration, variable transformation, and parameter estimation algorithm works, a form of equation V – 32 with an analytical solution is developed. Equation II – 32 is further reduced with the following assumptions. The reaction is first order in P, and $\mathcal{D}_{O_2}$ is constant. This is given in equation V – 18.

$$\mathcal{D}_{O_2}\frac{d^2P}{dx^2} = cRTk_PP \qquad \text{(V – 18)}$$

The boundary conditions are:

$$x = 0 \qquad P = P_{SI} \qquad \frac{dP}{dx} = 0$$

$$x = L \qquad P = P_{ES}$$

Specifying P_{SI} constrains equation V – 18 to a unique $\mathcal{D}_{O_2}$. The analytical solution for $\mathcal{D}_{O_2}$ is given in equation V – 19.

$$\mathcal{D}_{O_2} = \frac{cRTk_PL^2}{\cosh^{-1}(P_{ES}\,/\,P_{SI})} \qquad \text{(V – 19)}$$

R is 82.057 $\text{cm}^3 \cdot \text{atm} / \text{g mol} \cdot \text{K}$. T is in units of K. c is given in equation V – 2, and k_P is determined from T and the specific asphalt Arrhenius constants in Table IV-6. The units of k_P on a per day basis are converted to a per second basis. L is

the film thickness in meters. These parameters with accompanying units calculate $\mathcal{D}_{O_2}$ in units of m^2 / s. The difference between analytical $\mathcal{D}_{O_2}$ and $\mathcal{D}_{O_2}$ determined by trial and error, numerical integration, and variable transformation for all asphalts, aging temperatures, and pressures studied is within 0.02%. This confirms that the numerical integration, variable transformation, and $\mathcal{D}_{O_2}$ estimation techniques are correct.

With the numerical technique confirmed, $\mathcal{D}_{O_2}$ is estimated in more complex models. Specifying the order of reaction to be α is one level of complexity shown in equation V – 20.

$$\frac{d^2P}{dx^2} = \frac{cRTk_P}{\mathcal{D}_{O_2}} P^{\alpha} \qquad (V - 20)$$

The boundary conditions are the same as those for equation V – 18. This equation has no analytical solution, and numerical techniques are used to estimate $\mathcal{D}_{O_2}$.

Estimated constant $\mathcal{D}_{O_2}$ values for α of 0.27 and all aging pressures, temperatures and asphalts studied are given in Table V-11. For isobaric conditions and a given asphalt, $\mathcal{D}_{O_2}$ increases with temperature in all cases studied except Coastal AC-20 and Exxon AC-20 at 0.2 atm from 333.3 to 344.4 K and Texaco AC-20 at 2 atm from 333.3 to 344.4 K. For isothermal conditions and a given asphalt, $\mathcal{D}_{O_2}$ decreases with increasing pressure except for Exxon AC-20 at 355.5 K. These anomalies probably result from errors in determining P_{SI} based on $(r_{CA})_{SI}$.

From estimated $\mathcal{D}_{O_2}$ and P_{SI}, oxygen pressure profiles in the films were calculated. The source code that generates the oxygen pressure profiles is given in Appendix D. Figure V-14 shows the oxygen pressure profiles of 1 mm thick Ampet AC-20 at P_{ES} of 0.2 atm. The difference in line types designate the different aging temperatures of 333.3, 344.4, and 355.5 K, respectively. For increasing temperature,

Table V-11. Estimated $\mathcal{D}_{O_2}$ for Steady-State Constant $\mathcal{D}_{O_2}$ Oxygen Diffusion and Reaction[a]

Asphalt	T K	P_{ES} atm	P_{SI} atm	$\mathcal{D}_{O_2} \times 10^{13}$ m^2/s
Ampet AC-20	333.3	0.2	0.0673	20.0
	344.4	0.2	0.115	88.5
	355.5	0.2	0.161	486.0
	333.3	2	0.393	2.80
	344.4	2	0.857	11.5
	355.5	2	1.80	176.1
Coastal AC-20	333.3	0.2	0.149	64.9
	344.4	0.2	0.0345	39.3
	355.5	0.2	0.0789	160.0
	333.3	2	0.925	5.16
	344.4	2	0.408	7.83
	355.5	2	1.105	43.2
Cosden AC-20	333.3	0.2	0.0331	20.0
	344.4	0.2	0.130	141.0
	355.5	0.2	–[b]	–
	333.3	2	0.937	7.07
	344.4	2	0.363	8.86
	355.5	2	1.48	86.1
Exxon AC-20	333.3	0.2	0.175	150.0
	344.4	0.2	0.108	99.3
	355.5	0.2	0.0775	127.0
	333.3	2	1.09	6.88
	344.4	2	1.17	20.8
	355.5	2	1.86	249.0
Texaco AC-20	333.3	0.2	0.124	38.9
	344.4	0.2	0.122	92.5
	355.5	0.2	0.170	598.3
	333.3	2	1.39	9.11
	344.4	2	0.57	8.04
	355.5	2	1.28	44.6

[a] α of 0.270 and 1 mm thick films
[b] This calculation was not done.

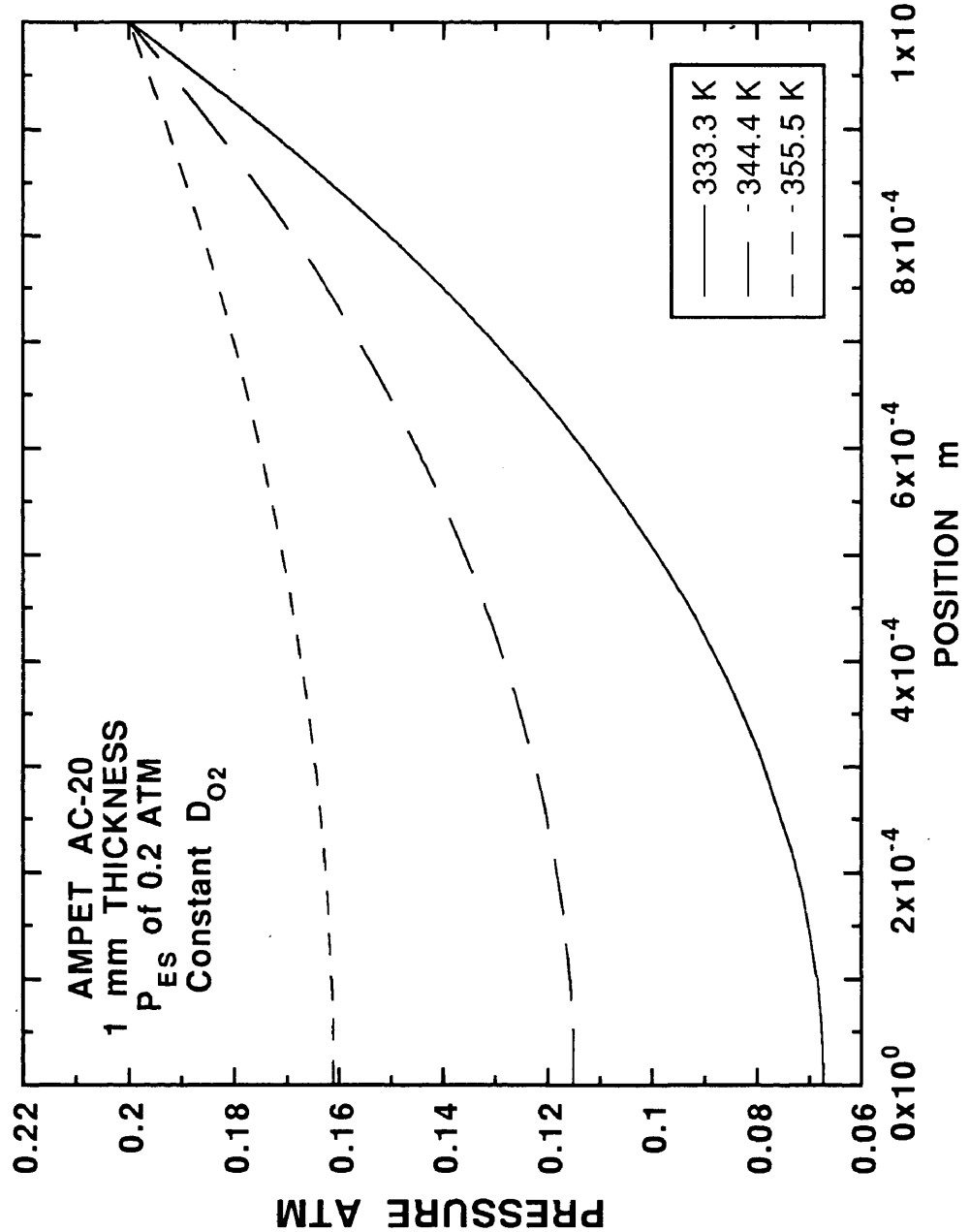

Figure V-14. Calculated oxygen pressure profiles in 1 mm thick film Ampet AC-20 at 333.3, 344.4, and 355.5 K with P_{ES} of 0.2 atm for estimated $\mathcal{D}_{O_2}$ from steady-state constant $\mathcal{D}_{O_2}$ oxygen diffusion and reaction.

the profile is less steep; P_{SI} approaches P_{ES}. This figure shows that diffusion resistance decreases with increasing temperature. Data from Table V-8 also support this conclusion. In comparison, Figure V-15 shows calculated oxygen pressure profiles for Cosden AC-20 at P_{ES} of 2.0 atm. From this figure, one would conclude that diffusion resistance decreases from 333.3 to 344.4 K. This is not physically reasonable, and one of the profiles is incorrect. Comparing $\mathcal{D}_{O_2}$ in Table V-11 holding other measurable aging variables constant may not be sufficient to detect errors in the data. A combination of both P_{SI} and $\mathcal{D}_{O_2}$ must be considered.

Even though there are some unrealistic values, a comparison of estimated $\mathcal{D}_{O_2}$ with literature values validates the technique of using r_{CA}. There are only two sources reporting $\mathcal{D}_{O_2}$ in asphalt. Van Oort (1956) gives $\mathcal{D}_{O_2}$ of 8.0×10^{-16} m^2 / s for neat asphalt at 323.2 K. In 1959, Blokker and van Horn (1959) report $\mathcal{D}_{O_2}$ as 1.2×10^{-10} m^2 / s at 323.2 K. These literature values range six orders of magnitude. Estimated $\mathcal{D}_{O_2}$ values in Table V-11 are within the range of literature values. In both literature sources, no surface properties were measured. Van Oort assumed a first order reaction with $\mathcal{D}_{O_2}$ varying inversely proportional to bound oxygen. Blokker and van Horn assumed $\mathcal{D}_{O_2}$ did not change with oxidative aging, but the reactivity of the asphalt decreased with aging time. They assumed the order of reaction in oxygen concentration to be 0.6.

The propagation of errors is a significant problem since $(r_{CA})_{SI}$ was used to determine P_{SI} and to estimate $\mathcal{D}_{O_2}$. Table V-11 contains some unrealistic values. With a 10% uncertainty in $(r_{CA})_{SI}$, the corresponding error band for P_{SI} is 40%. This results from small α. To determine the error in estimated $\mathcal{D}_{O_2}$, a range of $\pm$ 40% was established for P_{SI}. $\mathcal{D}_{O_2}$ was estimated at each end of the range. The calculation was not possible for some cases since P_{SI} exceeded P_{ES}. The calculated

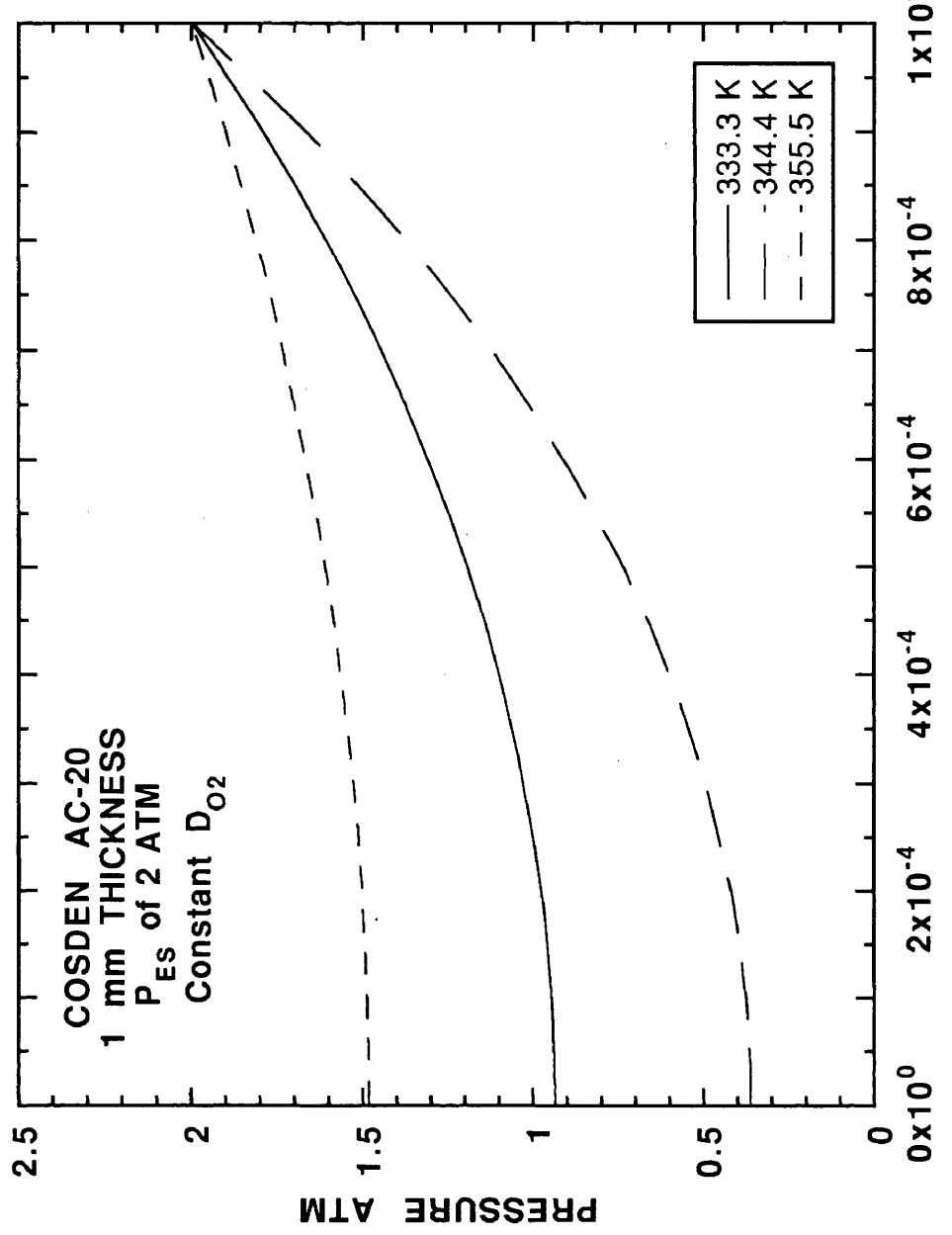

Figure V-15. Calculated oxygen pressure profiles in 1 mm thick film Cosden AC-20 at 333.3, 344.4, and 355.5 K with P_{ES} of 2 atm for estimated $\mathcal{D}_{O_2}$ from steady-state constant $\mathcal{D}_{O_2}$ oxygen diffusion and reaction.

$\mathcal{D}_{O_2}$ are given in Table V-12. The error in $\mathcal{D}_{O_2}$ is directly related to the magnitude of $\mathcal{D}_{O_2}$. Small $\mathcal{D}_{O_2}$ shows a small error band. The range of error varies from asphalt to asphalt and across aging conditions. For example, the error band in $\mathcal{D}_{O_2}$ is from 4.35 to 86.4 $\times 10^{-13}$ m^2 / s for Texaco AC-20 at 333.3 K and 2 atm at the *ES*. In contrast, Coastal AC-20 at the same aging conditions shows a range of $\mathcal{D}_{O_2}$ from 3.48 to 8.43 $\times 10^{-13}$ m^2 / s.

Establishing a suitable criterion to discard data is next to impossible since the actual values of estimated $\mathcal{D}_{O_2}$ are still unknown. Screening the data in a attempt to remove anomalous points before the estimation of $\mathcal{D}_{O_2}$ was difficult. Using a criterion of large variability in $\mathcal{D}_{O_2}$ may not be the best criterion either. For example, values of P_{SI} that err on the low side tend to produce low variability in $\mathcal{D}_{O_2}$. From P_{SI} and $\mathcal{D}_{O_2}$ together, Table V-13 lists questionable $\mathcal{D}_{O_2}$ and P_{SI} for the asphalts and specified aging conditions. At 0.2 atm, the data for Coastal AC-20 and Exxon AC-20 at 333.3 and 355.5 are questionable. At 2 atm, all of the $\mathcal{D}_{O_2}$ at 344.4 K appear to be too low. Other questionable data at 2 atm include Ampet AC-20 at 333.3 K and Coastal AC-20 and Texaco AC-20 at 355.5 K. Since most of the questionable data were at 2 atm, the diffusion resistance was probably extremely low. The difference in r_{CA} at the *SI* and *ES* could be accounted for in the measurement error. However, these data points are not removed from the data set at this time.

Estimated $\mathcal{D}_{O_2}$ changes with pressure for isothermal aging and a given asphalt. This suggests that $\mathcal{D}_{O_2}$ varies in the asphalt film as a result of aging. Changes in η_o^* as a result of *CA* formation affect changes in $\mathcal{D}_{O_2}$. A model relating $\mathcal{D}_{O_2}$ to η_o^* is given in equation II – 34 for isothermal conditions.

$$\mathcal{D}_{O_2} = D_o(\eta_o^*)^B \qquad \text{(II – 34)}$$

Table V-12. Estimated $\mathcal{D}_{O_2}$ at ±40% P_{SI} for Steady-State Constant $\mathcal{D}_{O_2}$ Oxygen Diffusion and Reaction[a,b]

Asphalt	T K	P_{ES} atm	P_{SI} atm	$\mathcal{D}_{O_2} \times 10^{13}$ m^2/s		
				-40% P_{SI}	P_{SI}	+40% P_{SI}
Ampet AC-20	333.3	0.2	0.0673	15.2	20.0	26.9
	344.4	0.2	0.115	51.8	88.5	207.5
	355.5	0.2	0.161	164.3	486.0	–
	333.3	2	0.393	2.35	2.80	3.29
	344.4	2	0.857	8.06	11.5	17.6
	355.5	2	1.80	35.0	176.1	–
Coastal AC-20	333.3	0.2	0.149	26.8	64.9	–
	344.4	0.2	0.0345	33.5	39.3	45.5
	355.5	0.2	0.0789	115.4	160.0	231.6
	333.3	2	0.925	3.48	5.16	8.43
	344.4	2	0.408	6.54	7.83	9.26
	355.5	2	1.105	26.1	43.2	91.7
Cosden AC-20	333.3	0.2	0.0331	17.1	20.0	23.0
	344.4	0.2	0.130	73.3	141.0	579.4
	355.5	0.2	–	–	–	–
	333.3	2	0.937	4.74	7.07	11.7
	344.4	2	0.363	7.52	8.86	10.3
	355.5	2	1.48	36.0	86.1	–
Exxon AC-20	333.3	0.2	0.175	35.0	150.0	–
	344.4	0.2	0.108	61.2	99.3	199.8
	355.5	0.2	0.0775	92.0	127.0	181.8
	333.3	2	1.09	4.19	6.88	14.3
	344.4	2	1.17	12.0	20.8	50.7
	355.5	2	1.86	35.2	249.0	–
Texaco AC-20	333.3	0.2	0.124	21.3	38.9	118.4
	344.4	0.2	0.122	51.1	92.5	270.2
	355.5	0.2	0.170	166.1	598.3	–
	333.3	2	1.39	4.35	9.11	86.4
	344.4	2	0.57	6.34	8.04	10.2
	355.5	2	1.28	23.4	44.6	170.0

[a] α of 0.270 and 1 mm thick films
[b] – Signifies the values were not determined.

Table V-13. Suspect $\mathcal{D}_{O_2}$ and POV-Aging Conditions for Steady-State Constant $\mathcal{D}_{O_2}$ Oxygen Diffusion and Reaction[a]

Asphalt	T K	P_{ES} atm	P_{SI} atm	$\mathcal{D}_{O_2} \times 10^{13}$ m^2/s
Ampet AC-20	333.3	2	0.393	2.80
	344.4	2	0.857	11.5
Coastal AC-20	333.3	0.2	0.149	64.9
	355.5	0.2	0.0789	160.0
	344.4	2	0.408	7.83
	355.5	2	1.105	43.2
Cosden AC-20	344.4	2	0.363	8.86
Exxon AC-20	333.3	0.2	0.175	150.0
	355.5	0.2	0.0775	127.0
	344.4	2	1.17	20.8
Texaco AC-20	344.4	2	0.57	8.04
	355.5	2	1.28	44.6

[a] α of 0.270 and 1 mm thick films

Comparing estimated $\mathcal{D}_{O_2}$ with average η_o^* on a log-log plot should yield a straight line if equation II – 34 models the asphalt behavior.

The calculation of average η_o^* for a given asphalt, aging temperature, and pressure is described. From Tables C-2 through C-11 in Appendix C, the average CA in the film during the aging experiment was approximated by the arithmetic average of the minimum and maximum CA. Neat CA was not used. Using HS and m of the different asphalts and aging temperatures from Table V-4, average η_o^* of the asphalt during the aging experiment was calculated from equation I – 6. Table V-14 reports average CA, η_o^*, and estimated $\mathcal{D}_{O_2}$ at the aging conditions for all the asphalts studied. The data denoted with * in the table are the questionable data set

Table V-14. Estimated $\mathcal{D}_{O_2}$, Average CA and η_o^*, and POV-Aging Conditions for Steady-State Constant $\mathcal{D}_{O_2}$ Oxygen Diffusion and Reaction[a,b]

Asphalt	T K	P_{ES} atm	CA_{avg} CA	$\eta^*_{o\,avg}$ P	$\mathcal{D}_{O_2} \times 10^{13}$ m^2 / s
Ampet AC-20	333.3	0.2	0.729	10200	20.0
	344.4	0.2	0.726	1320	88.5
	355.5	0.2	0.806	230	486.1
	333.3*	2	1.001	23400	2.80
	344.4*	2	0.985	2760	11.5
	355.5	2	1.099	510	176.1
Coastal AC-20	333.3*	0.2	0.734	12100	64.9
	344.4	0.2	0.815	4350	39.3
	355.5*	0.2	0.837	330	160.0
	333.3	2	1.030	39100	5.16
	344.4*	2	1.032	4910	7.83
	355.5*	2	1.140	1000	43.2
Cosden AC-20	333.3	0.2	0.834	12100	20.0
	344.4	0.2	0.778	1290	141.0
	355.5	0.2	–	–	–
	333.3	2	1.172	32800	7.07
	344.4*	2	1.098	3200	8.86
	355.5	2	1.302	750	86.1
Exxon AC-20	333.3*	0.2	0.802	11400	150.0
	344.4	0.2	0.839	1640	99.3
	355.5*	0.2	0.970	330	127.0
	333.3	2	1.096	24600	6.88
	344.4*	2	1.066	2900	20.8
	355.5	2	1.065	410	249.0
Texaco AC-20	333.3	0.2	0.669	6600	38.9
	344.4	0.2	0.736	1170	92.5
	355.5	0.2	0.746	190	598.3
	333.3	2	0.876	13400	9.11
	344.4*	2	0.904	1990	8.04
	355.5*	2	1.009	400	44.6

[a] α of 0.270 and 1 mm thick films
[b] – Signifies the values were not determined.
* These data were not used to estimate parameters in Figure V-16.

given in Table V-13.

Figure V-16 shows estimated $\mathcal{D}_{O_2}$ with error bars versus average η_o^* for all asphalts. Circles, squares and diamonds denote aging temperatures 333.3, 344.4, and 355.5 K, respectively. Even with the questionable data, the conclusion that increases in η_o^* decrease $\mathcal{D}_{O_2}$ can be reached. For modeling, a specific mathematical relationship must be developed from this generality. To develop this model, the questionable data are first discussed and then discarded from the parameter estimation. Solid symbols denote the questionable data in Table V-13 and V-14. The asphalt and aging pressure for each questionable point are given on the figure. The questionable data are both unrealistically high and low for 333.3 K. The questionable data are low for 344.4 and 355.5 K. Furthermore, at 344.4 K, the questionable data are at one aging pressure, 2 atm, possibly suggesting a systematic error in this experiment. Hollow symbols represent the data used in the parameter estimation. With the questionable data removed, it appears that equation II−34 models the asphalt behavior. Surprisingly, the $\mathcal{D}_{O_2}$-η_o^* relationship appears to be independent of the asphalts studied. Furthermore, the temperature dependence on $\mathcal{D}_{O_2}$ is completely masked by average η_o^*. From the parameter estimation, a value of -0.84 is determined for B as shown in the figure. This value lies in the range of literature values, -1 to -0.5. The pre-exponential factor, D_o, is 4.039×10^{-9} m / s^2.

Several data points were discarded from the parameter estimation. These errors are traced to the uncertainty in $(r_{CA})_{SI}$. At 333.3 K, two data points are too high and one is too low. The discarded data are three different asphalts and two different pressures. The lower bound of the error bar for Exxon AC-20 and Coastal AC-20 approaches the model. The error bar for Ampet AC-20 is very small, and this is probably a bad point. At 344.4 K, all data at 2 atm are below the regression line.

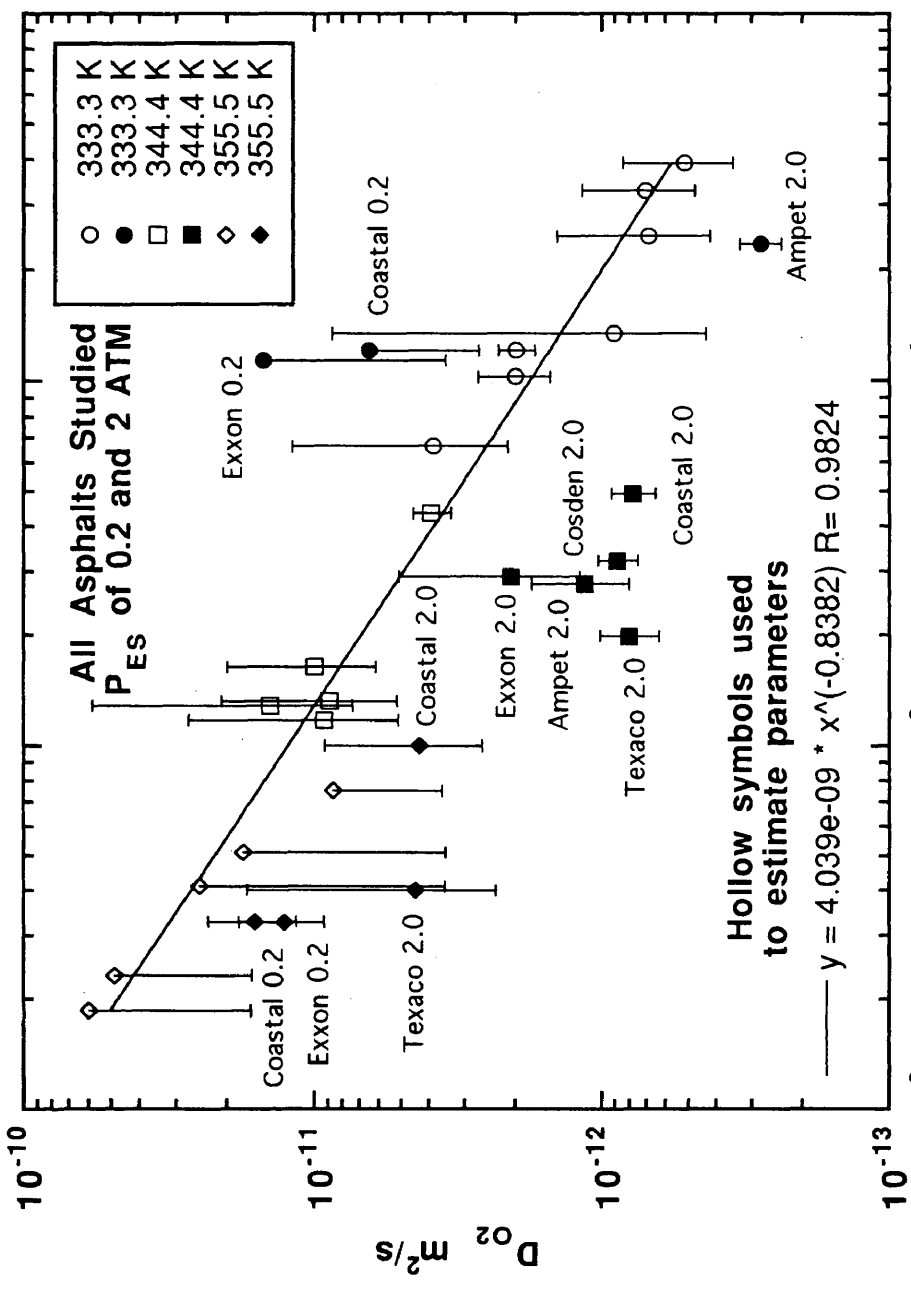

Figure V-16. Estimated $\mathcal{D}_{O_2}$ versus average η_o^* of all 1 mm thick film POV-aged asphalts and conditions studied.

One may argue that the temperature was not 344.4 K but actually lower. However, $(r_{CA})_{ES}$ shows good linearity in Figure IV-14 suggesting that the temperature was correct. Low $\mathcal{D}_{O_2}$ and P_{SI} would result if the film thickness was actually greater than 1 mm. For Exxon AC-20, the upper region of the error bar approaches the model suggesting that this datum is at most 10% in error in $(r_{CA})_{SI}$. At 355.5 K, the discarded data are below the model. Four different asphalts and two different pressures are included in this set. High temperatures and thin films minimize diffusion resistance. Small differences in $(r_{CA})_{ES}$ and $(r_{CA})_{SI}$ are difficult to measure. Fortunately, the upper region of the error band for $\mathcal{D}_{O_2}$ is very close to the model.

The measurement of the relative rates of diffusion and reaction is a primary concern for catalytic reactions (Froment and Bischoff, 1979). Although the oxidative aging in asphalts may not be catalytic in nature, a measure of the relative diffusion and reaction rates does provide valuable information for future experimental design. The Thiele modulus, ϕ, is a measure of the relative rates of diffusion and reaction. ϕ greater than unity indicates a diffusion controlled regime either from small diffusivity, large diffusion length, or very rapid reaction. As ϕ approaches 0, there is no appreciable transport resistance.

The effective ϕ for oxygen diffusion and reaction in asphalt is given in equation V – 21.

$$\phi = L\sqrt{\frac{cRT(r_{CA})_{\text{avg}}}{P_{\text{avg}}\mathcal{D}_{O_2}}} \qquad \text{(V – 21)}$$

$(r_{CA})_{\text{avg}}$ is evaluated at the arithmetic average pressure in the film. Calculated values of ϕ are presented in Table V-15. ϕ for the set of questionable data was not calculated.

ϕ decreases with increasing temperature for isobaric aging and a given asphalt in all cases studied except Texaco AC-20 from 333.3 to 344.4 K. This suggests that

Table V-15. Thiele Modulus, Estimated $\mathcal{D}_{O_2}$ and Average P for All Asphalts and POV-Aging Conditions Studied[a,b]

Asphalt	T K	P_{ES} atm	P_{SI} atm	P_{avg} atm	$\mathcal{D}_{O_2} \times 10^{13}$ m^2/s	ϕ
Ampet AC-20	333.3	0.2	0.0673	0.134	20.0	0.750
	344.4	0.2	0.115	0.158	88.5	0.529
	355.5	0.2	0.161	0.181	486.1	0.327
	333.3	2	0.393	–	2.80	–
	344.4	2	0.857	–	11.5	–
	355.5	2	1.800	1.90	176.1	0.231
Coastal AC-20	333.3	0.2	0.149	–	64.9	–
	344.4	0.2	0.0345	0.117	39.3	0.957
	355.5	0.2	0.0789	–	160.0	–
	333.3	2	0.925	1.46	5.16	0.617
	344.4	2	0.408	–	7.83	–
	355.5	2	1.105	–	43.2	–
Cosden AC-20	333.3	0.2	0.0331	0.117	20.0	0.933
	344.4	0.2	0.130	0.165	141.0	0.491
	355.5	0.2	–	–	–	–
	333.3	2	0.937	1.47	7.07	0.623
	344.4	2	0.363	–	8.86	–
	355.5	2	1.48	1.74	86.1	0.388
Exxon AC-20	333.3	0.2	0.175	–	150.0	–
	344.4	0.2	0.108	0.154	99.3	0.525
	355.5	0.2	0.0775	–	127.0	–
	333.3	2	1.09	1.54	6.88	0.574
	344.4	2	1.17	–	20.8	–
	355.5	2	1.86	1.93	249.0	0.193
Texaco AC-20	333.3	0.2	0.124	0.162	38.9	0.502
	344.4	0.2	0.122	0.161	92.5	0.514
	355.5	0.2	0.170	0.185	598.3	0.287
	333.3	2	1.39	1.70	9.11	0.440
	344.4	2	0.570	–	8.04	–
	355.5	2	1.28	–	44.6	–

[a] α of 0.270 and 1 mm thick films
[b] – Signifies the values were not determined.

diffusion resistance in asphalt decreases with increasing temperature. The exception is due to lower average pressure at higher temperature. However, ϕ for all aging conditions is less than one. Even at 0.2 atm and 333.3 K the reaction was not diffusion limited. Blokker and van Hoorn (1959) concluded that the depth of oxygen penetration in an asphalt film was about 2.5 mm at 323.2 K and 1 atm oxygen. The maximum depth of penetration was 5 mm based on their assumptions of constant $\mathcal{D}_{O_2}$ and the order of reaction of 0.6. From these calculations, 1 mm thick films may be too thin even at 0.2 atm for studying $\mathcal{D}_{O_2}$. Experiments designed to increase ϕ would provide better $\mathcal{D}_{O_2}$. A modification of the existing experimental design increases the asphalt film thickness.

To summarize, for steady-state constant $\mathcal{D}_{O_2}$, equation II – 34 describing a $\mathcal{D}_{O_2}$-η_o^* relationship was developed. $\mathcal{D}_{O_2}$ versus η_o^* showed significant scatter when all data were included. Questionable data were removed and the errors could be traced to the estimation of $(r_{CA})_{SI}$. The model parameters are B of -0.838 and D_o of 4.0389×10^{-9} for η_o^* in poise and $\mathcal{D}_{O_2}$ in m^2 / s. The parameters are independent of temperature and asphalts for the asphalts studied. Furthermore, the parameter B was in the range of literature values. The $\mathcal{D}_{O_2}$-T dependence is completely masked by η_o^*. This does not suggest that all asphalts have the same $\mathcal{D}_{O_2}$. Asphalt dependent parameters determine r_{CA}, CA_o, HS, and m. These are used to calculate η_o^*, and each asphalt has unique η_o^* from oxidative aging. With unique η_o^* and asphalt independent parameters B and D_o, unique values of $\mathcal{D}_{O_2}$ are calculated for each asphalt. The Thiele modulus, ϕ, providing a measure of the relative rates of diffusion to reaction, was calculated for POV aging in the asphalt films. All calculated values of ϕ were less than unity suggesting that the experimental design was not in a diffusion control regime. Experiments designed to increase ϕ should yield more significant oxygen

diffusion data.

Steady-state variable diffusivity

With the $\mathcal{D}_{O_2}$-η_o^* relationships confirmed, a steady-state variable $\mathcal{D}_{O_2}$ oxygen diffusion and reaction model is studied. Oxygen transport and reaction with variable $\mathcal{D}_{O_2}$ is given in equation II – 31.

$$0 = \left(\frac{d\mathcal{D}_{O_2}}{dx}\right)\left(\frac{dP}{dx}\right) + \mathcal{D}_{O_2}\left(\frac{d^2P}{dx^2}\right) - \left(\frac{cRT}{h}\right)r_{CA} \qquad \text{(II – 31)}$$

The boundary conditions are equivalent to equation II – 30. Using the chain rule, equation II – 31 is rewritten as equation V – 22.

$$0 = \left(\frac{d\mathcal{D}_{O_2}}{dP}\right)\left(\frac{dP}{dx}\right)^2 + \mathcal{D}_{O_2}\left(\frac{d^2P}{dx^2}\right) - \left(\frac{cRT}{h}\right)r_{CA} \qquad \text{(V – 22)}$$

$\mathcal{D}_{O_2}$ is defined in terms of the amount of aging by equation II – 37.

$$\mathcal{D}_{O_2}(t,x) = D_o\left[\exp\left\{HS\left[T(t,x)\right]\left(\int_0^t r_{CA}\left[T(\theta,x),P(\theta,x)\right]d\theta + CA_o\right) + m\left[T(t,x)\right]\right\}\right]^B \qquad \text{(II – 37)}$$

Unlike the steady-state constant $\mathcal{D}_{O_2}$ oxygen diffusion and reaction model, CA_o is estimated for these calculations. Since CA_o is determined from equation IV – 2 and model parameters given in Table V-10, some error may be introduced. The derivative of $\mathcal{D}_{O_2}$ with respect to P is given in equation II – 39.

$$\left(\frac{\partial\mathcal{D}_{O_2}}{\partial P}\right) = B \cdot HS \cdot \mathcal{D}_{O_2} \cdot \int_0^t \left(\frac{\partial r_{CA}}{\partial P}\right)d\theta \qquad \text{(II – 39)}$$

Since B is negative and all of the other terms are positive, this term is negative. Therefore, variable $\mathcal{D}_{O_2}$ decreases the overall rate of oxygen transport compared to constant $\mathcal{D}_{O_2}$. At P equal zero, equation II – 39 is undefined. However, r_{CA} is zero

at P equal zero. Eliminating this singularity, equation V – 23 evaluates the first term in equation II – 37 at P equals zero.

$$P = 0 \qquad \left(\frac{d\mathcal{D}_{O_2}}{dP}\right)\left(\frac{dP}{dx}\right)^2 = -\mathcal{D}_{O_2}\left(\frac{d^2P}{dx^2}\right) \qquad \text{(V - 23)}$$

This equation is only valid for the steady-state assumption.

A multi-variable optimization of both D_o and B with the steady-state assumption and variable $\mathcal{D}_{O_2}$ for discrete aging times was not performed. Instead a series of calculations determined the sensitivity of the oxygen pressure profile to aging time. For the first set of calculations, D_o was optimized for fixed B, P_{SI}, and P_{ES}. This calculation confirmed the accuracy of the numerical solution with variable $\mathcal{D}_{O_2}$. Next, D_o and B were fixed based on the estimation in Figure V-16. P_{SI} was determined at different aging times for known P_{ES}. This calculation is important, establishing a range of P_{SI} for the experimental time period. This also yields more realistic oxygen pressure profiles with aging time. Finally, the magnitudes of $\left(\frac{d\mathcal{D}_{O_2}}{dx}\right)\left(\frac{dP}{dx}\right)$ and $\mathcal{D}_{O_2}\left(\frac{d^2P}{dx^2}\right)$ are compared. This gives a measure of the limitation of oxygen transport due to variable $\mathcal{D}_{O_2}$. Both sets of calculations were performed at aging times of 10, 20, 40, 60, and 80 days for 333.3 K; 5, 10, 20, 30, and 40 days for 344.4 K; and 2, 5, 10, 15, and 20 for 355.5 K. Both calculations used variable transformation, incremental search, and method of false-position to optimize the objective function. Source code for the programs that optimize the specific parameters, D_o or P_{SI}, and generate the oxygen pressure profiles is given in Appendix D.

Figures V-17, V-18, and V-19 show oxygen pressure profiles for Ampet AC-20 at 0.2 atm, 333.3, 344.4, and 355.5 K with optimized values of D_o at various aging times. The optimized D_os are not reported; however, the profile for constant $\mathcal{D}_{O_2}$ is shown on the figures in the solid line for comparison. It appears that the numerical calculation

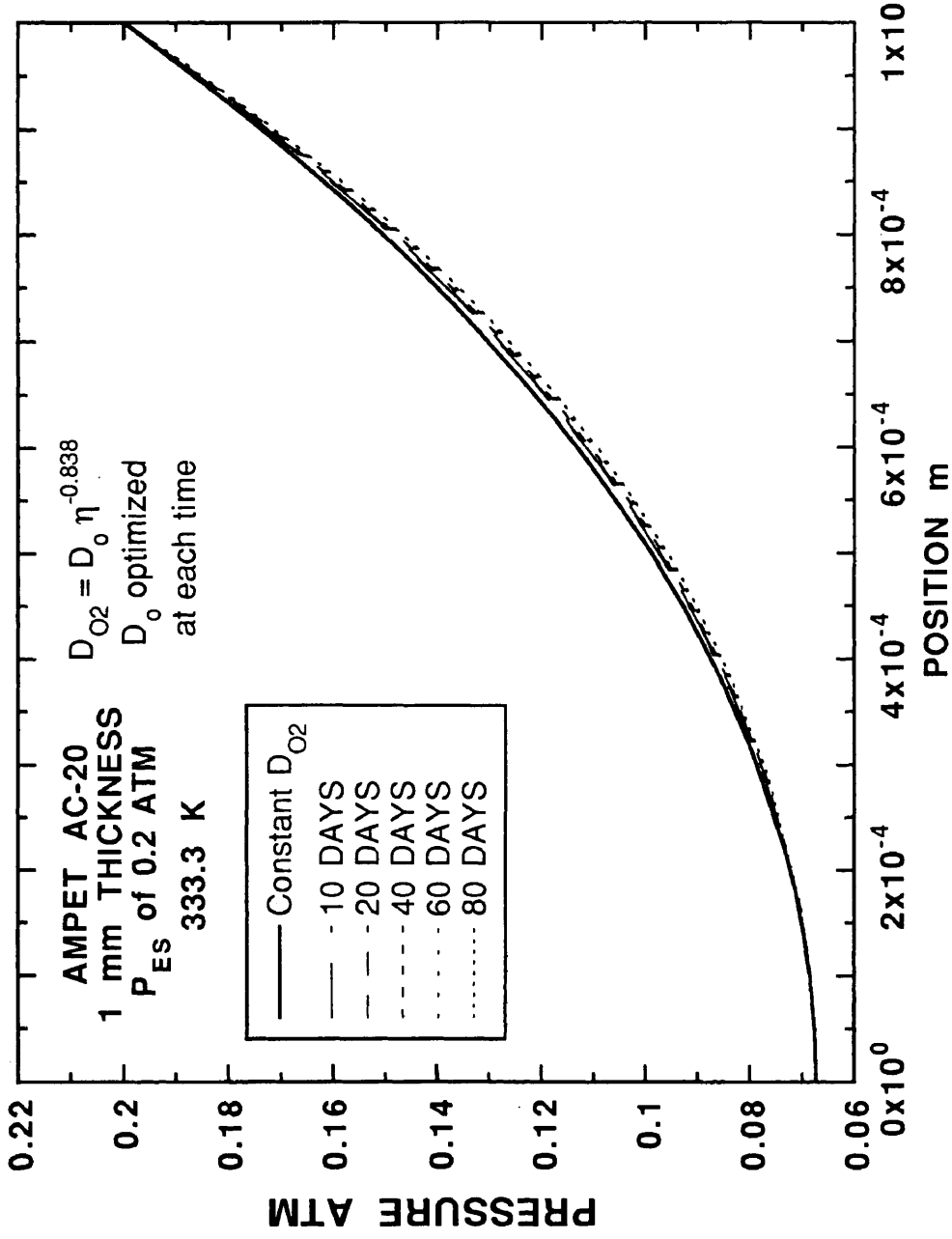

Figure V-17. Calculated oxygen pressure profiles in 1 mm thick film Ampet AC-20 at 333.3 K and P_{ES} of 0.2 atm for estimated D_o from steady-state variable $\mathcal{D}_{O_2}$ oxygen diffusion and reaction.

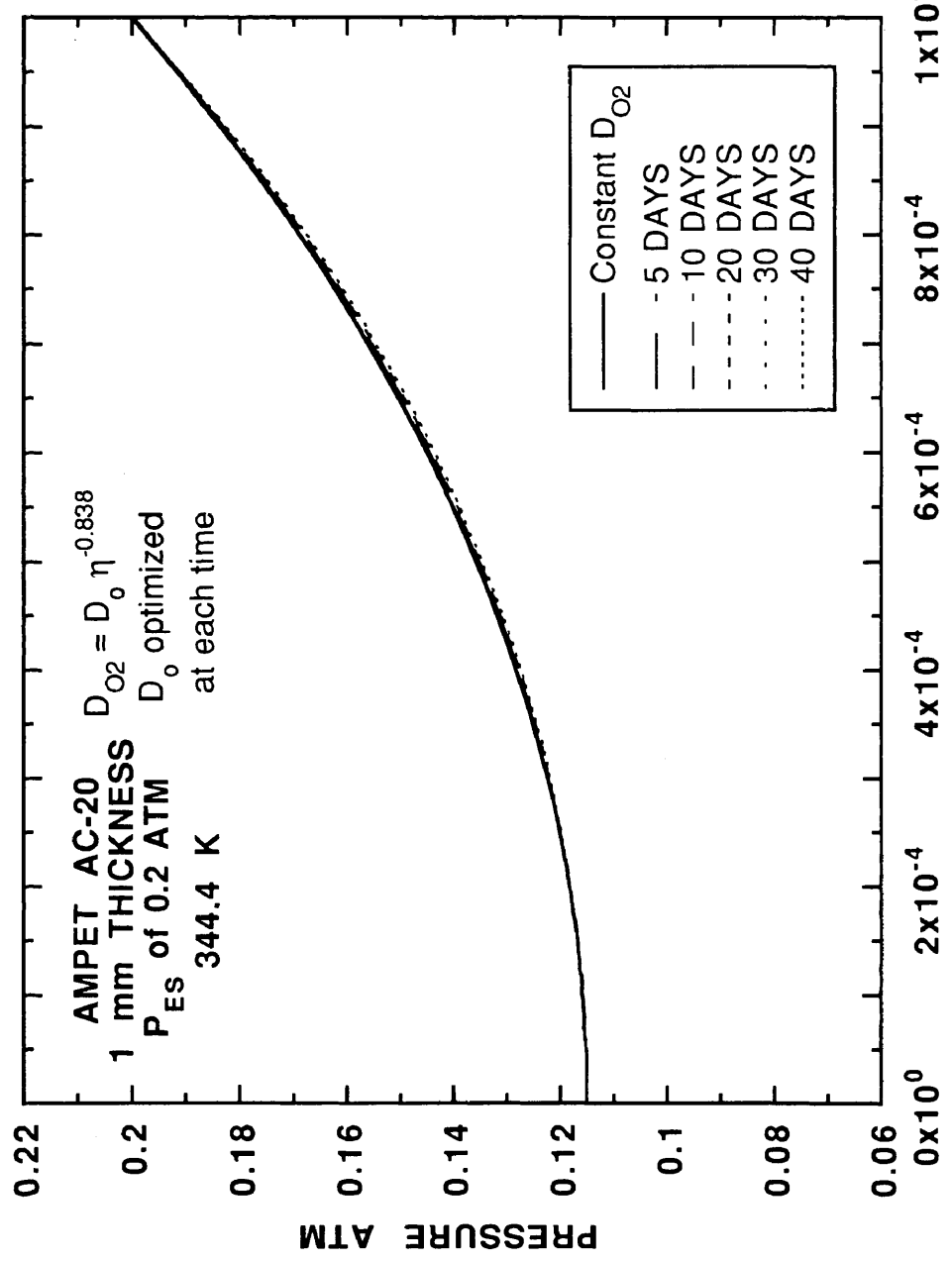

Figure V-18. Calculated oxygen pressure profiles in 1 mm thick film Ampet AC-20 at 344.4 K and P_{ES} of 0.2 atm for estimated D_o from steady-state variable $\mathcal{D}_{O_2}$ oxygen diffusion and reaction.

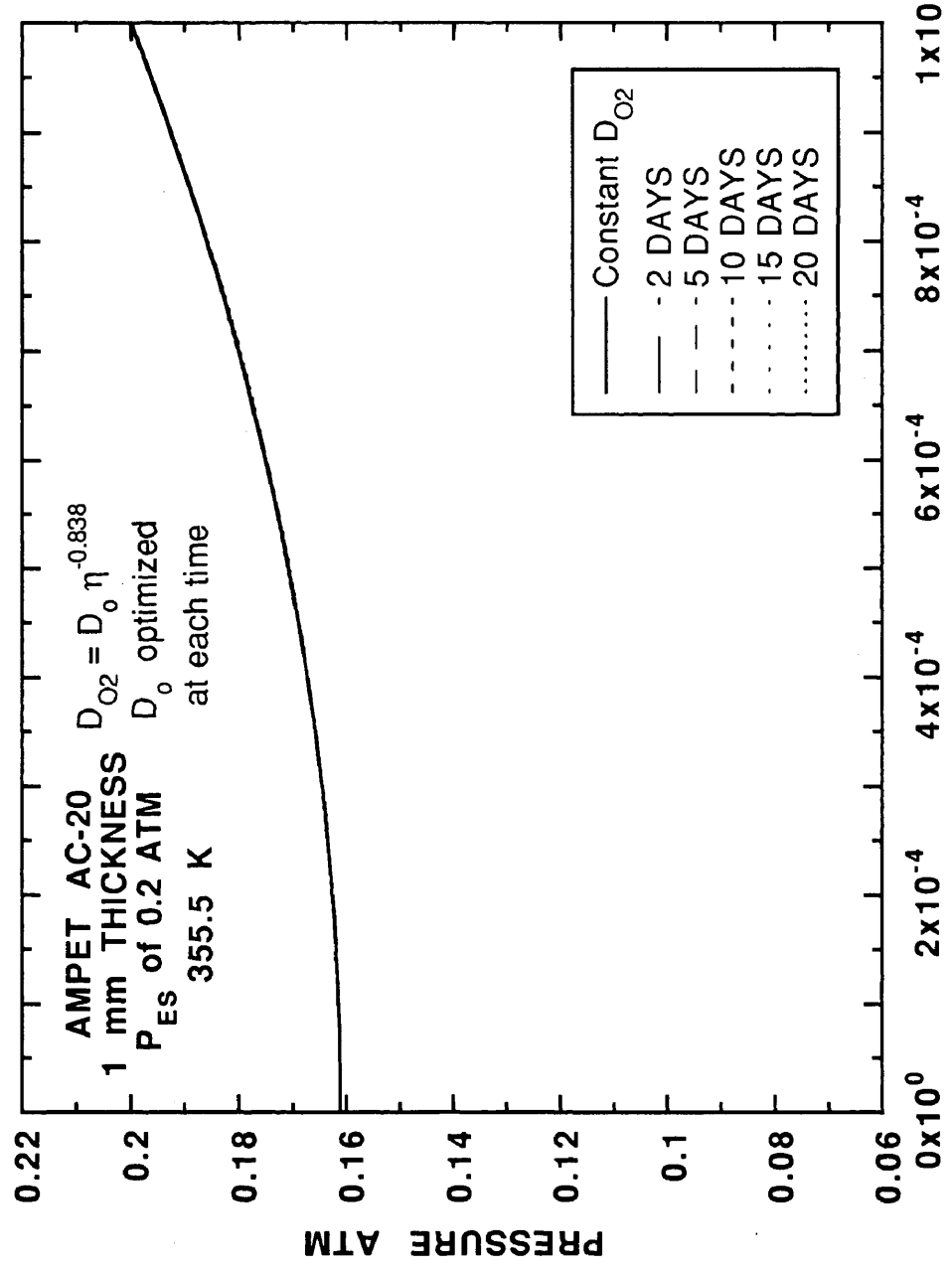

Figure V-19. Calculated oxygen pressure profiles in 1 mm thick film Ampet AC-20 at 355.5 K and P_{ES} of 0.2 atm for estimated D_o from steady-state variable $\mathcal{D}_{O_2}$ oxygen diffusion and reaction.

is accurate from Figures V-17, V-18, and V-19 and Figure V-14 for constant $\mathcal{D}_{O_2}$. For increasing aging time at isothermal conditions, oxygen pressure profiles become steeper as x approaches the ES. This diminishes for increasing temperature; therefore, temperature probably reduces η_o^* more significantly than increases r_{CA}. There is little change in the profile at all temperatures given the constraints on the solution. At 355.5 K, oxygen pressure profiles are insensitive to optimized D_o. Overall, given the criterion for solution, oxygen pressure profiles change little by including variable $\mathcal{D}_{O_2}$. Although these calculations are purely hypothetical, they support Blokker and van Hoorn's (1959) conclusion that a hard skin is formed on the ES inhibiting oxygen transport through the film. Oxygen pressure profiles for the other asphalts and aging conditions studied were not produced.

In the second set of calculations, B and D_o were fixed for all asphalts and aging conditions. P_{SI} was optimized such that all boundary conditions were satisfied. This calculation is more realistic than the previous set, predicting decreases in P_{SI} with increasing aging time. $\mathcal{D}_{O_2}$ at the ES decreases due to increases in η_o^* from CA. This complex phenomenon limits further oxygen transport into the asphalt film.

Figures V-20, V-21, V-22 show the oxygen pressure profile in a 1 mm film for Ampet AC-20 at P_{ES} of 0.2 atm for aging temperatures of 333.3, 344.4, 355.5 K, respectively. The oxygen pressure profile at the ES becomes steeper with increasing aging time for isothermal conditions. P_{SI} decreases with increasing aging time to satisfy the boundary conditions. The difference in P_{ES} and P_{SI} decreases at constant aging time with increasing temperature. At high temperature, the rate of oxygen transport and reaction are about the same magnitude. At low temperature, the rate of oxygen transport is lower than reaction, and decreasing oxygen pressure reduces r_{CA} in the film. The change in P_{SI} with respect to change in aging time appears

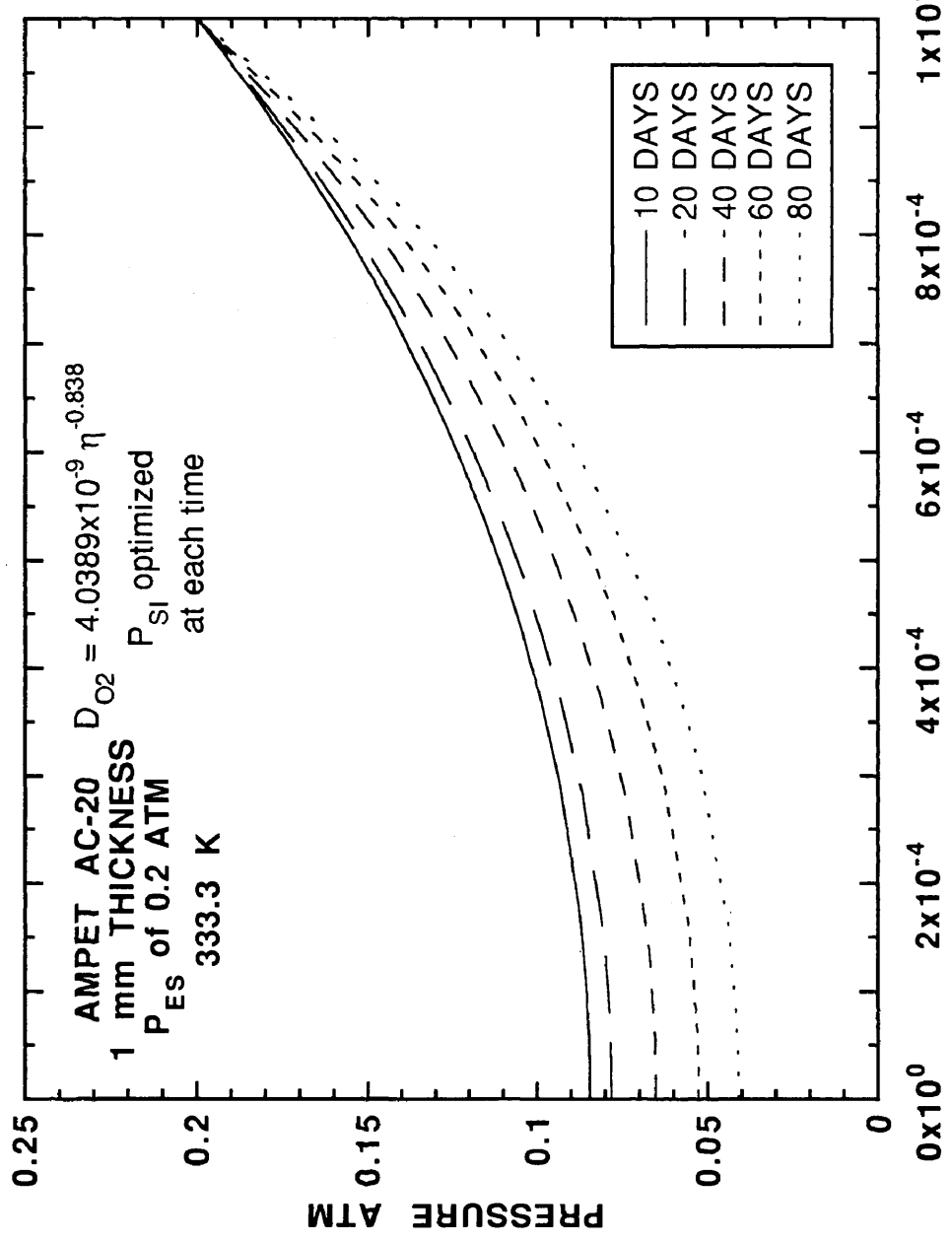

Figure V-20. Calculated oxygen pressure profiles in 1 mm thick film Ampet AC-20 at 333.3 K and P_{ES} of 0.2 atm for estimated P_{SI} from steady-state variable $\mathcal{D}_{O_2}$ oxygen diffusion and reaction.

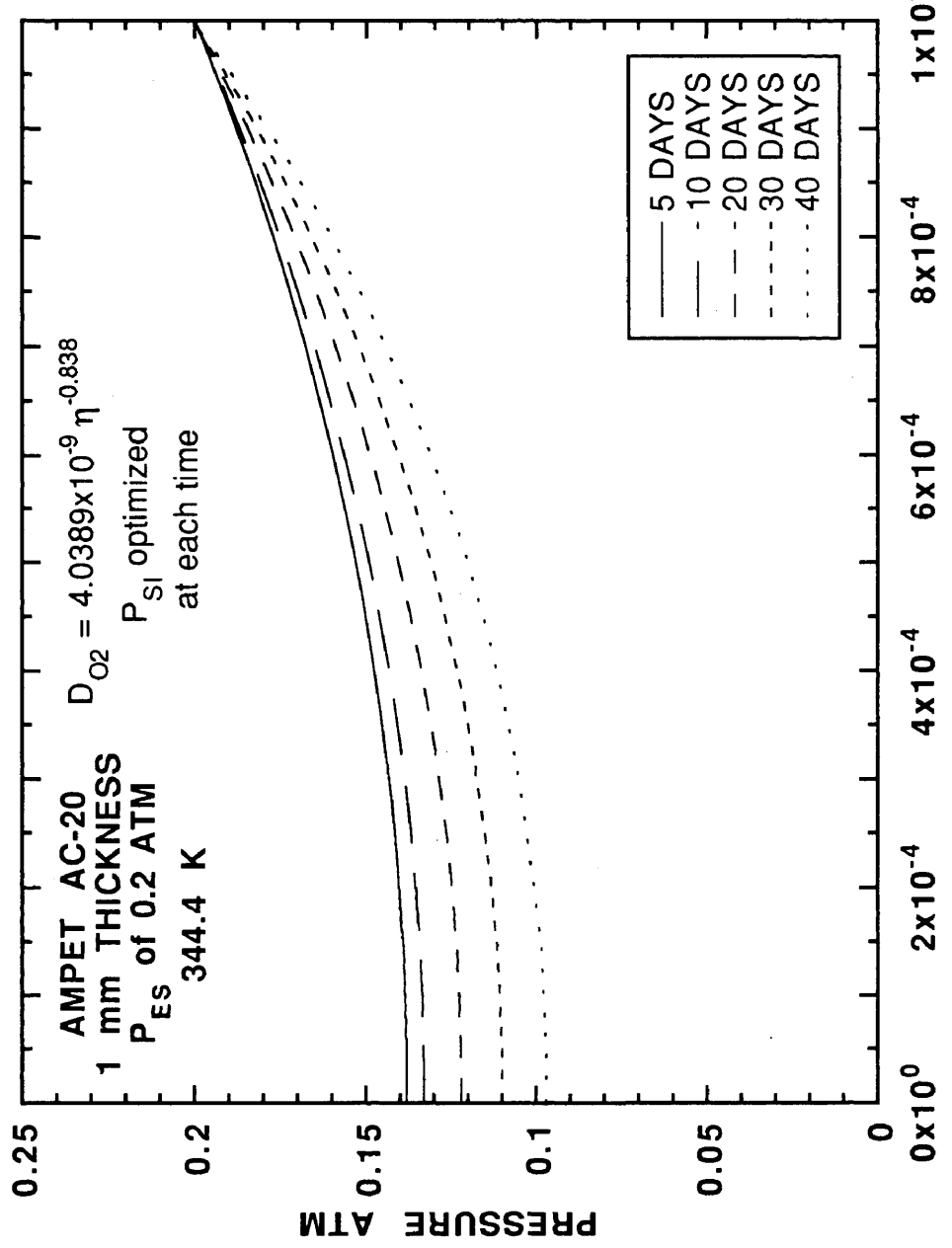

Figure V-21. Calculated oxygen pressure profiles in 1 mm thick film Ampet AC-20 at 344.4 K and P_{ES} of 0.2 atm for estimated P_{SI} from steady-state variable $\mathcal{D}_{O_2}$ oxygen diffusion and reaction.

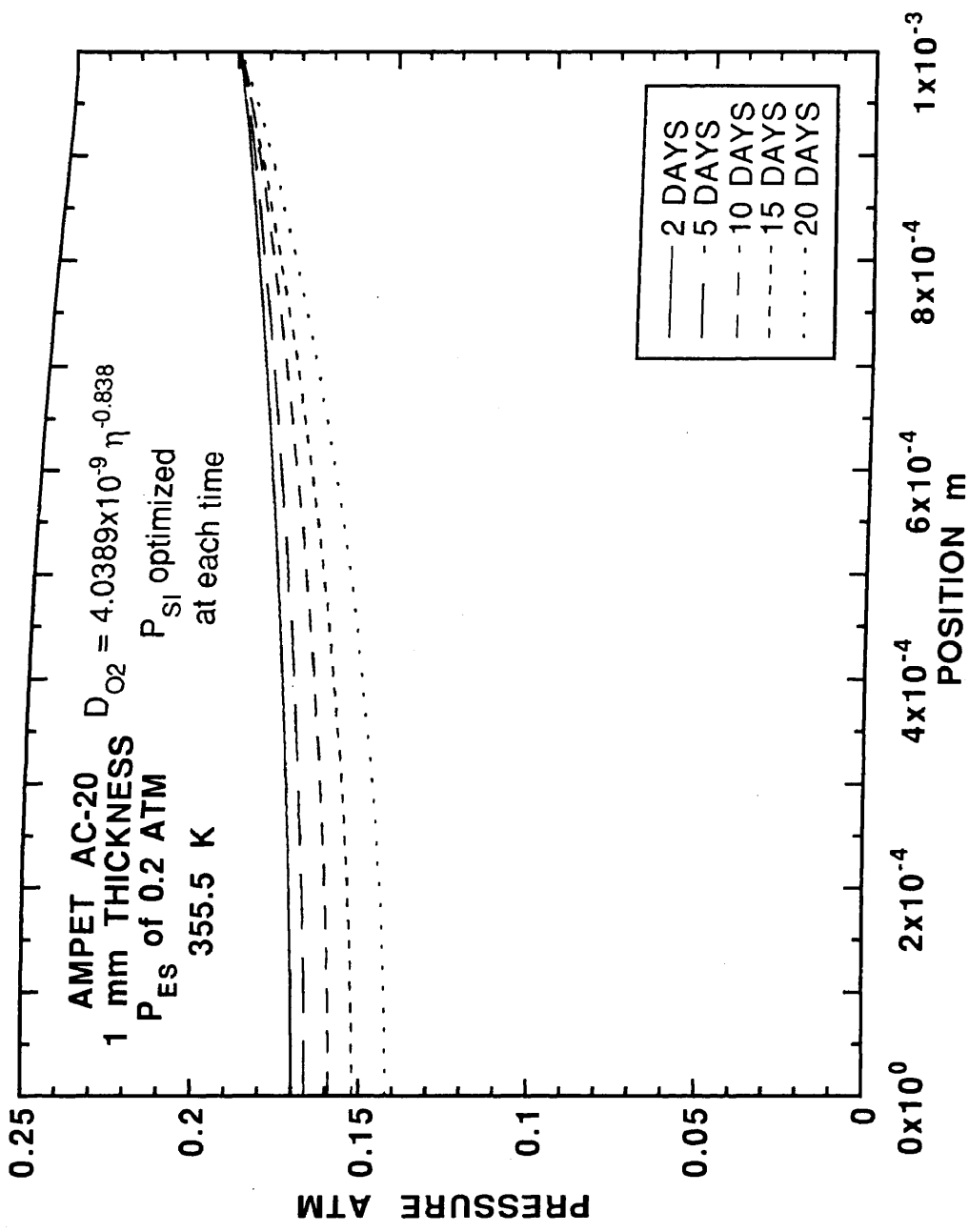

Figure V-22. Calculated oxygen pressure profiles in 1 mm thick film Ampet AC-20 at 355.5 K and P_{ES} of 0.2 atm for estimated P_{SI} from steady-state variable D_{O_2} oxygen diffusion and reaction.

to increase with aging temperature. For example, changes in P_{SI} from 10 to 20 days are largest for 355.5 and decreases for 344.4 and 333.3 K respectively. This observation, although appearing to contradict the fact that increasing temperature decreases diffusion resistance, does not factor in the magnitude of P_{SI}. This may have resulted purely from the constraints on the equation. Finally, the steady-state assumption is violated since the oxygen pressure profiles change with time. Profiles of the other asphalts and aging conditions studied were not generated.

Comparisons between estimated P_{SI} at the experimental initial and ending aging times based on equation II – 31 with variable $\mathcal{D}_{O_2}$ and P_{SI} determined from $(r_{CA})_{SI}$ are given in Table V-16 and V-17. All of the asphalts and aging conditions are given, including 20 atm. The tables are organized by asphalts for increasing aging temperature and P_{ES}. The initial and final aging times are 10, 5, 2, and 80, 40, 20, for 333.3, 344.4, 355.5 K, respectively. The percent difference in the arithmetic average of the initial and final P_{SI} versus P_{SI} determined from $(r_{CA})_{SI}$ is also shown. The set of questionable data shows the largest percent difference. This set was not used to estimate $\mathcal{D}_{O_2}$-η_o^* model parameters.

Figures V-20, V-21, and V-22 show that P_{SI} decreases with increasing aging time for all asphalts and aging conditions studied. In Table V-16 for Ampet AC-20 at 333.3 K and P_{ES} of 2 atm, P_{SI} is 1.66 atm at 10 days and 1.41 atm at 80 days. At the initial time, all asphalts show decreasing pressure gradients relative to P_{ES} with increasing P_{ES} for isothermal aging. Comparisons at constant temperature are for equivalent aging time ranges. However, comparisons at different aging temperatures do not represent the same time range. The percent decrease in P_{SI} relative to P_{ES} for 0.2, 2, and 20 atm is 58, 17, and 5% respectively for Ampet at 333.3 K at 10 days aging. At the final time, the relative gradient increases for all cases. Furthermore, the

Table V-16. Comparisons between Estimated P_{SI} from r_{CA} and Calculated P_{SI} for Steady-State Variable $\mathcal{D}_{O_2}$ Oxygen Diffusion and Reaction for Ampet AC-20, Coastal AC-20, and Cosden AC-20[a,b]

Asphalt	T K	P_{ES} atm	P_{SI} Initial atm	P_{SI} Kinetics atm	P_{SI} Final atm	P_{SI} Avg atm	% Diff[c]
Ampet AC-20	333.3	0.2	0.0846	0.0673	0.0411	0.0629	7
		2.0	1.66	0.393*	1.16	1.41	-72
		20.0	19.0	–	14.0	16.5	–
	344.4	0.2	0.138	0.115	0.0967	0.117	-2
		2.0	1.83	0.857*	1.49	1.66	-48
		20.0	19.5	–	15.9	17.7	–
	355.5	0.2	0.170	0.161	0.142	0.156	3
		2.0	1.92	1.80	1.72	1.82	-1
		20.0	19.8	–	17.6	18.7	–
Coastal AC-20	333.3	0.2	0.0820	0.149*	0.0290	0.0555	168
		2.0	1.49	0.925	0.630	1.06	-13
		20.0	17.4	–	4.85	9.78	–
	344.4	0.2	0.132	0.0345	0.0698	0.101	-66
		2.0	1.74	0.476*	0.918	1.33	-64
		20.0	18.7	–	5.89	12.3	–
	355.5	0.2	0.163	0.0789*	0.105	0.134	-41
		2.0	1.86	1.10	1.12	1.49	-26
		20.0	19.4	–	6.25	12.8	–
Cosden AC-20	333.3	0.2	0.0444	0.0331	0.0063	0.0254	30
		2.0	1.33	0.936	0.403	0.868	8
		20.0	17.1	–	3.85	10.5	–
	344.4	0.2	0.117	0.130	0.0576	0.0873	49
		2.0	1.70	0.363*	0.962	1.33	-73
		20.0	18.8	–	7.98	13.4	–
	355.5	0.2	0.160	0.400*	0.121	0.140	186
		2.0	1.87	1.48	1.35	1.61	-8
		20.0	19.5	–	11.1	15.3	–

[a] α of 0.270 and 1 mm thick films

[b] – Signifies the values were not determined

[c] $\%\ \text{Diff} = 100\left(\frac{P_{\text{rea}} - P_{\text{dif}}}{P_{\text{dif}}}\right)$

* These data were not used in the parameter estimation in Figure V-16.

Table V-17. Comparisons between Estimated P_{SI} from r_{CA} and Calculated P_{SI} for Steady-State Variable $\mathcal{D}_{O_2}$ Oxygen Diffusion and Reaction for Exxon AC-20 and Texaco AC-20[a,b]

Asphalt	T K	P_{ES} atm	P_{SI} Initial atm	P_{SI} Kinetics atm	P_{SI} Final atm	P_{SI} Avg atm	% Diff[c]
Exxon AC-20	333.3	0.2	0.0686	0.175*	0.0284	0.0485	260
		2.0	1.54	1.09	0.958	1.25	-13
		20.0	18.4	–	15.7	17.0	–
	344.4	0.2	0.120	0.108	0.0696	0.0948	14
		2.0	1.75	1.17*	1.21	1.48	-21
		20.0	19.1	–	12.4	15.8	–
	355.5	0.2	0.169	0.0776*	0.146	0.158	-51
		2.0	1.91	1.86	1.74	1.82	2
		20.0	19.7	–	17.8	18.8	–
Texaco AC-20	333.3	0.2	0.119	0.124	0.0749	0.0970	28
		2.0	1.74	1.38	1.28	1.51	-9
		20.0	19.1	–	13.4	16.2	–
	344.4	0.2	0.157	0.122	0.123	0.140	-13
		2.0	1.87	0.570*	1.58	1.72	-67
		20.0	19.6	–	15.9	17.8	–
	355.5	0.2	0.178	0.170	0.155	0.166	2
		2.0	1.94	1.28 *	1.75	1.84	-30
		20.0	19.8	–	17.5	18.6	–

[a] α of 0.270 and 1 mm thick films

[b] – Signifies the values were not determined.

[c] % Diff $= 100\left(\frac{P_{\text{rea}} - P_{\text{dif}}}{P_{\text{dif}}}\right)$

* These data were not used in the parameter estimation in Figure V-16.

effect of P_{ES} on the relative pressure gradient diminishes. The percent decrease in P_{SI} relative to P_{ES} is 79, 42, and 30% for 0.2, 2, and 20 atm respectively for Ampet AC-20 at 80 days and 333.3 K.

Not all asphalts show this behavior. Coastal AC-20 and Cosden AC-20 show increased pressure gradients relative to P_{ES} for P_{ES} from 2 to 20 atm for all aging temperatures at the final aging time. Texaco AC-20 at 355.5 K shows no decrease

in relative pressure gradient from 2 to 20 atm at the final aging time. These results for Coastal AC-20, Cosden AC-20, and Texaco AC-20 can be related to previously measured properties and estimated parameters. Coastal AC-20 has the highest *HS* at all temperatures studied in Table V-4. Cosden AC-20 has relatively high r_{CA} from Table V-5. At 355.5 K, Texaco AC-20 r_{CA} approaches that of Cosden AC-20, and Texaco AC-20 *HS* approaches that of Coastal AC-20. At the conditions for this unusual behavior, these asphalts become very hard due to *CA* and *HS* in a relatively short time compared to the other asphalts. With very high η_o^*, $\mathcal{D}_{O_2}$ is low. For asphalts with high r_{CA} or *HS*, increasing P_{ES} for long term aging studies may not necessarily diminish the relative pressure gradient in the film. However, the magnitude of the pressure may be high enough such that relatively homogenous-aged material is obtained. In Chapter IV, this problem was discussed for Cosden AC-20 at 20 atm and 333.3 K where bulk *CA* was determined.

P_{SI} from $(r_{CA})_{SI}$ and P_{SI} values estimated from the steady-state variable $\mathcal{D}_{O_2}$ and reaction model are compared. The range of initial and final P_{SI} should bound P_{SI} determined from $(r_{CA})_{SI}$. This is not always true even for the data included in the parameter estimation of the $\mathcal{D}_{O_2}$-η_o^* model. The range of initial and final P_{SI} does not bracket P_{SI} estimated from $(r_{CA})_{SI}$ for Texaco AC-20 at 333.3 K, P_{ES} of 0.2 atm; Coastal AC-20, Cosden AC-20, and Texaco AC-20 to 344.4 K, P_{ES} of 0.2 atm; and Coastal AC-20 at 355.5 K, P_{ES} of 2.0 atm. These errors may result from the steady-state assumption or from the estimation of CA_o. CA_o was not in the model when steady-state constant $\mathcal{D}_{O_2}$ was determined, and the $\mathcal{D}_{O_2}$-η_o^* model was developed. P_{SI} estimated from $(r_{CA})_{SI}$ is outside initial and final P_{SI} for all questionable data that was not used to estimate $\mathcal{D}_{O_2}$-η_o^* model parameters.

The effective average P_{SI} was calculated as the arithmetic average of initial and final P_{SI}. The percent difference in P_{SI} determined from $(r_{CA})_{SI}$ and the effective average P_{SI} is also shown in the table. The difference is extremely large, over 200%, for some of the questionable data. The data set at 344.4 K shows the largest overall percent difference if one neglects the extreme outliers, data for Coastal AC-20 and Exxon AC-20 at 333.3 K and Cosden AC-20 at 355.5 K at P_{ES} of 0.2. A majority of P_{SI} determined from $(r_{CA})_{SI}$ is below the effective average P_{SI}. At 344.4 K the difference is fairly large even for the data used to estimate $\mathcal{D}_{O_2}$-η_o^* model parameters. This difference may result from the kinetic parameters as described in Chapter IV or CA_o from equation IV – 2.

The magnitudes of $\left(\frac{d\mathcal{D}_{O_2}}{dP}\right)\left(\frac{dP}{dx}\right)^2$ and $\mathcal{D}_{O_2}\left(\frac{d^2P}{dx^2}\right)$ are compared. This provides a relative measure of the limitation of oxygen transport due to variable diffusivity. Since $\left(\frac{d\mathcal{D}_{O_2}}{dP}\right)$ is negative, variable diffusivity decreases overall oxygen transport. The absolute value of the ratio of the two quantities defines a new, dimensionless, variable in equation V – 24.

$$\xi = \left| \frac{\left(\frac{d\mathcal{D}_{O_2}}{dP}\right)\left(\frac{dP}{dx}\right)^2}{\mathcal{D}_{O_2}\left(\frac{d^2P}{dx^2}\right)} \right| \qquad (V-24)$$

The denominator is never zero over the range of x; the value of ξ is always defined. Substituting equation II – 37 into V – 24 gives equation V – 25.

$$\xi = \left| \frac{\mathcal{D}_{O_2} \cdot B \cdot HS \cdot k_P \cdot \alpha \cdot t \cdot P^{(\alpha-1)}\left(\frac{dP}{dx}\right)^2}{\mathcal{D}_{O_2}\left(\frac{d^2P}{dx^2}\right)} \right| \qquad (V-25)$$

$\mathcal{D}_{O_2}$ is eliminated yielding equation V – 26.

$$\xi = -B \cdot HS \cdot k_P \cdot \alpha \cdot t \cdot P^{(\alpha-1)} \left[\frac{\left(\frac{dP}{dx}\right)^2}{\left(\frac{d^2P}{dx^2}\right)} \right] \qquad (V-26)$$

B and α were constant and dimensionless with values of -0.838 and 0.27 respectively, for the asphalts studied. HS has units of $1/CA$ and is a function of T and asphalt as given in Table V-4. k_P has units of CA / day atm$^{\alpha-1}$ and is a function of T and asphalt, also. It is calculated from the Arrhenius parameters in Table IV-6. The aging time, t, is in days.

Figures V-23, V-24, and V-25 show ξ as a function of position for Ampet AC-20 at P_{ES} of 0.2 atm and aging temperatures of 333.3, 344.4, and 355.5 K. The first and second derivatives of P with respect to x were numerically evaluated from the profile data in Figures V-20, V-21, and V-22. Therefore, the lines are jagged. From the figures, ξ increases with position from the SI at constant time. At constant position, ξ increases with increasing aging time; i.e., the more the aging extent, the greater the effect of variation of $\mathcal{D}_{O_2}$ on position. Variable $\mathcal{D}_{O_2}$ limits oxygen transport more severely with increasing time. Surprisingly, at constant aging time and position, the data suggest that increases in temperature also increase ξ. For example, Figure V-23 shows higher ξ at 20 days for 355.5 K than ξ at 20 days for 344.4 or 333.3 K. This suggests that both k_P and P increase to a greater extent than HS and the derivatives decrease the increasing temperature. For Ampet AC-20 at P_{ES} of 0.2 atm, the highest ξ for the laboratory experiments was 0.2. The calculations were not performed for the other asphalts studied. Asphalts such as Coastal AC-20 and Cosden AC-20 may have higher ξ than those calculated for Ampet AC-20.

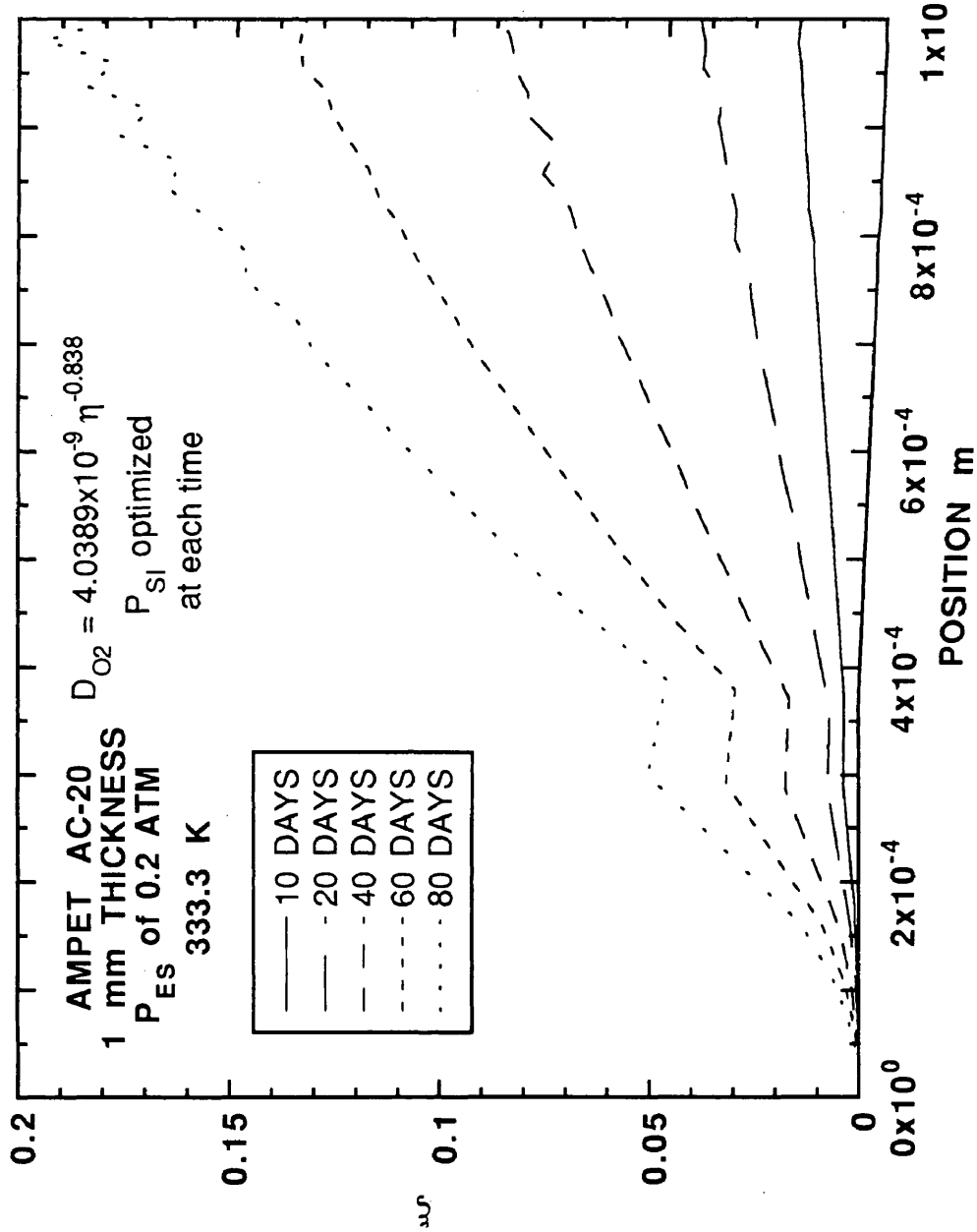

Figure V-23. ξ versus position in 1 mm thick film Ampet AC-20 at 333.3 K and P_{ES} of 0.2 atm for estimated P_{SI} from steady-state variable $\mathcal{D}_{O_2}$ oxygen diffusion and reaction.

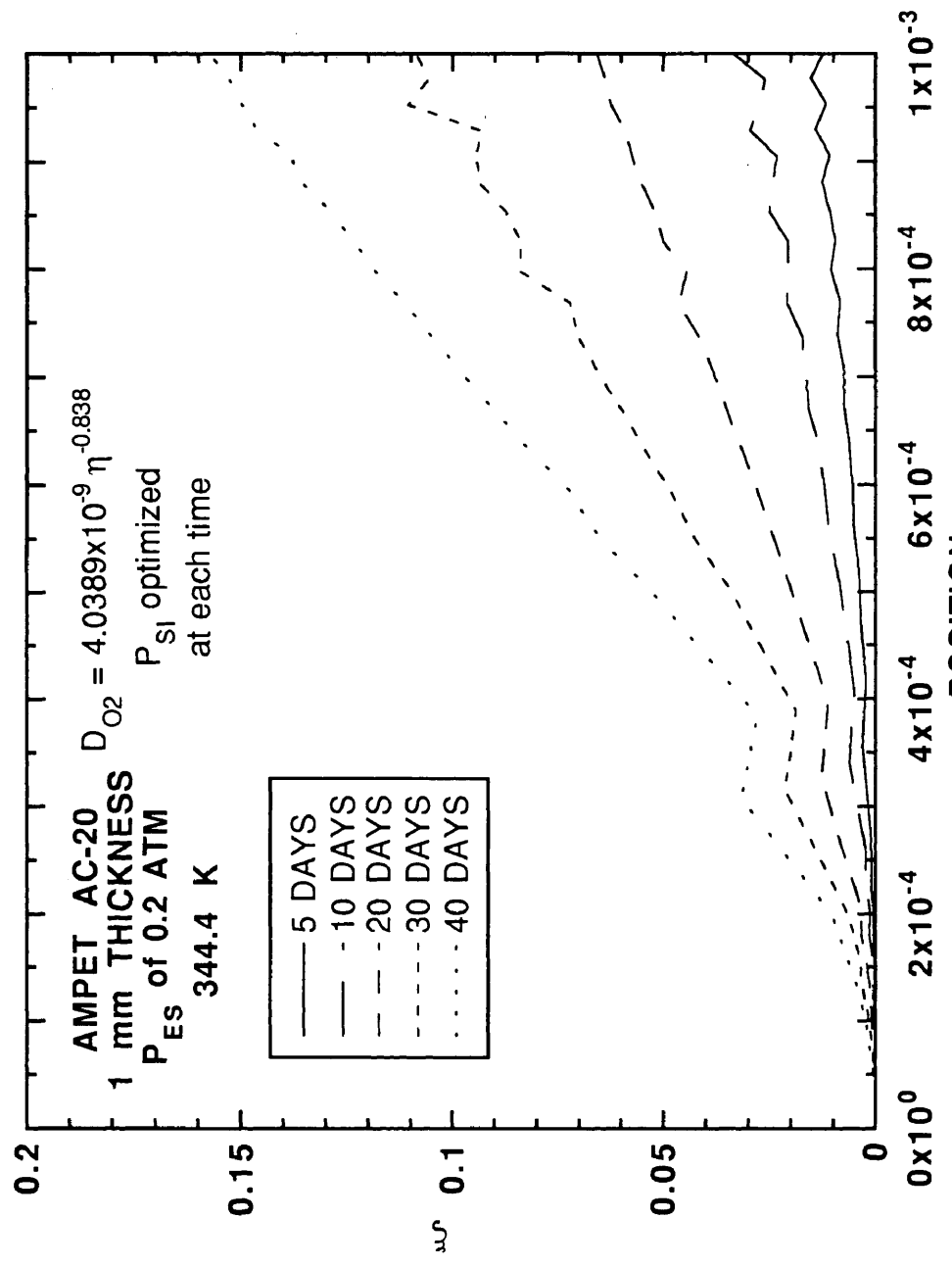

Figure V-24. ξ versus position in 1 mm thick film Ampet AC-20 at 344.4 K and P_{ES} of 0.2 atm for estimated P_{SI} from steady-state variable $\mathcal{D}_{O_2}$ oxygen diffusion and reaction.

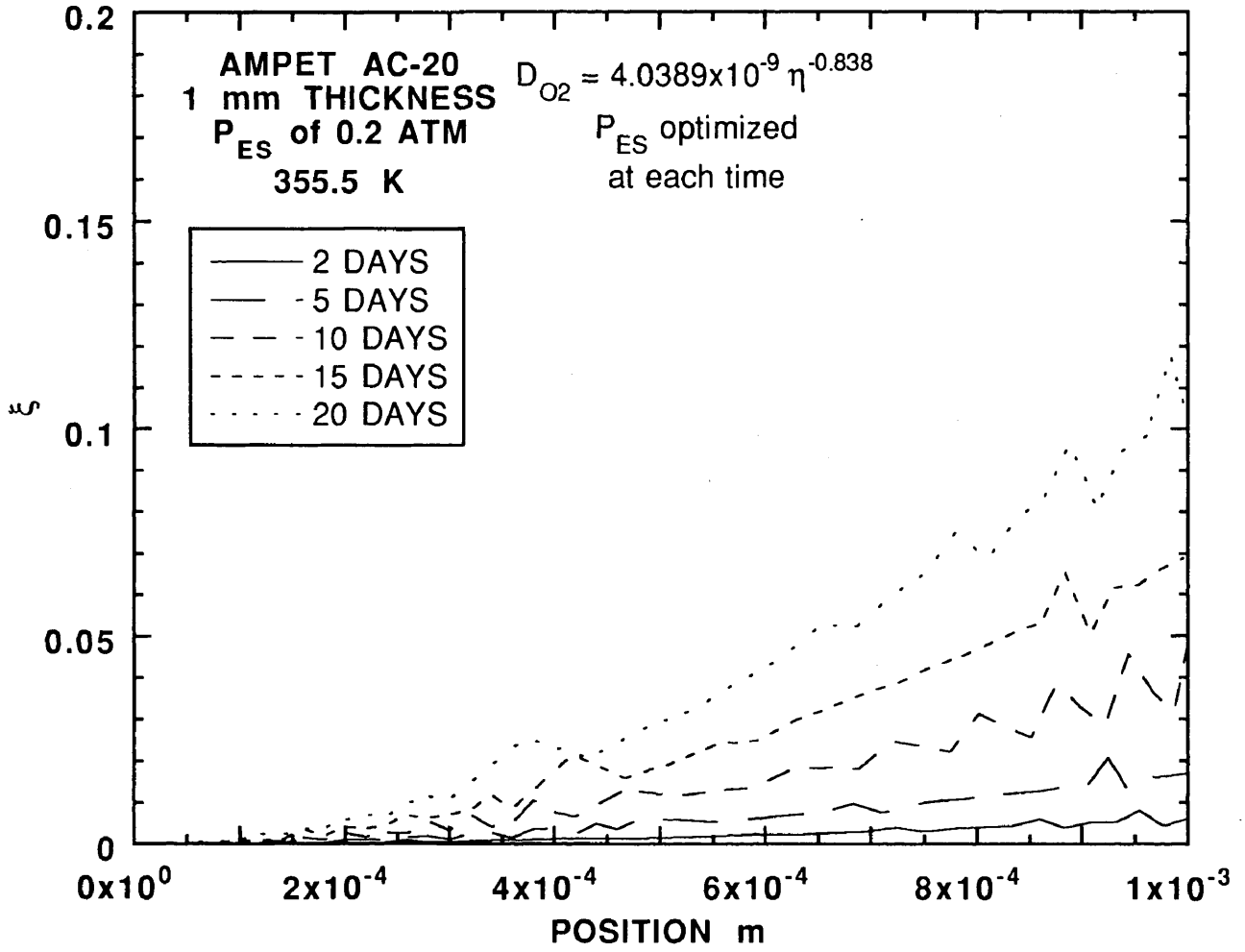

Figure V-25. ξ versus position in 1 mm thick film Ampet AC-20 at 355.5 K and P_{ES} of 0.2 atm for estimated P_{SI} from steady-state variable $\mathcal{D}_{O_2}$ oxygen diffusion and reaction.

In summary, with a model relating $\mathcal{D}_{O_2}$ and η_o^*, a steady-state variable $\mathcal{D}_{O_2}$ oxygen diffusion and reaction equation was numerically solved. The solution of the equation produced the oxygen pressure profile in an asphalt film. This solution satisfied both boundary conditions at the *SI* for zero oxygen flux and the *ES* for known P. It was concluded that the numerical solution was accurate comparing the profiles for constant $\mathcal{D}_{O_2}$ and optimized D_o at discrete aging times. Given the constraints for the equation, the oxygen pressure profile is insensitive to changes in D_o. P_{SI} was optimized for discrete aging times and fixed B, D_o, and P_{ES}. These profiles were more realistic showing decreasing P_{SI} with increasing aging time. These figures also showed that the steady-state assumption is probably not valid. The range of P_{SI} determined from the oxygen transport and reaction model was compared to P_{SI} estimated from $(r_{CA})_{SI}$. Even the data set used to estimate $\mathcal{D}_{O_2}$-η_o^* model parameters showed some differences in the comparison. This probably resulted by introducing CA_o into the model. The questionable data set, not used to estimate $\mathcal{D}_{O_2}$-η_o^* model parameters, showed rather large differences in the comparison. The calculations and data revealed an interesting phenomenon. In the past, researchers have used elevated pressure to decrease the oxygen gradient in the film. However, for asphalts with high *HS* or r_{CA}, increasing P_{ES} may actually increase the oxygen pressure gradient on a relative basis for long-term aging. For these asphalts, a very hard material with low $\mathcal{D}_{O_2}$ forms rapidly at the *ES* inhibiting further oxygen transport. Even though the pressure gradient in the film on a relative basis may be more severe, the magnitude of the pressure may be such that relatively uniform aging samples are obtained. Finally, a dimensionless variable ξ was defined as the absolute value of the ratio of $\left(\frac{d\mathcal{D}_{O_2}}{dP}\right)\left(\frac{dP}{dx}\right)^2$ to $\mathcal{D}_{O_2}\left(\frac{d^2P}{dx^2}\right)$. For Ampet AC-20 at P_{ES} of 0.2 atm, ξ increased with both position from the *SI* and aging time. ξ also increased with aging

temperature for constant time; P and k_P increased more than HS and the ratio of the derivatives decreased. The maximum value of ξ for Ampet AC-20 was 0.2. ξ for the other asphalts was not determined.

Unsteady-state oxygen diffusion and reaction

From Figures V-20, V-21, and V-22, it is obvious that a steady-state assumption is not valid for oxygen diffusion and reaction in an asphalt film. Therefore, the unsteady-state variable $\mathcal{D}_{O_2}$ oxygen diffusion and reaction model given in equation II – 40 is solved.

$$\left(\frac{\partial P}{\partial t}\right) = \left(\frac{\partial \mathcal{D}_{O_2}}{\partial P}\right)\left(\frac{\partial P}{\partial x}\right)^2 + \mathcal{D}_{O_2}\left(\frac{\partial^2 P}{\partial x^2}\right) - \left(\frac{cRT}{h}\right) r_{CA} \qquad \text{(II – 40)}$$

This equation not only requires two boundary conditions but also an initial condition.

$\left(\frac{\partial P}{\partial x}\right) = 0$	at	$x = 0$	Substrate interface
$P = P_{\text{gas}}$	at	$x = L$	Exposed surface
$P = 0$	at	$t = 0$	Initial condition

h is assumed to be unity in the absence of reliable oxygen solubility data. A model relating $\mathcal{D}_{O_2}$ to the amount of aging is given in equation II – 37.

$$\mathcal{D}_{O_2}(t,x) = D_o\left[\exp\left\{HS\left[T(t,x)\right]\left(\int_0^t r_{CA}\left[T(\theta,x),P(\theta,x)\right]d\theta + CA_o\right) + m\left[T(t,x)\right]\right\}\right]^B \qquad \text{(II – 37)}$$

The partial derivative of $\mathcal{D}_{O_2}$ with respect to P is given in equation II – 39.

$$\left(\frac{\partial \mathcal{D}_{O_2}}{\partial P}\right) = B \cdot HS \cdot \mathcal{D}_{O_2} \cdot \int_0^t \left(\frac{\partial r_{CA}}{\partial P}\right) d\theta \qquad \text{(II – 39)}$$

This model contains 12 estimated parameters: three for r_{CA}, two for CA_o, four to determine HS and m, one relating r_{CA} to r_{O_2}, and two relating $\mathcal{D}_{O_2}$ to η_o^*. For these calculations, B and D_o were estimated in Figure V-16. No multi-variable parameter estimation is performed from the solution of the PDE. From the unsteady-state oxygen profile, CA at both the ES and SI are calculated. These values are compared to measured CA. This comparison is used to judge how well the model and estimated parameters performed.

To numerically solve equation II – 40 with II – 37 and II – 39, finite difference equations are written for the spatial variable, x. The boundary conditions are satisfied by these finite difference equations. This expands equation II – 40 into a set of first order ODEs. Along with the equations for oxygen pressure, carbonyl formation at each point in the finite difference grid is also calculated from equation II – 1.

$$\left(\frac{\partial CA}{\partial t}\right) = r_{CA} \qquad \text{(II – 1)}$$

Two sets of equations, one accounting for oxygen pressure and one for carbonyl content, are solved simultaneously. With the known boundary and initial conditions and all the model parameters, the set of equations are numerically integrated forward in time yielding the oxygen pressure and carbonyl profiles. Finally, CA at the ES and SI are compared to experimental data.

The equation for variable diffusivity cannot be solved for the initial condition of zero oxygen pressure. $\left(\frac{\partial \mathcal{D}_{O_2}}{\partial P}\right)$ is undefined. Using equation V – 23 is not appropriate since this equation only applies for steady-state conditions. To eliminate this problem, equation V – 27 assuming a constant $\mathcal{D}_{O_2}$ is integrated for a time period of one day.

$$\left(\frac{\partial P}{\partial t}\right) = \mathcal{D}_{O_2}\left(\frac{\partial^2 P}{\partial x^2}\right) - cRTr_{CA} \qquad \text{(V – 27)}$$

After a one day time period, $\mathcal{D}_{O_2}$ varies according to equation II – 37.

Initial $\mathcal{D}_{O_2}$ must also be calculated. Since P_{ES} is known, bulk P in the film is approximated as one half P_{ES}. From equation IV – 2 an initial value of CA is calculated. With known HS and m at given T, η_o^* is determined from equation I – 6. Finally, $\mathcal{D}_{O_2}$ is calculated from equation II – 34. With this constant $\mathcal{D}_{O_2}$, equation V – 27 is integrated for one day establishing an initial oxygen pressure profile in the film. After one day, equations II–40 and II–1 are integrated forward until the desired time period is reached.

After the initial profile has been established, P at the SI becomes smaller and smaller because of reaction. Depending of the rates of oxygen transport and reaction, P in the film may increase or decrease. As P approaches zero, numerical instabilities occur because of equation II – 39. As P goes to zero, $\left(\frac{\partial \mathcal{D}_{O_2}}{\partial P}\right)$ goes to negative infinity. To overcome these instabilities, two conditions are artificially set. First, when P is zero, $\left(\frac{\partial \mathcal{D}_{O_2}}{\partial P}\right)$ is zero. Second, at decreasing pressures, if $P^{(\alpha-1)}$ exceeds one, $P^{(\alpha-1)}$ is artificially defined as one. $P^{(\alpha-1)}$ is used to calculate $\left(\frac{\partial \mathcal{D}_{O_2}}{\partial P}\right)$ from equation II – 39. This insures that ξ is less that one. These two conditions were imposed to decrease the numerical instabilities.

A set of first order ODEs with respect to time are formulated by numerically approximating the spatial derivatives using finite differences. For the interior points, the derivatives are approximated by equation V – 28.

$$\left(\frac{\partial P}{\partial x}\right) = \frac{P_{j+1} - P_{j-1}}{2\Delta x}$$
$$\left(\frac{\partial^2 P}{\partial x^2}\right) = \left(\frac{P_{j+1} - 2P_j + P_{j-1}}{\Delta x^2}\right) \qquad (V - 28)$$

Equation V – 29 gives the set of first order ODEs for constant $\mathcal{D}_{O_2}$ at the interior nodes.

$$\left(\frac{\partial P_j}{\partial t}\right) = \mathcal{D}_{O_2}\left(\frac{P_{j+1} - 2P_j + P_{j-1}}{\Delta x^2}\right) - cRTr_{CA}(T, P_j) \qquad (V - 29)$$

For the zero flux boundary at the SI, an imaginary node is defined by equation V – 30.

$$P_{\text{ima}} = P_2 \qquad (V - 30)$$

Equation V – 31 gives the ODE at the first node.

$$\left(\frac{\partial P_1}{\partial t}\right) = \mathcal{D}_{O_2}\left(\frac{P_2 - 2P_1 + P_{\text{ima}}}{\Delta x^2}\right) - cRTr_{CA}(T, P_1) \qquad (V - 31)$$

Equation V – 32 gives the ODE at the last node where P_{ES} is known.

$$\left(\frac{\partial P_N}{\partial t}\right) = \mathcal{D}_{O_2}\left(\frac{P_{ES} - 2P_N + P_{N-1}}{\Delta x^2}\right) - cRTr_{CA}(T, P_N) \qquad (V - 32)$$

For the initial condition, P is zero.

For variable $\mathcal{D}_{O_2}$, a second set of equations are derived. Equation V – 33 gives the ODE for the interior nodes.

$$\left(\frac{\partial P_j}{\partial t}\right) = \mathcal{D}'_{O_2}(P_j)\left(\frac{P_{j+1} - P_{j-1}}{2\Delta x}\right) + \mathcal{D}_{O_2}(P_j)\left(\frac{P_{j+1} - 2P_j + P_{j-1}}{\Delta x^2}\right) - cRTr_{CA}(T, P_j) \qquad (V - 33)$$

$\mathcal{D}'_{O_2}(P)$ is shorthand for $\left(\frac{\partial D_{O_2}}{\partial P}\right)$. Using the imaginary node from equation V – 30, equation V – 34 gives the ODE at the first node.

$$\left(\frac{\partial P_1}{\partial t}\right) = \mathcal{D}'_{O_2}(P_1)\left(\frac{P_2 - P_{\text{ima}}}{2\Delta x}\right) + \mathcal{D}_{O_2}(P_1)\left(\frac{P_2 - 2P_1 + P_{\text{ima}}}{\Delta x^2}\right) - cRTr_{CA}(T, P_1) \qquad (V - 34)$$

At the free surface, equation V – 35 provides the ODE.

$$\left(\frac{\partial P_N}{\partial t}\right) = \mathcal{D}'_{O_2}(P_N)\left(\frac{P_{ES} - P_{N-1}}{2\Delta x}\right) + \mathcal{D}_{O_2}(P_N)\left(\frac{P_{ES} - 2P_N + P_{N-1}}{\Delta x^2}\right) - cRTr_{CA}(T, P_N) \qquad (V - 35)$$

Together with P, CA at each node is also determined from equation V – 36.

$$\left(\frac{\partial CA_J}{\partial t}\right) = r_{CA}(T, P_J) \qquad \text{(V – 36)}$$

The source code for this program is given in Appendix D.

A comparison between measured and calculated CA at the ES and SI gives an indication of the model's ability to predict aging characteristics. Figures V-26 through V-31 compared Texaco AC-20 at 333.3, 344.4, and 355.5 K, and P_{ES} of 0.2 and 2 atm. Measured CA_{ES} is designated with the hollow circle; calculated CA_{ES} is shown with the solid line. Measured CA_{SI} is shown in the hollow square; calculated CA_{SI} is designated with the dashed line. Neat CA is shown with the solid circle. Calculated CA shows the same initial jump as the experimental data, because CA_o estimated the integration constant. It appears that calculated CA_{ES} is always lower than measured CA_{ES} for the same aging times, temperatures, and P_{ES}. At the SI, calculated CA is higher for some cases and lower in others relative to measured CA_{SI}. For Figures V-27 and V-29, the agreement is best. Although there are significant differences between measured and calculated CA, the figures suggest better agreement between r_{CA}. This results from errors in the estimation of CA_o at the beginning of the integration. An empirical model, equation IV – 2 was used with the estimated parameters from Table V-10. A more accurate model between P and CA_o such as equation I – 5 along with more experimental data to estimate parameters would diminish these discrepancies. A fundamental model, equation II – 7 calculates r_{CA}. Large amounts of data were collected with the intent of extracting kinetic model parameters. Thus, agreement between the calculated and measured r_{CA} is better.

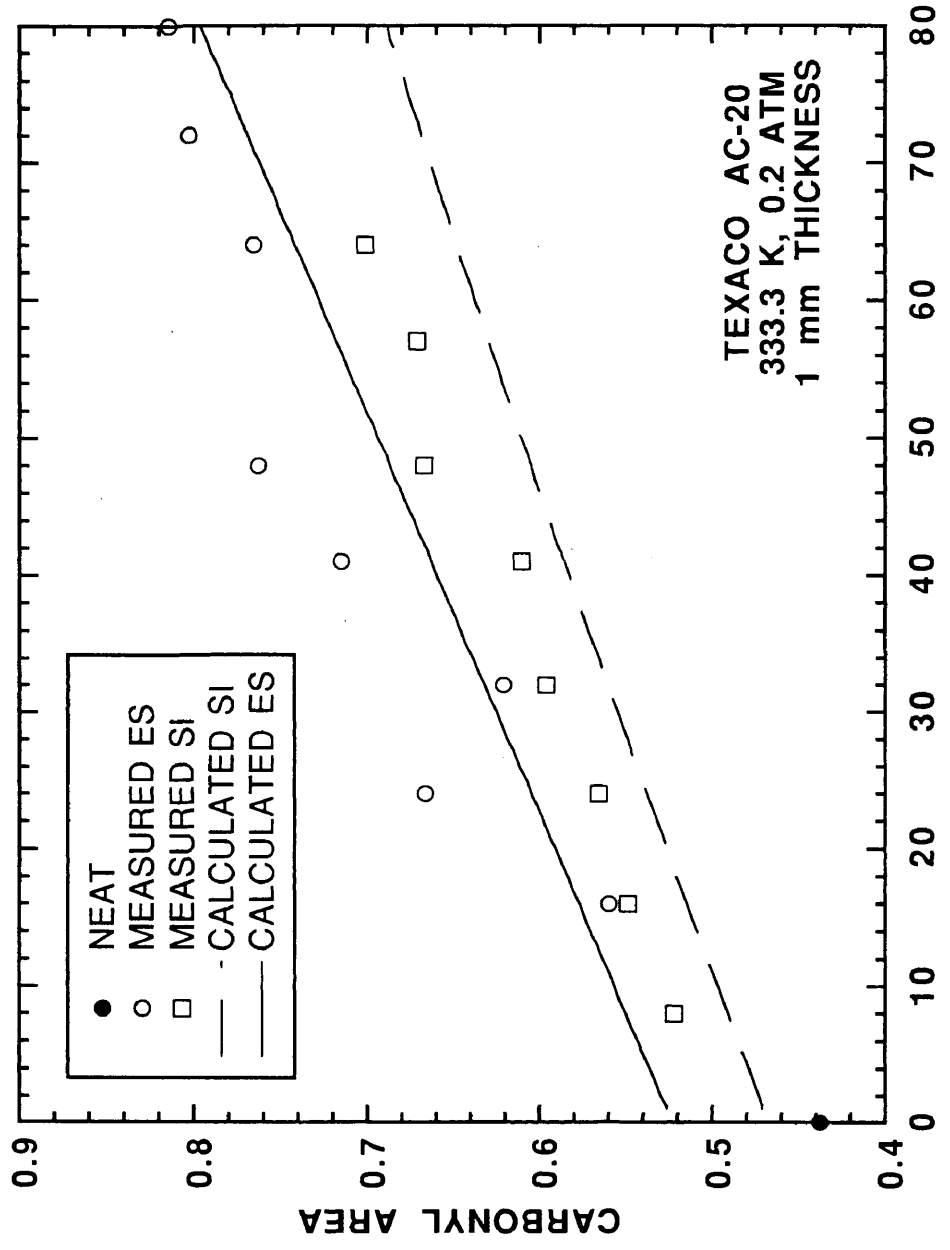

Figure V-26. Comparisons between measured and calculated CA at the ES and SI of 1 mm thick film POV-aged Texaco AC-20 at 333.3 K and P_{ES} of 0.2 atm.

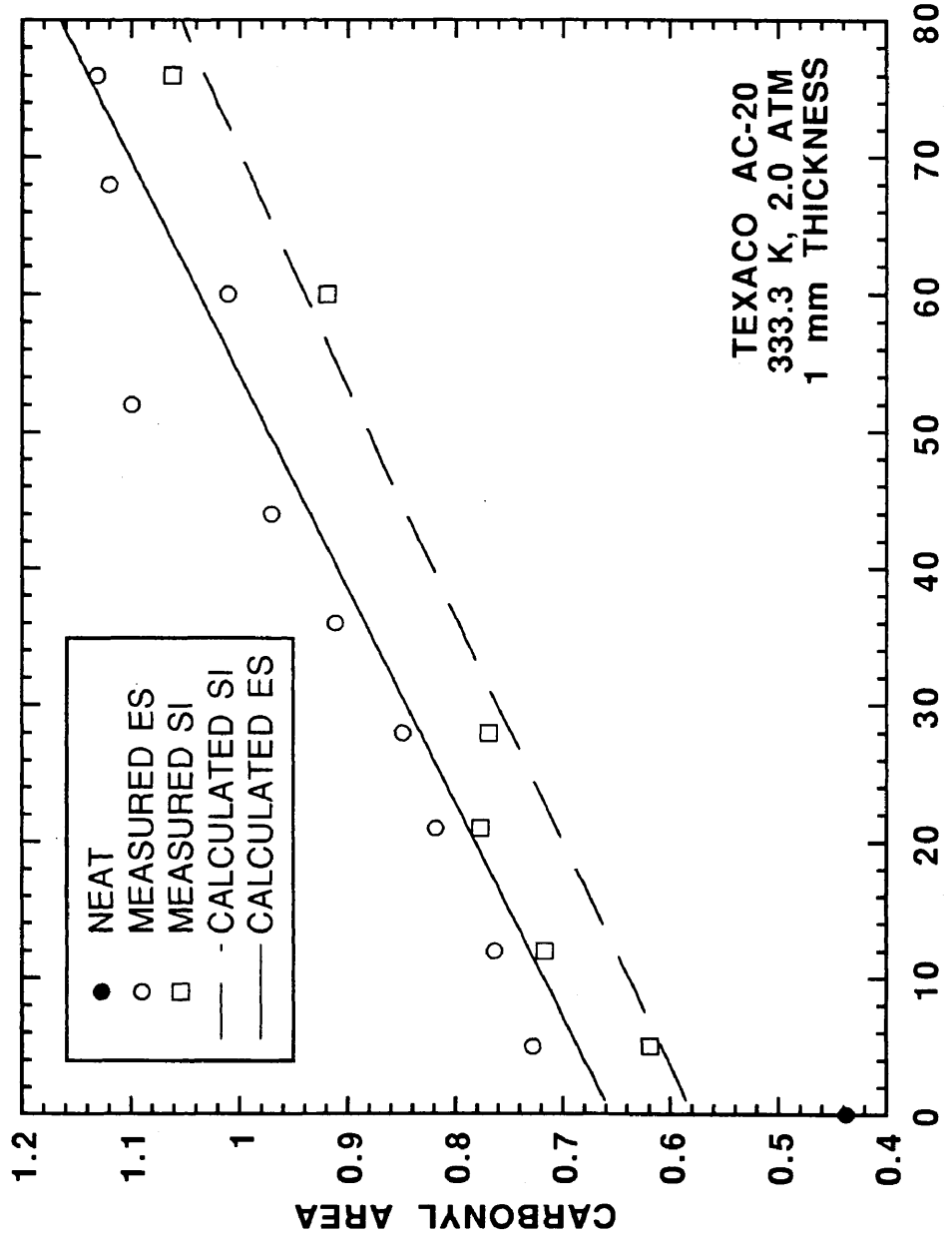

Figure V-27. Comparisons between measured and calculated CA at the ES and SI of 1 mm thick film POV-aged Texaco AC-20 at 333.3 K and P_{ES} of 2 atm.

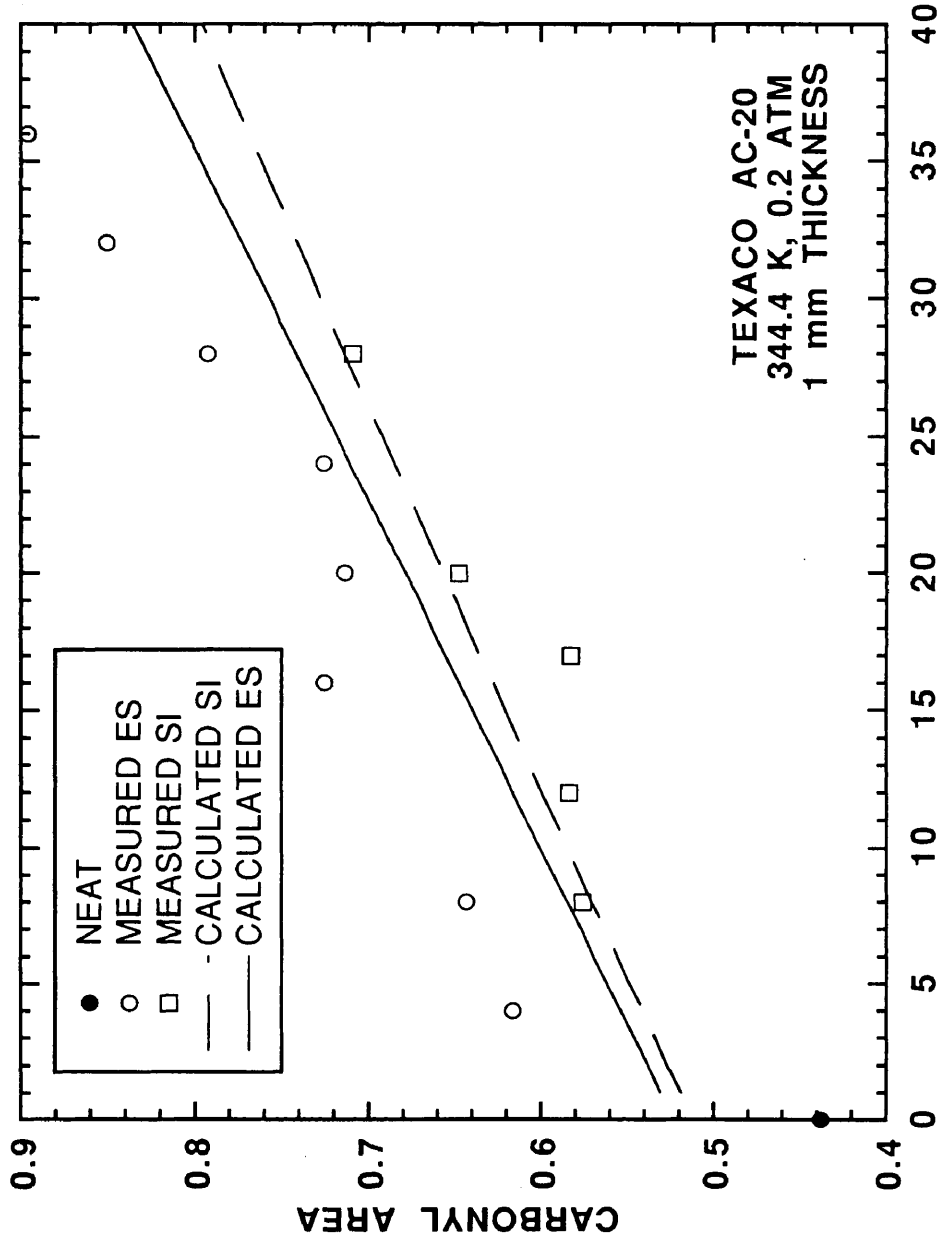

Figure V-28. Comparisons between measured and calculated CA at the ES and SI of 1 mm thick film POV-aged Texaco AC-20 at 344.4 K and P_{ES} of 0.2 atm.

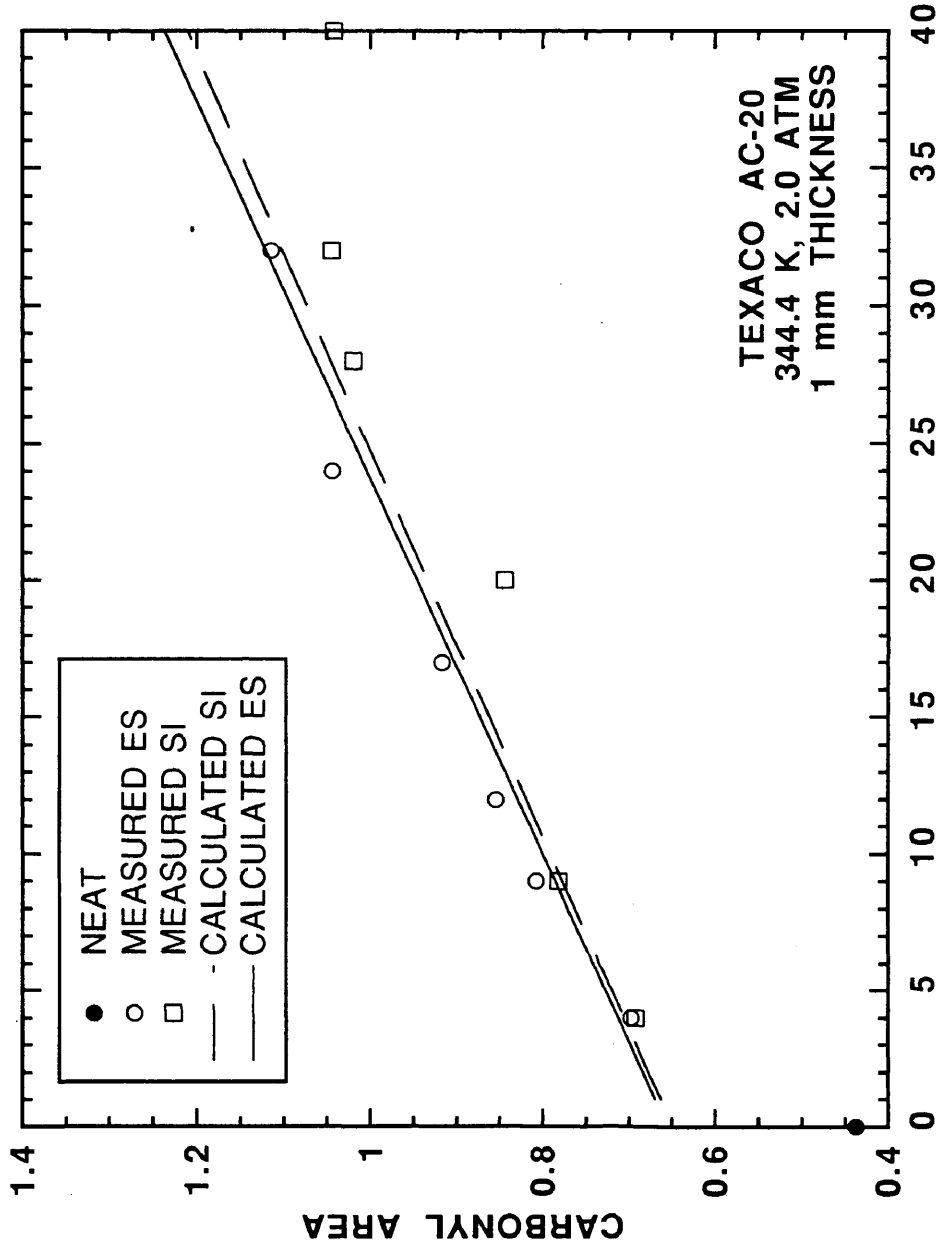

Figure V-29. Comparisons between measured and calculated CA at the ES and SI of 1 mm thick film POV-aged Texaco AC-20 at 344.4 K and P_{ES} of 2 atm.

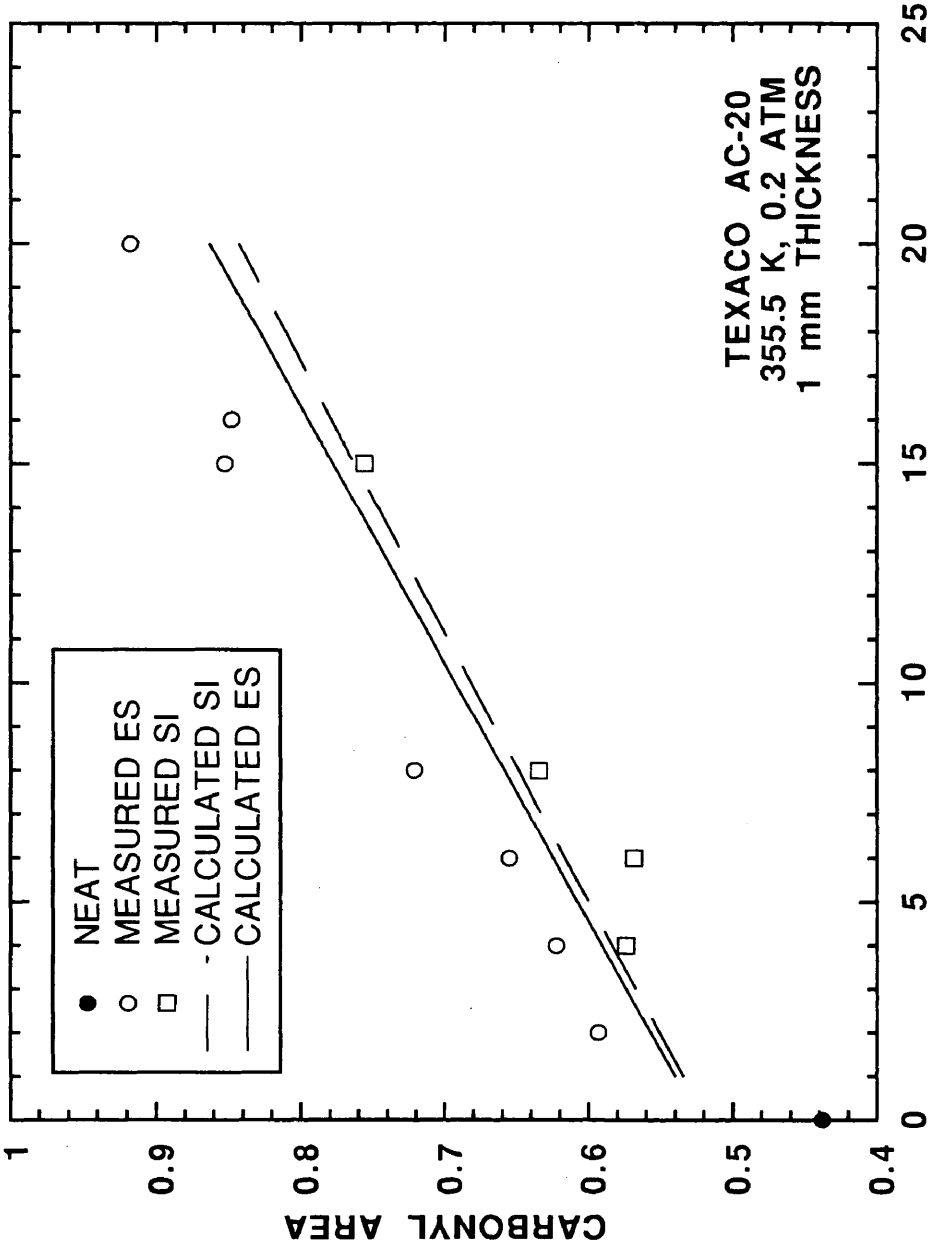

Figure V-30. Comparisons between measured and calculated CA at the ES and SI of 1 mm thick film POV-aged Texaco AC-20 at 355.5 K and P_{ES} of 0.2 atm.

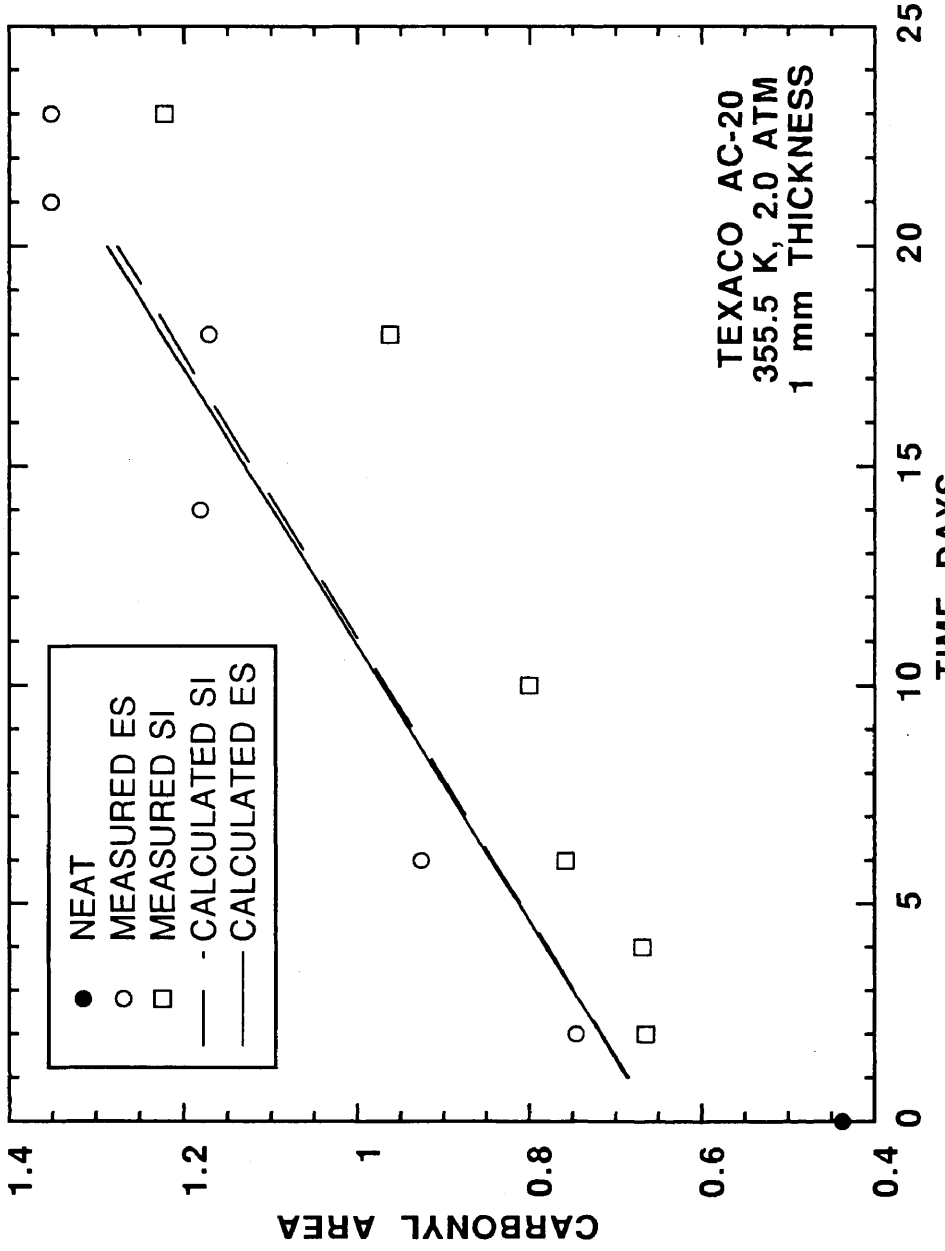

Figure V-31. Comparisons between measured and calculated CA at the ES and SI of 1 mm thick film POV-aged Texaco AC-20 at 355.5 K and P_{ES} of 2 atm.

Figures C-29 through C-52 show the other asphalts studied, and similar conclusions are drawn. Unlike Texaco AC-20, calculated CA_{ES} is sometime greater relative to measured CA_{ES} for the other asphalts studied. The most dramatic figures, C-35 and C-41 for Coastal AC-20 and Cosden AC-20 at 333.3 K and P_{ES} of 0.2 atm, show oxygen limited reaction at the *SI*. However, calculated and measured *CA* do not agree for these figures. The Thiele modulus from Table V-15 for Cosden AC-20 at these conditions is very close to one and relatively high compared with the other asphalts. Coastal AC-20 at these conditions was in the questionable data set, and the Thiele modulus was not determined. For those asphalts and aging conditions from the questionable data set, the agreement between calculated and measured *CA* is as good if not better than the data set used to estimated $\mathcal{D}_{O_2}$-η_o^* model parameters. Surprisingly, parameters relating $\mathcal{D}_{O_2}$ to η_o^* based on steady-state constant $\mathcal{D}_{O_2}$ oxygen diffusion and reaction could be applied to the unsteady-state variable $\mathcal{D}_{O_2}$ oxygen diffusion and reaction with some success.

From calculated *CA* at constant P_{ES}, increasing temperature decreases the difference between CA_{SI} and CA_{ES}. This suggests that oxygen diffusion resistance decreases with increasing temperature. At constant T, increases in P_{ES} also decrease the difference between CA_{SI} and CA_{ES}. This suggests that the difference in the pressures at the *ES* and *SI* is less. Previously, it was discovered that for long-term aging the relative pressure gradient in films of some asphalts may actually increase with increasing pressure. For this study, it appears the pressure is high enough, and since r_{CA} is relatively insensitive to pressure, more homogenous films in terms of *CA* are produced with increasing pressure.

An averaged P_{SI} was determined from calculated P_{SI} for the aging simulation. Table V-18 compares averaged P_{SI} and estimated P_{SI} from $(r_{CA})_{SI}$. The percent difference is also calculated and given in the table. Average P_{SI} agree closely with average P_{SI} reported in Table V-16 and V-17 for steady-state variable $\mathcal{D}_{O_2}$. Comparison with P_{SI} from $(r_{CA})_{SI}$ is not very good, especially for those in the questionable data sets.

Figures V-32 through V-35 show the oxygen pressure, CA, $\log \eta_o^*$, and $\log \mathcal{D}_{O_2}$ profiles for Texaco AC-20 at 333.3 K and P_{ES} of 0.2 atm. These figures provide a qualitative understanding of the aging phenomenon. Similar figures were not generated for the other asphalts and aging conditions studied. Maximum P_{SI} occurs at about six days from Figure V-32. This suggests that initially the rate of oxygen diffusion exceeds that of reaction. After the maximum, P decreases as a result of CA and decreasing $\mathcal{D}_{O_2}$ at the ES. Figure V-33 shows CA profiles. The difference between CA_{ES} and CA_{SI} increases with aging time at isothermal aging conditions. This results from decreasing P in the film. $\mathrm{Log}\eta_o^*$ profiles in Figure V-34 show similar trends as CA profiles. HS and m along with CA were used to calculate $\log \eta_o^*$ profiles. Finally, Figure V-35 shows $\log \mathcal{D}_{O_2}$ profiles. In this figure, maximum and minimum $\mathcal{D}_{O_2}$ are at the SI and ES, respectively. This profile is inverted compared with the other profiles. Furthermore, values of $\mathcal{D}_{O_2}$ do not intersect at $t = 0$ since the integration over time was divided into two separate regions. From zero to one day, equation V – 27 was used. From one day to the end of the integration, equation II – 40 was used. The difference at the ES and SI increases with aging time similar to CA and $\log \eta_o^*$. For the other asphalt and aging conditions, similar phenomena are expected; however, profiles were not generated.

Table V-18. Comparisons between P_{SI} Estimated from r_{CA} and Average P_{SI} Calculated from Unsteady-State Variable $\mathcal{D}_{O_2}$ Oxygen Diffusion and Reaction[a]

Asphalt	P_{ES}	T	P_{SI}		% Diff[b]
			Kinetics	Diffusion	
	atm	K	atm	atm	
Ampet AC-20	0.2	333.3	0.0673	0.06	12
		344.4	0.115	0.125	-8
		355.5	0.161	0.17	-5
	2.0	333.3*	0.393	1.4	-72
		344.4*	0.857	1.7	-49
		355.5	1.80	1.85	-3
Coastal AC-20	0.2	333.3*	0.149	0.06	148
		344.4	0.0345	0.1	-65
		355.5*	0.0789	0.14	-44
	2.0	333.3	0.925	1.2	-23
		344.4*	0.408	1.4	-71
		355.5*	1.105	1.6	-31
Cosden AC-20	0.2	333.3	0.0331	0.03	10
		344.4	0.130	0.09	44
		355.5*	0.416	0.14	197
	2.0	333.3	0.937	0.9	4
		344.4*	0.363	1.35	-73
		355.5	1.480	1.7	-13
Exxon AC-20	0.2	333.3*	0.175	0.04	338
		344.4	0.108	0.11	-2
		355.5*	0.0775	0.16	-52
	2.0	333.3	1.09	1.3	16
		344.4*	1.17	1.6	-27
		355.5	1.86	1.85	0
Texaco AC-20	0.2	333.3	0.124	0.09	38
		344.4	0.122	0.14	-13
		355.5	0.170	0.17	0
	2.0	333.3	1.39	1.5	-7
		344.4*	0.570	1.7	-66
		355.5*	1.28	1.9	-33

[a] α of 0.270 and 1 mm thick films

[b] % Diff $= 100\left(\frac{P_{\text{rea}} - P_{\text{dif}}}{P_{\text{dif}}}\right)$

* These data were not used in the parameter estimation in Figure V-16.

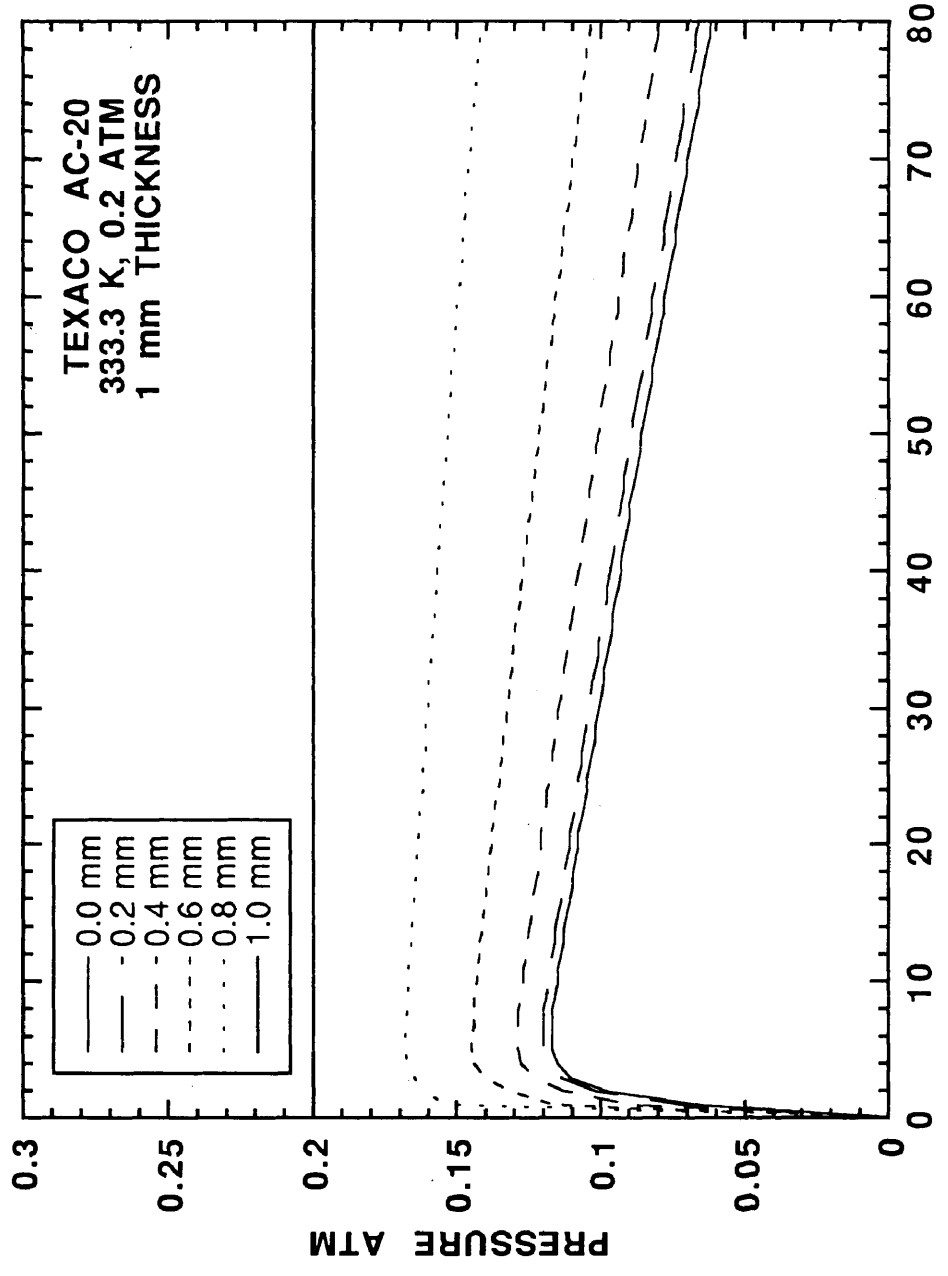

Figure V-32. Calculated oxygen pressure profiles in 1 mm thick film Texaco AC-20 at 333.3 K and P_{ES} of 0.2 atm from unsteady-state variable $\mathcal{D}_{O_2}$ oxygen diffusion and reaction.

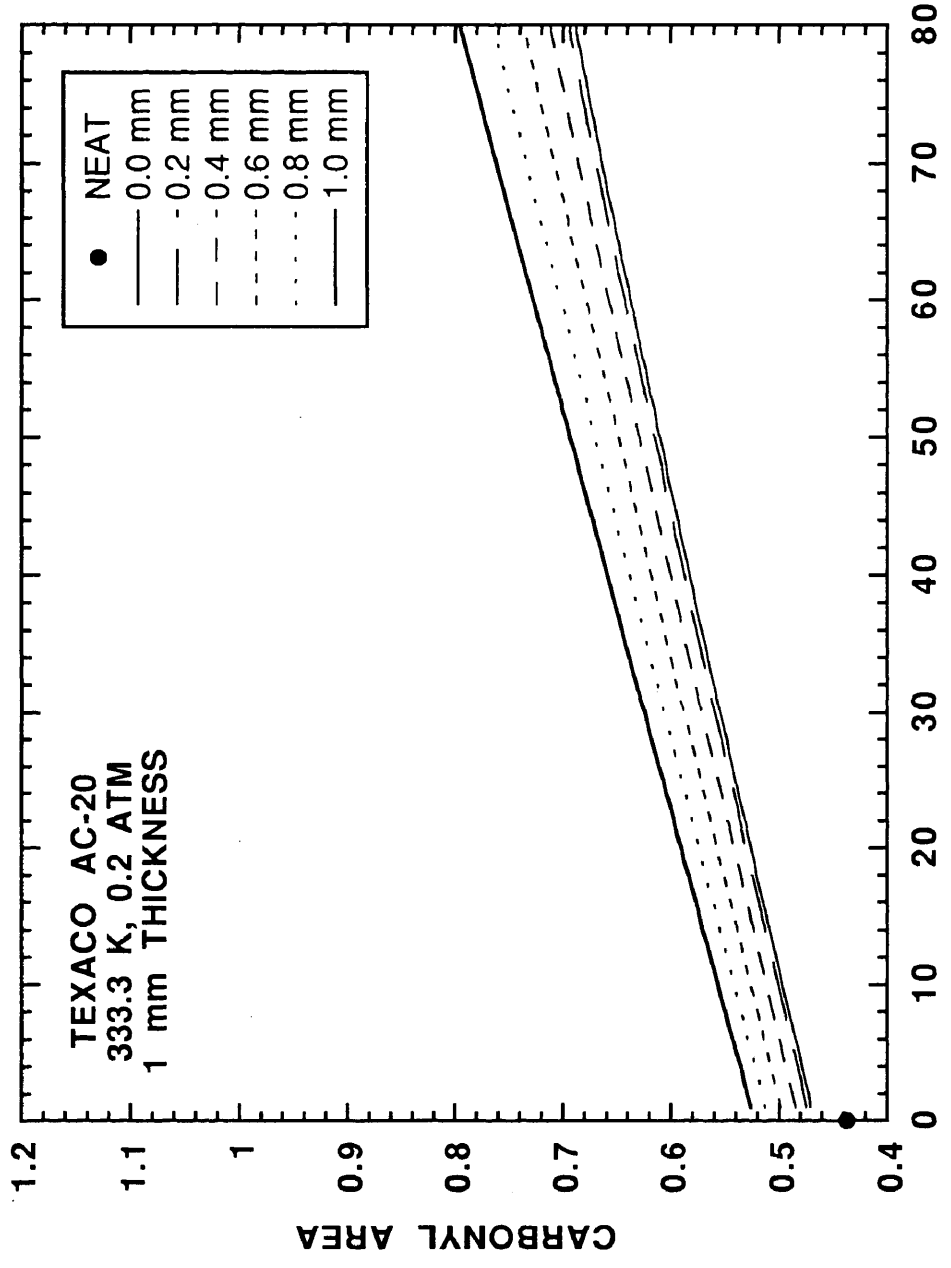

Figure V-33. Calculated CA profiles in 1 mm thick film Texaco AC-20 at 344.4 K and P_{ES} of 0.2 atm from unsteady-state variable $\mathcal{D}_{O_2}$ oxygen diffusion and reaction.

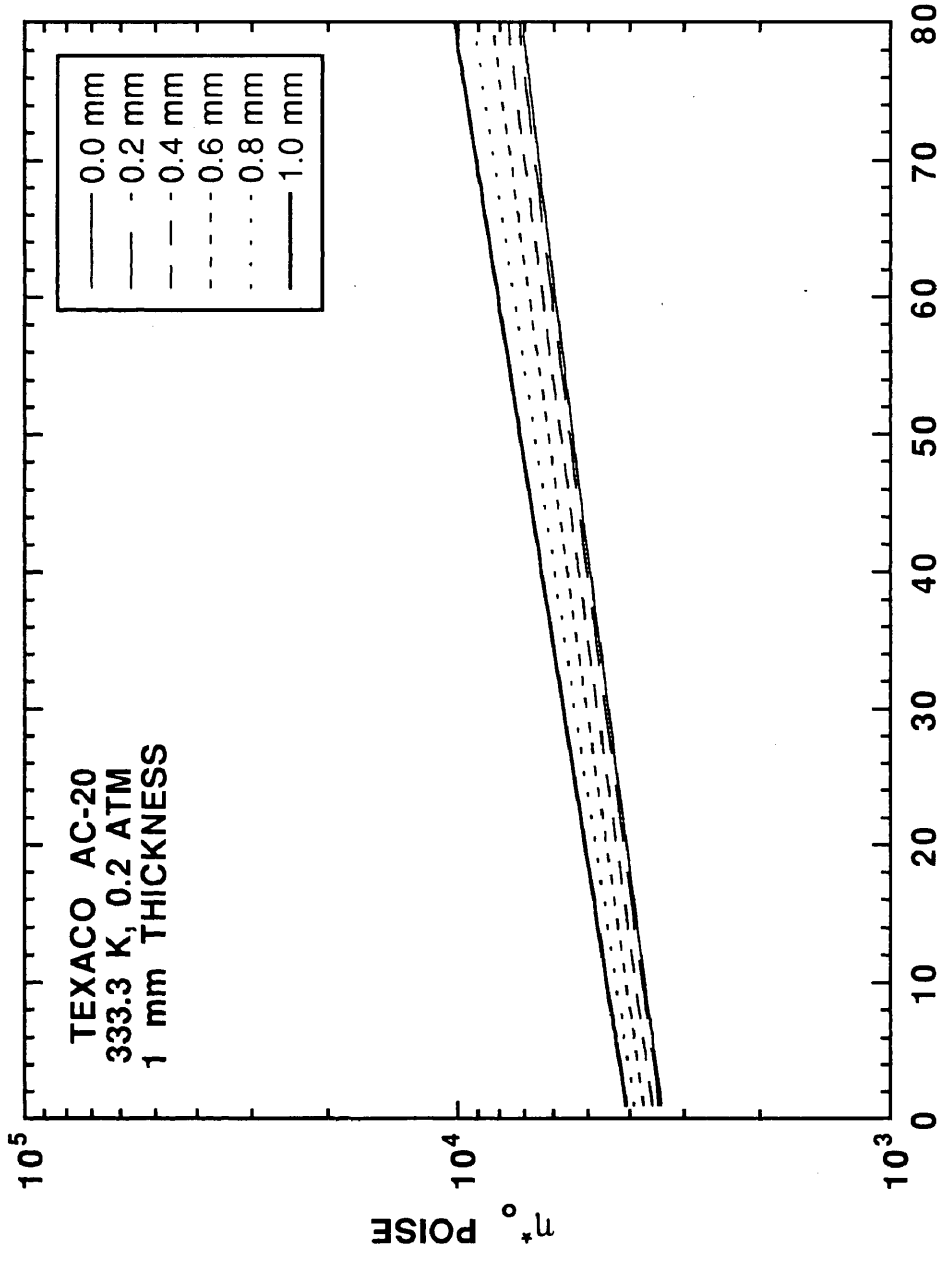

Figure V-34. Calculated η_o^* profiles in 1 mm thick film Texaco AC-20 at 355.5 K and P_{ES} of 0.2 atm from unsteady-state variable $\mathcal{D}_{O_2}$ oxygen diffusion and reaction.

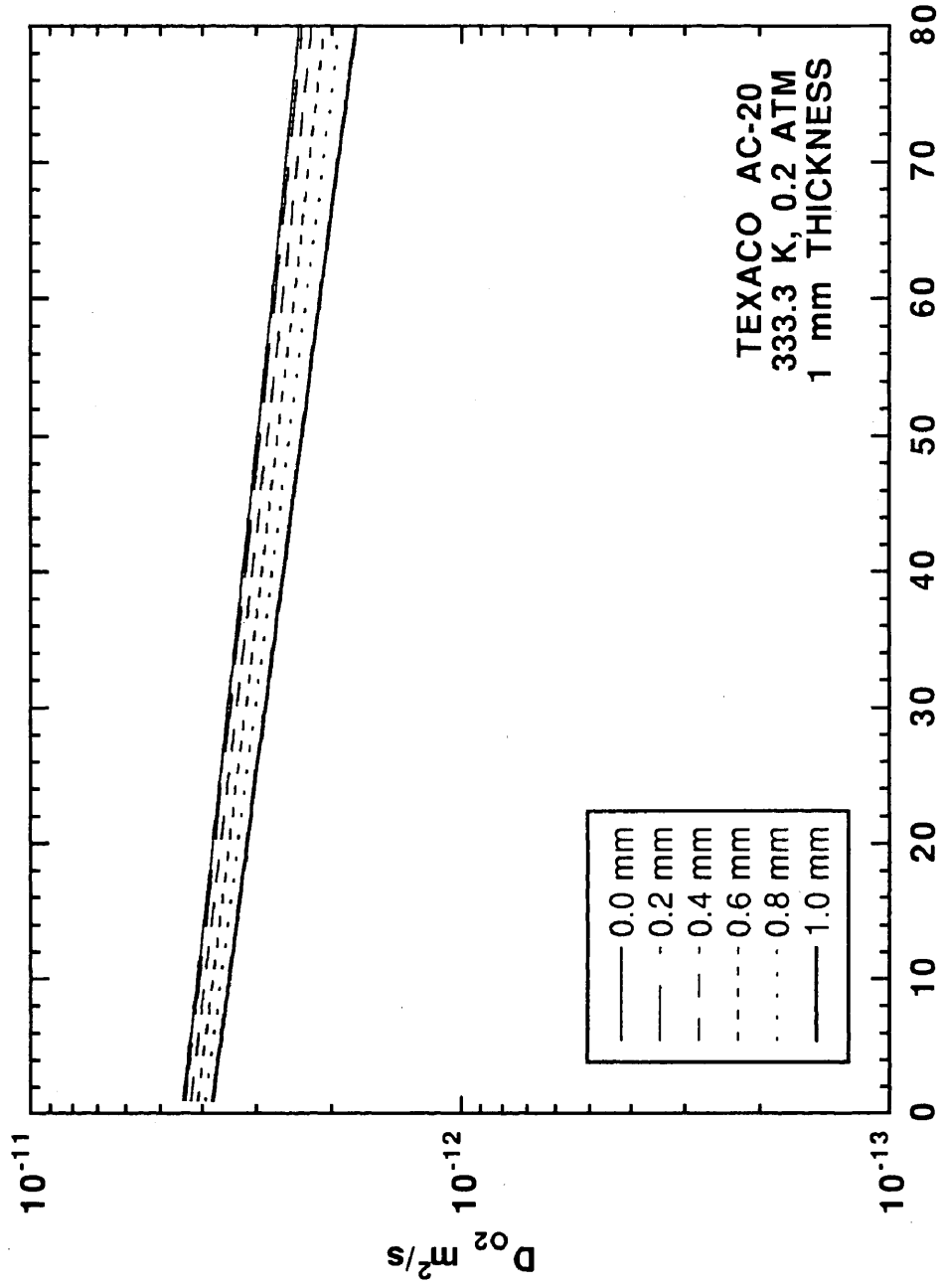

Figure V-35. Calculated $\mathcal{D}_{O_2}$ profiles in 1 mm thick film Texaco AC-20 at 355.5 K and P_{ES} of 0.2 atm from unsteady-state variable $\mathcal{D}_{O_2}$ oxygen diffusion and reaction.

An unsteady-state variable $\mathcal{D}_{O_2}$ oxygen transport and reaction model was numerically solved. Numerical problems associated with $\left(\frac{\partial \mathcal{D}_{O_2}}{\partial P}\right)$ as P approaches zero had to be addressed. To start the integration, an unsteady-state constant $\mathcal{D}_{O_2}$ model was used. During the aging simulation, the value of $\left(\frac{\partial \mathcal{D}_{O_2}}{\partial P}\right)$ was artificially updated decreasing numerical instabilities. Calculated and measured CA were compared. The data showed that measured and calculated CA differ significantly but measured and calculated r_{CA} agree more closely. This suggested that the empirical model for estimating CA_o needs further refinement. However, the fundamental model that calculates r_{CA} was sufficient for simulating long-term rates. The parameters estimated for the $\mathcal{D}_{O_2}$-η_o^* relationships from a steady-state constant $\mathcal{D}_{O_2}$ model showed surprising success in an unsteady-state variable $\mathcal{D}_{O_2}$ oxygen diffusion and reaction model. A comparison of average P_{SI} for the experimental time range and P_{SI} estimated from $(r_{CA})_{SI}$ showed large differences for the questionable data set. Averaged P_{SI} for the unsteady-state model showed excellent agreement with averaged P_{SI} for the steady-state variable $\mathcal{D}_{O_2}$ model in Tables V-16 and V-17. Finally, oxygen pressure, CA , $\log \eta_o^*$, and $\log \mathcal{D}_{O_2}$ profiles were generated for Texaco AC-20 at 333.3 K and P_{ES} of 0.2 atm. These figures provided a qualitative picture of the aging process in an asphalt film.

Diffusion and Reaction in Asphalt Aging Tests

Davison *et al.*, (1992) proposed an asphalt aging test. From kinetic parameters determined by POV aging at several temperatures and physicochemical property relationships, the authors calculated the time required to reach a certain pre-defined failure criterion. A relative ranking of the asphalts studied was provided. The POV experiments were at 20 atm.

This test showed the dramatic difference that oxidation temperature has on the ability of an asphalt to resist aging. However, the test neglected certain critical factors. First, POV data were only at one elevated pressure. No pressure correction to atmospheric conditions was provided. This does not change the relative rankings of the asphalts since the order of reaction is the same for the asphalts studied, Chapter IV. Second, the authors assumed that CA_o for all of the asphalts was the same. Current data have shown that this is not true. Pressure affects CA_o, and CA_o is different for each asphalt. Since the change in CA relates to the time required to reach the failure criterion, the relative rankings of the asphalts could possibly change when atmospheric aging pressures and asphalt specific CA_o are taken into account. Finally, the previous aging test neglected any diffusion resistance.

Using this same idea, an isothermal aging test including diffusion and reaction is studied. The isothermal aging temperature was 322.2 K. P_{ES} was constant 0.2 atm. Kinetic parameters were taken from Table IV-6. CA_o was determined from parameters in Table V-10. Four different calculations were done. The first assumed no oxygen diffusion resistance. The last three calculations included diffusion resistance for film thicknesses of 0.8, 1.0, and 1.2 mm. Table V-19 shows the years required to reach a 500 kP η_o^* at 333.3 K. The source code for this calculation is provided in Appendix D.

Including diffusion resistance increases the required time for all of the asphalts studied. This increase is about three fold. For a given asphalt, increasing asphalt film thickness also increases the time required to reach the failure criterion because the effective diffusion length has increased. Including the effect of diffusion resistance changes the relative rankings which is a surprising result. For example, with no diffusion resistance, Cosden AC-20 is the least resistant of the asphalts studied

Table V-19. Comparisons between Calculated Time to Reach 500 kP η_o^* at 333.3 K, Aging at 322 K and P_{ES} of 0.2 atm with and without Diffusion Resistance for Film Thicknesses of 0.8, 1.0, and 1.2 mm

Asphalt	No Diff yrs	Film Thickness 0.8 mm yrs	1.0 mm yrs	1.2 mm yrs
Ampet AC-20	3.01	6.55	7.32	10.38
Coastal AC-20	2.30	3.10	4.30	5.45
Cosden AC-20	1.88	4.36	6.33	7.15
Exxon AC-20	2.59	5.51	9.45	9.73
Texaco AC-20	2.75	4.30	7.10	7.97

to oxidative aging at 322.2 K. However, for a 0.8 mm thick film including oxygen diffusion, Coastal AC-20 is the least resistant to oxidative aging relative to the other asphalts at 322.2 K. This change in the rankings is caused by the two competing phenomena, the relative rates of oxygen diffusion and reaction in a particular asphalt film. Further complicating this process, the physical properties are changing as a function of both time and position. Asphalts with low *HS* show more significant aging resistance with diffusion included. For example, Coastal AC-20 has the highest *HS* and the failure time changes the least with diffusion and reaction included. On the other hand, asphalts with relatively low *HS* show more dramatic aging resistance with diffusion included.

The previous table has some peculiar results however. It is difficult to explain why Ampet AC-20 is the best asphalt at 0.8 mm, the second best asphalt at 1.0 mm, and the best asphalt again at 1.2 mm. The reverse is true for Exxon AC-20. The other asphalts do not exhibit this rather erratic behavior. Although this is only a

preliminary study, one conclusion can be made. It appears that asphalt film thickness and diffusion must be included in an asphalt-aging test.

Oxygen Solubility

In Chapter IV, a Henry's law model was used to describe the relationship between the measured P in the gas to the pressure at the ES.

$$P_{ES} = P = hP_{\text{gas}} \qquad \text{(IV - 14)}$$

If the reference frame is the true oxygen pressure in the film, r_{CA} is expressed as:

$$r_{CA} = Ah^{-\alpha} \exp\left(\frac{-E_A}{RT}\right) P^{\alpha} \qquad \text{(V - 37)}$$

Estimating P_{SI} from r_{CA} at the ES and SI is given in equation V – 6 with respect to the pressure in the film.

$$P_{SI} = P_{ES}\left(\frac{(r_{CA})_{SI}}{(r_{CA})_{ES}}\right)^{1/\alpha} \qquad \text{(V - 6)}$$

If the reference frame is switched to the measured pressure in the gas, P_{ES} is substituted with equation IV – 14 giving equation V – 38. r_{CA} is independent of the reference frame.

$$P_{SI} = hP_{\text{gas}}\left(\frac{(r_{CA})_{SI}}{(r_{CA})_{ES}}\right)^{1/\alpha} \qquad \text{(V - 38)}$$

Comparing equation V – 6 with V – 38, the actual P_{SI} as determined from measured pressure in the gas is multiplied by the Henry's law constant.

$$P_{SI} = hP_{SI\ \text{gas}} \qquad \text{(V - 39)}$$

The relative pressures at the ES and SI from r_{CA} are independent of oxygen solubility considerations assuming Henry's law.

Neglecting the Henry's law constant in the oxygen diffusion and reaction model is also analyzed. A dimensionless pressure, Π, is defined in equation V – 40

$$\Pi = \frac{P - P_{SI}}{P_{ES} - P_{SI}} \qquad (V - 40)$$

Π is independent of oxygen solubility parameters assuming Henry's law. Now P is defined in terms of Π by equation V – 41

$$P = \Pi(P_{ES} - P_{SI}) + P_{SI} \qquad (V - 41)$$

Equation II – 40 is written in terms of Π.

$$(P_{ES} - P_{SI})\left(\frac{\partial \Pi}{\partial t}\right) = (P_{ES} - P_{SI})\left(\frac{\partial \mathcal{D}_{O_2}}{\partial \Pi}\right)\left(\frac{\partial \Pi}{\partial x}\right)^2 + (P_{ES} - P_{SI})\mathcal{D}_{O_2}\left(\frac{\partial^2 \Pi}{\partial x^2}\right) - cRTk_P\left(\Pi(P_{ES} - P_{SI}) + P_{SI}\right)^{\alpha} \qquad (V - 42)$$

The boundary conditions are given below.

$\left(\frac{\partial \Pi}{\partial x}\right) = 0$	at	$x = 0$	Substrate interface
$\Pi = 1$	at	$x = L$	Exposed surface
$\Pi = 0$	at	$t = 0$	Initial condition

$\mathcal{D}_{O_2}$ was estimated with respect to the measured gas pressure. However, these values should be related to the true oxygen pressure in the film. Changing the frame of reference to the true pressure in the film and assuming a Henry's law model, equation V – 42 becomes:

$$h(P_{ES} - P_{SI})\left(\frac{\partial \Pi}{\partial t}\right) = h(P_{ES} - P_{SI})\left(\frac{\partial \mathcal{D}_{O_2}}{\partial \Pi}\right)\left(\frac{\partial \Pi}{\partial x}\right)^2 + h(P_{ES} - P_{SI})\mathcal{D}_{O_2}\left(\frac{\partial^2 \Pi}{\partial x^2}\right) - cRTk_P\left(\Pi(P_{ES} - P_{SI}) + P_{SI}\right)^{\alpha} \qquad (V - 43)$$

P_{ES} and P_{SI} are still measured with respect to the gas. The boundary conditions are not affected. r_{CA} was not modified since this term is independent of the reference

frame. For steady-state constant $\mathcal{D}_{O_2}$, the difference between $\mathcal{D}_{O_2}$ with respect to the measured gas pressure and $\mathcal{D}_{O_2}$ with respect to the true pressure is given by equation V – 44.

$$(\mathcal{D}_{O_2})_{\text{actual}} = h(\mathcal{D}_{O_2})_{\text{gas measured}} \qquad \text{(V – 44)}$$

Since h is about 0.1 for asphalts (Baldwin and Daniel, 1953), actual $\mathcal{D}_{O_2}$ is about one order of magnitude less than the value determined from gas pressure measurements. D_o in the model relating $\mathcal{D}_{O_2}$ and η_o^* is also decreased by an order of magnitude. B needs no modification. Even with these changes, $\mathcal{D}_{O_2}$ in this study is still in the range of the literature values reported by Van Oort (1956) and Blokker and van Horn (1959).

Summary

The ultimate objective of this study was to estimate $\mathcal{D}_{O_2}$ for asphalt. To achieve this goal, several other relationships between measurable properties and fundamental variables in the oxygen diffusion and reaction equation were developed. First, with limited experimental data, r_{CA} and r_{O_2} were related by the proportionality constant, c. The value of c is 6.56×10^{-6} gmol O_2/mL CA. Second, a model describing η_o^* as a function of both CA and T was developed. All of the model parameters appeared to be composition dependent. Furthermore, HS was relatively insensitive to temperature compared with m.

To estimate $\mathcal{D}_{O_2}$ from equation II – 30, an additional constraint was required. Along with zero flux at the SI and the known P_{ES} from the experimental design, P_{SI} was specified. However, the estimation of P_{SI} was not trivial. CA at the ES and SI was measured for POV-aged asphalt films. Assuming steady-state conditions,

estimates of P_{SI} were determined solely from $(r_{CA})_{SI}$. Error analysis showed that 10% error in $(r_{CA})_{SI}$ increased to 40% error in P_{SI} because of small α.

With the required constraints, preliminary estimates of $\mathcal{D}_{O_2}$ were calculated for a steady-state constant $\mathcal{D}_{O_2}$ model. Due to error propagation of $(r_{CA})_{SI}$ to P_{SI}, errors in $\mathcal{D}_{O_2}$ for some cases were large. The data showed that, at isothermal conditions for a given asphalt, $\mathcal{D}_{O_2}$ decreased with increasing aging pressure. This suggested that $\mathcal{D}_{O_2}$ was not constant but changed as a result of oxidation in the film. Figure V-16 compared $\mathcal{D}_{O_2}$ and average η_o^* from average carbonyl content in the film for the aging experiment. Based on this figure, $\mathcal{D}_{O_2}$ decreased as a result of increased η_o^*. The model describing the behavior is supported in the literature. The estimated parameter B of -0.84 for η_o^* in poise and $\mathcal{D}_{O_2}$ in m^2/s is within the range of literature values. Not all of the data were used for this parameter estimation. Error analysis in the estimation of $\mathcal{D}_{O_2}$ showed that most of data is in the neighborhood of the parameter estimation.

Using constant $\mathcal{D}_{O_2}$, the Thiele modulus, ϕ, was calculated. For the experimental design, this showed that a diffusion limited condition did not dominate even for aging conditions at 0.2 atm and 333.3 K. More significant oxygen diffusion data should be obtained from experiments designed to increase ϕ. A simple modification to achieve this goal is to age thicker asphalt films.

With a model relating $\mathcal{D}_{O_2}$ to η_o^* along with the estimated model parameters, the change in P_{SI} during the POV aging experiment was calculated from steady-state variable $\mathcal{D}_{O_2}$ oxygen diffusion and reaction, equation II – 31. Average P_{SI} and P_{SI} determined from $(r_{CA})_{SI}$ compared favorably. Those data discarded from the $\mathcal{D}_{O_2}$-η_o^* parameter estimation showed rather large differences. The magnitude of the rate of oxygen transport due to variable $\mathcal{D}_{O_2}$ and that due to the pressure gradient

was compared. For the laboratory aging experiments, Ampet AC-20 showed that a maximum of 20% of the oxygen transport in the film was limited by ξ as a result of variable $\mathcal{D}_{O_2}$. Even though this contribution was not significant in POV aging experiments, for lower temperatures and longer aging times in highway-pavement aging, ξ may significantly limit oxygen transport in the asphalt.

Using all of the twelve previously estimated parameters, an unsteady-state variable $\mathcal{D}_{O_2}$ oxygen diffusion and reaction model was numerically integrated for the POV aging conditions studied. From these integrations, calculated CA at the ES and SI were compared to measured CA. Agreement between the magnitudes of measured and calculated CA was not very good. The empirical model estimating CA_o from aging P along with the limited data set for parameter estimation probably accounts for these differences. Agreement between calculated and measured r_{CA} was better. The r_{CA} model is based on fundamental principles, and a large set of data was used to estimate the model parameters. For one asphalt and one aging condition, an example of oxygen pressure, CA, $\log \eta_o^*$, and $\log \mathcal{D}_{O_2}$ profiles from oxidative aging in an asphalt film were produced.

An aging test was evaluated. The time to reach a pre-determined failure criterion of 500 kP η_o^* at 333.3 K was calculated for isothermal aging at 322.2 K and constant P_{ES} of 0.2 atm. For the thickest films, including diffusion resistance increased the required time five fold in some asphalts compared to aging without diffusion resistance. The relative ranking of the asphalts changed when diffusion resistance was included. Including both diffusion and reaction has a more significant effect on the calculated time for asphalts with relatively low HS as compared to those asphalts with relatively high HS.

To account for oxygen solubility, estimated $\mathcal{D}_{O_2}$ from measured gas pressure has to be multiplied by the Henry's law constant if $\mathcal{D}_{O_2}$ is expressed in terms of the true oxygen pressure. Finally, the models developed in Chapter IV and V are the foundation for an asphalt-aging model. This model accounts for both temperature and pressure for unsteady-state variable $\mathcal{D}_{O_2}$ oxygen diffusion and reaction in an asphalt film.

CHAPTER VI
COMPARISON BETWEEN LABORATORY AND FIELD AGING

Much effort has been devoted to developing kinetic and diffusion models from laboratory-aged asphalts. These models, together, form an asphalt-aging model. The ultimate objective is to develop a highway-pavement aging model using this fundamental asphalt-aging model. The highway-pavement aging and asphalt-aging models would allow highway engineers to monitor and predict field aging. Also, these models could be used to rank asphalts by their predicted resistance to field aging. With the knowledge from accurate aging models, highway engineers and governments can better allocate resources for improving and maintaining the highway system.

A favorable comparison between field- and POV-aged material would confirm that low temperature, high pressure laboratory oxidation simulates field aging. Unfortunately, previous comparisons have been flawed by extraction and recovery procedures (Burr *et al.*, 1990; Burr *et al.*, 1991), or the complete lack of a kinetic model or data. However, in this work, the field- and POV-aged asphalts are compared by two different methods. The first method takes advantage of the physicochemical relationship developed by Lau *et al.*, (1992). This relationship was independent of the kinetics describing the aging process. Therefore, a comparison using this method is independent of any kinetic model. Having the ability to make field- and laboratory-aged comparisons independent of the kinetics is a truly remarkable achievement. The second method of comparison includes the asphalt-aging model. From laboratory-determined kinetic and diffusion parameters along with climatic data, estimations of the effective asphalt film thickness, L_{eff}, and effective oxygen pressure in the void,

P_{eff}, are attempted. These estimations are made by comparing field-aged data to values calculated from the asphalt-aging model.

The same oxidation products resulting from field aging over a long period of time should also result from POV aging over a relatively short time period for accurate laboratory simulation. Only the rate at which the products are formed differ. If the same oxidation products are formed, the same physicochemical relationship should result. If both aging methods produce the same physicochemical model parameters, the laboratory simulation is correct. This confirmation must be done before proceeding with the asphalt-aging model.

With positive confirmation between field- and laboratory-aged materials from physicochemical properties, the field-aged data and asphalt-aging model are used to develop a highway-pavement aging model. Laboratory experiments are designed to extract the asphalt specific parameters, E_A, A, HS, and m. Since α and the diffusivity parameters are independent of asphalt composition, these values are taken from Chapters IV and V. The parameters relating CA_o to aging P are not determined for these asphalts. With the known kinetic and diffusion parameters and climatic information for the specific region, L_{eff} and P_{eff} are estimated by comparing field-aged data with values calculated from integrating equations II – 1 and II – 40 for the given aging times. The model relating L_{eff} and P_{eff} to measurable core properties is the highway-pavement aging model.

Materials and Laboratory Experimental Design

Neat asphalts and field-aged material from three test sections located in the state of Texas were acquired. The test sections are located in Dickens, Pineland, and Bryan. For the Dickens test section, the original pavement was placed in 1982, and

seven asphalts were used (Adams and Holmgreen, 1986). The Pineland test section was an overlay in 1983, and six asphalts were used. The aggregate at Dickens and Pineland was river gravel and limestone/iron ore mix, respectively. The Dickens and Pineland test sections are important for two reasons. Different asphalts were used in the same test section, and several literature sources describe the test section aging (Adams and Holmgreen, 1986; Martin *et al.*, 1990; Davison *et al.*, 1989). The Bryan test section was placed in 1987 and was constructed of asphalt from one refinery. Tank asphalt and hot-mix were sampled at different locations during construction. The numbers in Table III-1 following the Bryan Exxon AC-20 designation correspond to the sample locations.

Neat asphalts from the test sections were POV-aged using procedures described in Chapter III. The POV aging temperature and time were selected such that the measured field-aged properties should lie within the range of laboratory data to compare physicochemical properties. The aging pressure in all cases was 20 atm pure oxygen. Table VI-1 gives viscosity, η, percent air voids, % V, and percent asphalt, % Asp, for Dickens and Pineland asphalts from extracted cores in 1987 (Davison *et al.*, 1989). Carbonyl content was also measured in this report, but the KBr method was used. Comparing IR spectra obtained by two different techniques was not attempted or recommended. From the data in Table VI-1, POV aging temperatures for Dickens and Pineland asphalts were 355.5 and 333.3 K, respectively. For both, the maximum aging time was 22 days. From the Bryan test section, six asphalts were aged at 344.4 K, and three of the six were aged at 355.5 K. Aging times ranged from 40 and 20 days for 344.4 and 355.5 K experiments. Ten trays per asphalt per temperature were prepared for all of the POV aging experiments. Changes in CA, rheological properties, and MW were measured by FTIR, DMA, and GPC, respectively.

Table VI-1. Properties of 1987 Samples from Dickens and Pineland Test Sections[a,b]

Location	Asphalt	η (333.3 K) Poise	% V	% Asp
Dickens	Cosden AC-10	342000	12.0	5.6
	Cosden AC-20	376000	11.0	4.0
	Diamond Shamrock AC-20	260000	12.0	–
	Dorchester AC-20	222000	13.0	4.6
	Exxon AC-20	900000	9.0	5.1
	MacMillan AC-20	159000	8.0	6.2
Pineland	Cosden AC-20	5400	1.8	6.9
	Dorchester AC-20	–	–	–
	Exxon AC-20	2500	2.5	7.7
	MacMillan AC-20	–	–	–
	Texaco AC-20	–	–	–

[a] From Davison *et al.*, 1989
[b] – Signifies the values were not determined.

The cores from Dickens and Pineland were extracted by two different methods, the auto extraction by Burr (1993) and a modification of method A (ASTM D-2172-81). The modified method is called the micro extraction since one core was partitioned into four equal masses. The four masses were extracted independently. The final recovery of the asphalt for both methods used a rotary evaporator. The cores from Bryan were extracted using the auto extraction method only. All extractions used a solvent solution of 25% ethanol and 85% TCE by volume. After extraction and recovery, GPC analysis confirmed that solvent removal was complete (Burr *et al.*, 1990; Burr *et al.*, 1991). Furthermore, GPC data were used to identify and verify the asphalts. This confirmed that the samples were cored in the correct location (Glover *et al.*, 1987).

POV- and Field-Aging Comparisons by Physicochemical Properties

In this section, POV- and field-aged asphalts are compared by physicochemical relationships. Based on the agreement in the comparisons a conclusions about the ability of POV aging to simulate field aging is reached. Since field-aged asphalt requires extraction and recovery, GPC confirmed complete solvent removal and verified the coring location and asphalt. η_o^*-CA and $(1\ /\ J'')$-CA relationships for POV and field aging are compared. η_o^*-MW relationships for POV- and field-aged samples are analyzed. Finally, IR spectra of POV- and field-aged asphalts are compared. For both POV- and field-aged materials, CA, η_o^* at 333.3 K, $(1\ /\ J'')$ at 333.3 K and 10 rad/s, and MW based on polystyrene standards and RI detection are given in Appendix E. Tables E-1 through E-6 contain the properties for the asphalts from the Dickens test section. The Pineland test section asphalts are given in Tables E-7 through E-11. The Bryan POV aging data are reported in Tables E-12 through E-17, and the field-aged samples from Bryan are given in Table E-18.

Confirming complete solvent removal and coring location

The extracted asphalt and the POV-aged material were analyzed by GPC. This confirmed complete solvent removal during extraction and recovery and verified the location with POV-aged neat asphalt.

Figure VI-1 shows GPC chromatograms for field-aged Dickens Cosden AC-10. The bold line designates the auto extraction method and the thin dashed lines represent the micro extractions. The two micro extraction chromatograms overlay each other. The chromatogram is divided into three sections for descriptive purposes. The first section, between 21 and about 26 minutes, represents the asphalt molecules of large molecular size. This is designated the LMS region. The second section, from

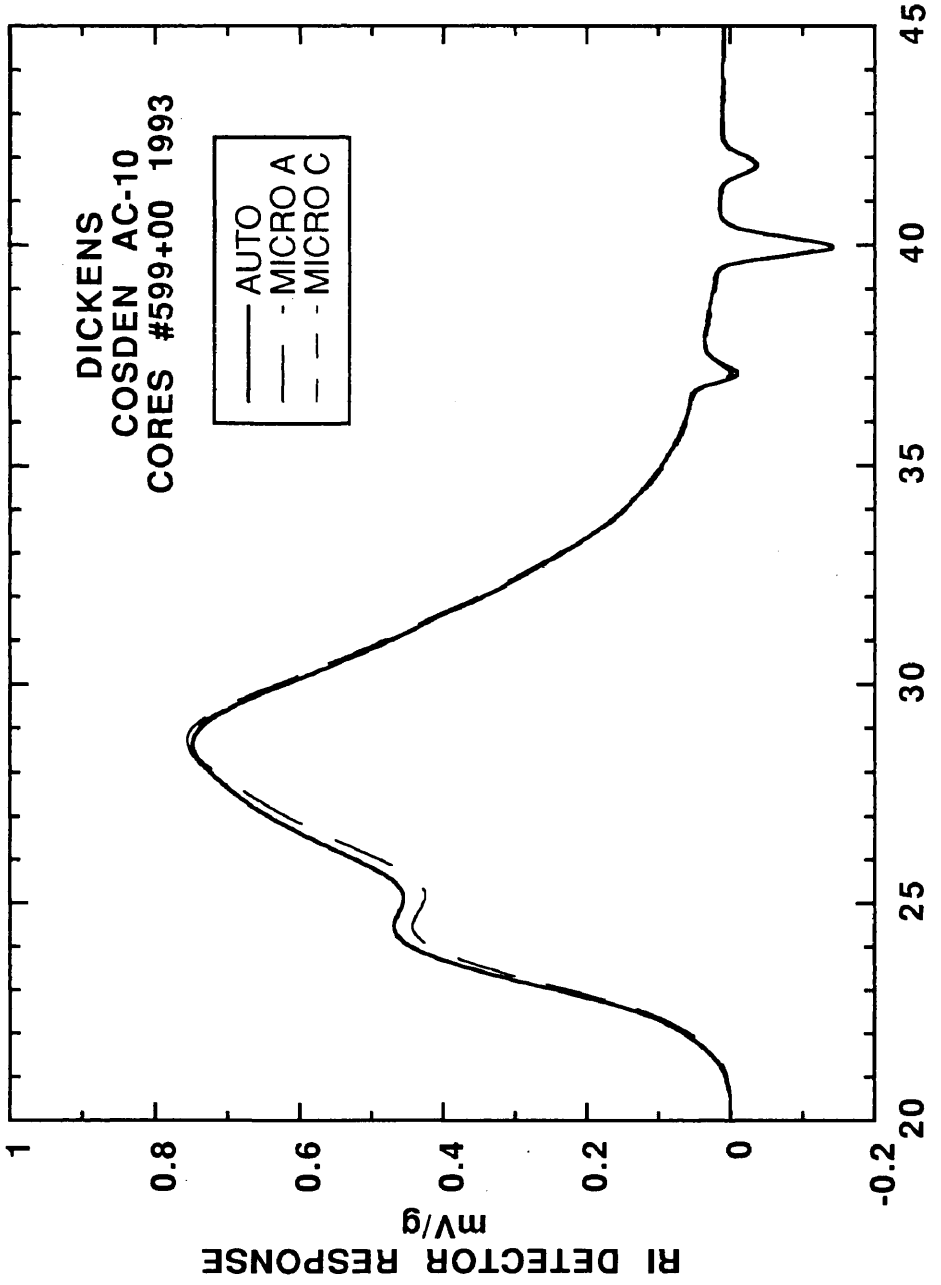

Figure VI-1. GPCs of field-aged Dickens Cosden AC-10 extracted asphalt from #550+00. Cored February, 1993.

26 minutes to 35 minutes, is the medium molecular size, *MMS*. The third and final section, from 35 to 45 minutes, is the solvent and dissolved gases region. The negative peaks at 37, 40, and 42 minutes represent water, nitrogen, and oxygen, respectively. Since the *RI* of these compounds is less than the *RI* of the carrier solvent, THF, negative peaks result. The presence of the extraction solvent produces a positive peak at about 38 minutes between the water and nitrogen peaks.

From the absence of the solvent peak at 37 minutes, it was concluded that solvent removal was complete. The shape of chromatograms suggests that the auto extraction method either removed or produced more *LMS* than the micro extractions for this asphalt. Other than that discrepancy, the shape of the chromatograms are nearly identical. Chromatograms of the extracted asphalt from the other locations are shown in Figures E-1 through E-15 in Appendix E. There appears to be no residual solvent present after extraction and recovery for all of the field-aged asphalts. Furthermore, the difference between the auto and micro extraction methods appears to be random with respect to the *LMS* region.

Some of the POV-aged asphalt were analyzed by GPC to generate a finger print of the asphalt as described by Glover *et al.*, (1987). POV- and field-aged finger prints were compared verifying that equivalent asphalts were being examined. Discrepancies in the comparison suggest that the asphalts are not equivalent. Furthermore, physicochemical comparisons with these samples are not valid. Figure VI-2 shows GPC chromatograms of neat and POV-aged Dickens Cosden AC-10. The neat sample is designated by the solid, bold line. The POV-aged samples are designated by the thin, dashed lines. This figure shows that at isobaric and isothermal aging conditions, increases in aging time increases *LMS* and decreases *MMS*. These results confirm Lau's (1992) observations for POV aging. GPC chromatograms of the other POV-

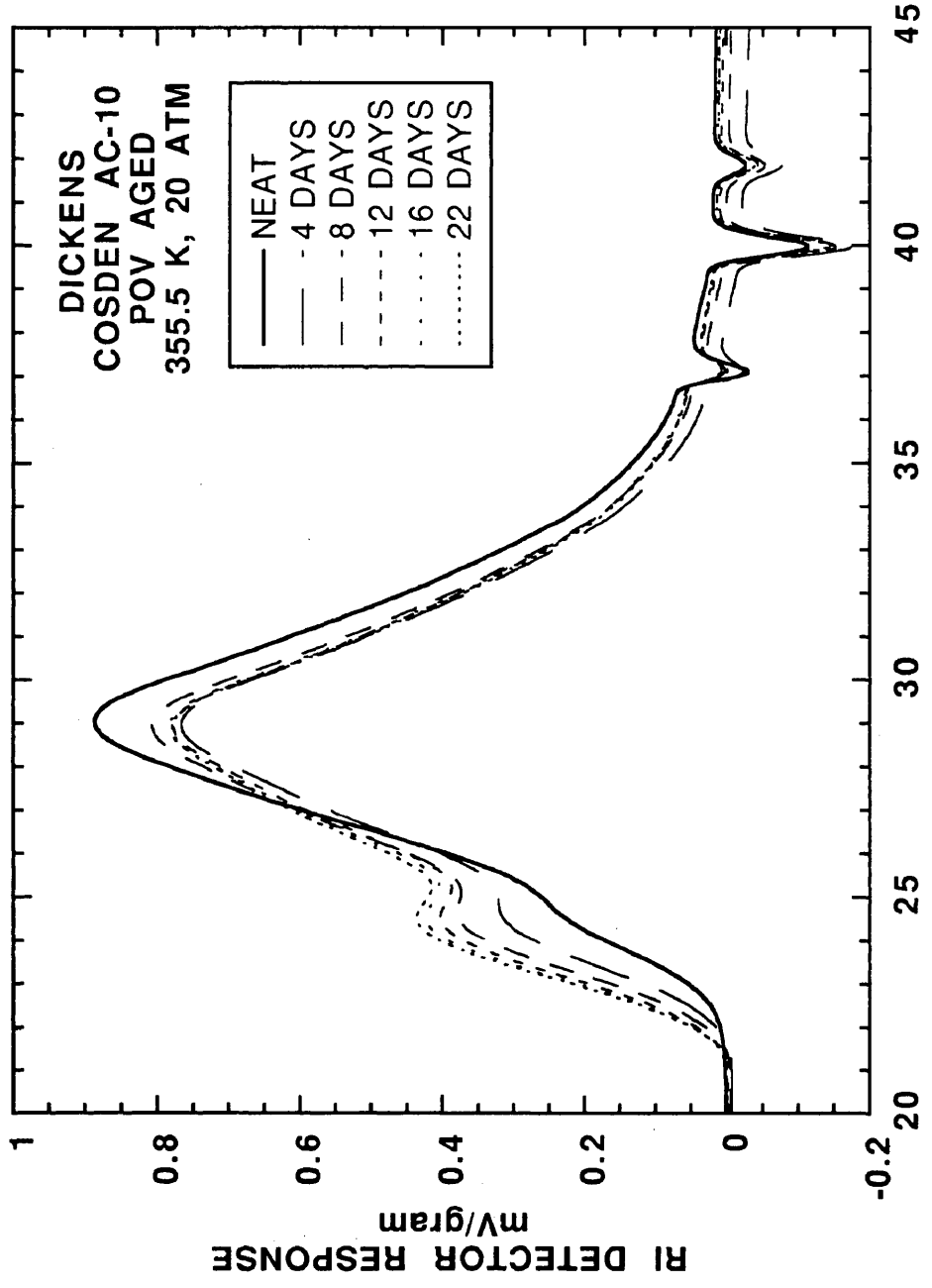

Figure VI-2. GPCs of neat and POV-aged Dickens Cosden AC-10 at 355.5 K and 20 atm.

aged asphalts are shown in Figures E-16 through E-26.

Figure VI-3 overlays POV- and field-aged GPC chromatograms for Dickens Cosden AC-10. The bold, solid line designates the auto extracted sample; the thin, dashed lines represent the POV-aged material. Overall, the chromatograms are very similar. The extracted field-aged material has a much higher peak and broader shoulder in the *LMS* region than the POV-aged samples. Furthermore, the extracted sample has larger shoulder at 27 minutes in the *MMS* region compared with POV-aged samples. Despite these differences, it is concluded that these asphalts are equivalent from the overall shape.

For Dickens Diamond Shamrock AC-20 and Dickens Dorchester AC-20, the comparisons are not as favorable. Figures VI-4 and VI-5 show the overlays of POV- and field-aged GPCs. The characteristic very high *LMS* peak is shown for POV-aged Dickens Diamond Shamrock AC-20 (Davison *et al.*, 1989). The field-aged material extracted from station #458+00, reported to be Diamond Shamrock AC-20, does not show this characteristic. POV-aged Dorchester AC-20 shows a narrow *MMS* peak with a sharp *LMS* peak. However, field-aged material from station #391+00 shows a broad *MMS* peak and a large, dispersed *LMS* peak. The POV aging experiments were designed such that field-aged data would lie in the range of laboratory data. The field-aged *LMS* exceeds the range of POV-aged *LMS* for this asphalt. It was concluded that the field-aged samples for these two asphalts were not equivalent to the POV-aged material. The field-aged samples could have been contaminated, or the coring location was incorrect. It was concluded that all of the other asphalts and locations from the Dickens, Pineland, and Bryan test sections were equivalent based on GPC analysis.

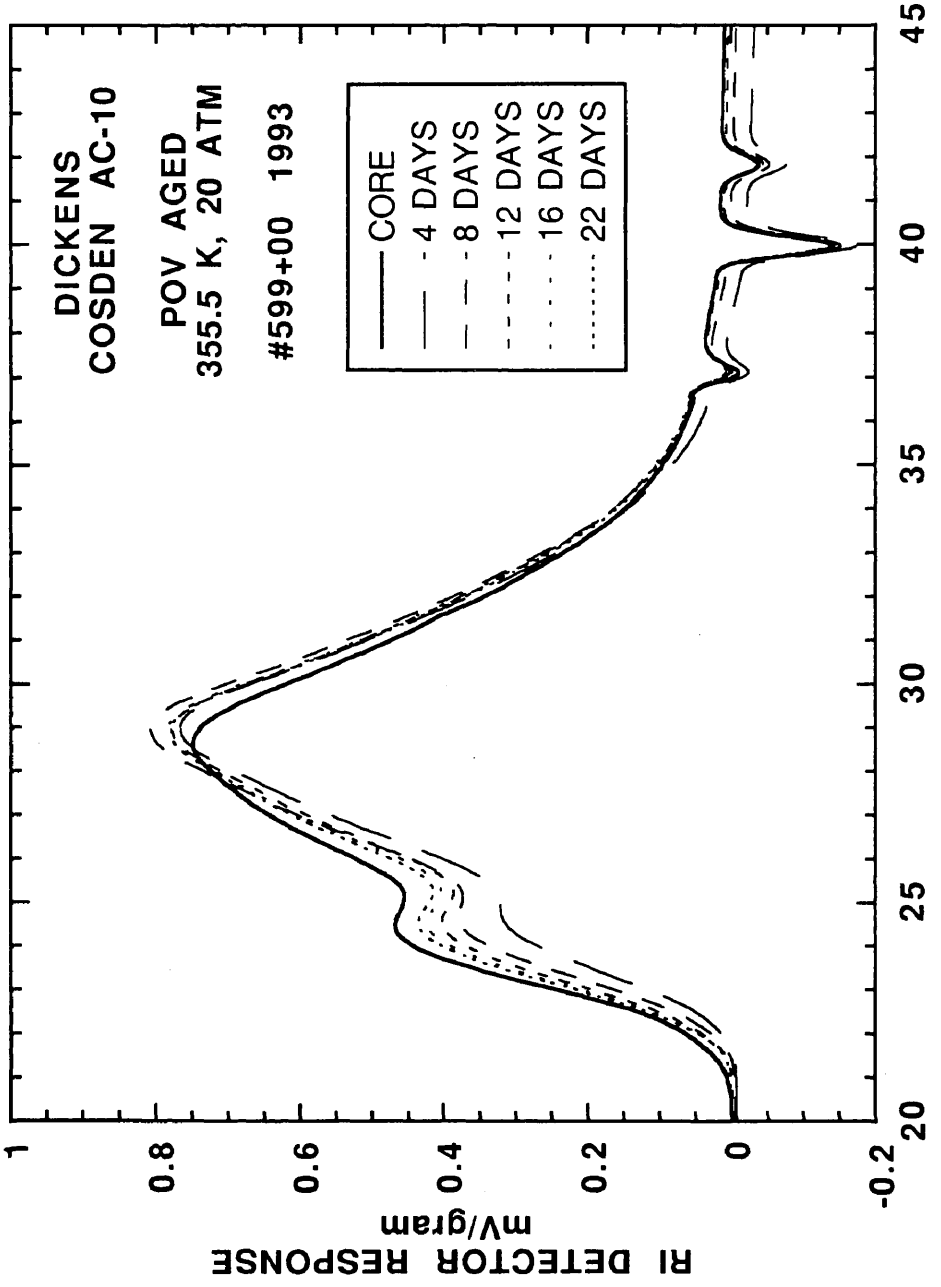

Figure VI-3. Comparisons between GPCs from POV (355.5 K, 20 atm) and field-aged (#550+00, February 1993) Dickens Cosden AC-10.

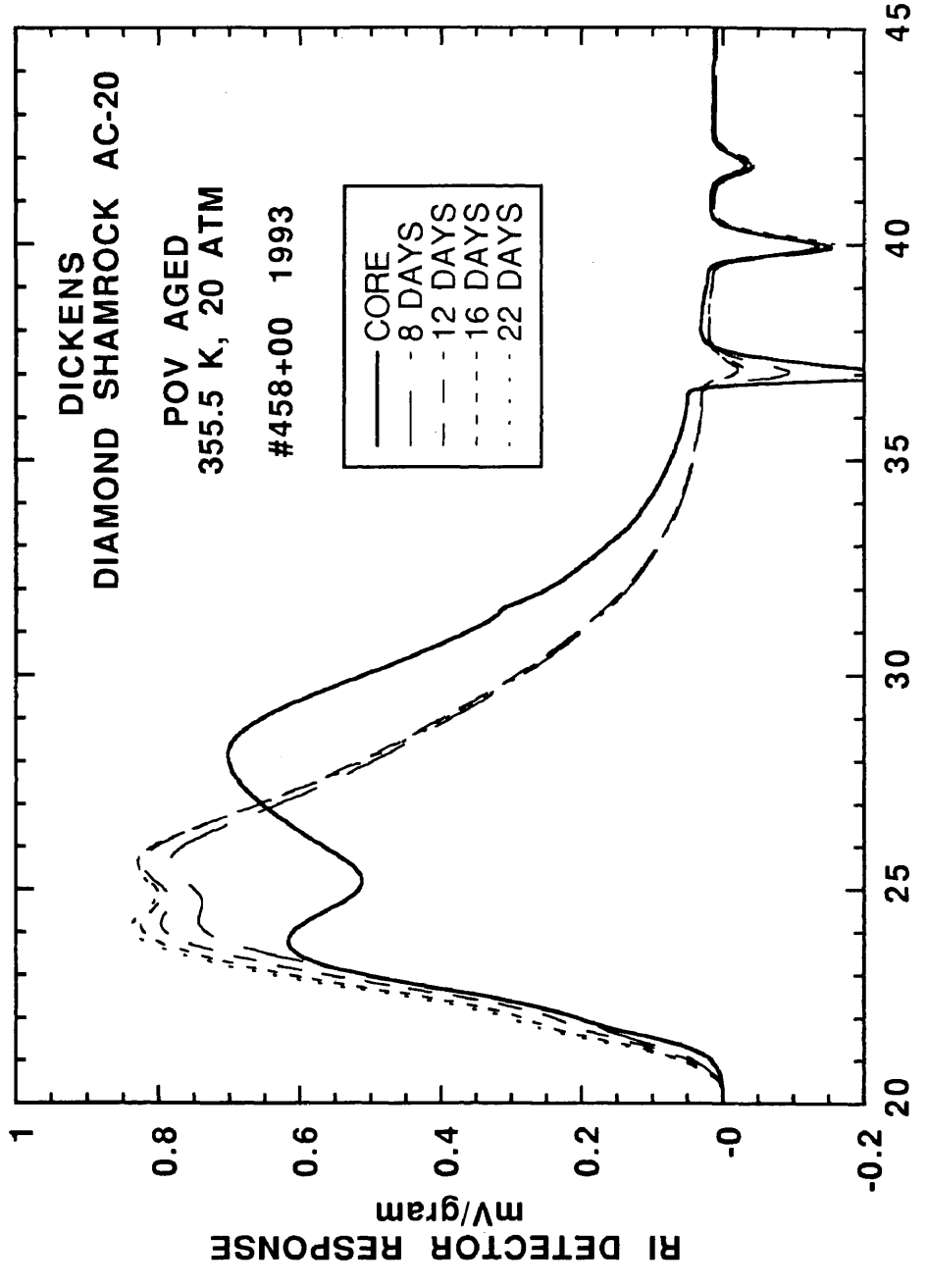

Figure VI-4. Comparisons between GPCs from POV (355.5 K, 20 atm) and field-aged (#458+00, February 1993) Dickens Diamond Shamrock AC-20.

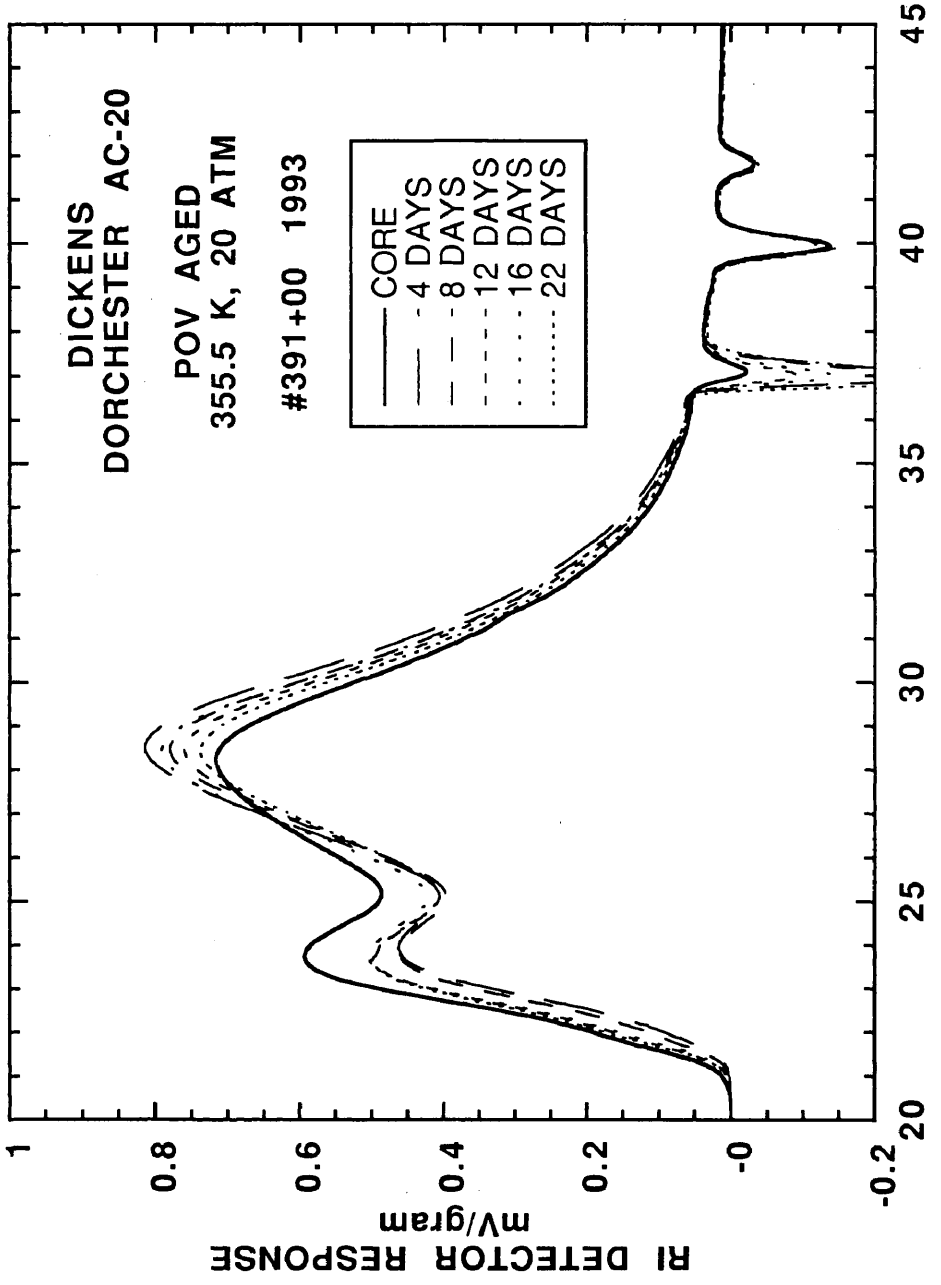

Figure VI-5. Comparisons between GPCs from POV (355.5 K, 20 atm) and field-aged (#391+00, February 1993) Dickens Dorchester AC-20.

The *LMS* region of the field-aged material is larger than that of the POV-aged material at the same *CA*, η_o^*, or $(1/J'')$ for all of the asphalts studied. Jemison *et al.*, (1991) also reports on the differences of GPC chromatograms by comparing extracted hot-mix and oven-aged residue. For the same viscosity increase, the extracted hot-mix shows a larger *LMS* region compared to the oven-aged residue. The oven-aged residue was not extracted and recovered. From these observations, one may conclude that POV aging does not simulate field aging. However, that conclusion assumes that the extraction and recovery procedure does not, in any way, alter the properties of the asphalt. Although much work has been done to increase precision of asphalt extraction and recovery with respect to viscosity changes (Burr, 1993), the extraction process may irreversibly change other aspects of the asphalt. These results and Jemison's work both support this conclusion. The larger *LMS* for field-aged extracted and recovered materials compared with POV-aged materials requires more research to understand. However, this was not the focus of this work.

Comparisons between η_o^* and CA

GPC analysis provides a qualitative characterization of asphalt based on unique chromatographic features, but the information contained in the chromatogram is difficult to correlate with chemical and physical properties. A much better relationship between η_o^* and *CA* due to oxidative aging exists. Lau *et al.*, (1992) showed that for POV aging, equation I – 6 describes the η_o^*-*CA* relationship. The model parameters, *HS* and *m*, are dependent on asphalt composition.

$$\eta_o^* = \exp\left\{ HS \cdot CA + m \right\} \qquad (I-6)$$

GPC analysis has confirmed that similar asphalts from field- and POV-aged samples

are equivalent. Agreement between POV- and field-aged *HS* and *m* should provide evidence that POV experiments are simulating field aging.

Figure VI-6 shows η_o^* at 333.3 K versus *CA* for Dickens Cosden AC-10. POV-aged data are represented by the hollow circle; the neat material is depicted by the filled circle, and the field-aged samples are designated by the square with slash symbol. The parameter estimation is based only on POV-aged data. This figure shows excellent agreement between the POV- and field-aged asphalt. η_o^* of field-aged material is slightly higher relative to POV-aged material for equivalent *CA*. The other asphalts from the Dickens test section are also compared. Figure VI-7 shows η_o^* at 333.3 K versus *CA* for Dickens Cosden AC-20. The field-aged extracted asphalt has higher η_o^* for the same *CA* as compared with POV-aged asphalt. The difference is approximately 30% in η_o^*. However, *HS* for both POV- and field-aged asphalt appears to be the same. Figure VI-8 shows the POV- and field-aged data for Exxon AC-20. Agreement is better than Cosden AC-20; however, field-aged asphalt has lower η_o^* relative to POV-aged asphalt for the same *CA*. For MacMillan AC-20, field-aged asphalt shows slightly lower η_o^* for equivalent *CA* relative to POV-aged asphalt as illustrated in Figure VI-9. Except for Cosden AC-20, the asphalts show very good agreement based on this η_o^*-*CA* relationship.

Figures VI-10 and VI-11 show dramatic differences between field- and POV-aged asphalts for Dickens Diamond Shamrock AC-20 and Dorchester AC-20. This difference is expected. It was concluded that the asphalts were not equivalent based on GPC analysis, Figures VI-4 and VI-5. Field-aged Diamond Shamrock was contaminated from Figure VI-4. For Dorchester AC-20, Figure VI-11 shows that η_o^* of the field-aged asphalt is significantly lower, almost one order of magnitude, compared to the POV-aged asphalt at the same *CA*. From GPC analysis, Figure VI-5 shows

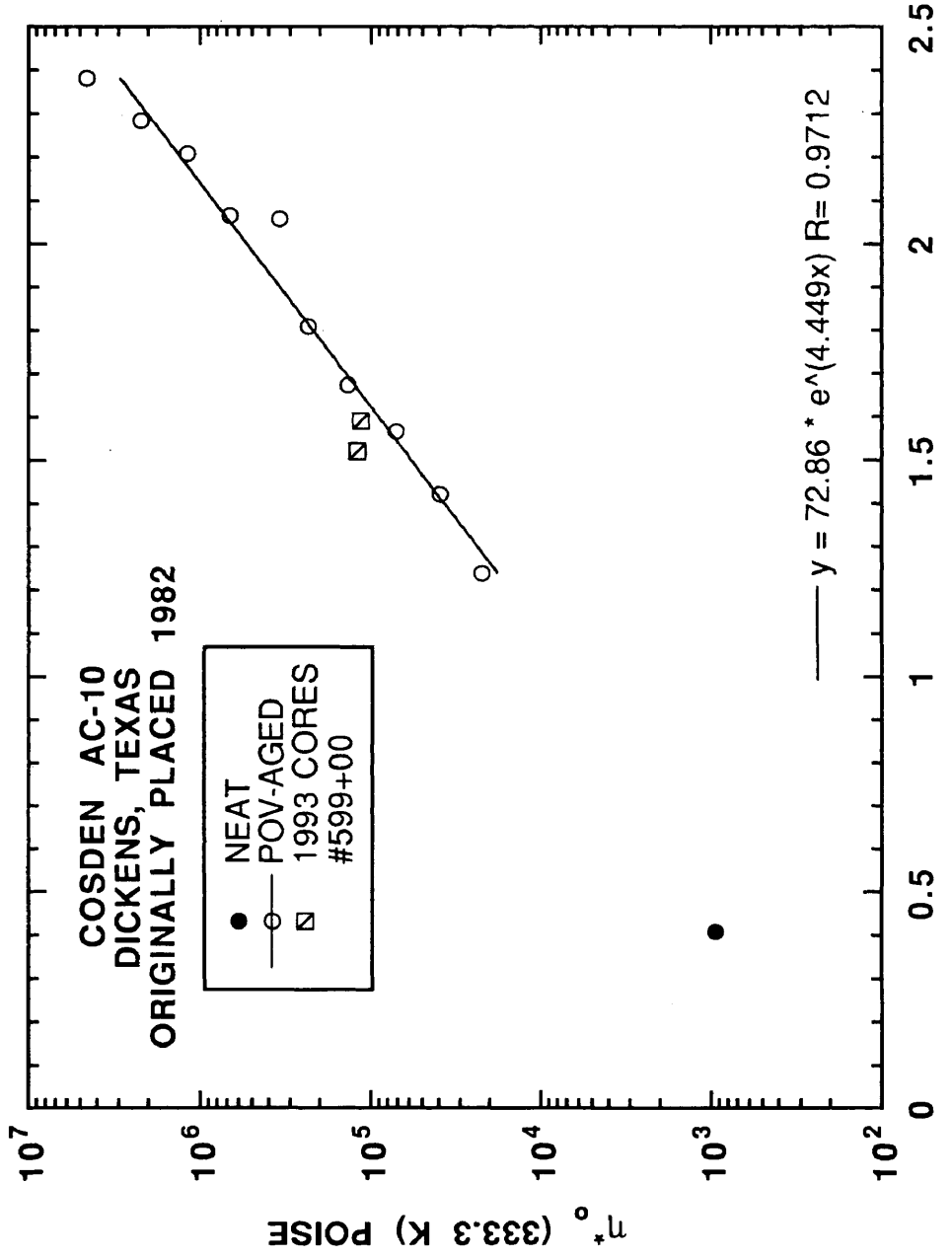

Figure VI-6. Comparison between η_o^* at 333.3 K and CA of neat, POV- (355.5 K, 20 atm), and field-aged (#599+00, February 1993) Dickens Cosden AC-10.

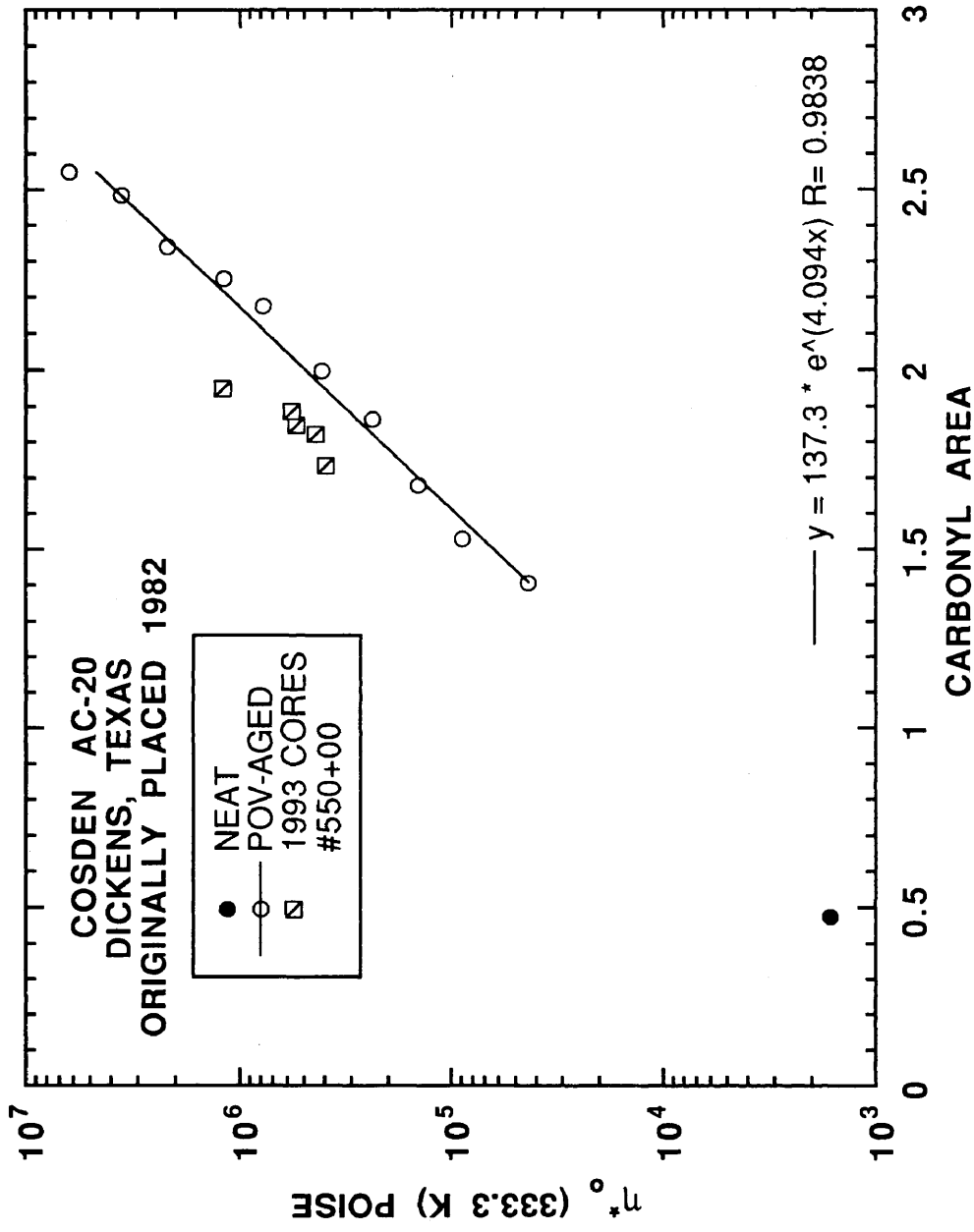

Figure VI-7. Comparisons between η_o^* at 333.3 K and CA of neat, POV- (355.5 K, 20 atm), and field-aged (#550+00, February 1993) Dickens Cosden AC-20.

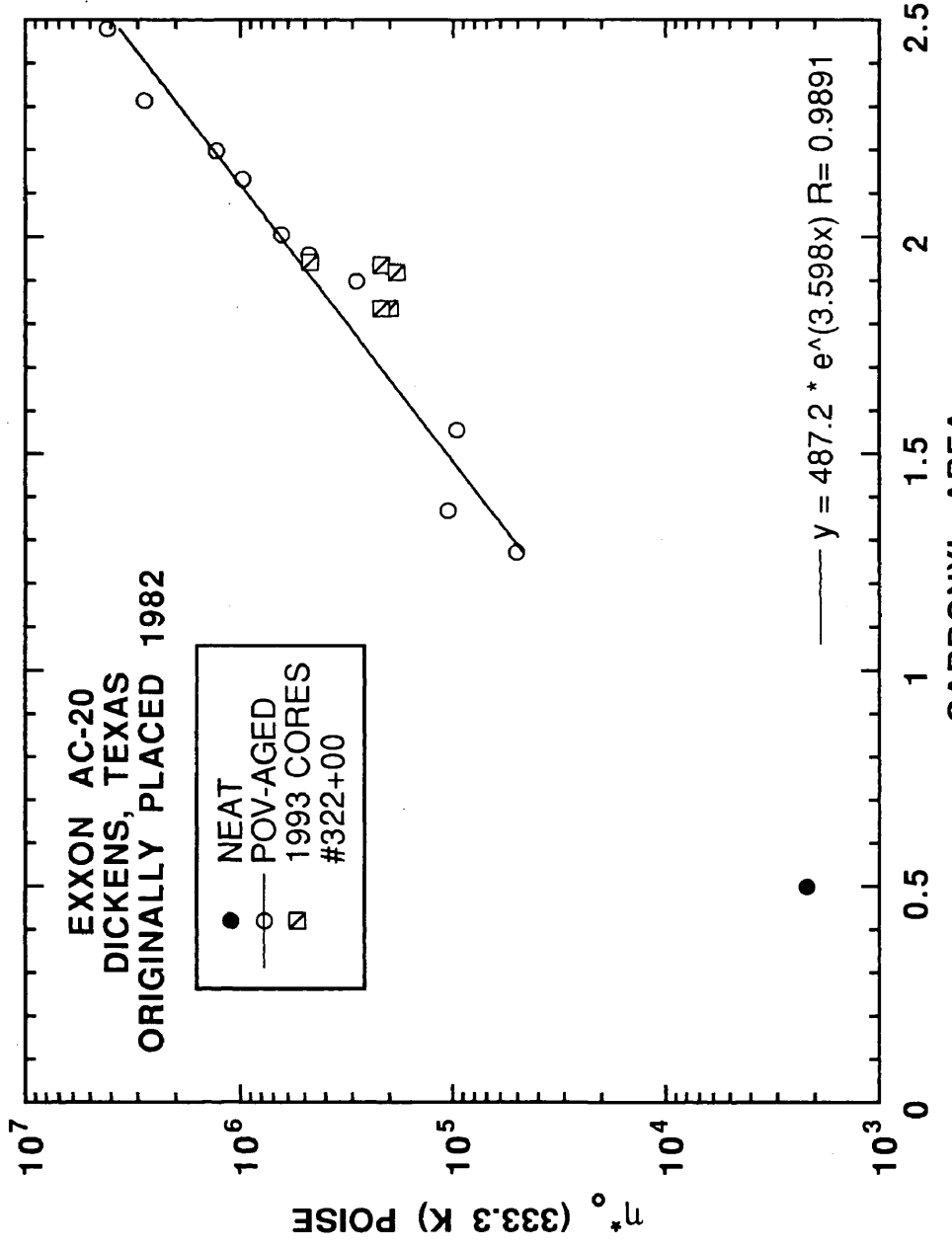

Figure VI-8. Comparisons between η_o^* at 333.3 K and CA of neat, POV- (355.5 K, 20 atm), and field-aged (#322+00, February 1993) Dickens Exxon AC-20.

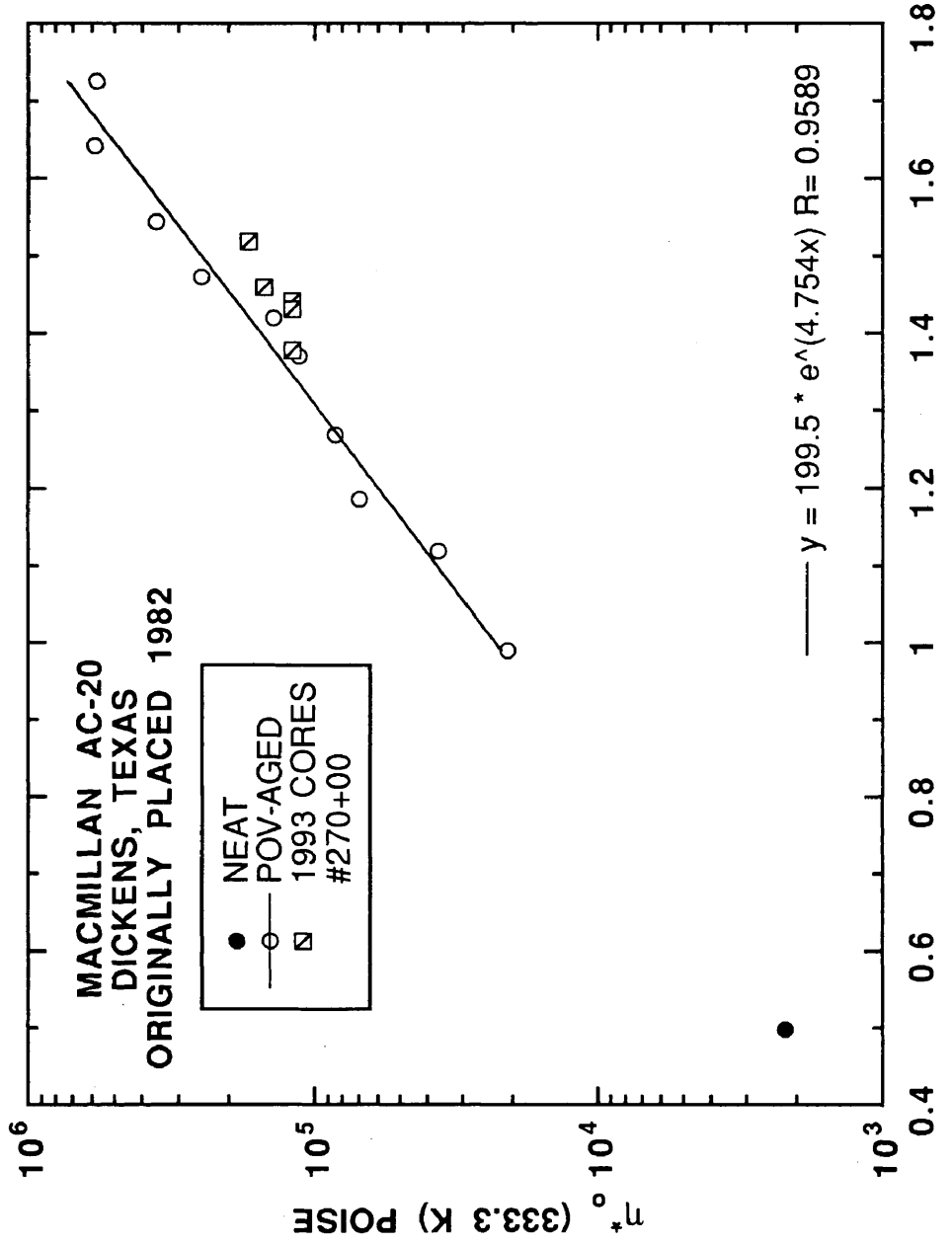

Figure VI-9. Comparisons between η_o^* at 333.3 K and CA of neat, POV- (355.5 K, 20 atm) and field-aged (#270+00, February 1993) Dickens MacMillan AC-20.

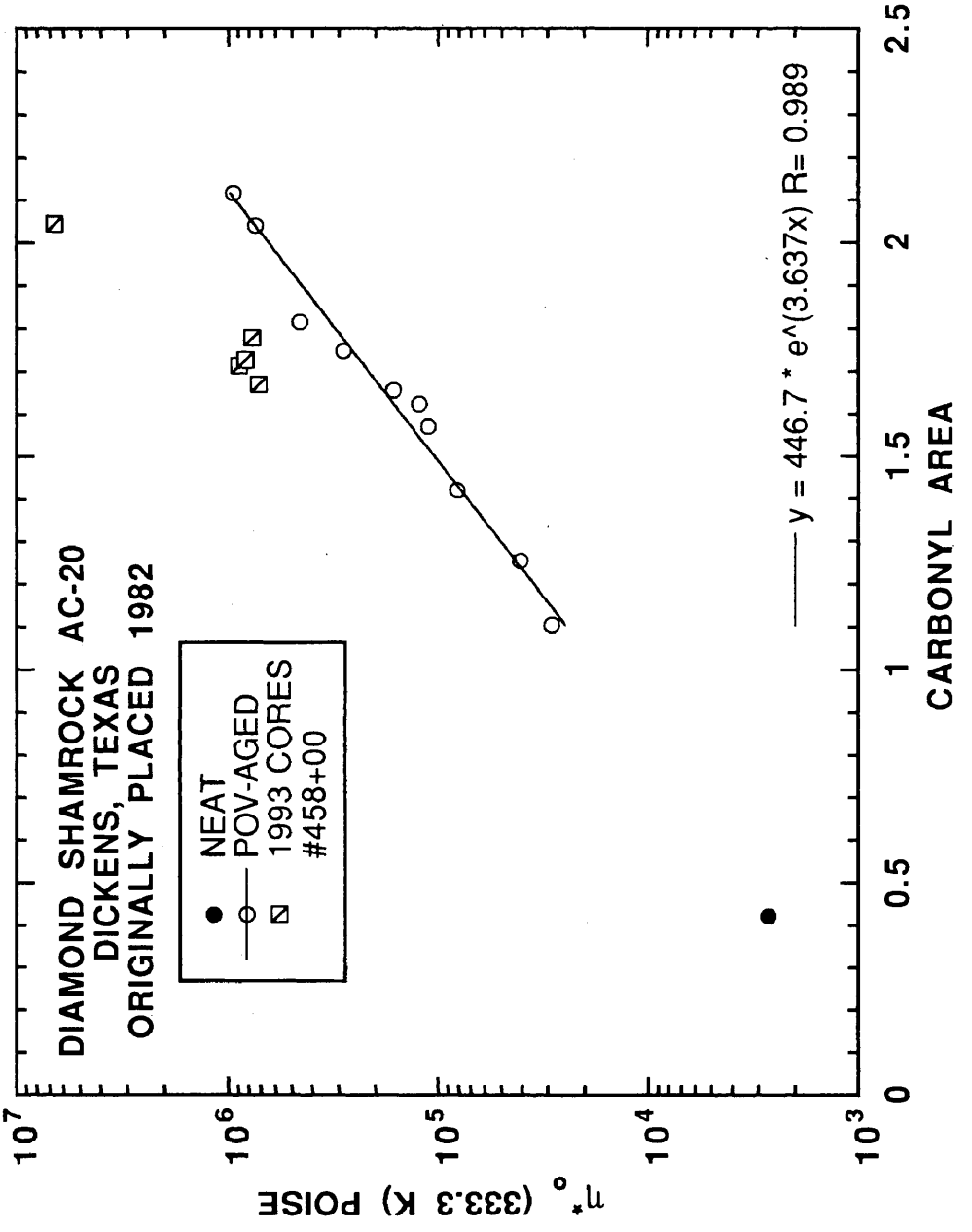

Figure VI-10. Comparisons between η_o^* at 333.3 K and CA of neat, POV- (355.5 K, 20 atm), and field-aged (#458+00, February 1993) Dickens Diamond Shamrock AC-20.

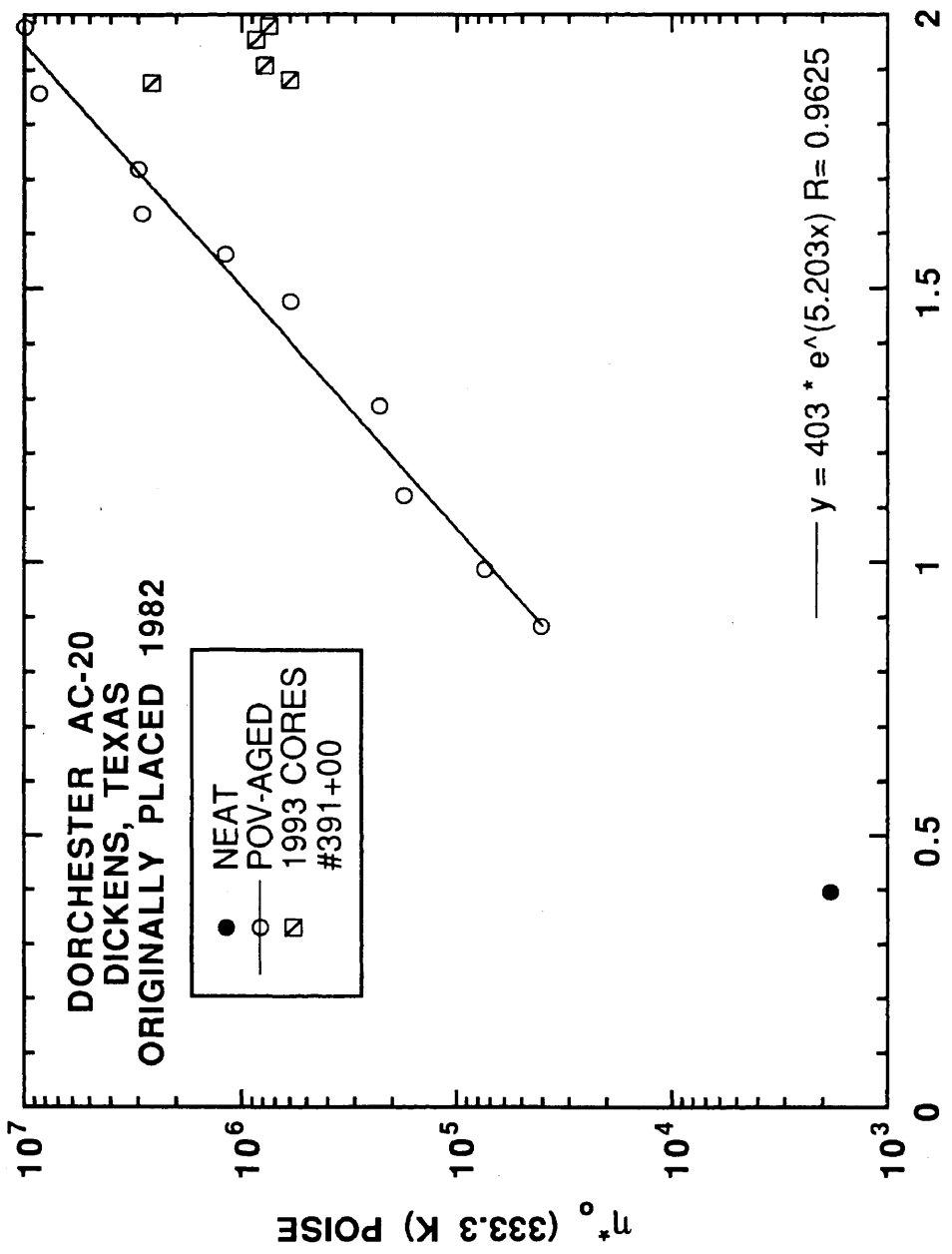

Figure VI-11. Comparisons between η_o^* at 333.3 K and CA of neat, POV- (355.5 K, 20 atm), and field-aged (#391+00, February 1993) Dickens Dorchester AC-20.

field-aged asphalt with larger *LMS* region compared to POV-aged asphalt. This larger *LMS* region also suggests a higher η_o^*. Furthermore, the extracted asphalt was not contaminated with solvent based on the absence of the solvent peak. These conclusions suggest that field-aged Dorchester AC-20 was also contaminated or cored in the wrong location.

These figures show the differences between physicochemical properties of two different asphalts. Compared to the figures where the asphalts are equivalent these differences are enormous. Therefore, even though there are errors in the equivalent asphalts when comparing POV and field aging, the errors are relatively small.

The asphalts from Pineland are also compared. Figures VI-12 through VI-16 compare η_o^* at 333.3 K and *CA* for POV- and field-aged Cosden AC-20, Dorchester AC-20, Exxon AC-20, MacMillan AC-20 and Texaco AC-20, respectively. From the magnitude of η_o^*, the asphalts at this test section did not age much relative to the Dickens test section. In fact, the POV simulation at 333.3 K and 20 atm for one day was more severe than ten years of service for Cosden AC-20 at Pineland shown in Figure VI-12. Since the field-aged data are outside the range of the laboratory data, conclusions about the field- and POV-aged asphalt are not made. However, it appears that field-aged asphalt has slightly lower η_o^* relative to POV-aged asphalt at the same *CA*. Figure VI-13 gives Dorchester AC-20. Field-aged asphalt shows about 40% higher η_o^* compared with POV-aged asphalt for the same *CA*. *HS* appears to be the same in both cases. For Exxon AC-20 shown in Figure VI-14, agreement between field- and POV-aged data is better. Field-aged asphalt has 20% lower η_o^* at the same *CA* compared to POV-aged asphalt. MacMillan AC-20, in Figure VI-15, shows field-aged asphalt with lower η_o^* by about 25% relative to POV-aged asphalt. *HS* for both field- and POV-aged asphalt appears to be equivalent. Texaco AC-20, in Figure

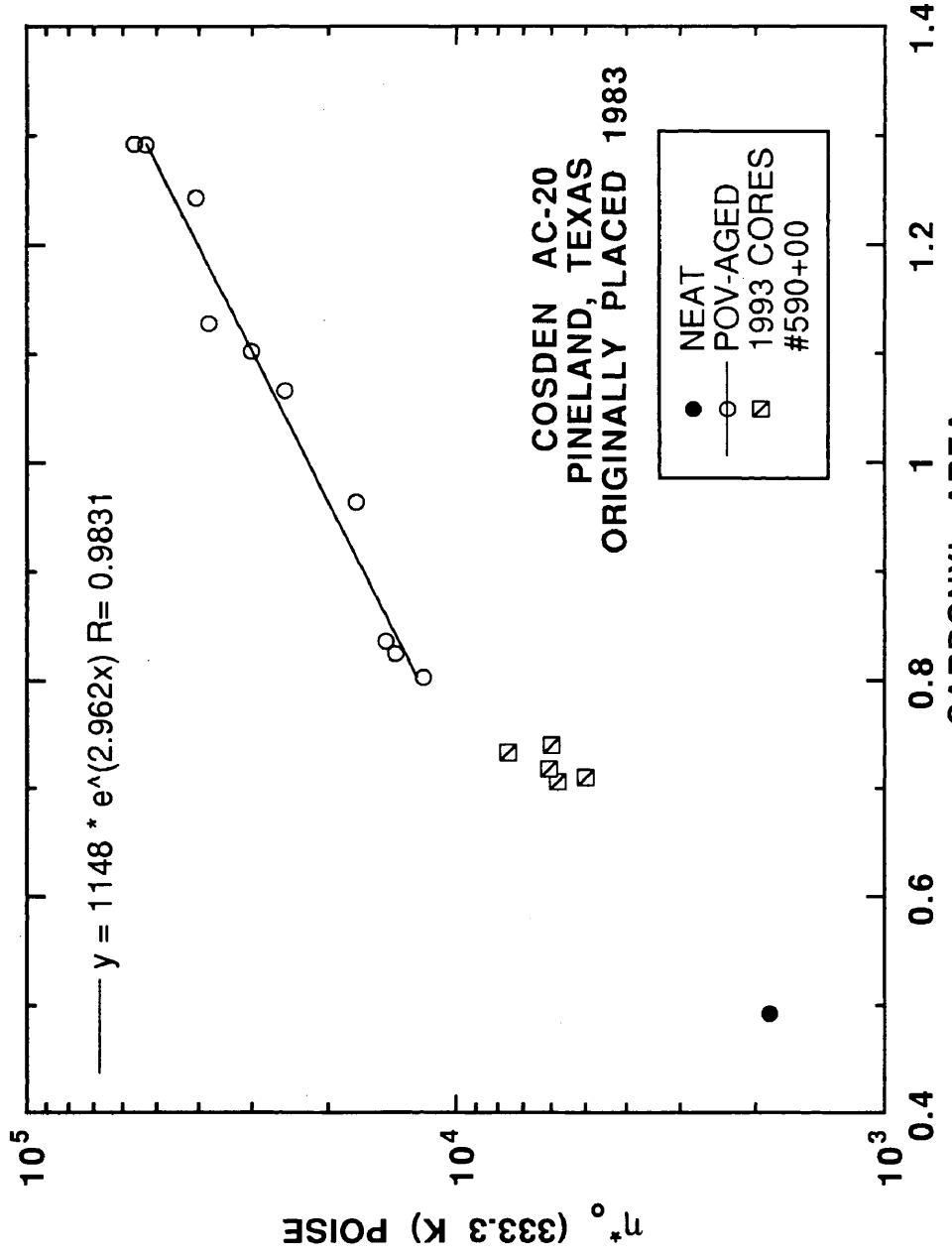

Figure VI-12. Comparisons between η_o^* at 333.3 K and CA of neat, POV- (333.3 K, 20 atm), and field-aged (#590+00, March 1993) Pineland Cosden AC-20.

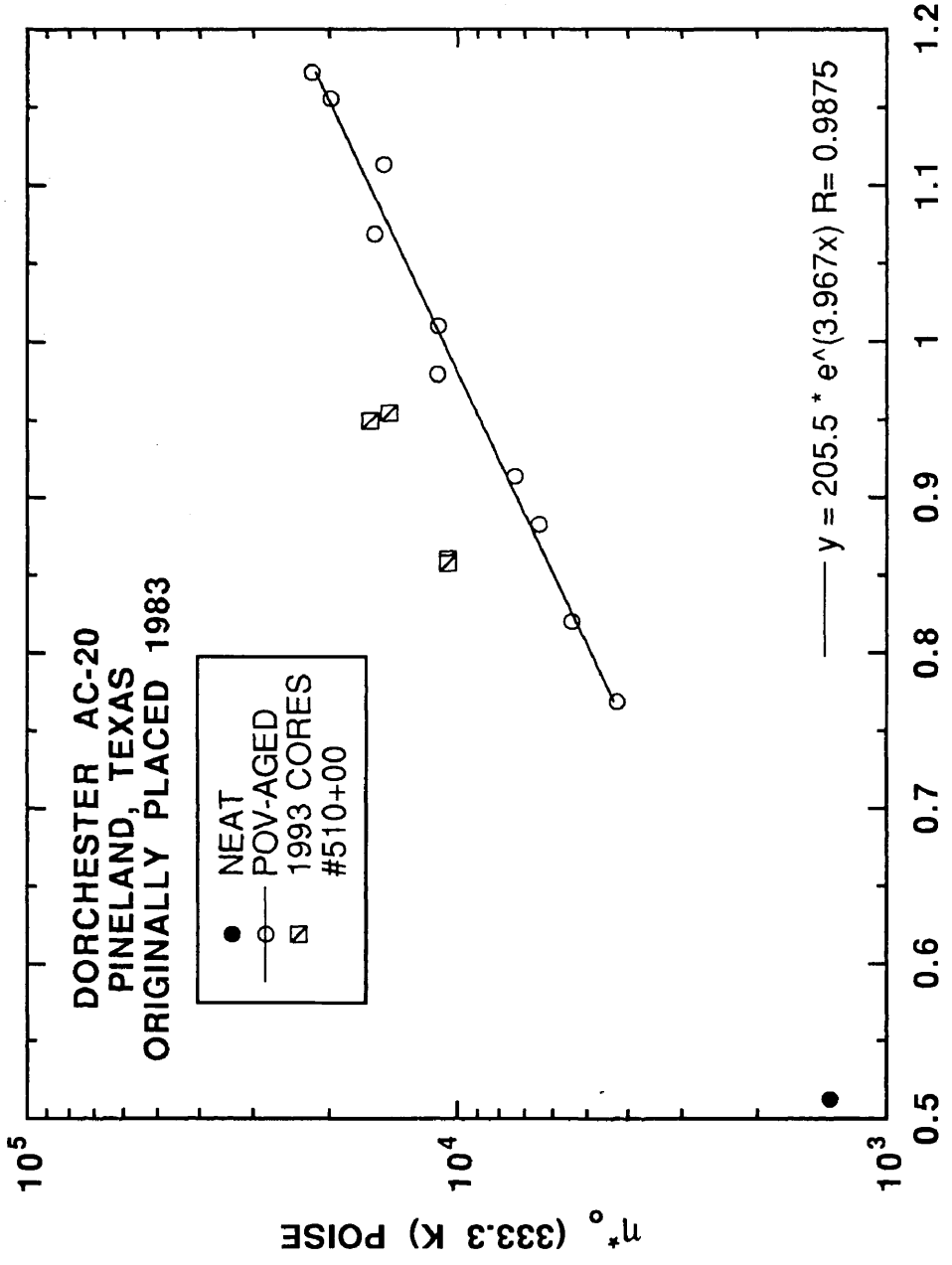

Figure VI-13. Comparisons between η_0^* at 333.3 K and CA of neat, POV- (333.3 K, 20 atm), and field-aged (#510+00, March 1993) Pineland Dorchester AC-20.

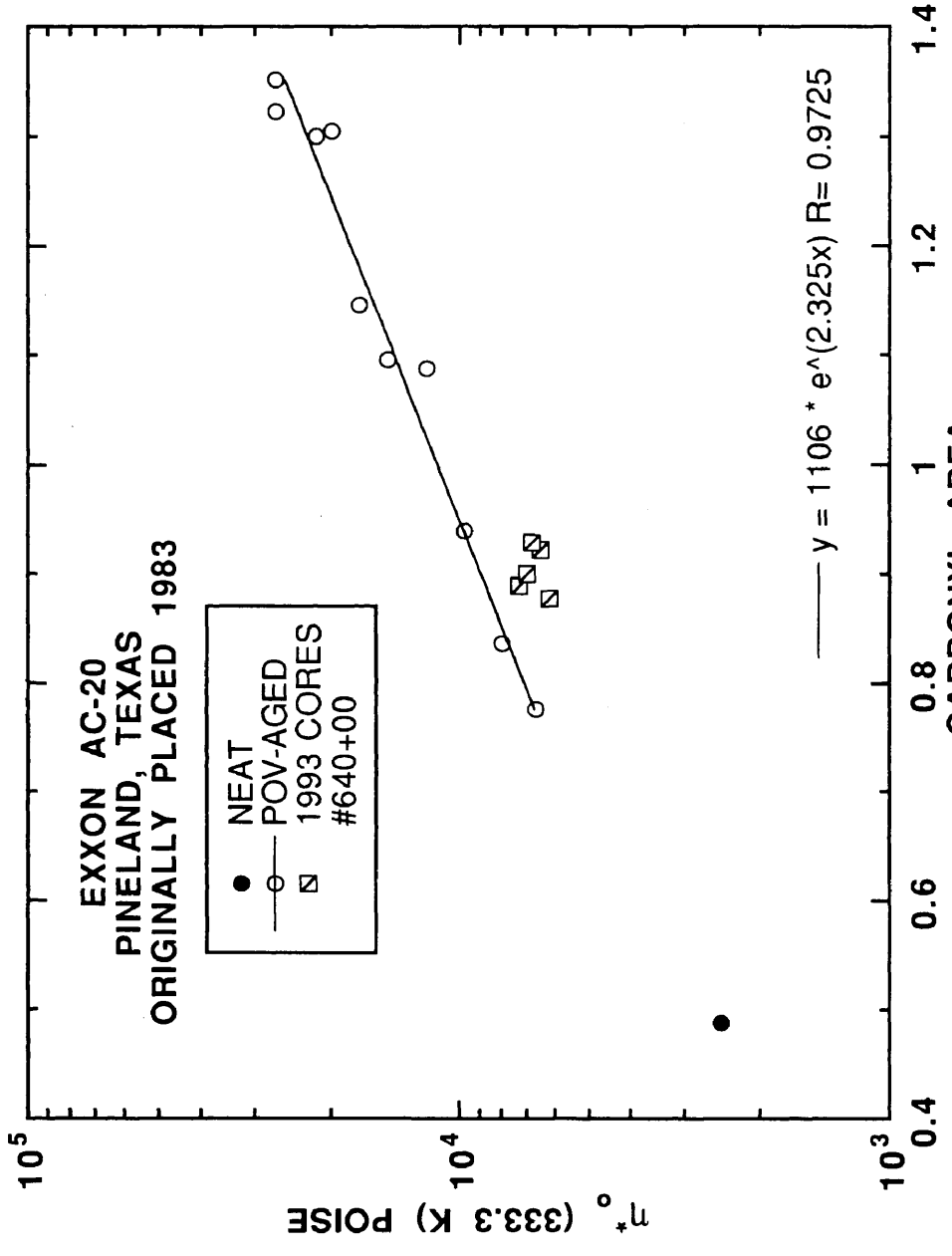

Figure VI-14. Comparisons between η_o^* at 333.3 K and CA of neat, POV- (333.3 K, 20 atm), and field-aged (#640+00, March 1993) Pineland Exxon AC-20.

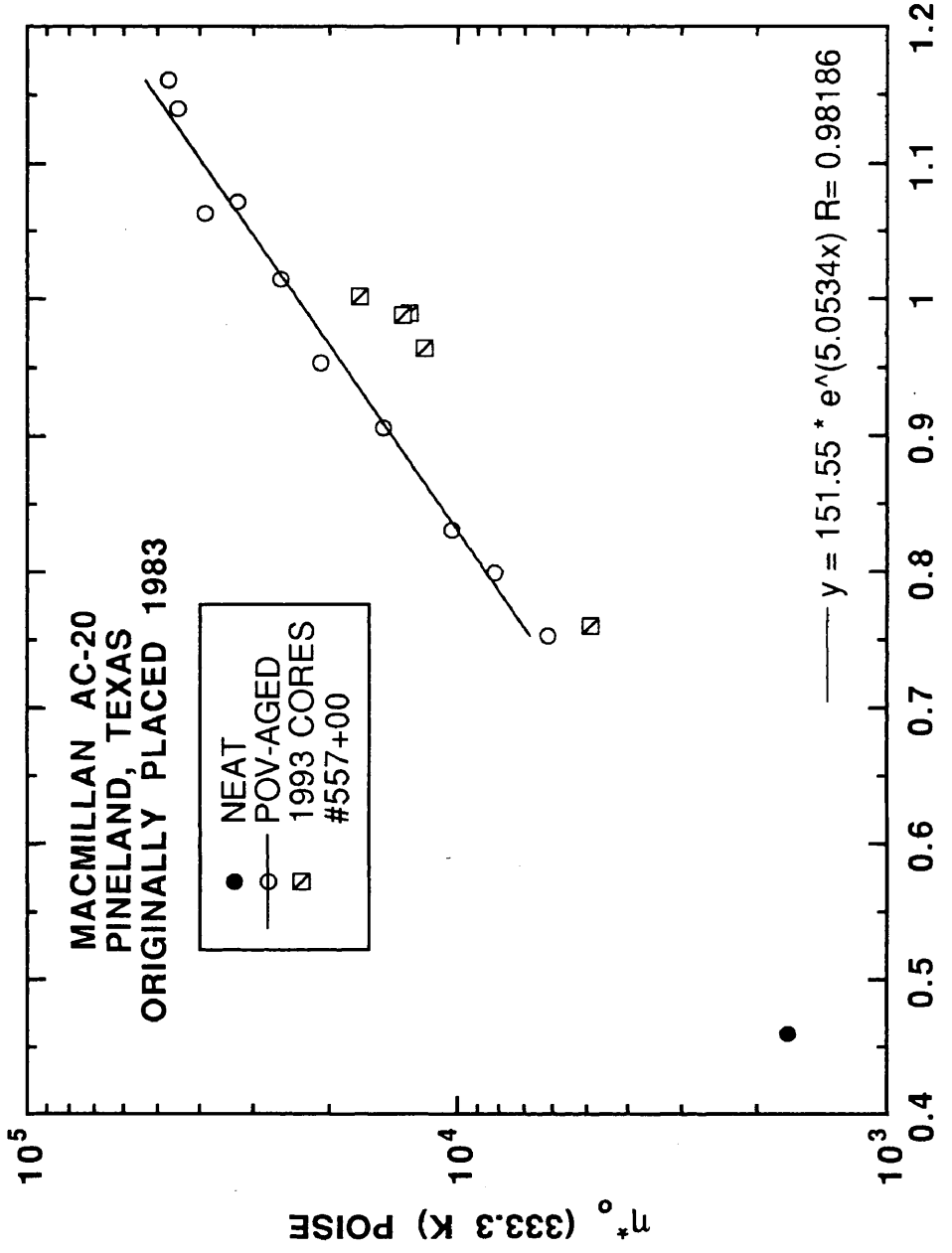

Figure VI-15. Comparisons between η_0^* at 333.3 K and CA of neat, POV- (333.3 K, 20 atm), and field-aged (#557+00, March 1993) Pineland MacMillan AC-20.

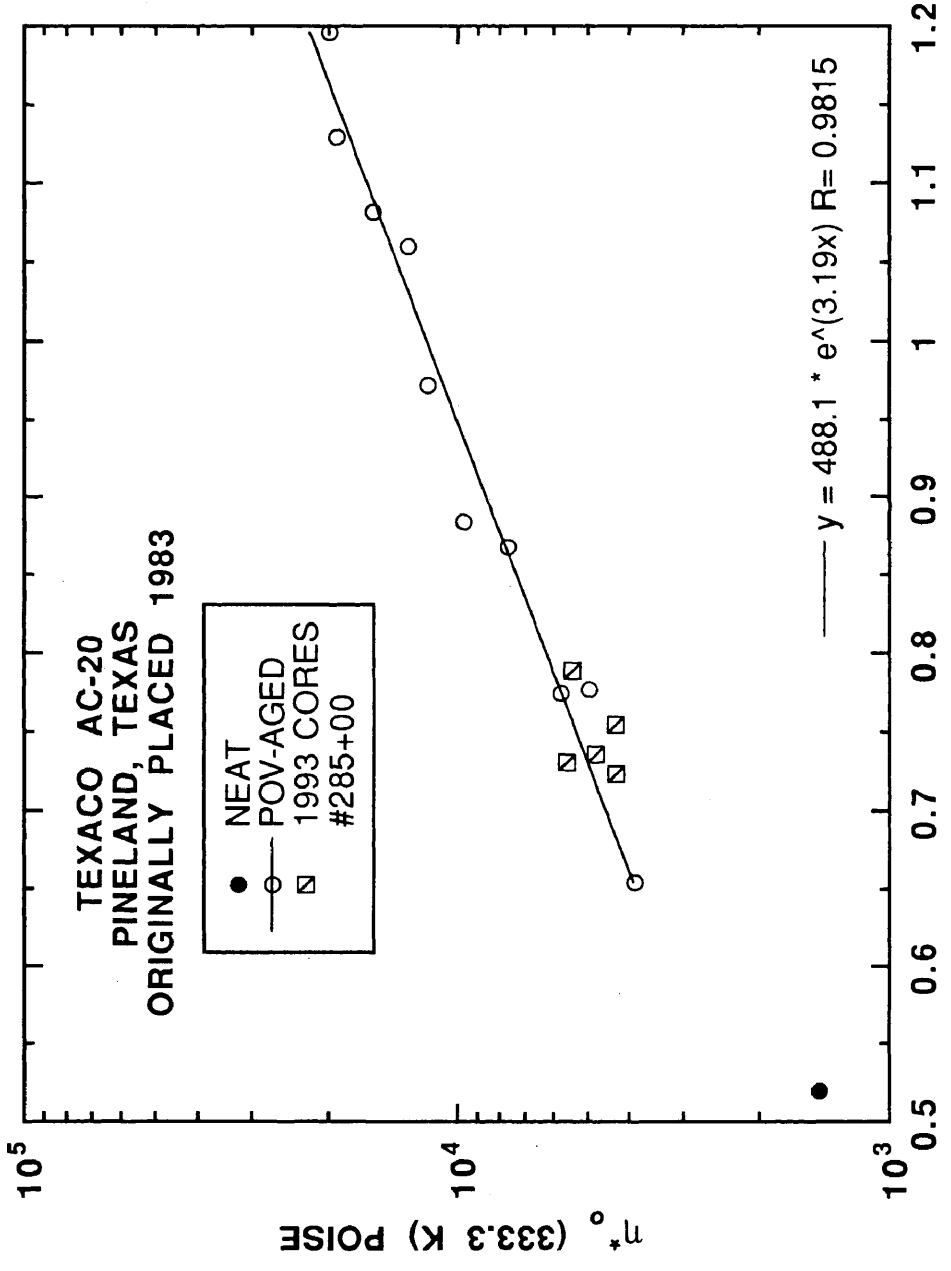

Figure VI-16. Comparisons between η_o^* at 333.3 K and CA of neat, POV- (333.3 K, 20 atm), and field-aged (#285+00, March 1993) Pineland Texaco AC-20.

VI-16, shows excellent agreement between field- and POV-aged asphalt. Since GPC confirmed that there was no residual solvent after extraction and recovery, lower η_o^* for field-aged Exxon AC-20 and MacMillan AC-20 compared to POV-aged material results from other undetermined factors.

Sixteen different extractions were performed for the Bryan test section. Six different Bryan Exxon AC-20 asphalts were POV aged. All of the extracted asphalt and POV simulation data are found in Tables E-12 through E-18. A clearer picture emerges with many extractions in determining if POV aging is simulating field aging. Figure VI-17 shows all of the field-aged extracted asphalt and three of the POV-aged asphalts. These POV-aged asphalts were selected since they have the highest, lowest, and median *HS* of the six asphalts studied for this test section. These asphalts give the variability of *HS* for the Bryan Exxon AC-20 asphalts studied. The extracted asphalts, shown by the slashed square, have significant scatter with respect to η_o^* at a given *CA* compared to the POV-aged asphalts. The scatter is random with respect to the mean defined as the POV-aged asphalt. A parameter estimation with the 1992 extraction data appears to give the same parameters as the POV-aged data. POV simulation at 344.4 K, 20 atm and four days produced material that was more severely aged than two years of field aging at this location.

POV experiments are simulating field aging based on the agreement between η_o^* and *CA*. The model parameters, *HS* and m, from POV-aged asphalt are given in Table VI-2. Other aspects of the data need to be addressed however. There is rather large variability in the properties of the extracted asphalt for the same age and location. For example, Dickens Cosden AC-20 has a range of *CA* from 1.7 to 1.95. η_o^* at 333.3 K ranges from 600 to 1,500 kP. Also, Pineland Dorchester AC-20 and Pineland MacMillan AC-20 show large variability with respect to the

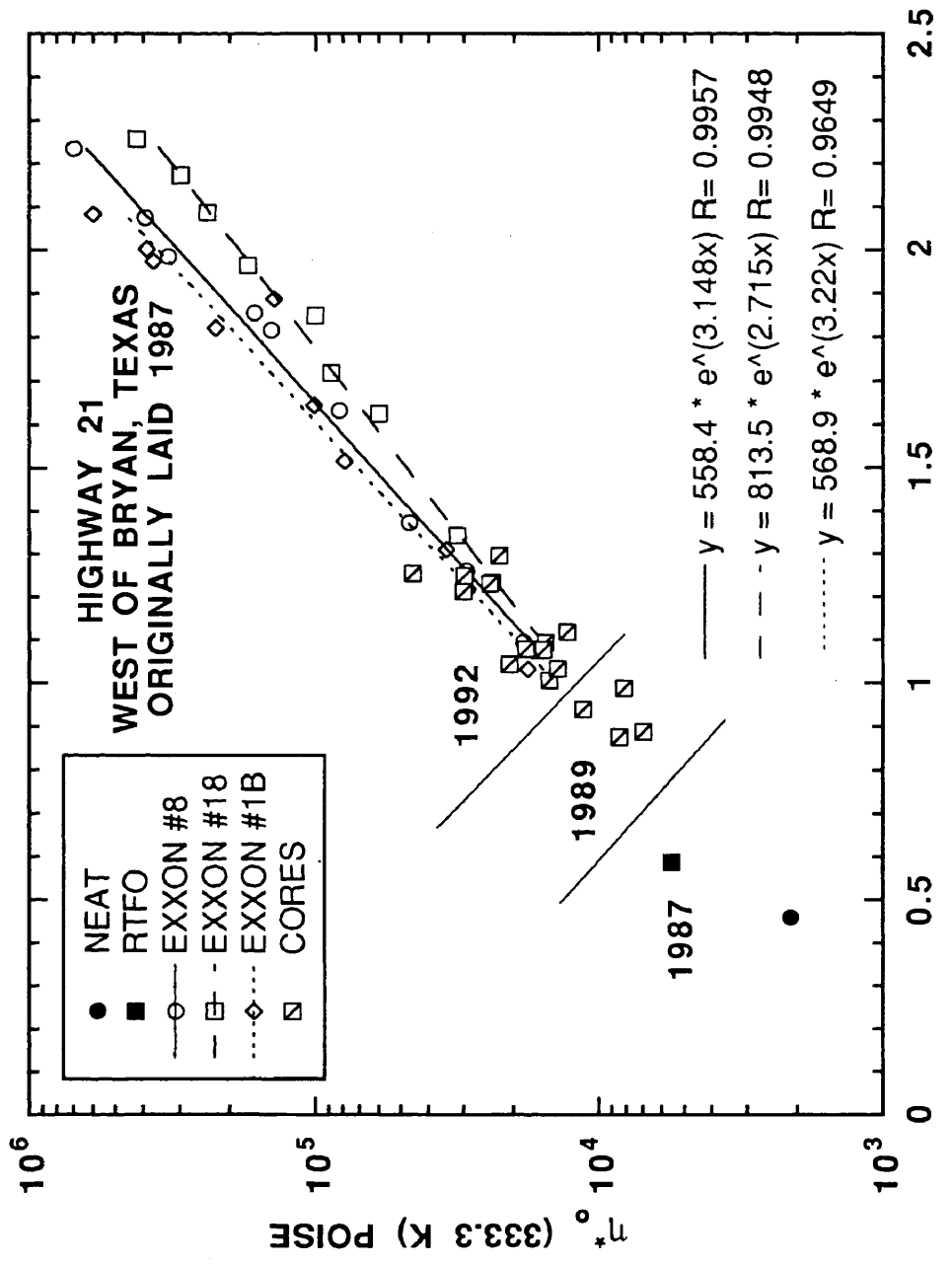

Figure VI-17. Comparisons between η_0^* at 333.3 K and CA of neat, RTFO, POV-(344.4 K, 20 atm), and field-aged Bryan Exxon AC-20.

Table VI-2. Model Parameters for All Physicochemical Relationships Based on POV-Aging Data of All Neat Asphalts Studied [a,b]

Location	Asphalt	η_o^*-CA[c]		$(1/J'')$-CA[d]		η_o^*-MW[e]	
		HS	$\exp(m)$	RS	$(1/J'')_o$	N	v
Dickens	Cosden AC-10	4.45	72.8	3.23	3147	24.3	3.67×10^{-76}
	Cosden AC-20	4.09	137	2.89	6513	24.9	3.56×10^{-78}
	D.S. AC-20	3.36	447	2.44	12581	20.1	1.03×10^{-69}
	Dorchester AC-20	5.20	403	3.01	19134	23.8	1.29×10^{-77}
	Exxon AC-20	3.60	487	3.60	487	16.9	2.01×10^{-51}
	MacMillan AC-20	4.75	199	3.20	6739	13.4	2.90×10^{-43}
Pineland	Cosden AC-20	2.96	1148	2.67	12849	16.4	8.31×10^{-50}
	Dorchester AC-20	3.97	206	3.53	2693	16.8	1.99×10^{-53}
	Exxon AC-20	2.32	1106	2.19	11864	16.2	3.24×10^{-49}
	MacMillan AC-20	5.05	152	4.17	2500	23.3	1.63×10^{-76}
	Texaco AC-20	3.19	488	2.88	5674	14.0	1.99×10^{-43}
Bryan	Exxon AC-20 #8	3.15	558	2.54	10368	16.2	2.30×10^{-49}
	Exxon AC-20 #15	2.93	579	2.48	9450	–	–
	Exxon AC-20 #16	2.86	670	2.42	10542	–	–
	Exxon AC-20 #18	2.71	813	2.36	11628	–	–
	Exxon AC-20 #19	3.10	501	2.60	8483	–	–
	Exxon AC-20 #1B	3.22	569	2.61	10034	–	–

[a] From Davison *et al.*, 1989. D.S represents Diamond Shamrock
[b] – Signifies the values were not determined
[c] Model: $\eta_o^*(333.3\text{ K}) = \exp(HS \cdot CA + m)$
[d] Model: $(1/J'')(333.3\text{ K},\ 10\text{ rad/s}) = (1/J'')_o \exp(RS \cdot CA)$
[e] Model: $\eta_o^*(333.3\text{ K}) = v(MW)^N$

measured properties for field-aged extracted asphalt. It is unrealistic to suggest that the properties of the asphalt in the cores change that dramatically within a few inches of each other. A more realistic explanation is that the variability results from the extraction and recovery procedures. Second, the products of asphalt oxidation are independent of aggregate composition. At Dickens, Pineland, and Bryan the

aggregate is river gravel, limestone/iron ore mix, and limestone, respectively. POV simulation accurately describes changes in η_o^* and *CA* for all test sections studied within a tolerance of error. Even though aggregate composition does not affect the oxidation products, the rate at which the oxidation products form may depend on aggregate composition. Unfortunately, the data shown thus far contain no information about the kinetics of field aging. Finally, ultimate precision in comparing POV- and field-aged asphalt at this point is unrealistic. From the data, *HS* is independent of aging method. However, the parameter m is more sensitive to field-aging or extraction and recovery since some of the field-aged data are shifted off the POV-aged model. The direction of the shift is somewhat random. Two asphalts, Dickens Cosden AC-20 and Pineland Dorchester AC-20, shift up; two asphalts, Pineland Exxon AC-20 and Pineland MacMillan AC-20, shift down, and the rest have no shift at all. Dickens Diamond Shamrock AC-20 and Dorchester AC-20 are excluded from this list. The downward shift is not caused by residual solvent after extraction and recovery. GPC analysis confirmed complete solvent removal. Since field-aged asphalts required extraction and recovery and POV-aged asphalts did not, more work is needed to confirm that this offset in the field-aged data is not an artifact of the extraction and recovery process.

Comparisons between $(1 / J'')$ *and CA*

Recently, SHRP discovered that the reciprocal of the loss compliance $(1 / J'')$ of an asphalt binder correlates with the rate of rut depth when the asphalt is in a mix (SHRP, 1993). $(1 / J'')$ is measured at 333.3 K and 10 rad/s. Furthermore, Lin *et al.*, (1993) showed that $(1 / J'')$ and percent hexane asphaltenes correlated for oxidative aging. Since η_o^* and *CA* provides a physicochemical relationship for comparing field

and POV aging, the development of a $(1 / J'')$-CA relationship was studied.

Figure VI-18 shows $(1 / J'')$ at 333.3 K and 10 rad/s versus CA for field- and POV-aged Dickens Cosden AC-10. The data suggest a model given in equation VI – 1.

$$(1 / J'') = (1 / J'')_o \exp\left\{ RS \cdot CA \right\} \qquad (\text{VI} - 1)$$

The parameters, RS and $(1 / J'')_o$, are defined as the *Rutting Susceptibility* and model intercept, respectively. This physicochemical property is novel, and similar to HS, provides a measure of an asphalt's resistance to rut with CA due to oxidative aging. Figure VI-18 also shows that the field- and POV-aged asphalts are in very close agreement. Not only is equation VI – 1 a new physicochemical relationship for characterizing asphalts with respect to oxidative aging, but also it shows that POV experiments are simulation field aging. Figures E-27 through E-37 show $(1 / J'')$ at 333.3 K and 10 rad/s and CA for the other asphalts and test sections. From all asphalts studied, for both field and POV aging, CA not only correlates with η_o^* but also $(1 / J'')$. The model parameters for all of the asphalts studied are given in Table VI-2.

The differences discussed in the η_o^*-CA relationship for POV- and field-aged asphalt are similar in the $(1 / J'')$-CA relationship. The magnitude of the difference varies; however, the direction is the same. This suggests that either η_o^* and $(1 / J'')$ are not truly independent, or that the offset in the rheological property exists for all linear visco-elastic rheological properties. The first reason is false from the definitions of η_o^* and $(1 / J'')$. Furthermore, comparing HS and RS for different asphalts shows there is no direct correlation. Therefore, the offset affects all linear visco-elastic rheological properties to some degree. Again it is proposed that this offset results from extraction and recovery procedures and requires additional research to fully understand.

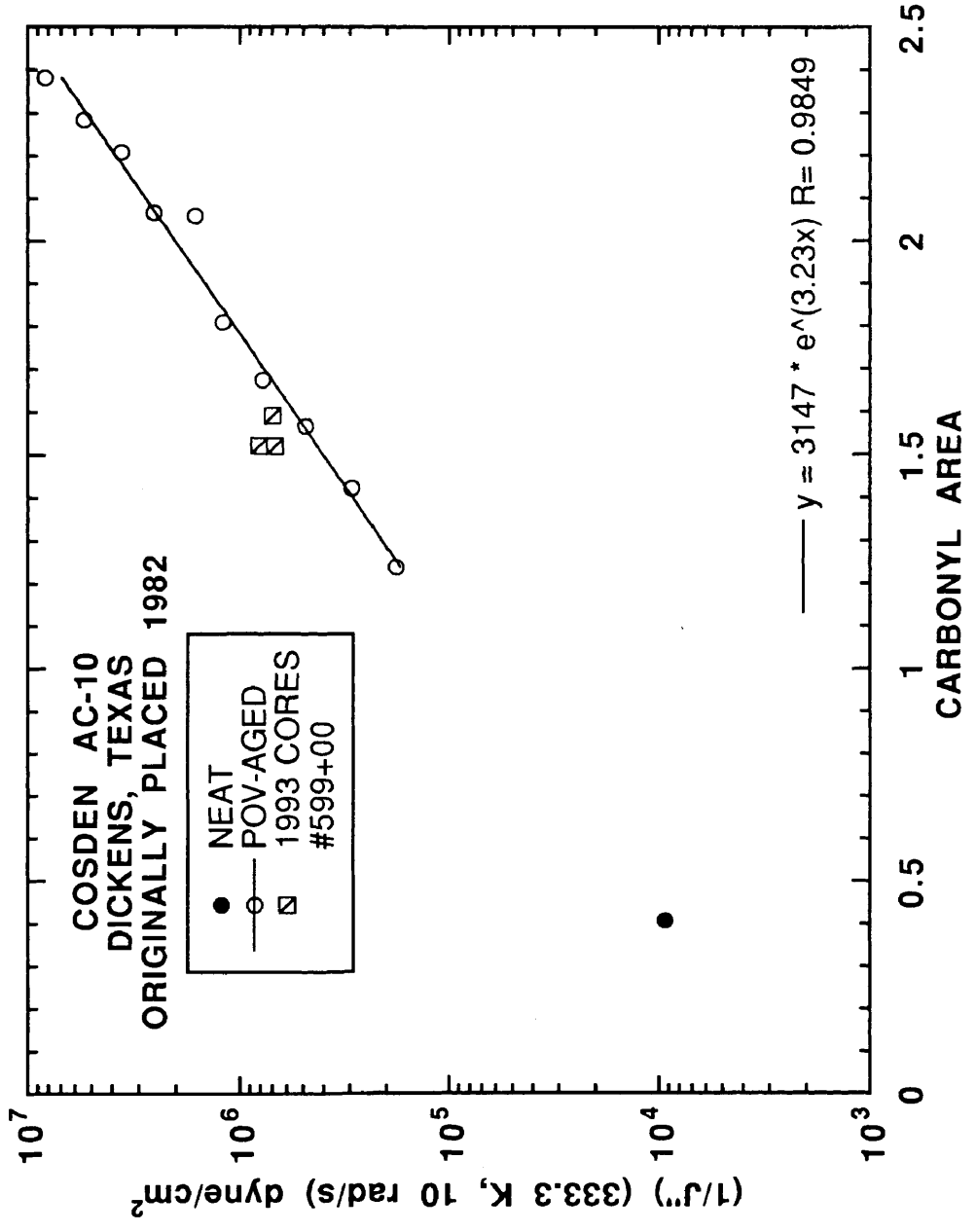

Figure VI-18. Comparisons between $(1 / J'')$ at 333.3 K, 10 rad/s and CA of neat, POV- (355.5 K, 20 atm), and field-aged (#599+00, February 1993) Dickens Cosden AC-10.

Comparisons between η_o^* and MW

A model relating η_o^* and MW for polymers is provided in Rosen (1982) and given in equation VI – 2.

$$\eta_o^* = v(MW)^N \qquad \text{(VI – 2)}$$

The model parameters, N and v, are determined from experimental data. N is unity for polymers if MW is below a critical MW. Above that critical MW, N is 3.4. The critical MW is defined as the point where molecular entanglements start to dominate the flow properties. Since both GPC and η_o^* data are available, the ability of equation VI – 2 to model aging characteristics of asphalt is studied.

GPC analysis was used primarily to confirm complete solvent removal after extraction and recovery and verify the asphalts and location. The data were used to determine a weight average molecular weight, MW. The calculation was based on known polystyrene standards and the calibration curve relating MW to retention time, Figure III-13.

Figure VI-19 shows the POV- and field-aged η_o^* at 333.3 K and MW for Dickens Cosden AC-10. The POV-aged asphalts are designated by open circles. The neat asphalt is shown in the filled circle. The field-aged samples are the slashed squares. First, only the POV-aged data are discussed. Since the scales on both axes are logarithmic and the POV data show good linearity this suggests that equation VI – 2 should accurately describe the η_o^*-MW relationship for POV-aged asphalt. However, the change in MW is not very large. A parameter estimation was performed, and N is 24.3 for Dickens Cosden AC-10 at 333.3 K as shown in the figure. Figures E-38 through E-47 show the other asphalts studied. The model parameters for all of the asphalts studied are given in Table VI-2. POV-aged data show a strong correlation

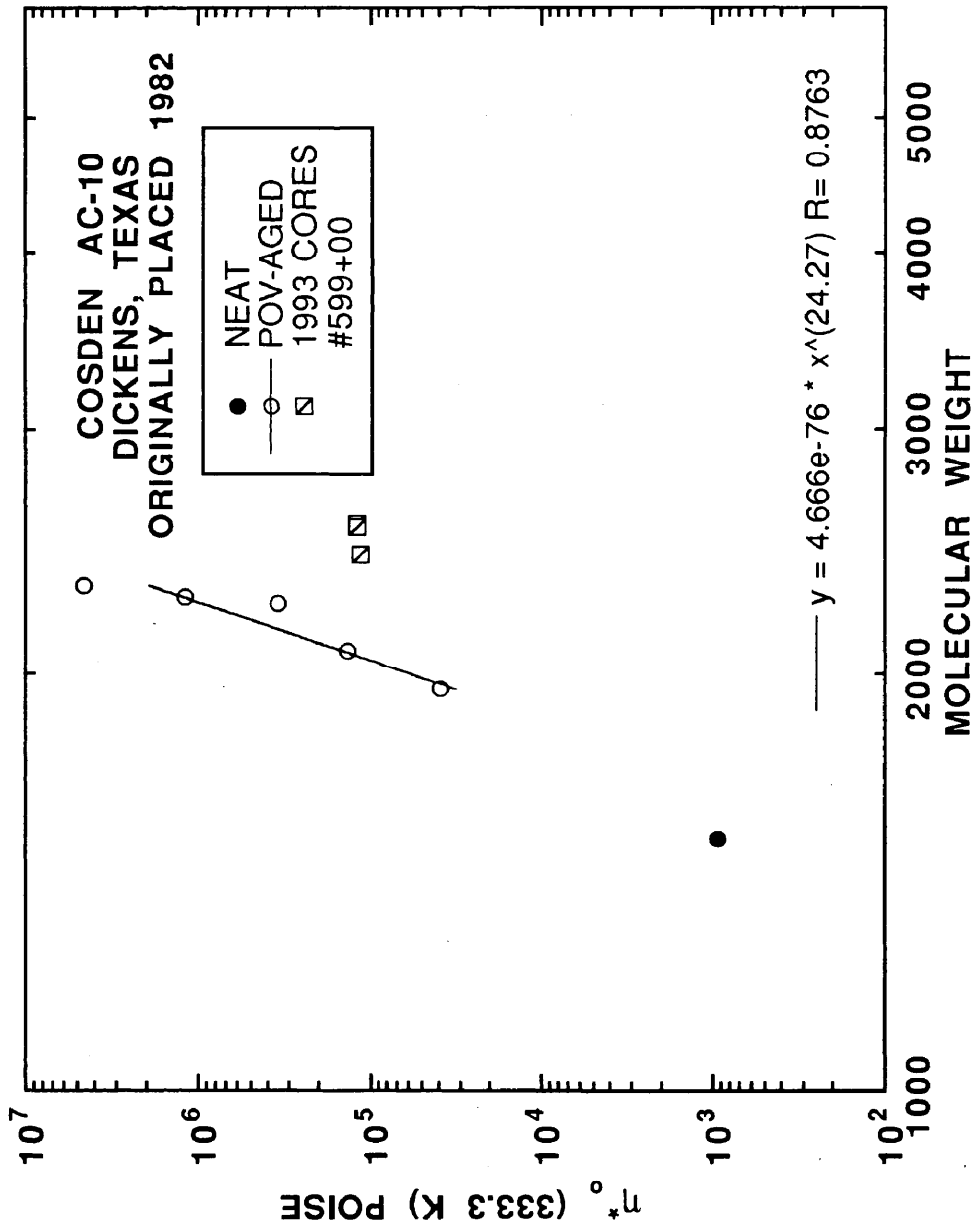

Figure VI-19. Comparisons between η_o^* at 333.3 K and MW of neat, POV- (355.5 K, 20 atm), and field-aged (#599+00, February 1993) Dickens Cosden AC-10.

between η_o^* and MW for all the asphalts studied, and N is much greater than 3.4. Therefore, η_o^* measurements at 333.3 K are dominated by molecular entanglements.

Different asphalts show different model parameters. For example, η_o^* at 333.3 K is relatively insensitive to MW increases for Dickens Diamond Shamrock AC-20 although it has a very large molecular weight compared to the other asphalts. η_o^* at 333.3 K for Dickens Cosden AC-20 is very sensitive to MW increases. The model parameters are only a function of the initial asphalt composition and do not change with oxidative aging. This provides another physicochemical relationship between GPC and DMA to characterize an asphalt with respect to oxidative aging.

Since the model parameters do not appear to change with oxidative aging and are only dependent on initial composition, the overall structure of the asphalt molecules are not changing due to aging. Furthermore, the asphalt-specific model parameters should relate to structural differences. There are some fundamental asphalt structures that have the desirable characteristic, the material resists hardening with increased MW or CA. By knowing which structures cause the desired behavior, asphalts of known aging characteristics can be designed and manufactured.

Since field-aged asphalts showed larger LMS regions relative to POV-aged asphalts at equivalent η_o^*, comparisons between POV- and field-aged asphalts based on η_o^* and MW are not very good. This larger LMS region corresponds to higher MW as shown in the Figure VI-19 for Dickens Cosden AC-10. Larger MW in the extracted field-aged asphalt was independent of the differences in η_o^*-CA comparisons. In other words, regardless if the field-aged asphalt η_o^* was lower or higher relative to POV-aged asphalt at the same CA, field-aged asphalt MW was always higher than POV-aged asphalt MW. Only one asphalt studied, Pineland Texaco AC-20 in Figure VI-20 shows good agreement between POV and field aging based on η_o^* and MW.

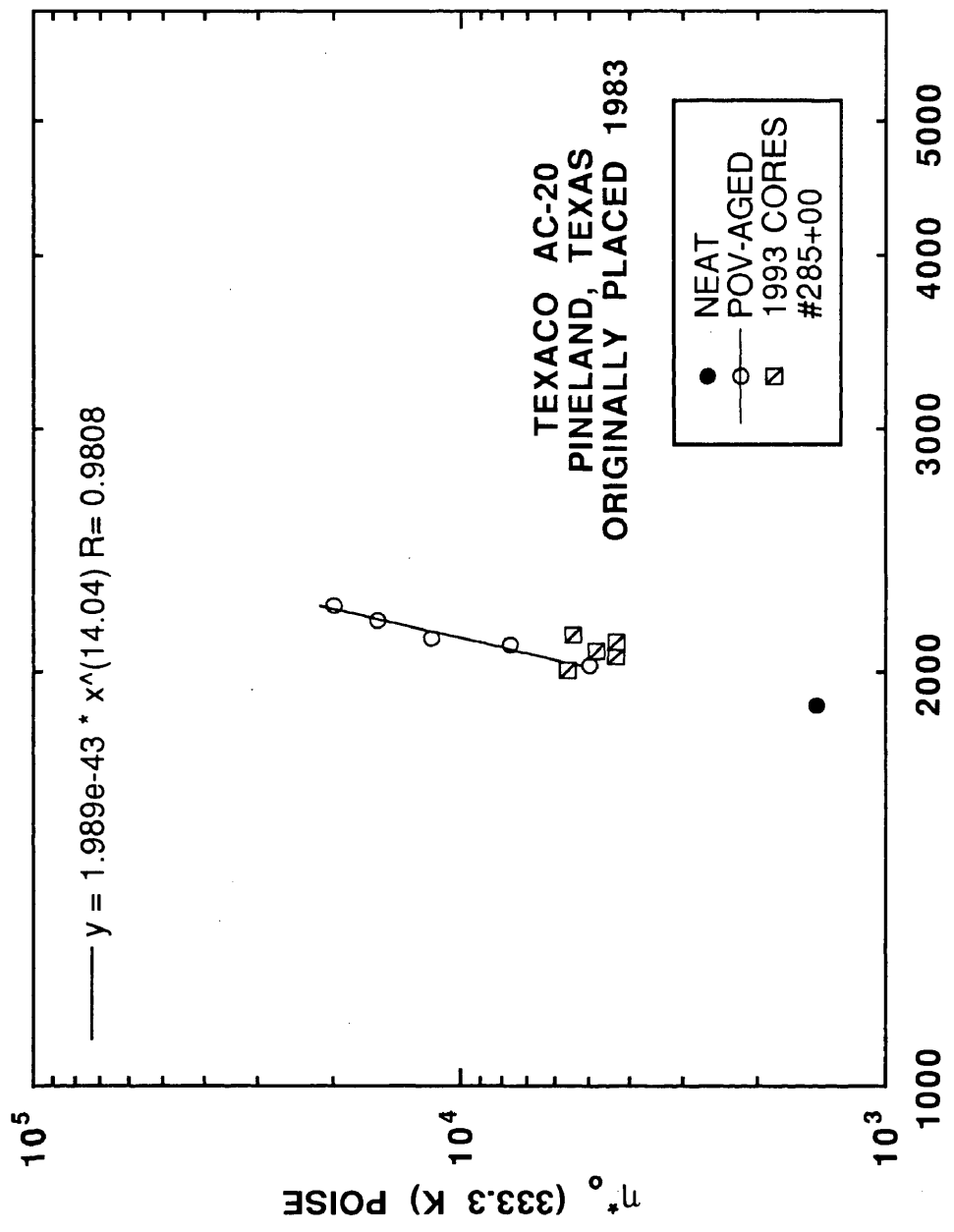

Figure VI-20. Comparisons between η_o^* at 333.3 K and MW of neat, POV- (333.3 K, 20 atm) and field-aged (#285+00, March 1993) Pineland Texaco AC-20.

Physicochemical relationships for all asphalts studied

From POV simulation data for the asphalts from Dickens, Pineland, and Bryan, a set of relationships between CA, η_o^* at 333.3 K, $(1/J'')$ at 333.3 K and 10 rad/s, and MW were discussed. Table VI-2 summarizes the model parameters for all asphalts studied. All of the parameters were only functions of initial composition and did not change as a result of POV oxidative aging. Comparisons between POV- and field-aged asphalts show that, for the most part, the model parameters in the CA, η_o^* , and $(1 / J'')$ relationship are independent of aging method. However, field-aged asphalt showed larger MW compared with the POV-aged asphalt for equivalent η_o^*. This larger MW is a direct result of the larger LMS region in the GPC chromatogram.

Comparisons between IR spectra

The IR spectra of POV- and field-aged asphalts are compared in an effort to understand why field-aged asphalt showed such large differences in terms of MW and large variability for other physicochemical properties. Figure VI-21 shows the IR spectra of the extracted field-aged asphalt at #599+00 for Dickens Cosden AC-10. For comparison, Figure VI-22 shows IR spectra of the POV-aged Dickens Cosden AC-10. The only difference between the spectra appears in the shape of the sulfoxide peak located at 1000 cm^{-1}. Comparing Figures VI-23 and VI-24 for field- and POV-aged Dickens Exxon AC-20, larger differences in the shape and size of the sulfoxide peak exists. Figures E-48 through E-67 show the IR spectra of the other field- and POV-aged asphalts. The shape and size of the sulfoxide peak is different comparing field-aged asphalt after extraction and recovery to POV-aged asphalt. From the previous observations for η_o^*-CA, this extraneous peak appears to have a larger effect on the magnitude of η_o^* and does not appear to change HS.

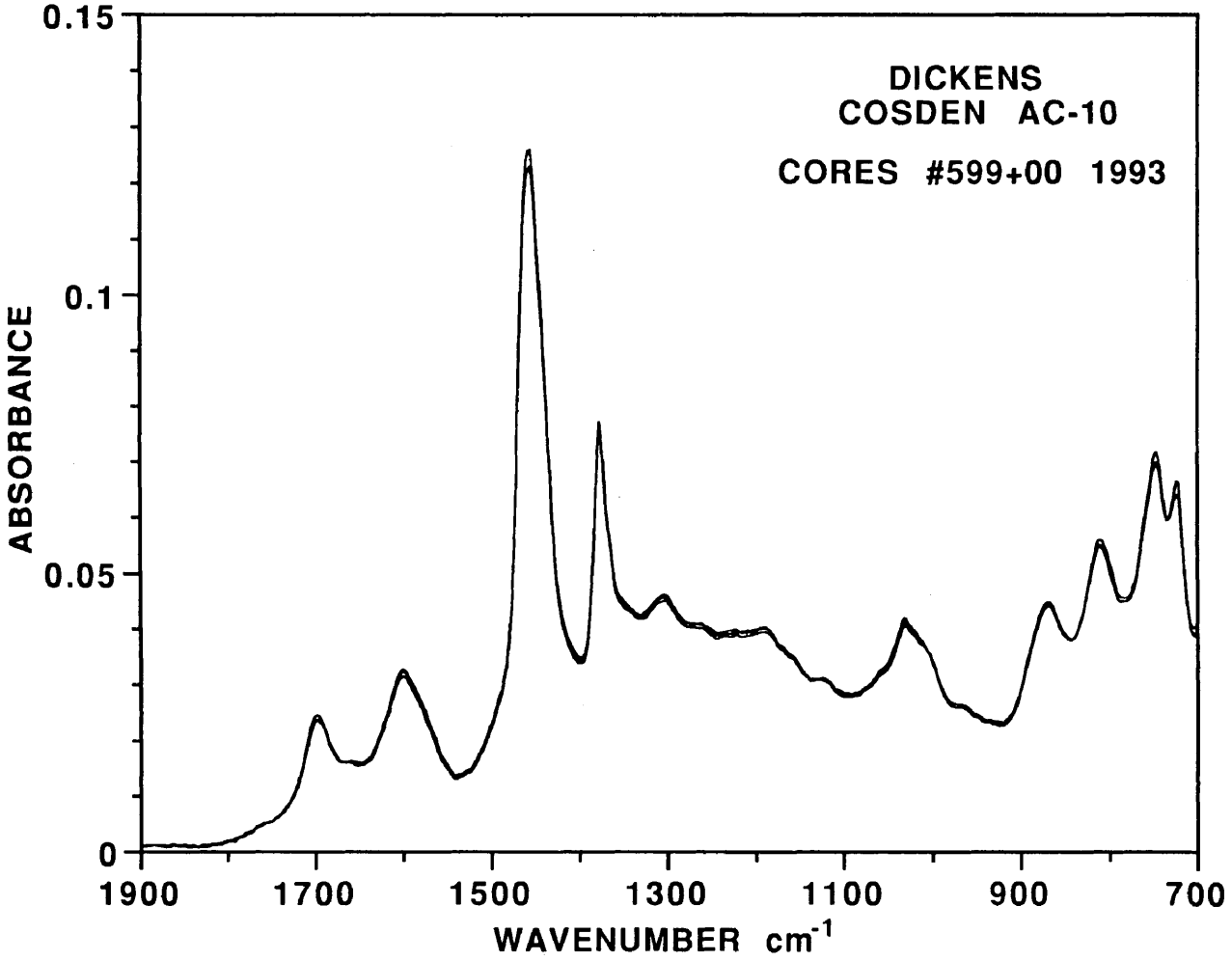

Figure VI-21. IR spectra of field-aged Dickens Cosden AC-10 extracted asphalt from #550+00. Cored February, 1993.

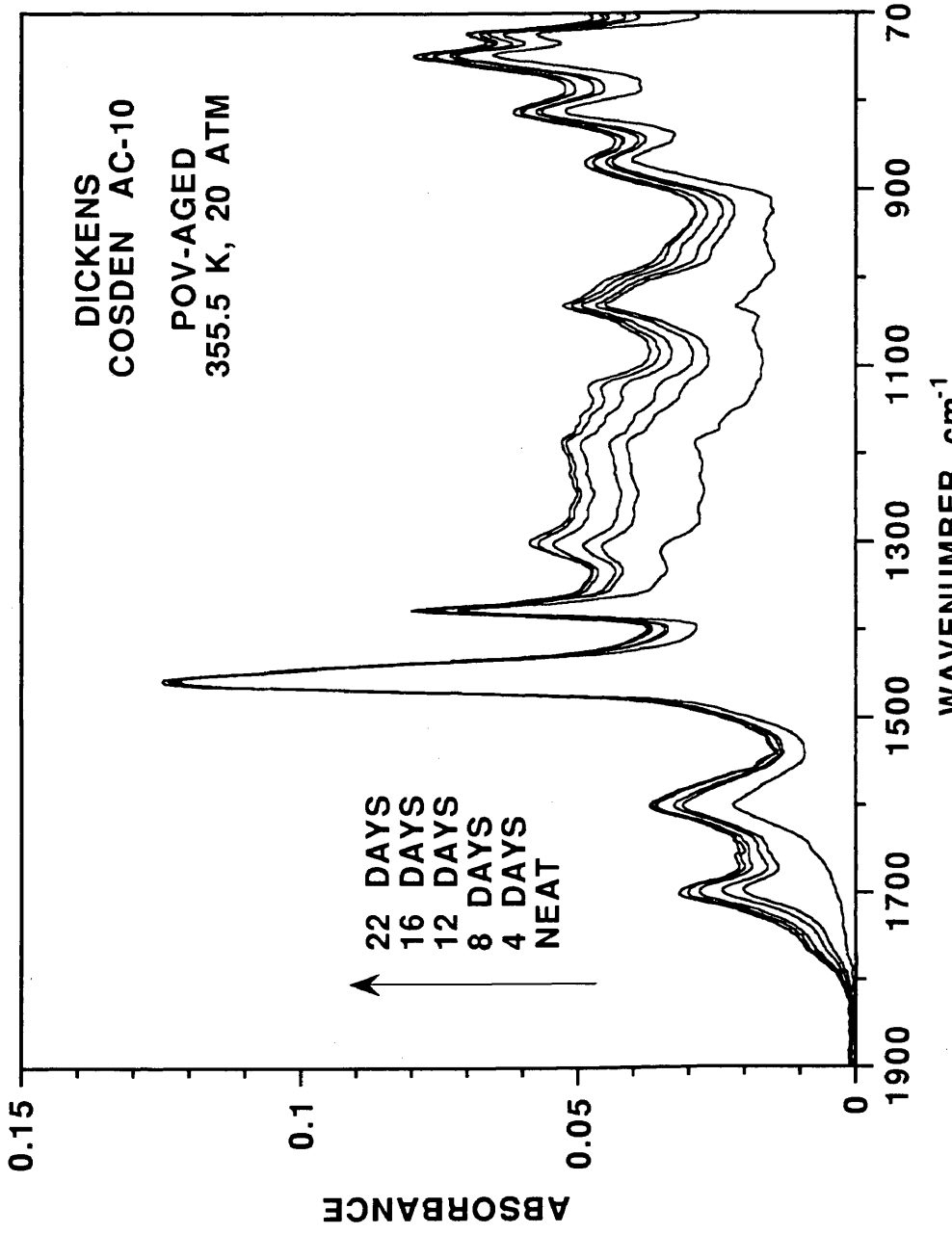

Figure VI-22. IR spectra of neat and POV-aged Dickens Cosden AC-10 at 355.5 K and 20 atm.

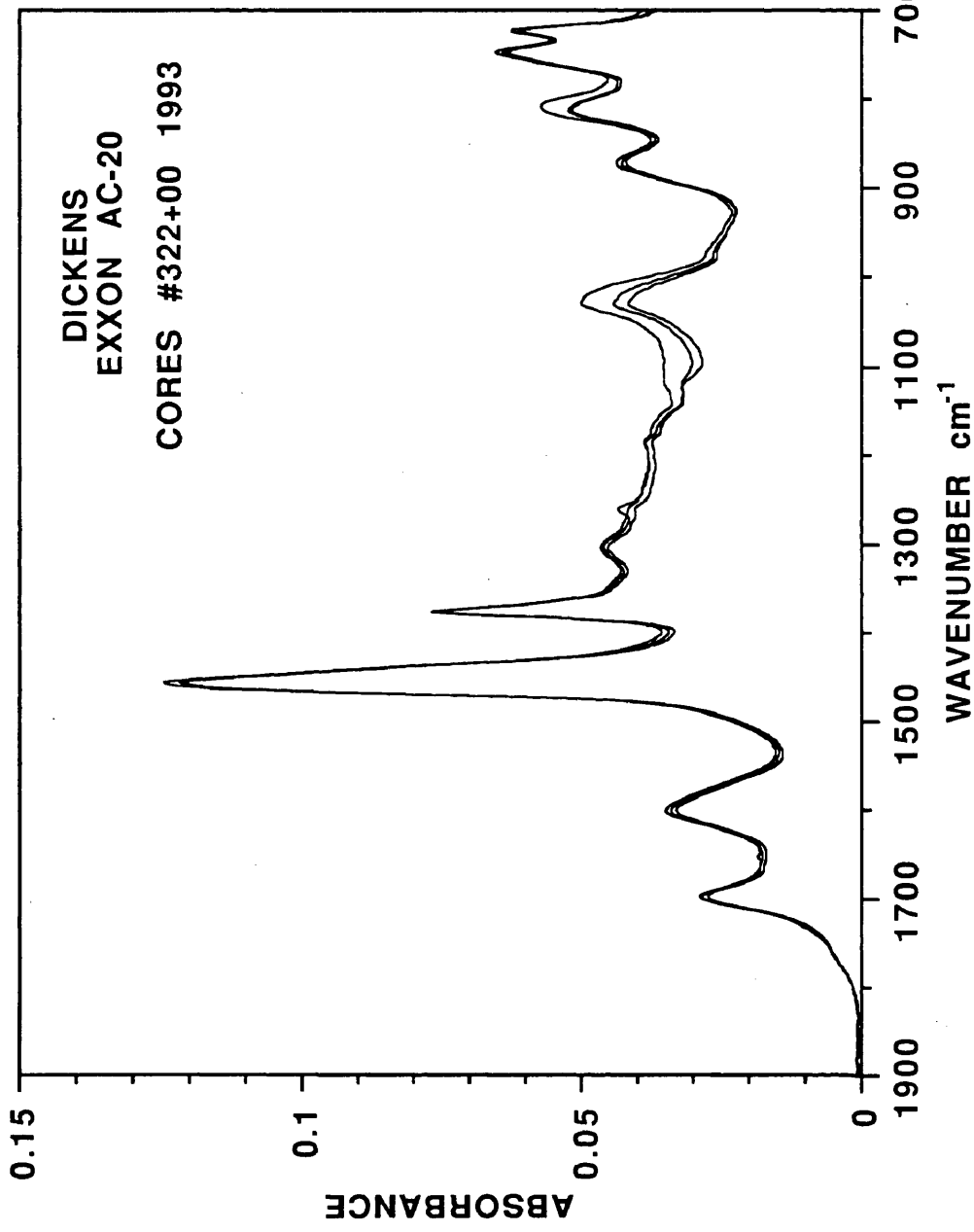

Figure VI-23. IR spectra of field-aged Dickens Exxon AC-20 extracted asphalt from #322+00. Cored February, 1993.

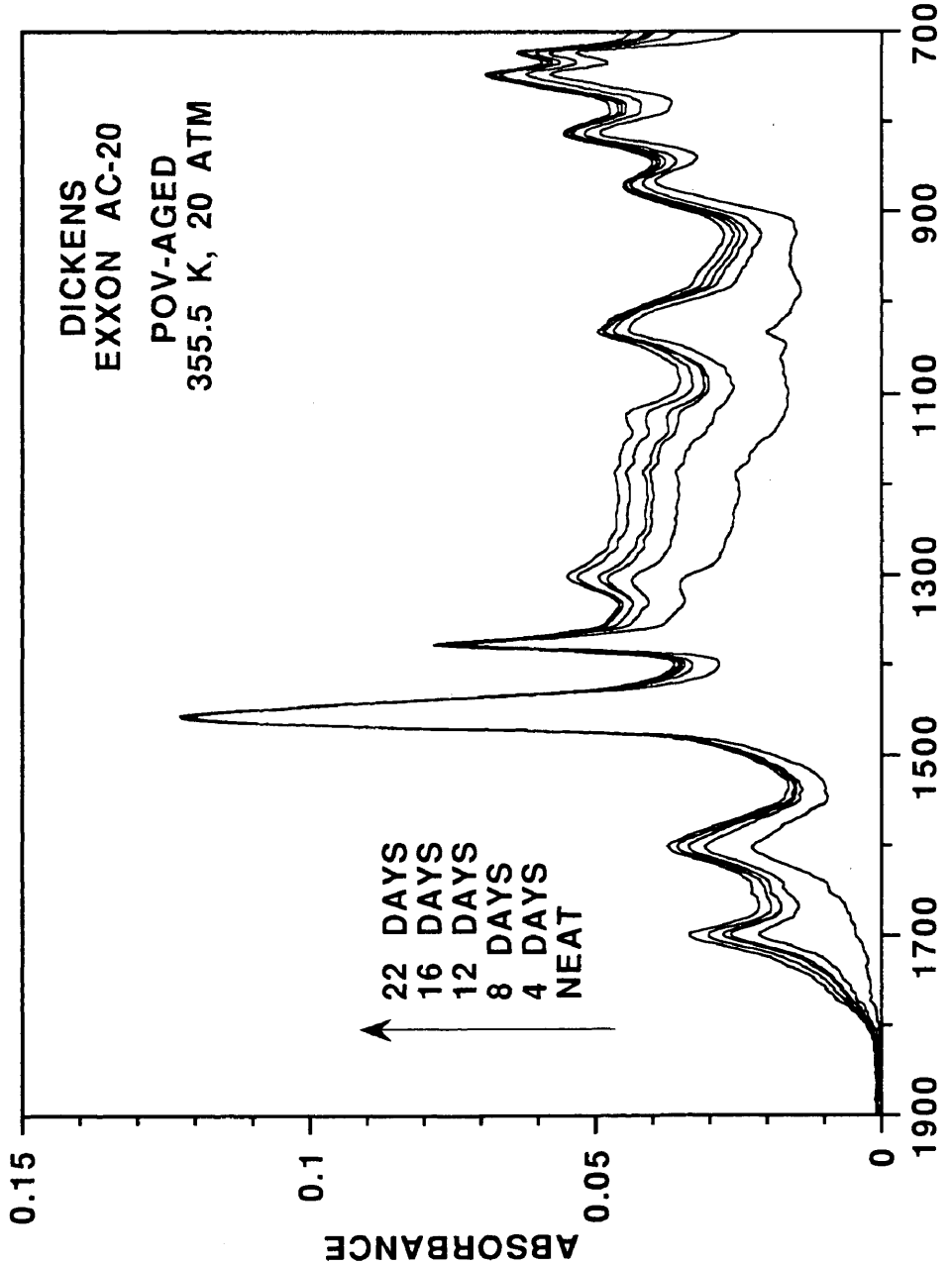

Figure VI-24. IR spectra of neat and POV-aged Dickens Exxon AC-20 at 355.5 K and 20 atm.

The sulfoxide region did not correlate with changes in physical properties as a result of POV or field aging (Lau *et al.*, 1992; Martin *et al.*, 1990). However, these studies did not compare POV with field aging. There appears to be a difference in the shape and size of the sulfoxide peak depending of the method of aging, field or POV. However, this difference may not result solely from field aging. Extraction and recovery processes may produce this difference, and more research is required to fully understand this phenomenon.

Extraction and recovery procedures

It appears that the field- and POV-aged samples are not chemically the same from the differences in the GPC chromatograms and the IR spectra in the sulfoxide region. However, agreement between CA, η_o^*, and $(1/J'')$ is excellent for the most part. With many extractions, Figure VI-17, POV- and field-aged asphalt properties are indistinguishable. Since agreement between field- and POV-aged asphalt properties increases with the number of cores extracted, the variability in the extraction and recovery process accounts for most of the error.

Comparing Dickens and Pineland data for 1987 and 1993 cores shows other discrepancies in the properties of the extracted asphalt. Table VI-3 gives η_o^*, % V, and % Asp, for the 1987 and 1993 asphalts at Dickens and Pineland. The reported values for 1993 are arithmetic averages of all the extractions for that particular asphalt and location. The differences between % V and % Asp for 1987 and 1993 are very small, even on a percentage basis. In all cases except Dickens Exxon AC-20 and Pineland Cosden AC-20 and Exxon AC-20, 1993 % V decreases compared to 1987 as expected. 1993 % Asp tends to be greater for Dickens and less for Pineland compared to 1987 % Asp. % V measurement requires no extraction and recovery, and only total

asphalt removed from the aggregate affects % *Asp*.

The most notable discrepancy is η_o^* in a comparison of 1987 and 1993 extracted asphalts. At Dickens, all of the asphalts became softer from 1987 to 1993. At Pineland, the asphalts became harder from 1987 to 1993. The Pineland result is more realistic and supported in the literature. The actual values of η_o^* for 1987 are larger than that reported in Table VI-3 since viscosity was measured with vacuum capillary viscometers. Unfortunately, comparisons of *CA* are not possible since two different techniques were used. Since physical properties are most affected by extraction and recovery procedures, the physically inconsistent results probably stem from errors in extraction and recovery.

From the data of the three test sections, the chemical and rheological properties of field aged asphalt change during the extraction and recovery process. The strategy behind this asphalt extraction and recovery was to remove as much material as possible. This may not have been a good idea since it included removing the strongly absorbed material that behaves much like the aggregate. The strongly-absorbed material has different chemical and material properties relative to the bulk (Burr, 1993). The presence of the strongly-absorbed material may account for the scatter in the comparison of field- and POV-aged asphalts. It may also account for the larger *LMS* region of field-aged asphalt relative to POV-aged asphalt. A method of measuring chemical and physical properties of the asphalt without extraction and recovery would eliminate most of the problems and be the ideal solution.

In summary, POV- and field-aged asphalt were compared using physicochemical relationships. The development of new physicochemical properties between $(1 / J'')$ and *CA* and η_o^* and *MW* was also accomplished. These relationships were dependent only on initial composition of an asphalt and did not change with POV aging. GPC

Table VI-3. Comparisons between 1993 and 1987 Properties from Dickens and Pineland Test Sections[a,b]

Location	Asphalt	η_o^*(333.3 K) P		% V		% Asp	
		1987[c]	1993	1987	1993	1987	1993
Dickens	Cosden AC-10	342000	118000	12.0	8.3	5.6	5.96
	Cosden AC-20	376000	375000	11.0	8.7	4.0	5.94
	D.S AC-20	260000	–	12.0	–	–	–
	Dorchester AC-20	222000	–	13.0	–	4.6	–
	Exxon AC-20	900000	206000	9.0	9.4	5.1	–
	MacMillan AC-20	159000	136000	8.0	5.8	6.2	6.10
Pineland	Cosden AC-20	5400	6100	1.8	1.8	6.9	6.10
	Dorchester AC-20	–	12900	–	2.2	–	6.30
	Exxon AC-20	2500	6760	2.5	2.6	7.7	6.36
	MacMillan AC-20	–	13900	–	2.8	–	6.20
	Texaco AC-20	–	4900	–	1.4	–	5.87

[a] From Davison *et al.*, 1989. D.S. represents Diamond Shamrock
[b] – Signifies the values were not determined
[c] These were measured by vacuum capillary

analysis showed the most pronounced differences in POV- and field-aged asphalts. Field-aged asphalt showed larger *LMS* compared with POV-aged asphalts for the same η_o^*. This larger *LMS* corresponded to larger *MW*. Comparisons based on *CA*, η_o^*, and $(1 / J'')$ showed that, for the most part, POV experiments were simulating field aging. Furthermore η_o^*-*CA* relationships for POV- and field-aged sample were indistinguishable with large numbers of extractions of the same asphalt. Agreement between POV- and field-aged asphalt was independent of the three aggregates, river gravel, limestone/iron ore mix, and limestone. Comparing POV- and field-aged asphalt IR spectra, the sulfoxide region was different for the two methods of aging. These results show promise; however, more data are needed. The solvent effect on the extracted and recovered asphalt needs to be studied more carefully.

POV- and Field-Aging Comparisons with the Asphalt-Aging Model

This section proposes to show that field-aging is a predictable phenomenon and develops a highway-pavement aging model. This is a relationship between measurable core properties such as % V or % Asp and the effective asphalt film thickness, L_{eff}, and the effective oxygen pressure in the voids, P_{eff}. L_{eff} and P_{eff} can then be used in the asphalt-aging model to predict field aging both qualitatively and, with the addition of more experimental data to refine the model parameters, quantitatively.

A comparison between POV- and field-aged asphalt was given. It was concluded that POV experiments simulate field-aging based on physicochemical properties. These comparisons only show to what extent the physical and chemical properties change. With these physicochemical relationships determined from laboratory data, monitoring the aging of a highway requires fewer measurable variables. For example, with HS and m determined from POV data, η_0^* can be calculated from a CA measurement. These physicochemical relationships greatly reduce the burden of monitoring highway aging. Unfortunately, these comparisons between physicochemical properties provide no kinetic information. With the data given thus far, it is impossible to predict how fast the chemical and physical properties change with time especially at other aging temperatures.

This section is divided into several sub-sections as described below. The first section details the laboratory experiments required to estimate kinetic parameters for each field-aged asphalt. The next section describes the estimation of pavement-surface temperature as a function of time from climatic data and latitude. The follow section uses the kinetic information and field temperature, calculating a theoretical minimum time, t_{theor}, to reach the measured properties of field-aged asphalt. This calculation assumes that oxygen diffusion resistance is negligible or that asphalt film

thickness is infinitely thin. t_{theor} qualitatively measures an asphalt's susceptibility to age in a given climate. Using t_{theor}, asphalts can be ranked. Finally, the last section describes an attempt to correlate the measurable core properties of % V and % Asp to L_{eff} and P_{eff}. These correlations are the highway-pavement aging model. L_{eff} is estimated by comparing measured chemical properties to those predicted by the asphalt-aging model.

Experimental design to determine kinetic parameters

Multi-temperature POV experiments were designed to determine kinetic parameters for the asphalts from Dickens and Pineland. Aging temperatures were 333.3, 344.4, and 355.5 K, and pressure was 20 atm pure oxygen. Aging times ranged from 1 to 44 days depending on the aging temperature. CA and aging time are given in Tables E-19 through E-29 for the asphalts studied. r_{CA} was determined for each asphalt using the linear model, equation I – 2. Table E-30 reports r_{CA} and temperature for the asphalts studied. Figures E-68 and E-69 show r_{CA} versus $(1 / T)$ for the asphalts from Dickens and Pineland, respectively. Arrhenius parameters, E_A and A, for all of the asphalts studied are given in Table VI-4. Multi-pressure experiments were not designed. It is assumed that these asphalts have the same order of reaction with respect to oxygen pressure, α of 0.27, as those asphalts studied in Chapter IV.

The effect of P on CA_o and T on η_o^*, other asphalt specific relationships, were not determined. Instead, a set of equivalent asphalts was established between those asphalts in Chapter V and these asphalts. The criterion was based on the refiner. The equivalency is only for β and s presented in Table V-10 and γ and δ given in Table V-3 for the Lau *et al.*, (1992) asphalts. Cosden AC-20 and AC-10, Exxon AC-20, and Texaco AC-20 asphalts are equivalent. Dorchester AC-20 at Dickens and Pineland

is equivalent to Ampet AC-20 in Chapter V. For MacMillan AC-20, an arithmetic average for the individual parameters of the asphalts studied in Chapter V are used. Bryan Exxon AC-20 is assumed to have the same parameters as Lau *et al.*, (1992) Exxon AC-20.

Table VI-4. Arrhenius Parameters of POV- and Field-Aged Asphalts[a] Estimated from POV Data

Location	Asphalt	$A \times 10^{-8}$ CA / day atm$^{\alpha}$	E_A kJ / gmol
Dickens	Cosden AC-10	6132	87.5
	Cosden AC-20	5567	87.1
	D.S. AC-20	2893	85.9
	Dorchester AC-20	2516	85.4
	Exxon AC-20	382	79.4
	MacMillan AC-20	310	80.0
Pineland	Cosden AC-20	705	80.9
	Dorchester AC-20	6695	87.7
	Exxon AC-20	604	80.4
	MacMillan AC-20	436	80.2
	Texaco AC-20	1977	83.8
Bryan	Exxon AC-20	1.71	66.7

[a] From Davison *et al.*, 1989. D.S. represents Diamond Shamrock

Estimation of pavement surface temperature

Latitude and minimum and maximum ambient air temperatures of the location are needed to estimate an annual temperature cycle for the pavement. With this information, Solaimanian and Kennedy (1993) provide a method to estimate the highest surface temperature as given in equation I – 9.

$$(T_{sur} - T_{air})_{max} = -0.01113\psi^2 + 0.41202\psi + 43.877 \qquad (I-9)$$

ψ is the latitude, and the temperatures are in °F. Minimum and maximum air temperatures are from the National Oceanic and Air Administration (NOAA, 1988). Table VI-5 gives the latitude, maximum and minimum air temperatures, the correction factor for estimating the maximum surface temperature from equation I – 9, and the pavement surface maximum and minimum temperatures. The Dickens, Pineland, and Bryan air temperature are approximated with NOAA data from Lubbock, Lufkin, and Austin, respectively.

Table VI-5. Location and Climatic Data for Dickens, Pineland, and Bryan, Texas

Location	Latitude	Air T			Surface T	
		T_{min} °F	T_{max} °F	$(T_{sur} - T_{air})_{max}$ °F	T_{min} °F	T_{max} °F
Dickens	33	25	92	45	25	137
Pineland	30	41	92	46	41	138
Bryan	30	41	95	46	41	141

A sinusoidal function, given in equation II – 43,

$$T(t)_{sur} = T_{avg} + (T_{max} - T_{avg})\cos(\omega t) \qquad \text{(II – 43)}$$

approximates the annual temperature variation. The model parameters, T_{max} and T_{avg} are determined from surface data in Table VI-5. T_{avg} is the arithmetic average of T_{min} and T_{max} at the surface. The frequency, ω, is defined such that for one year, the product of ωt is 2π. For example, if t is in units of days, ω is 2π / 365 1/days. The variation of temperature in the pavement as a function of depth is not included.

Table VI-6. Comparisons between t_{act} and t_{theor} for Measured *CA* of Field-Aged Asphalt[a]

Location	Asphalt	t_{theor} days	t_{act} days	t_{act} / t_{theor}
Dickens	Cosden AC-10	730	4015	5.5
	Cosden AC-20	770	4015	5.2
	Exxon AC-20	730	4015	5.5
	MacMillan AC-20	770	4015	5.2
Pineland	Cosden AC-20	310	3650	11.8
	Dorchester AC-20	370	3650	9.9
	Exxon AC-20	350	3650	10.4
	MacMillan AC-20	370	3650	9.9
	Texaco AC-20	330	3650	11.1
Bryan	Exxon AC-20 1989	530	730	1.4
	Exxon AC-20 1992	730	1825	2.5

[a] From Davison *et al.*, 1989.

Calculation of t_{theor} to reach measured CA

With the laboratory determined kinetic parameters and an estimation of the annual temperature cycle of the pavement surface, equation II – 1 is integrated.

$$\left(\frac{\partial CA}{\partial t}\right) = r_{CA} \qquad \text{(II – 1)}$$

The integration constant, CA_o, is calculated from equation IV–2 with model parameters in Table V-10. The time period is from CA_o to *CA* measured at the time of coring. Thus, the unknown in this calculation is time. Equation II – 1 is valid for highway-pavement aging only when diffusion resistance is negligible. This is probably not valid, but the solution gives t_{theor}, the theoretical minimum time to reach measured *CA* in the cores. The source code, integrating equation II–1 with a sinusoidal varying temperature, is given in Appendix F. Table VI-6 gives the calculated t_{theor}, the actual time, t_{act}, and the ratio of t_{act} to t_{theor} for all of the asphalts studied.

The table shows that t_{act} is over five times t_{theor} for Dickens and over nine times t_{theor} for Pineland. t_{act} is 2.5 times t_{theor} for Bryan Exxon AC-20 1992. These data suggest that oxygen diffusion resistance is significant and cannot be neglected in modeling highway-pavement aging. Diffusion resistance increases with age as the ratio of t_{act} to t_{theor} increases for Bryan Exxon AC-20 from 1989 to 1992. The ratio of t_{act} and t_{theor} provides a measure of diffusion resistance for a given location. For example, diffusion resistance at Pineland is higher compared to Dickens. The Bryan test section appears to have the lowest diffusion resistance. This probably means that it will harden very quickly.

One other interesting observation is discussed for Dickens and Pineland. Asphalts at the Dickens test section showed much more severe aging than those at Pineland. However, t_{theor} for Dickens is only twice t_{theor} for Pineland. The temperature range at the two locations is approximately the same, Table VI-5. The asphalts at the different test sections show very similar E_A in Table VI-4. Measured CA at Dickens is about twice measured CA at Pineland, Tables E-1 through E-11. Since equation II – 1 is integrated with roughly the same temperature function and model parameters, one would expect that t_{theor} for Dickens should about twice as large as t_{theor} for Pineland.

t_{theor} could be used to rank a set of asphalts. For example, a hypothetical failure criterion is established based on a maximum value of CA or η_o^*. A worst case scenario, no diffusion limitation, is tested with equation II – 1. With laboratory-determined kinetic parameters and climatic data from specific locations, the asphalt requiring the longest time to reach the failure criterion is most resistant to oxidative aging at that specific climate. Since t_{theor} in Table VI-6 are not with respect to a given failure criterion, it cannot be concluded that asphalts with higher t_{theor} are more resistant

to oxidative aging relative to the other asphalts from the same location.

The asphalt-aging model and highway-pavement aging

Oxygen diffusion and reaction is significant in modeling highway-pavement aging. Therefore, only a model including both reaction and diffusion, such as the asphalt-aging model in this work, can be successful. A preliminary study examined how the cyclical annual temperature variation affects asphalt-aging model calculations.

With isothermal and isobaric conditions the oxygen pressure profile steadily decreased in an asphalt film after an initial maximum, Figure V-32. The pressure gradients at the surface increased with aging time; however, oxygen transport was limited by decreases in $\mathcal{D}_{O_2}$. For isothermal and isobaric conditions, the carbonyl profile grows at an ever decreasing rate at every point in the film except the *ES*, Figure V-33. r_{CA} at the *ES* is constant for isothermal and isobaric conditions. The oxygen pressure and *CA* profiles in an asphalt film are different with a periodic temperature compared with isothermal conditions. These profiles are fundamental to understanding the aging characteristics of asphalts. Furthermore, these calculations were performed to confirm that the asphalt-aging model with variable temperature computer program was working.

Figure VI-25 shows the oxygen pressure profile in a 1 mm film of Ampet AC-20 asphalt for seven years aging. With elevated temperature, in summer, the rate of oxygen diffusion exceeds that of reaction. The oxygen pressure in the film increases. With time, $\mathcal{D}_{O_2}$ decreases as a result of *CA*, and the magnitude of oxygen pressure in the film decreases with each successive summer. When the temperature is low, during the winter, the oxygen pressure in the film goes to zero. η_0^* is extremely high at low

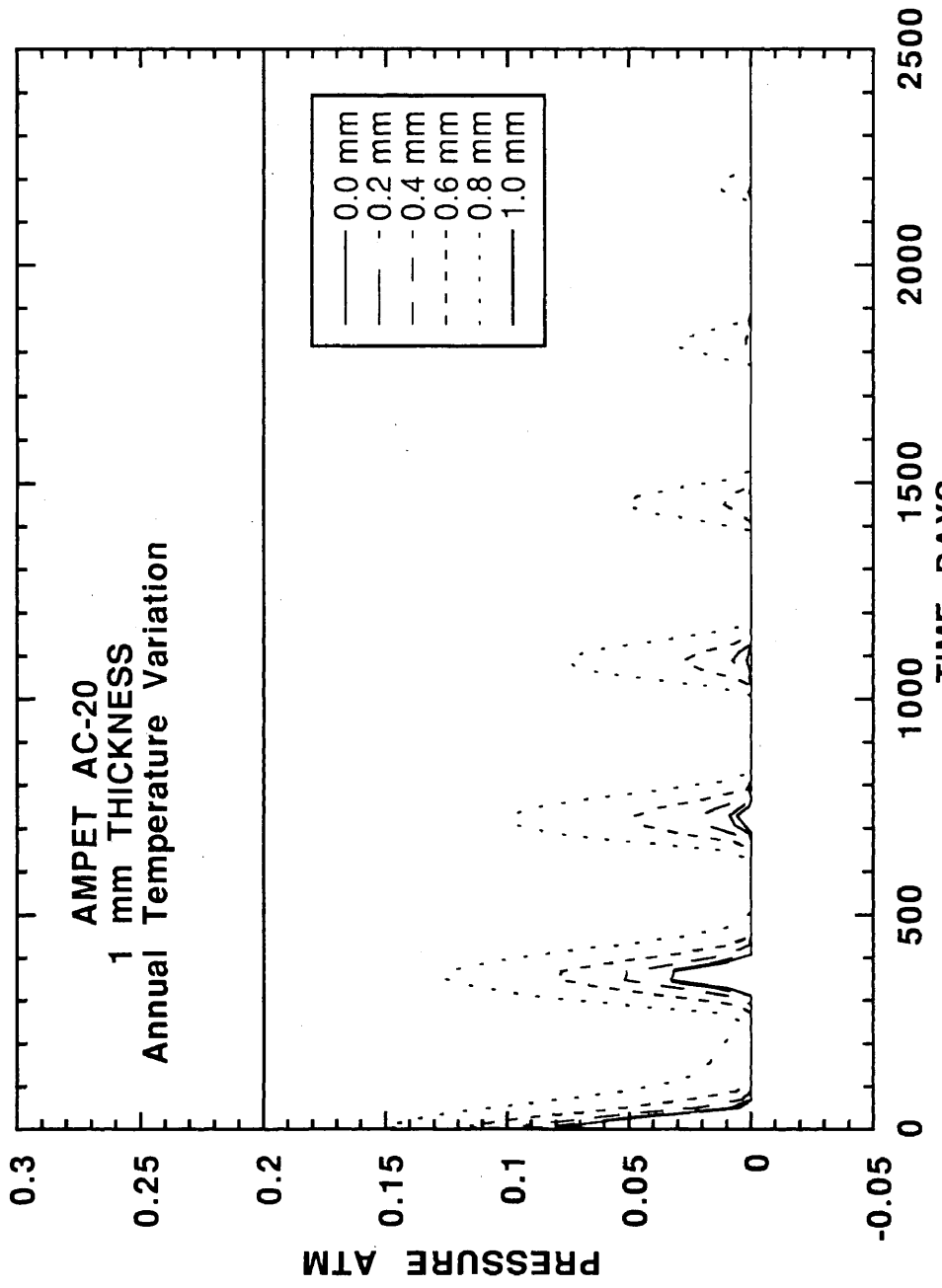

Figure VI-25. The effect of cyclical temperature on calculated oxygen pressure profiles in 1 mm thick Ampet AC-20 for unsteady-state variable $\mathcal{D}_{O_2}$ oxygen diffusion and reaction.

temperature and decreases $\mathcal{D}_{O_2}$ further. Even though r_{CA} is very slow at these low temperatures, the rate of oxygen transport is even slower. Oxygen does not enter the film fast enough to replace that consumed by reaction.

With cyclical temperature variation, CA in a 1 mm thick film of Ampet AC-20 is given in Figure VI-26. r_{CA} at low temperature during winter is practically zero even at the ES. In winter, r_{CA} in the film below the ES is close to zero, not only from low temperature but also from lack of oxygen. The lack of oxygen in the film below the ES becomes more significant with aging time. Only at the ES is the change in CA the same over a one year period. P_{ES} is assumed to be constant. In the film, P decreases with time. Therefore, the change in CA at points inside the film for a one year period decreases with aging time.

Since bulk properties of highway-pavement samples are measured, the integral average CA in the film was determined. This was calculated from equation II – 44.

$$CA_{\text{avg}} = \frac{1}{L_{\text{eff}}} \int^{L_{\text{eff}}} CA(x)dx \qquad \text{(II – 44)}$$

This represents a thoroughly mixed asphalt film measurement or bulk analysis. Figure VI-27 shows CA_{avg} in a 1 mm film of Ampet AC-20 as a function of aging time with a cyclical temperature variation. From profiles in Figure VI-26 and decreasing average P in the film, average annual r_{CA} decreases with age. This figure suggests that asphalts age faster when initially placed compared with aging rates after several years of service. Even for summer months, the rate of aging decreases as the asphalt becomes harder every successive year.

The asphalt-aging model has the same asymptotic behavior as has been noted from field data. However, the asymptotic nature was not achieved by empirically correlating field-aged data or devising empirical kinetic equations. Instead, the

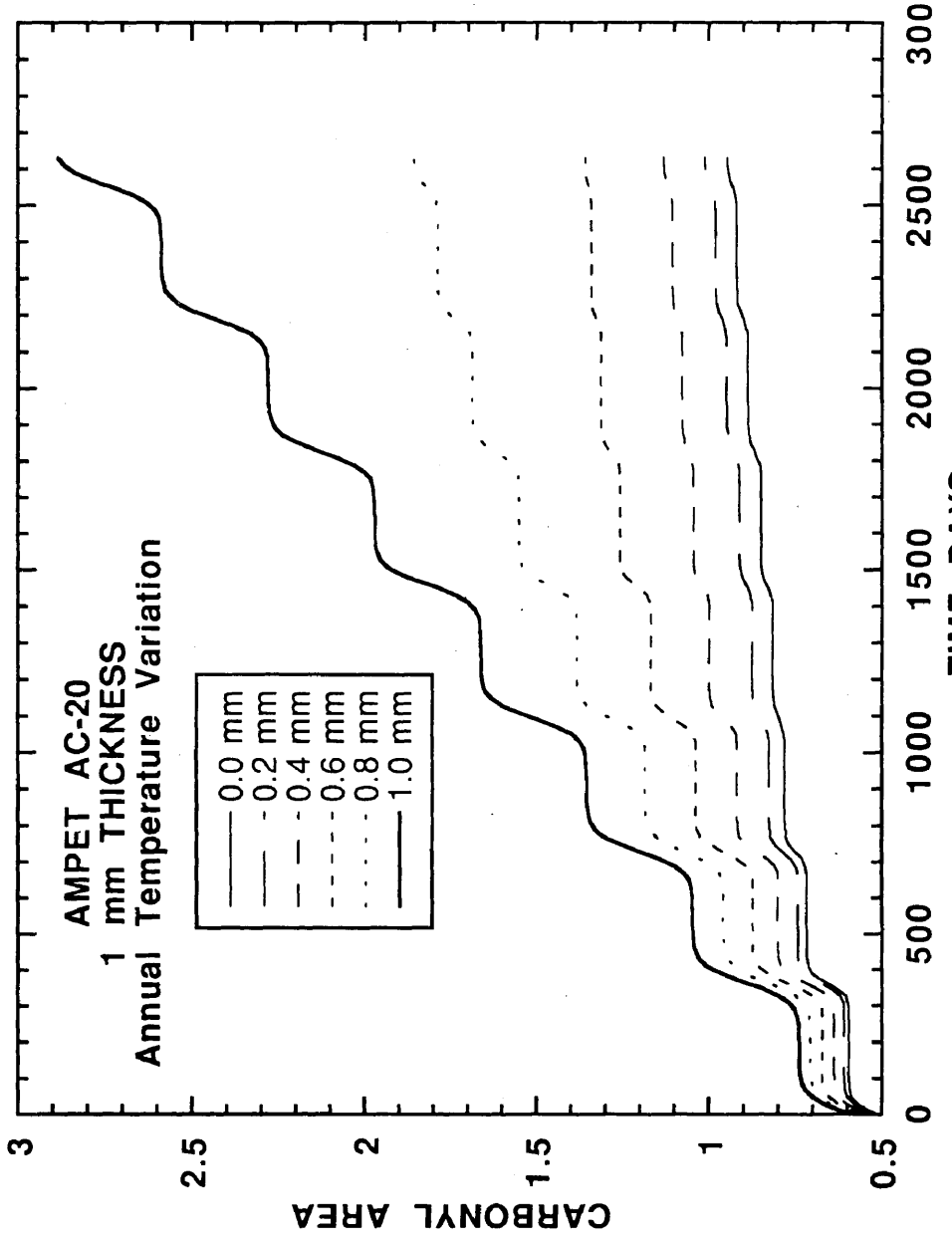

Figure VI-26. The effect of cyclical temperature on calculated CA profiles in 1 mm thick Ampet AC-20 for unsteady-state variable $\mathcal{D}_{O_2}$ oxygen diffusion and reaction.

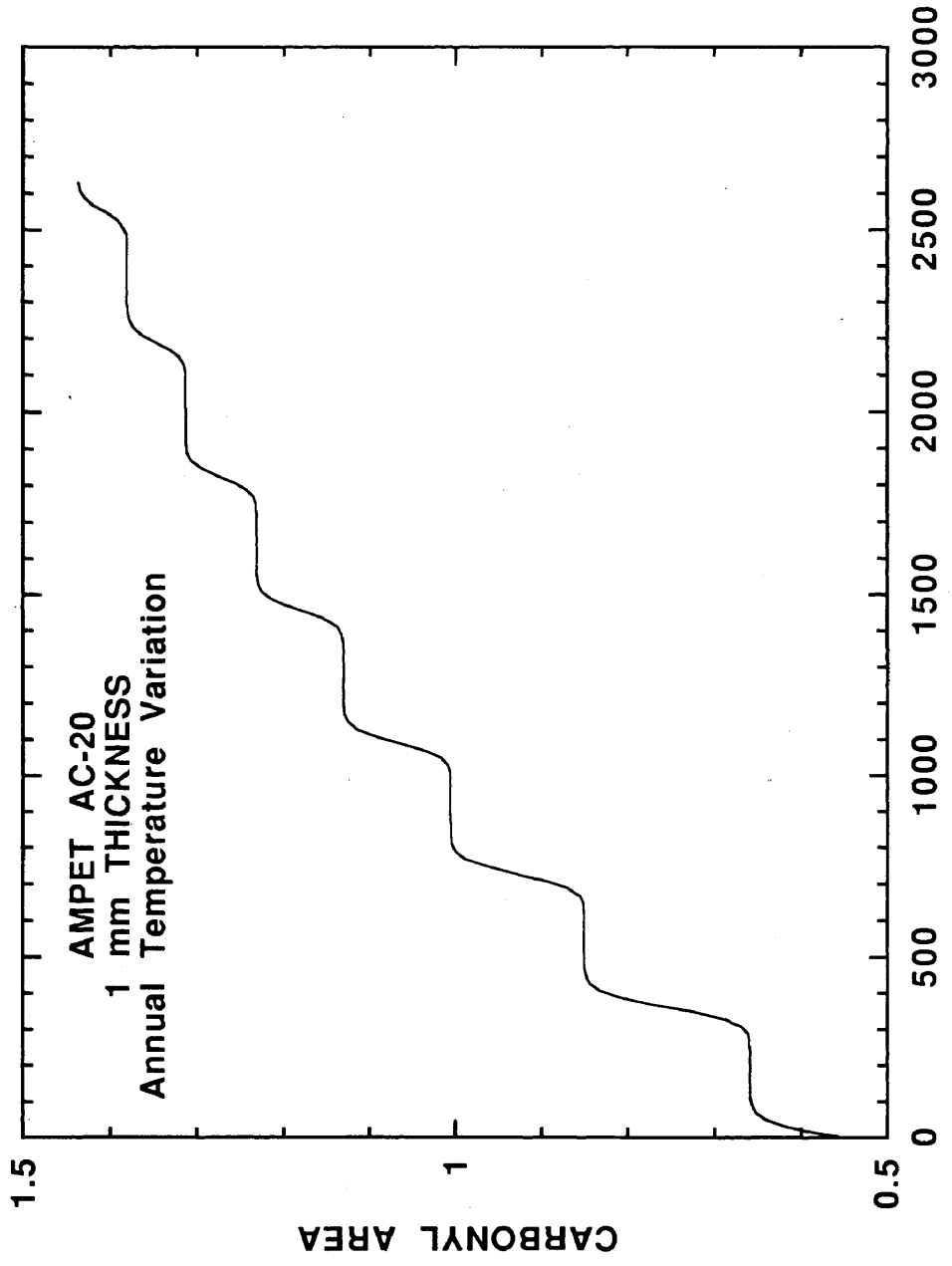

Figure VI-27. The effect of cyclical temperature on calculated CA_{avg} in 1 mm thick Ampet AC-20 for unsteady-state variable $\mathcal{D}_{O_2}$ oxygen diffusion and reaction.

asphalt-aging model is based on fundamental principles, both carbonyl formation and unsteady-state variable $\mathcal{D}_{O_2}$ oxygen diffusion and reaction. With the parameters estimated from laboratory data, the asphalt-aging model predicts the similar phenomenon of field aging. This is an extremely critical point, separating this work from the previously developed empirical aging models. The same type of behavior would be predicted for η_o^*, since CA relates to rheological properties, equation I – 6 and VI – 1.

The asphalt-aging model is based on fundamental principles whenever possible. Applying the model to actual field aging should be more successful than previously developed empirical correlations. However, before the asphalt-aging model is applied to field aging, correlations between measurable core properties, % V and % Asp, and fundamental quantities in the asphalt-aging model, L_{eff} and P_{eff}, must be developed. These correlations form the highway-pavement aging model.

Highway-pavement aging model development

Models relating the measurable core properties of % V and % Asp to fundamental quantities in the asphalt model are developed. These models are the highway-pavement aging model. Equations II–41 and II–42 respectively give the hypothesized models for P_{eff} and L_{eff} respectively.

$$P_{\text{eff}} = f(\%\ V, t) \qquad \text{(II – 41)}$$

$$L_{\text{eff}} = f(\%\ Asp, \%\ V) \qquad \text{(II – 42)}$$

CA of field-aged asphalt are measured and reported in Tables E-1 through E-18. The placement and coring times are known for these asphalts. The climatic conditions for these locations are also known, Table VI-5. The asphalt-aging model

has been developed for POV-aged asphalt films. This model includes carbonyl formation, equation II – 1, and unsteady-state variable $\mathcal{D}_{O_2}$ oxygen diffusion and reaction, equation II – 40. However, to use the asphalt-aging model, asphalt specific model parameters must be estimated from laboratory experiments. A series of three POV experiments at three different temperatures and one pressure yielded the necessary data to estimate the parameters, A, E_A, HS, and m. The other asphalt-specific model parameters, β, s, δ, and γ, were taken from equivalent asphalts in Chapter V. c, α, B, and D_o are assumed to be independent of asphalt composition. Furthermore, a comparison of POV- and field-aged asphalt showed that POV experiments simulate field aging with respect to physicochemical properties. With all of these conclusions, observations, and discoveries, the strategy of estimating L_{eff} is given.

L_{eff} in an asphalt-pavement core is estimated by comparing field-aged data with calculations from the asphalt-aging model. A trial and error procedure is used. First a thickness of L_{eff} is assumed. Equations II – 1 and II – 40 are integrated simultaneously from the time of placement to the time of coring. These integrations include the variation of temperature from the climatic data and the asphalt specific model parameters. When the time of coring is reached, CA_{avg} is calculated from equation II – 44. CA_{avg} is compared to measured CA for the field-aged asphalt. If CA_{avg} is greater than the measured CA, the assumed film thickness is too small. Conversely, if CA_{avg} is less than the measured CA, the film thickness is too large. The value of L_{eff} is updated until measured CA and CA_{avg} are within a pre-defined tolerance. An incremental search and method of false position was used to estimate L_{eff}. The source code for this program is given in Appendix F. This calculation assumes that oxygen diffusion resistance through the nitrogen gas in the air is negligible. Including the diffusion of oxygen through the nitrogen gas film should decrease the value of L_{eff}

determined in this study.

Estimation of L_{eff} with constant P_{eff}

In the first estimation of L_{eff} it is assumed that P_{eff} is constant, 0.2 atm. Table VI-7 shows estimated L_{eff}, % V, and % Asp for the Dickens and Bryan asphalts. It was not possible to determine reasonable values of L_{eff} for the Pineland asphalts with constant P_{eff}.

Table VI-7. Estimated L_{eff} for Dickens and Bryan Asphalts with Constant P_{eff} of 0.2 atm[a]

Location	Asphalt	L_{eff} mm	% V	% Asp
Dickens	Cosden AC-10	3.12	8.3	5.96
	Cosden AC-20	1.44	8.7	5.94
	Exxon AC-20	1.16	9.4	–
	MacMillan AC-20	1.79	5.8	6.10
Bryan	Exxon AC-20 1989	3.70	6.9	–
	Exxon AC-20 1992	2.92	6.4	–

– Signifies the values were not determined.

From the table, higher % V tends to yield lower L_{eff} for all asphalts except for Dickens MacMillan AC-20. Not enough data were collected for % Asp to make any conclusion about this property. The field-aged asphalts from Pineland show very little CA growth. From the numerical calculation, r_{CA} at the surface is so great with constant P_{ES} that estimated L_{eff} is unreasonable. Since no realistic values for L_{eff} could be determined for the Pineland test section asphalts, the assumption that P_{eff} is constant may not be valid especially for pavements with very low % V. Therefore, calculations with variable P_{eff} were performed. In order to compare Pineland

field-aged data with the laboratory determined properties, it was assumed that P_{eff} decreases with time.

Estimation of L_{eff} with variable P_{eff}

From conservation of mass in a void, the oxygen concentration in an inaccessible void decreases with time from oxygen diffusion and reaction in the asphalt film. At low enough % V levels, the number of inaccessible voids is significant. At high % V, the permeability of the core is such that most voids are accessible, the oxygen pressure in the void approaches 0.2 atm. A model relating P_{eff} as a function of time is hypothesized and given in equation VI – 3.

$$P_{\text{eff}} = (P_{\text{eff}})_o \exp(-\lambda t) \qquad \text{(VI – 3)}$$

The model parameter $(P_{\text{eff}})_o$ is the oxygen pressure at the initial time and is assumed to be 0.2 atm. The time constant, λ, is a function of % V. λ is large at low % V and small at high % V. Another model relating λ to % V is hypothesized in equation VI – 4.

$$\lambda = \lambda_o (\% V)^l \qquad \text{(VI – 4)}$$

With no experimental data, the model parameters λ_o and l were based on the numbers in Table VI-8. An estimation gives λ_o of 0.154 1/day and l of -2.41. Figure VI-28 shows the hypothesized function and numbers.

L_{eff} was estimated for the Dickens, Pineland, and Bryan asphalts with P_{eff} as the hypothesized function of time and % V and the hypothesized model parameters. Table VI-9 reports L_{eff}, % V, and % Asp for all the asphalts studied. Under the assumptions imposed by equations VI – 3 and VI – 4, all of the asphalts studied show L_{eff} of about 1 mm except for Pineland Cosden AC-20. L_{eff} for this asphalt is 4.18

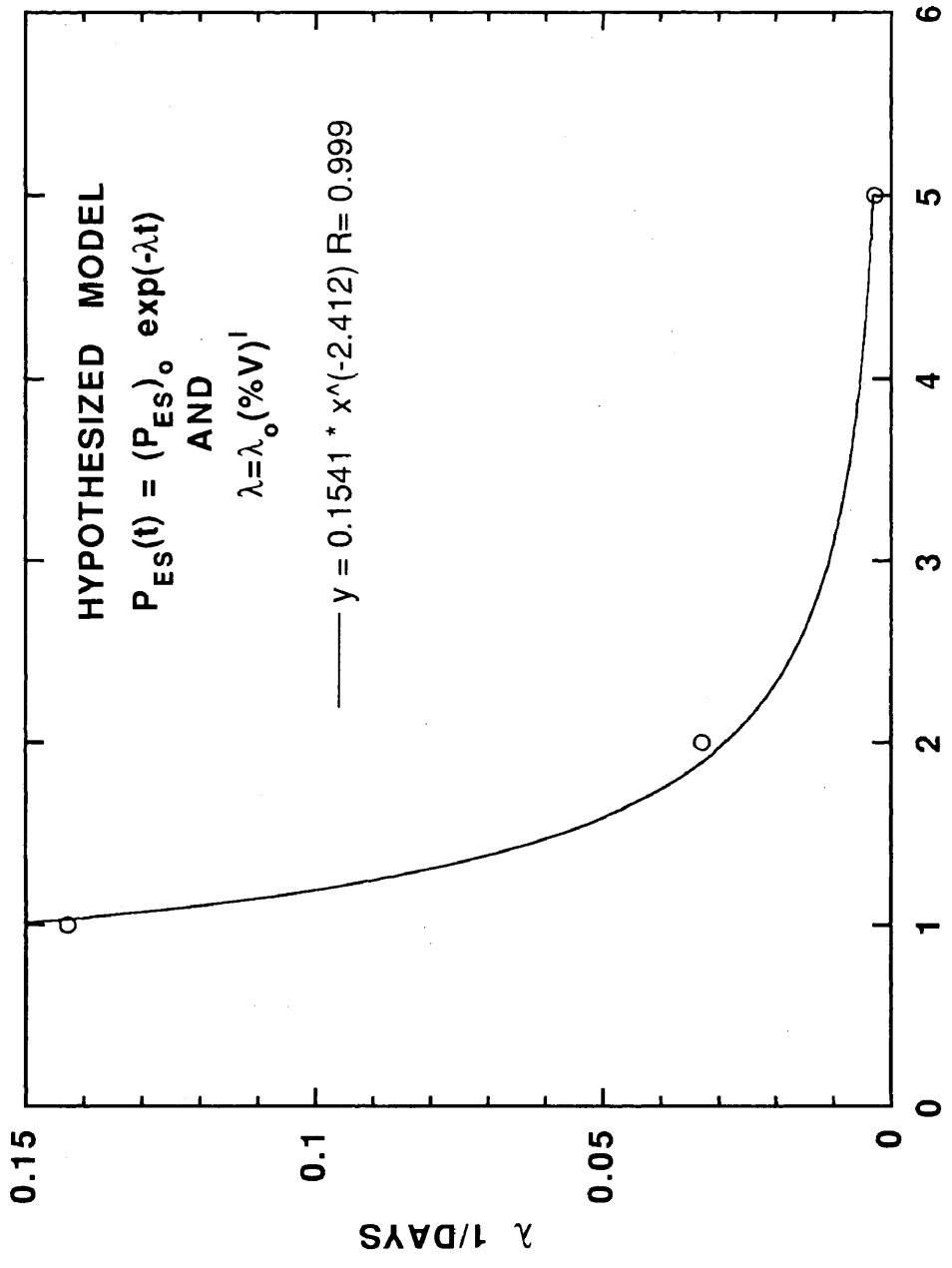

Figure VI-28. Hypothesized relationship between P_{eff} time constant λ and percent air voids.

Table VI-8. Hypothesized Model between % V and λ

% V	λ 1/day
1	1/7
2	1/30
5	1/365

mm. However, the field-aged data for Pineland Cosden AC-20 was outside the rate of POV-aged data as shown in Figure VI-12. This calculation may not be accurate. For Dickens and Bryan asphalts, L_{eff} for constant P_{eff} of 0.2 atm is greater than L_{eff} for variable P_{eff} from Tables VI-7 and VI-9. For equivalent CA at the end of the time period, constant P_{eff} requires a larger diffusion length compared with decreasing P_{eff}.

An attempt to correlate L_{eff} with % Asp is made with L_{eff} determined under the assumptions of equations VI – 3, VI – 4, and the model parameters. From Table VI-9, a relationship between L_{eff} and % Asp probably exists. However, the data set in this study is too small to make a conclusive development and parameter estimation. Most of the asphalts studied have % Asp ranging from 5.87 to 6.36. This is only an 8% difference. Unfortunately, % Asp for Bryan Exxon AC-20 was not measured.

Figure VI-29 shows % Asp and L_{eff}. Data for Pineland Cosden AC-20 are not shown on this figure. From this figure two conclusions can be drawn. The first conclusion is that L_{eff}, estimated under the assumptions of equations VI – 3, VI – 4 and the model parameters, is independent of % Asp. The second conclusion is based on the exclusion of the Dickens Cosden AC-10 and Pineland Texaco AC-20 data. These data show unusually high L_{eff} for the given % Asp. With these data excluded, it appears that there is a crude linear relationship between L_{eff} and % Asp as given

Table VI-9. Estimated L_{eff} for Dickens, Pineland, and Bryan Asphalts with Variable P_{eff}[a]

Location	Asphalt	L_{eff} mm	% V	% Asp
Dickens	Cosden AC-10	1.86	8.3	5.96
	Cosden AC-20	0.94	8.7	5.94
	Exxon AC-20	0.74	9.4	–
	MacMillan AC-20	1.16	5.8	6.10
Pineland	Cosden AC-20	4.18	1.8	6.10
	Dorchester AC-20	1.60	2.2	6.30
	Exxon AC-20	1.70	2.6	6.36
	MacMillan AC-20	1.15	2.8	6.20
	Texaco AC-20	1.57	1.4	5.87
Bryan	Exxon AC-20 1989	1.93	6.9	–
	Exxon AC-20 1992	1.97	6.4	–

[a]– Signifies the values were not determined.

by equation VI – 5.

$$L_{eff} = a(\%\ Asp) + e \qquad \text{(VI – 5)}$$

The model parameters are given in the figure with a of 1.82 mm/% Asp and e of -9.95 mm. Based on this model and parameters, pavements with asphalt contents less than 5.21 could not be used to predict valid L_{eff}.

% Asp is basically a measure of the volume of asphalt. L_{eff} is a measure of length. Since the asphalt is covering a surface of aggregate, the L_{eff}-% Asp relationship is probably not linear but quadratic. A data set with a larger range of % Asp is required to confirm this hypothesis. Furthermore, these conclusions should be taken in the context that L_{eff} was calculated assuming VI – 3, VI – 4 and the model parameters in VI – 4.

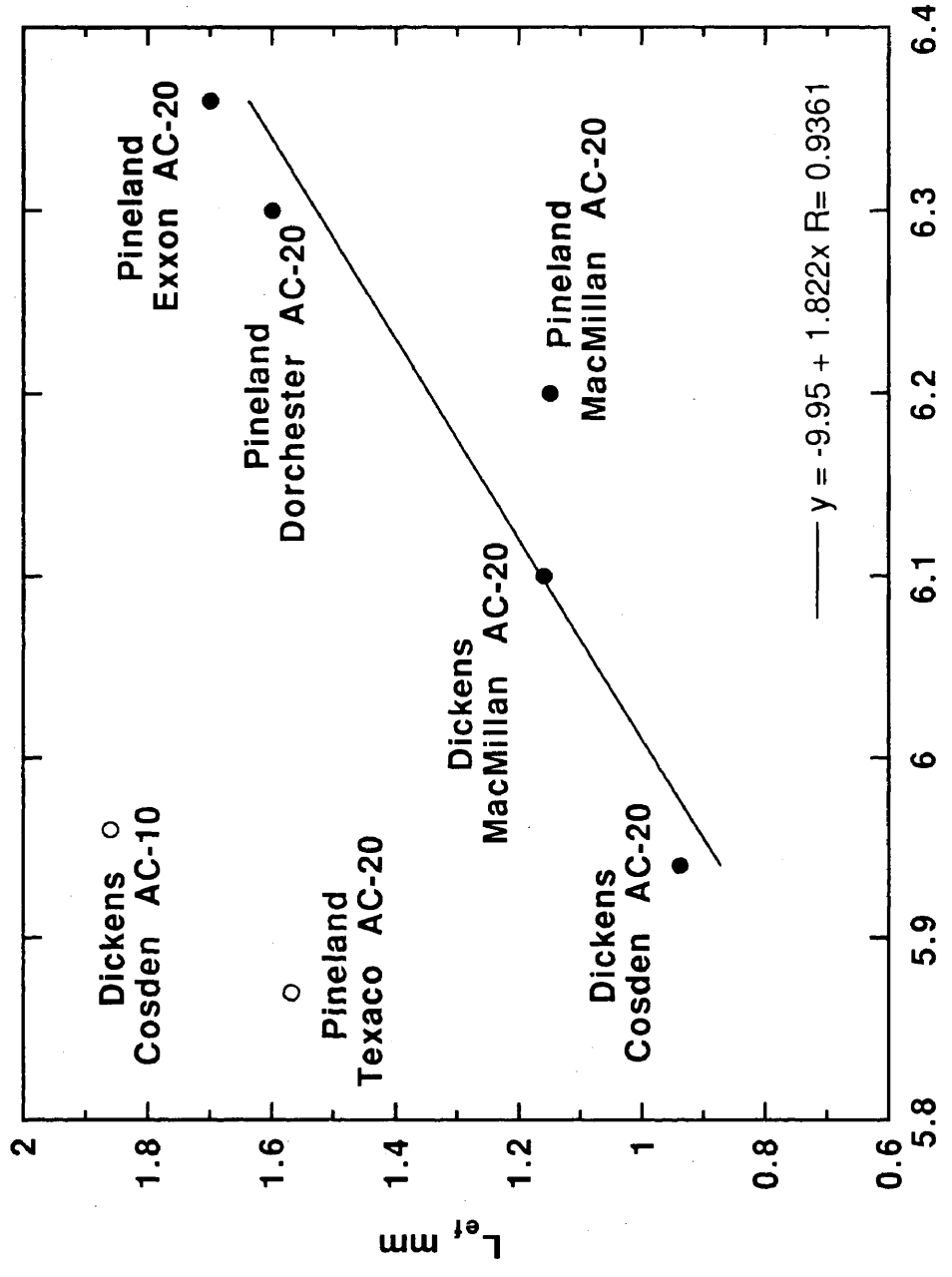

Figure VI-29. Hypothesized relationship between L_{eff} and percent asphalt.

From limited data, the initial development of the highway-pavement aging model relates P_{eff} to % V and t by equations VI – 3 and VI – 4. L_{eff} is related to % Asp by equation VI – 5. These are very crude models and need further refinement with larger data sets.

Summary

A comparison between POV- and field-aged asphalts was performed. In the first comparison, only physicochemical relationships were considered. These properties are independent of the kinetics of the aging process. From rheological properties and CA, it was concluded that POV aging simulates field aging. GPC and IR spectra analysis showed there were slight chemical differences. It was not determined if these differences resulted from extraction and recovery procedures or from field aging. A ($1/J''$)-CA relationship was developed for POV- and field-aged asphalts. A relationship between changes in η_o^* and MW as determined from GPC and was discovered for POV aging. Different asphalts showed different model parameters; however, for a given asphalt the model parameters did not change with aging. Similar to HS for η_o^*-CA, the η_o^*-MW relationship suggests that initial composition and structure of the molecules uniquely determines the physicochemical relationships for oxidative aging. With the discovery of the composition and structure that gives these favorable aging characteristics, superior asphalts can be designed and manufactured.

A comparison between field-aged asphalt and calculations from the asphalt-aging model was used to develop a highway-pavement aging model. To use the asphalt-aging model, POV experiments were designed to estimate the model parameters A, E_A, HS, and m. Other asphalt-specific parameters were taken from equivalent asphalts from Chapter V based on refiner. The parameters c, α, B, and D_o were

assumed to be independent of asphalt composition. Pavement-surface temperatures were estimated from latitude and climatic data. A sinusoidal function approximated the annual temperature variation. A theoretical minimum time, t_{theor} was calculated using and asphalt-aging model with no diffusion and resistance for each asphalt and location. The ratio of t_{act} and t_{theor} was 5 for Dickens and 10 for Pineland. This ratio is a qualitative measure of diffusion resistance. From this, it was concluded that diffusion resistance is significant in field aging.

Using the asphalt-aging model and field data, L_{eff} was estimated by two different calculations. First, P_{eff} was assumed to be constant, 0.2 atm. Reasonable values of L_{eff} were calculated for pavements with relatively high % V, Dickens and Bryan. However, no reasonable L_{eff} could be determined for Pineland, a pavement with low % V. The assumption of constant P_{eff} was probably not valid especially for cases with low % V.

A model was hypothesized accounting for decreasing P_{eff} with time.

$$P_{eff} = (P_{eff})_o \exp(-\lambda t) \qquad (VI-3)$$

This model is based somewhat on the conservation of mass in a void. Furthermore, it was assumed that (P_{eff}) was 0.2 atm and λ was a function of % V by another hypothesized model.

$$\lambda = \lambda_o(\%\ V)^l \qquad (VI-4)$$

The assumed model parameters were λ_o of 0.154 1/day and l of -2.41.

With variable P_{eff} from the hypothesized models, L_{eff} was estimated at all the locations studied. Values of L_{eff} ranged from 0.5 to 2.0 mm. Finally, an attempt to correlate L_{eff} with % Asp was made. With very limited data over a small range of

% *Asp* a crude linear model was developed.

$$L_{\text{eff}} = a(\%\ Asp) + e \qquad (\text{VI} - 5)$$

a was 1.82 mm/% *Asp*, and e was -9.95 mm. These parameters are not accurate; further refinements with additional data are needed. However, this is the initial development of a highway-pavement model relating measured core properties to fundamental quantities in the asphalt-aging model.

CHAPTER VII

SHORT TERM AGING

Long-term, LT, POV aging experiments provide kinetic information which can be used to simulate and possibly even predict field aging. Unfortunately, LT aging data are very costly in terms of experimental time. For example, POV aging experiments at 20 atm, 333.3 or 344.4 K require two months. This chapter attempts to relate short-term, ST, aging from one to five days to LT aging characteristics. ST aging data are also used in physicochemical relationships. Table III-1 reports the asphalts for ST aging studies.

Two comparisons between ST and LT aging are made. The first compares the Arrhenius parameters, A and E_A. No experiments were designed at multiple pressures; therefore, no pressure dependency was included. Successfully relating ST to LT aging kinetics should decrease the POV experimental test time. The second compares physicochemical relationships. Relationships between changes in rheological properties, η_o^* and $(1/J'')$, and chemical properties, CA and MW, were developed for LT and field aging. Furthermore, a relationship between η_o^* at 333.3 K and asphaltene formation, % A, is studied (Lin *et al.*, 1993).

Physicochemical relationships are important for two reasons, decreasing the number of required measurable variables to monitor asphalt aging and allowing researchers to study asphalt oxidation independent of the kinetic model. Since these physicochemical properties are independent of aging method, POV or field, physicochemical relationships are logical choices for asphalt specifications.

Experimental Design

POV aging experiments were at 20 atm oxygen and 322.2, 333.3, 344.4, 355.5, and 366.6 K. Aging times ranged from one to five days for all temperatures. Samples were removed from the POV every day for each asphalt. *CA* was measured by FTIR. η_o^* at 333.3 K and $(1 / J'')$ at 333.3 and 10 rad/s were measured by DMA. Percent hexane asphaltenes, % *A*, were measured for the Lau *et al.*, (1992) asphalts. Tables G-1 through G-15 report the data for the asphalts studied.

Aging Kinetics for *ST*

LT aging shows an initial non-linearity followed by a constant r_{CA} for isothermal and isobaric aging conditions. This initial non-linearity is a function of *P* from data in Chapters IV and V. Nicholas and Dickinson (1949) offer a more sophisticated model, equation I – 5, including the initial non-linearity in the kinetics. The kinetic model of Nicholas and Dickinson was not used in this study. The initial non-linearity for *LT* aging was treated as an integration constant, CA_o. For *ST* aging, the range of data is such that neat *CA* should be included in the r_{CA} estimation. This may give some indication of the initial non-linearity and, quite possibly, relate to the *LT* aging kinetics.

Figure VII-1 shows *ST* aging *CA* for Lau *et al.*, (1992) Exxon AC-20. Both r_{CA} and *CA* increase with aging temperature at isothermal and isobaric aging conditions for *ST* aging. An initial non-linearity still exists. A linear model, equation I – 2 describes *CA* and aging time. Equation I – 5 was not used to model the data. The linear model gives an average r_{CA} for the range of aging time. The data set included the neat datum, the black square, but not the RTFO residue, the square with center dot. The intercepts, CA_o, are greater than neat *CA* but lie in the neighborhood of

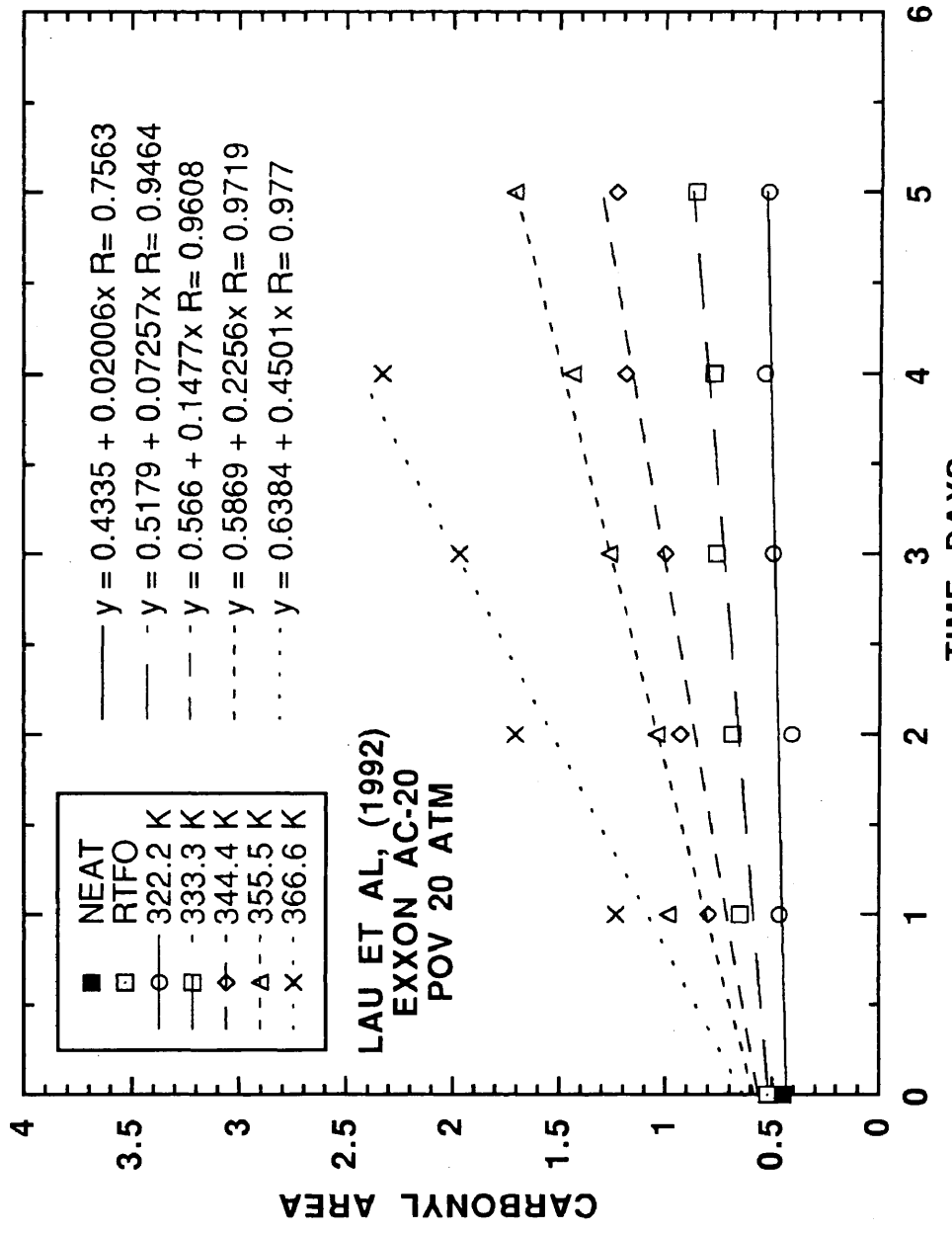

Figure VII-1. *CA*s of neat, RTFO, and POV-aged Lau *et al.*, (1992) Exxon AC-20 at 322.2, 333.3, 344.4, 355.5, and 366.6 K at 20 atm from 1 to 5 days.

RTFO CA. Figures G-1 through G-14 show CA as a function of time for the other asphalts studied.

r_{CA} and CA_o are reported in Table VII-1 and VII-2, respectively. Not all of the asphalts studied show good linearity for CA and t. However, the linear model was used in all cases for consistency. r_{CA} increases with increasing temperature for all of the asphalts. At 366.7 K, Lau *et al.*, (1992) Coastal AC-20 and SHRP (1990) AAD-1 and AAK-2 have r_{CA} two to three times greater than the other asphalts studied. These r_{CA} are abnormally high, possibly indicating a different oxidation mechanism at 366.7 K. SHRP (1990) AAG-1 has the highest r_{CA} of all the asphalts studied at all temperatures except 366.7 K. Both Lau *et al.*, (1992) and Jemison *et al.*, (1992b) Texaco AC-20 have the lowest r_{CA} at 322.2 K.

Some of the asphalts show increasing CA_o with increasing T in Table VII-2. At 366.7 K, many CA_os are below neat CA. The temperature dependence on CA_o may result from including the neat CA in the estimation of r_{CA}. Neat CA was not included for LT aging estimations of r_{CA} with the linear model. All of the ST aging experiments were conducted at one pressure, 20 atm. No pressure dependence on CA_o can be examined. CA_o is very much dependent on the asphalt composition. For example, SHRP (1990) AAG-1 CA_o is approximately 0.7 while Davison *et al.*, (1989) Dickens Diamond Shamrock AC-20 CA_o is 0.4. Unfortunately, it is still difficult to determine what variables control CA_o for ST and LT aging.

Figures VII-2, VII-3, and VII-4 show r_{CA} versus $(1\ /\ T)$ for ST isobaric and isothermal aging. The data suggest a linear relationship below 366.7 K for most asphalts, verifying that the Arrhenius relationship, equation I – 3, models the tem-

Table VII-1. r_{CA} for Short-Term Aging Studies

Group	Asphalt	r_{CA}				
		322.2 K CA/day	333.3 K CA/day	344.4 K CA/day	355.5 K CA/day	366.7 K CA/day
Lau *et al.*, (1992)						
	Ampet AC-20	0.027	0.116	0.152	0.213	0.525
	Coastal AC-20	0.033	0.049	0.078	0.137	0.743
	Cosden AC-20	0.025	0.071	0.159	0.230	0.534
	Exxon AC-20	0.020	0.073	0.148	0.226	0.450
	Texaco AC-20	0.016	0.034	0.130	0.132	0.501
Jemison *et al.*, (1992b)						
	Coastal AC-20	0.038	0.041	0.093	0.138	0.394
	Fina AC-20	0.040	0.078	0.181	0.226	0.430
	Texaco AC-20	0.016	0.041	0.118	0.137	0.425
Davison *et al.*, (1989)						
	Dickens D.S.[a]	0.056	0.092	0.183	0.247	0.354
SHRP (1990)						
	AAA-1	0.026	0.040	0.092	0.144	0.567
	AAC-1	0.055	0.093	0.151	0.204	0.308
	AAD-1	0.041	0.057	0.149	0.194	0.878
	AAG-1	0.100	0.208	0.380	0.464	0.500
	AAK-2	0.035	0.054	0.123	0.185	1.640
	AAM-1	0.063	0.088	0.176	0.177	0.339

[a] D.S. represents Diamond Shamrock.

Table VII-2. CA_o for Short-Term Aging Studies

Group	Asphalt	CA_o				
		322.2 K *CA*	333.3 K *CA*	344.4 K *CA*	355.5 K *CA*	366.7 K *CA*
Lau *et al.*, (1992)						
	Ampet AC-20	0.469	0.409	0.526	0.500	0.573
	Coastal AC-20	0.511	0.486	0.623	0.617	0.290
	Cosden AC-20	0.518	0.542	0.647	0.675	0.649
	Exxon AC-20	0.433	0.518	0.566	0.587	0.638
	Texaco AC-20	0.479	0.486	0.470	0.542	0.391
Jemison *et al.*, (1992b)						
	Coastal AC-20	0.504	0.511	0.555	0.652	0.598
	Fina AC-20	0.556	0.561	0.588	0.715	0.918
	Texaco AC-20	0.486	0.461	0.508	0.565	0.585
Davison *et al.*, (1989)						
	Dickens D.S.[a]	0.407	0.474	0.514	0.439	0.717
SHRP (1990)						
	AAA-1	0.516	0.520	0.566	0.565	0.636
	AAC-1	0.445	0.470	0.575	0.561	0.854
	AAD-1	0.724	0.784	0.803	0.872	0.746
	AAG-1	0.700	0.762	0.724	1.056	1.508
	AAK-2	0.640	0.672	0.638	0.750	0.518
	AAM-1	0.422	0.469	0.511	0.687	0.863

[a] D.S. represents Diamond Shamrock.

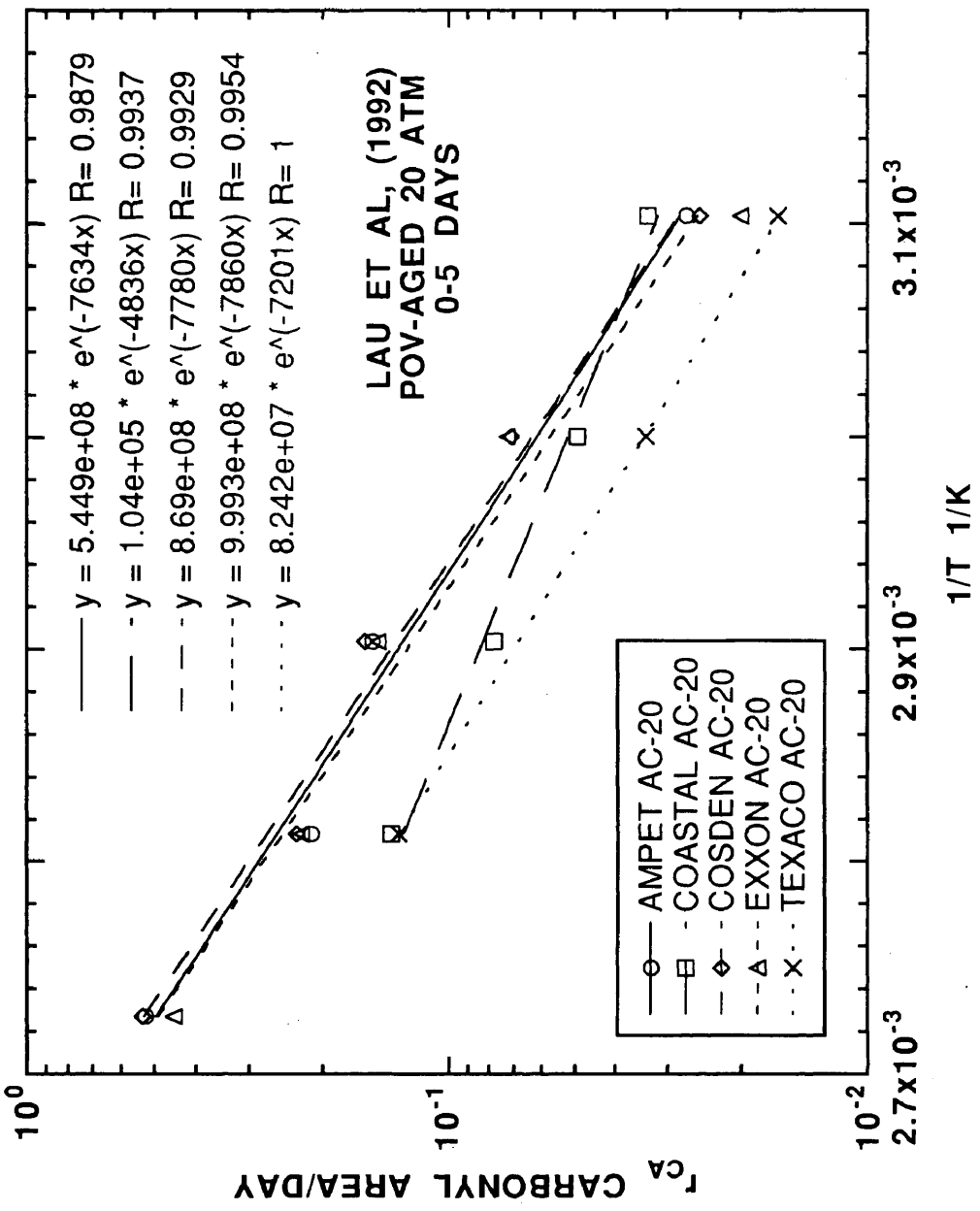

Figure VII-2. r_{CA} versus $(1\,/\,T)$ at 20 atm for all short term POV-aged Lau *et al.*, (1992) asphalts studied.

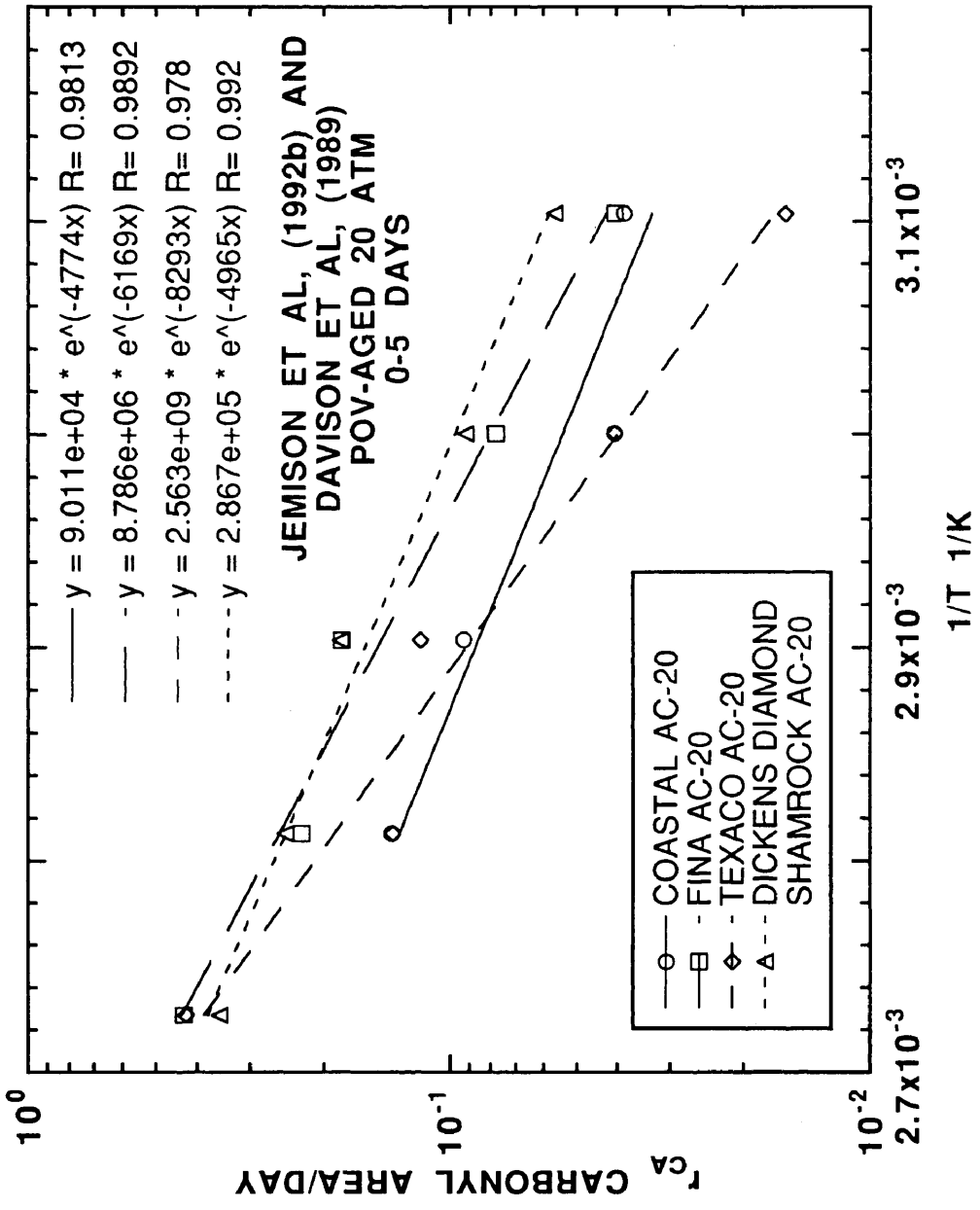

Figure VII-3. r_{CA} versus $(1\,/\,T)$ at 20 atm for all short term POV-aged Jemison *et al.*, (1992b) asphalts studied and Dickens Diamond Shamrock AC-20.

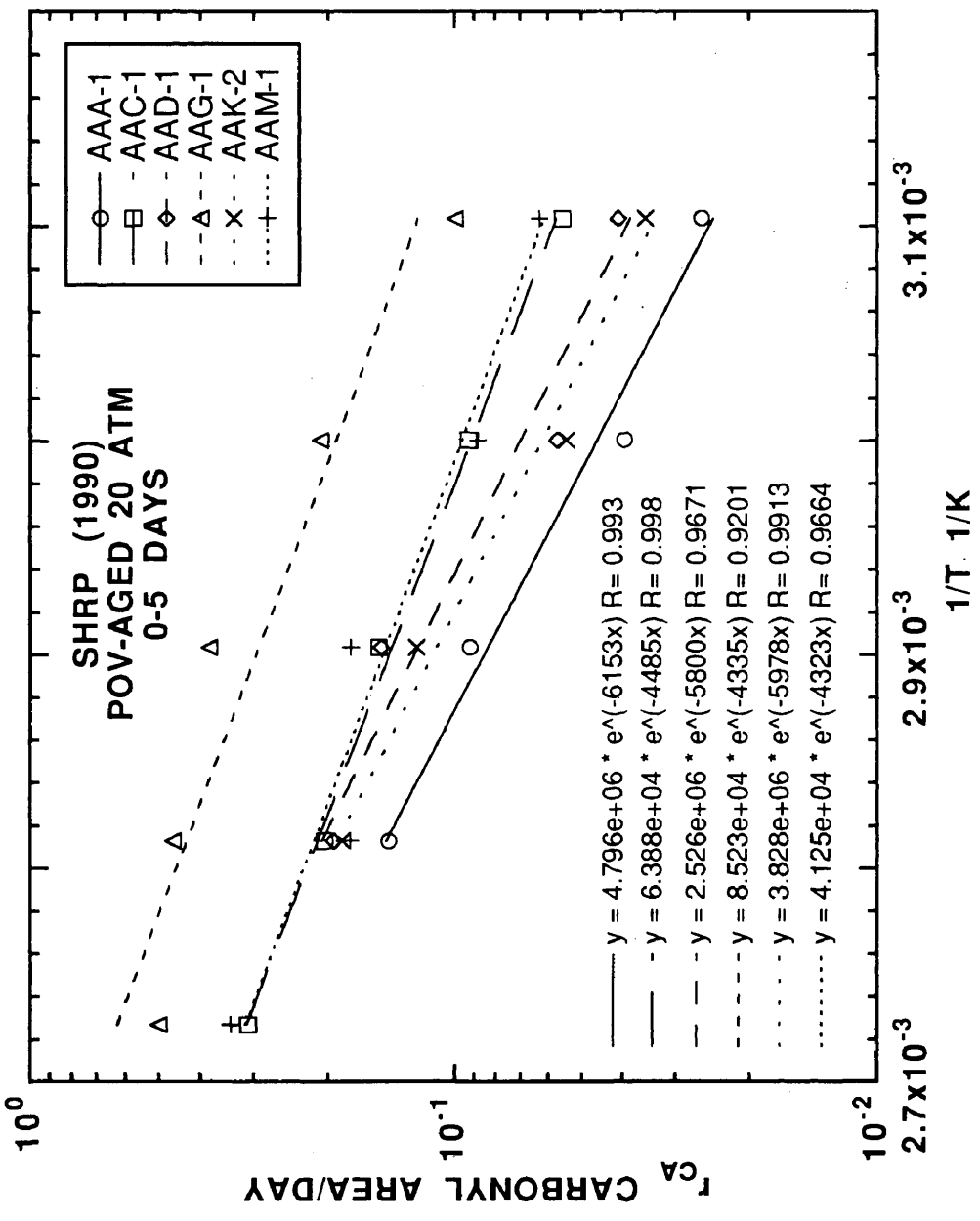

Figure VII-4. r_{CA} versus $(1/T)$ at 20 atm for all short term POV-aged SHRP asphalts studied.

perature dependence on r_{CA} for ST aging.

$$r_{CA} = A \exp\left(\frac{-E_A}{RT}\right) \qquad (I-3)$$

Figure VII-2 shows the Lau *et al.*, (1992) asphalts. The Arrhenius equation accurately describes the aging characteristics from 322.2 to 366.7 K for Ampet AC-20, Cosden AC-20, and Exxon AC-20. For Cosden AC-20 and Texaco AC-20, r_{CA} at 366.7 K were not included. At this temperature, r_{CA} were excessively high and may have resulted from different aging mechanisms. High r_{CA} at 366.7 K may have resulted since neat CA was included in the r_{CA} estimation. In any case, the high temperature data that did not fit the Arrhenius model were discarded. This is justified since the objective is to use estimated Arrhenius parameters to extrapolate r_{CA} to road conditions, 333.3 K or lower. Lau *et al.*, (1992) Coastal AC-20 shows the least resistance to CA at highway pavement conditions for ST aging. Lau *et al.*, (1992) Texaco AC-20 shows superior resistance to CA for ST aging at low temperature.

Figure VII-3 and VII-4 show the Arrhenius relationship for Jemison *et al.*, (1992b) and Davison *et al.*, (1987) Dickens Diamond Shamrock asphalts, and SHRP (1990) asphalts, respectively. r_{CA} at 366.7 K were too high for Jemison *et al.*, (1992b) Coastal AC-20, and SHRP (1990) AAA-1, AAD-1, and AAK-2 and could not be modeled with the Arrhenius relationship. As discussed in the previous paragraph, the data for the r_{CA} at high temperature were removed. Again, the objective is to estimate highway-condition r_{CA} from the Arrhenius parameters. From Figure VII-3 at 322.2 K, Dickens Diamond Shamrock AC-20 shows the highest r_{CA} while Jemison *et al.*, (1992b) Texaco AC-20 shows the lowest r_{CA}. However, at lower aging temperatures, Jemison *et al.*, (1992b) Coastal AC-20 eventually has the highest r_{CA} for these asphalts. From Figure VII-4 for the SHRP (1990) asphalts, AAG-1 shows

the highest r_{CA} at all temperatures studied. These asphalts can be divided into two families. The first family is AAA-1, AAD-1, and AAK-2 with high E_A and low r_{CA} at low aging temperature. The second family consists of AAC-1, AAG-1, and AAM-1 with low E_A and relatively high r_{CA} at low aging temperatures.

The Arrhenius parameters are asphalt dependent from Figures VII-2 through VII-4 for ST aging. Reliable extrapolations to road conditions can only be accomplished with Arrhenius parameters estimated from data at multiple elevated temperatures. A ST aging test at 355.5 K says that both Lau *et al.*, (1992) Coastal AC-20 and Texaco AC-20 have the lowest r_{CA} when compared to the other asphalts of Lau *et al.*, (1992). For this single temperature, the test would falsely discard the other asphalts in favor of Coastal AC-20 and Texaco AC-20. At road conditions of 322.2 K for ST aging, Lau *et al.*, (1992) Coastal AC-20 has a r_{CA} twice that of Lau *et al.*, (1992) Texaco AC-20 and greater than all of the Lau *et al.*, (1992) asphalts studied. For the lowest r_{CA} at road conditions for ST aging, Lau *et al.*, (1992) Texaco AC-20 and Exxon AC-20 is the correct choice. Clearly, a single elevated aging temperature for ST aging is not sufficient to characterize r_{CA} at other temperatures. Similar conclusions about r_{CA} and T were also made (Lau *et al.*, 1992) for LT aging.

Table VII-3 gives A and E_A for all of the asphalts studied with ST aging experiments. The model parameters are different for each asphalt, even across groups of asphalts from the same refinery. These asphalts, Lau *et al.*, (1992) Coastal AC-20 and Jemison *et al.*, (1992b) Coastal AC-20, may be the same from the Arrhenius parameters.

Table VII-3. Arrhenius Parameters for *ST* Aging Studies

Group	Asphalt	$A \times 10^{-8}$ CA / day	E_A kJ / gmol
Lau *et al.*, (1992)			
	Ampet AC-20	5.45	63.5
	Coastal AC-20	0.001	40.2
	Cosden AC-20	8.69	64.7
	Exxon AC-20	9.99	65.4
	Texaco AC-20	0.82	59.9
Jemison *et al.*, (1992b)			
	Coastal AC-20	0.0009	39.7
	Fina AC-20	0.09	51.3
	Texaco AC-20	25.6	69.0
Davison *et al.*, (1987)			
	Dickens D.S.[a]	0.003	41.3
SHRP (1990)			
	AAA-1	0.058	51.2
	AAC-1	0.0006	37.3
	AAD-1	0.025	48.2
	AAG-1	0.0008	36.0
	AAK-2	0.038	49.7
	AAM-1	0.0004	35.9

[a] D.S. represents Diamond Shamrock.

Comparing Arrhenius Parameters for *ST* and *LT* Aging

The information from *ST* experiments are compared with *LT* aging data. Only with a reliable correlation between *ST* and *LT* aging can the aging test time be decreased and still provide valuable kinetic information. Furthermore, r_{CA} at low temperature should be used to characterize an asphalt's resistance to oxidative aging and compare *ST* and *LT* aging.

A ranking of asphalts studied is done for qualitative comparisons of *ST* aging. From Figure VII-2, Lau *et al.*, (1992) Coastal AC-20 and Texaco AC-20 show the fastest and slowest r_{CA} at 322.2 K, respectively. For Jemison *et al.*, (1992b) and

Davison *et al.*, (1989) in Figure VII-3, the fastest r_{CA} at 322.2 K is Coastal AC-20 while the slowest is Texaco AC-20. For the SHRP (1990) asphalts at 322.2 K, AAG-1 has an order of magnitude greater r_{CA} relative to AAA-1.

It is uncertain how the kinetic parameters from *ST* aging relate to *LT* aging. Nine asphalts studied have both *LT* and *ST* aging data, Lau *et al.*, (1992) Ampet AC-20, Coastal AC-20, Cosden AC-20, Exxon AC-20, and Texaco AC-20, Davison *et al.*, (1989) Dickens Diamond Shamrock AC-20, and Jemison *et al.*, (1992b), Coastal AC-20, Fina AC-20, and Texaco AC-20. Lau *et al.*, (1992) Cosden AC-20 has the highest r_{CA} at 322.2 K based on both experimental data and extrapolation from high temperature data for *LT* aging, Table IV-8. From *ST* aging data, it was concluded that Lau *et al.*, (1992) Coastal AC-20 has the highest r_{CA}. Unfortunately, it appears that *ST* aging with the simple linear model, equation I – 2, cannot be directly related to *LT* aging.

E_A as determined from *ST* and *LT* aging are compared. E_As for *LT* aging are reported in Table IV-6, Table VI-4 and Chapter IV for literature values. E_A for *ST* aging are half relative to E_A for *LT* aging. At high temperature, r_{CA} for both *ST* and *LT* aging are about the same. At low temperature, r_{CA} are higher for *ST* aging compared to *LT* aging. This is partially caused by including neat *CA* in the estimation of r_{CA} for *ST* aging. Since low temperature r_{CA} are higher for *ST* aging relative to *LT* aging, E_A for *ST* aging is lower than E_A for *LT* aging.

Figures VII-5 and VII-6 compare E_A and A, respectively, for *ST* and *LT* aging. All of the *LT* activation energies are greater than *ST* activation energies. Even with this difference, perhaps *LT* and *ST* activation energies could be correlated. However, from Figure VII-5, it appears that there is no correlation between *ST* and *LT* aging activation energies for the asphalts studied. This provides further evidence that *ST*

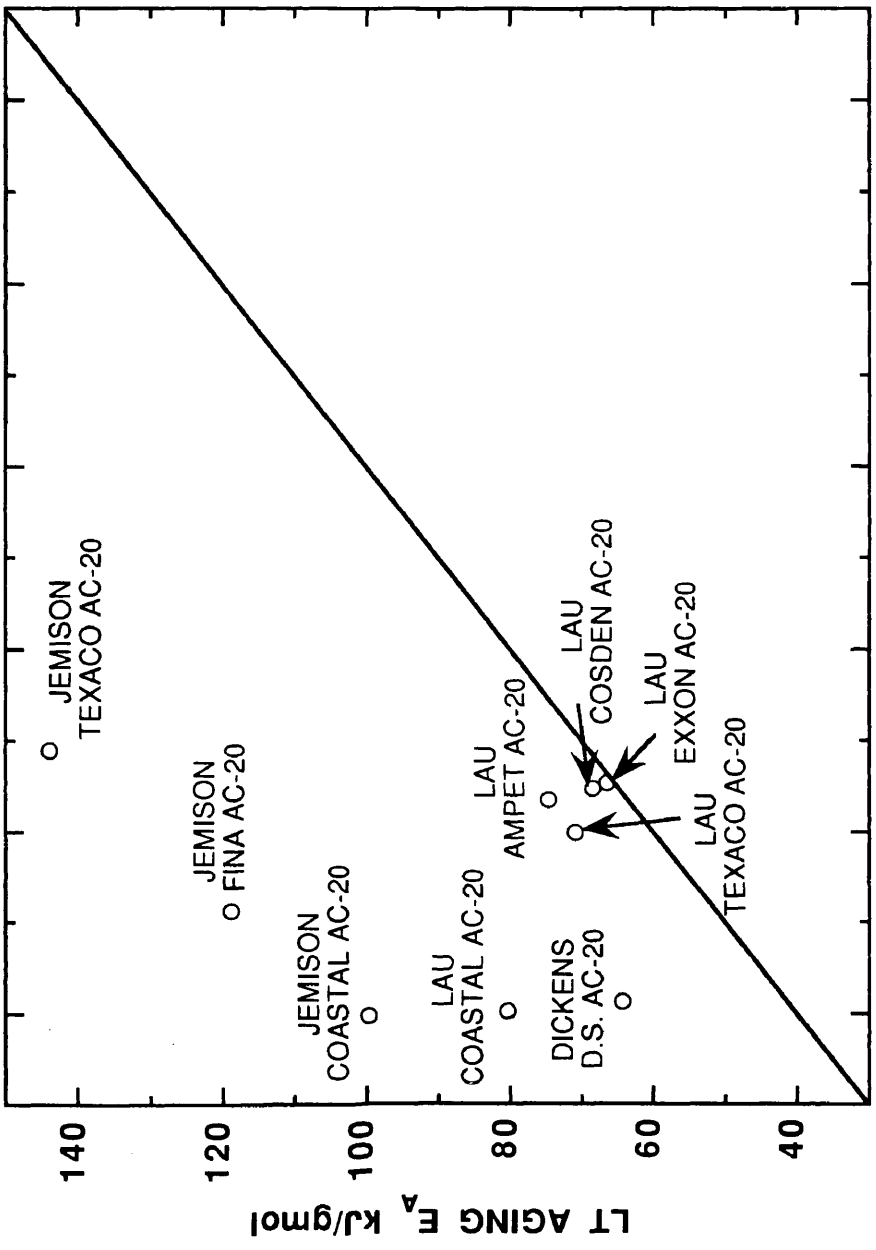

Figure VII-5. Comparisons between E_A for all short term and long term POV-aged asphalts studied.

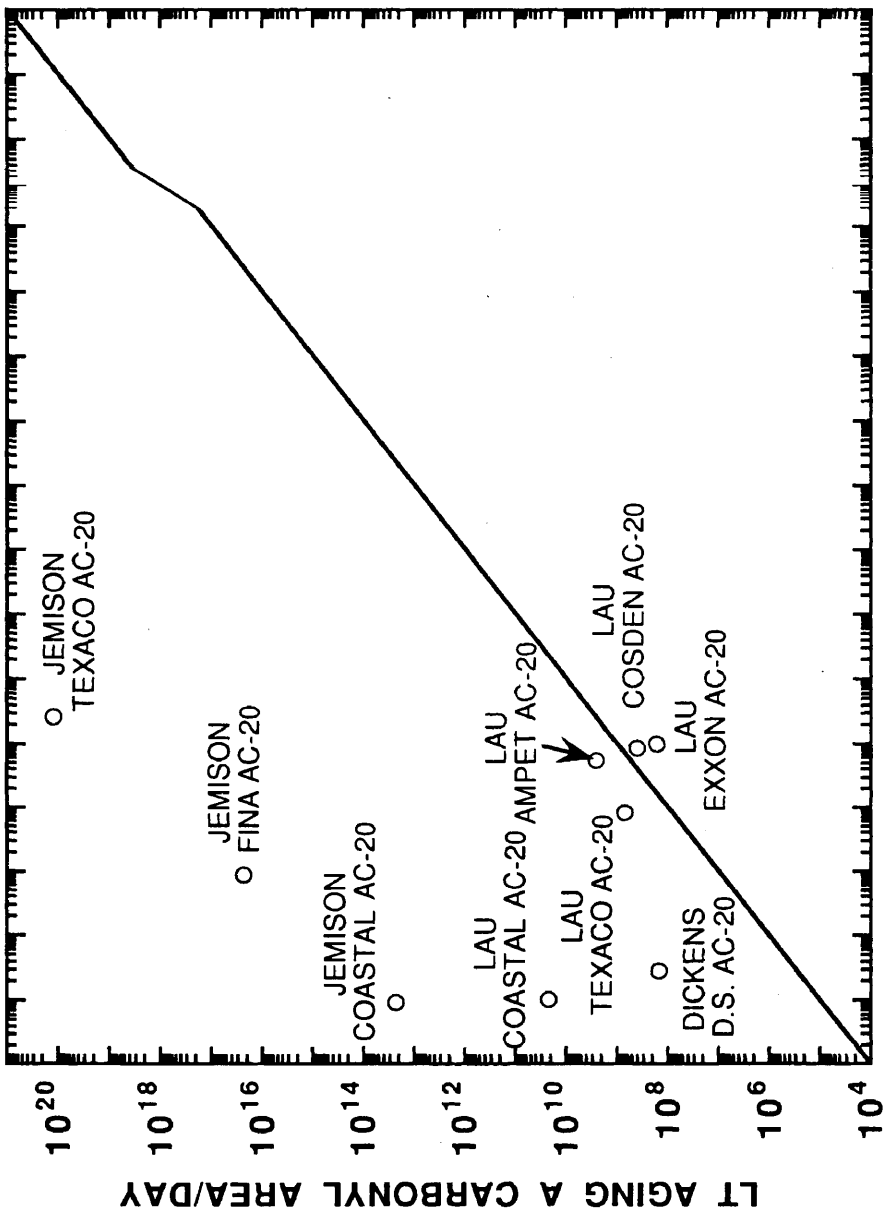

Figure VII-6. Comparisons between A for all short term and long term POV-aged asphalts studied.

and *LT* aging may occur by two different mechanisms and are not necessarily related (Dickinson and Nicholas, 1949). From the reported data for the Jemison (1992b) asphalts, E_As for *LT* aging are 100 kJ/gmol and outside the reported literature values. These E_A data are probably suspect.

The Arrhenius constant, *A*, for *ST* and *LT* aging are compared in Figure VII-6. This figure is log scale on both axes. *LT* and *ST* values are about the equality line for Lau *et al.*, (1992) Ampet AC-20, Cosden AC-20, Exxon AC-20, and Texaco AC-20. Lau *et al.*, (1992) Coastal AC-20 shows significant deviation from the equality line. *A* for *LT* aging is five orders of magnitude greater than *A* for *ST* aging. Davison *et al.*, (1989) Dickens Diamond Shamrock AC-20 also shows a significantly higher value for *A* from *LT* aging relative to *A* from *ST* aging. Jemison *et al.*, (1992b) asphalts for *LT* aging show markedly different *A* when compared to the other asphalts and *ST* aging. Again, this suggests that the estimated r_{CA} are probably in error for the *LT* aging experiments of Jemison (1992).

Physicochemical Relationships

Asphalts have unique physicochemical relationships that can be modeled and quantified for *LT* POV- and field-aged material. For example, log η_o^* and *CA* due to oxidative aging for a given asphalt are linearly related by the *HS*. Log $(1/J'')$ and *CA* are also linearly related as shown in Chapter VI for POV and field aging. Recently, Lin *et al.*, (1993) show that η_o^* at 333.3 K and % *A* are related by a modified Pal-Rhodes model. *ST* aging physicochemical relationships are developed and compared to *LT* aging results when possible.

η_o^*-CA relationships

CA and η_o^* at 333.3 K were measured for each asphalt for all aging temperatures and times. Figure VII-7 illustrates the data for Lau *et al.*, (1992) Coastal AC-20. The neat and RTFO residue are included on the figure. The parameter estimation used only the data from *ST* POV aging. A linear relationship between log η_o^* and *CA* exists over a given range for *ST* aging as given in equation I – 6.

$$\eta_o^* = \exp\Big\{ HS \cdot CA + m \Big\} \qquad (I-6)$$

Figures G-15 through G-27 show the other asphalts studied. Not all of the asphalts show such good linearity as Lau *et al.*, (1992) Coastal AC-20. Some of the asphalts studied show an increasing rate of change of log η_o^* with *CA* at relatively high *CA*, Figure VII-8 for Lau *et al.*, (1992) Cosden AC-20. Including the entire *ST* data set in the parameter estimation results in higher *HS* relative to a data set with low η_o^* or *CA*. All of the asphalts except SHRP (1990) AAG-1 show good linearity for η_o^* lower than 500 kP at 333.3 K.

Table VII-4 gives *HS* and exp(m) at 333.3 K for all of the asphalts studied for the *ST* aging. *HS* ranges from 6.23 to 0.96 $1/CA$. SHRP (1990) AAG-1 has the lowest *HS*, and Jemison, *et al.*, (1992b) Coastal AC-20 has the highest *HS*. From Arrhenius parameters, Lau *et al.*, (1992) Coastal AC-20 and Jemison *et al.*, (1992b) Coastal AC-20 may be the same asphalt. However, the asphalts are different based on *HS*. Lau *et al.*, (1992) Coastal AC-20 is more resistant to oxidative hardening than Jemison *et al.*, (1992b) Coastal AC-20 even though r_{CA} is the same. *HS* are very similar for Lau *et al.*, (1992) Texaco AC-20 and Jemison *et al.*, (1992b) Texaco AC-20; however, r_{CA}s for the two asphalts are not the same.

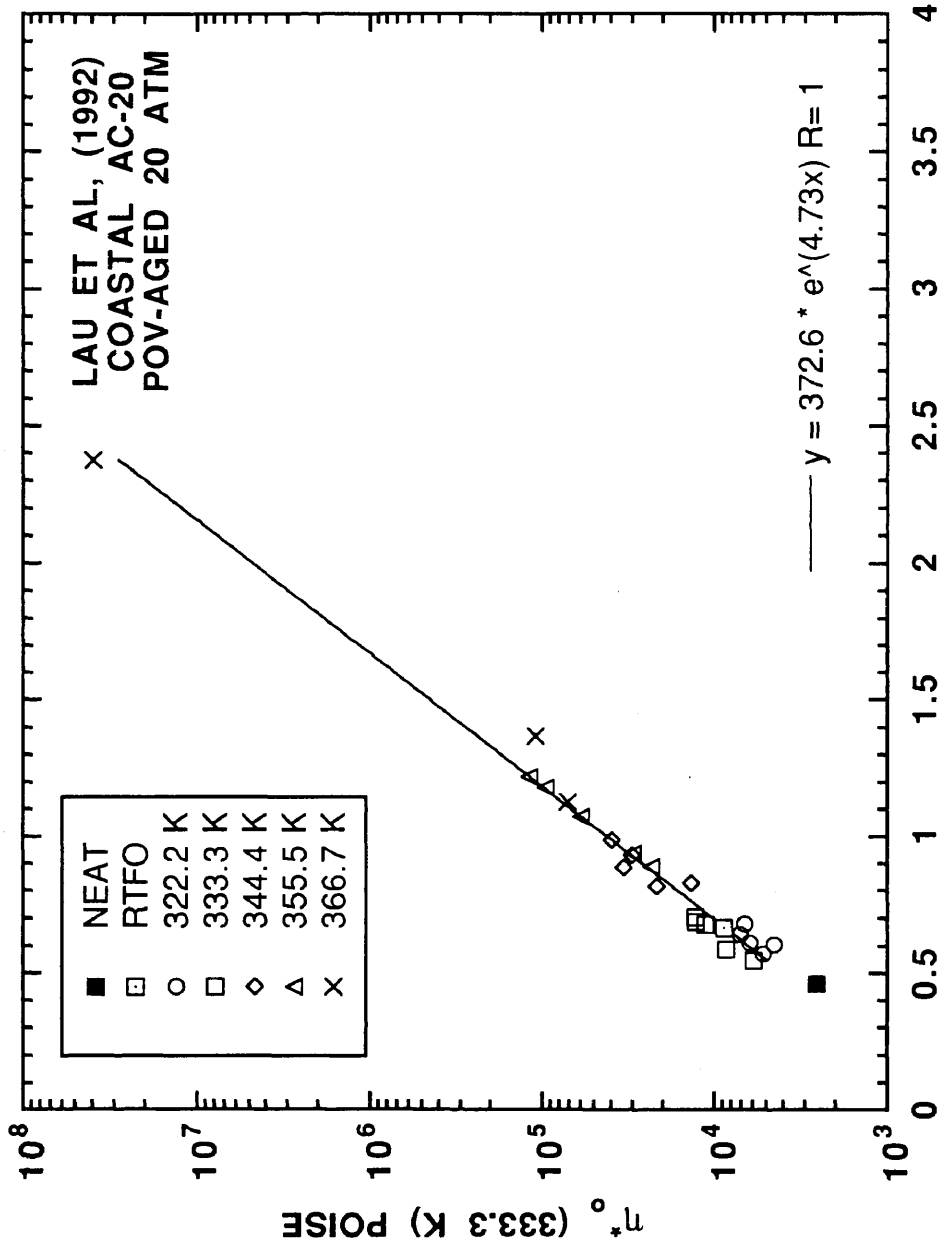

Figure VII-7. η_o^* at 333.3 K and CA of neat, RTFO, and all short term POV-aging conditions studied for Lau *et al.*, (1992) Coastal AC-20.

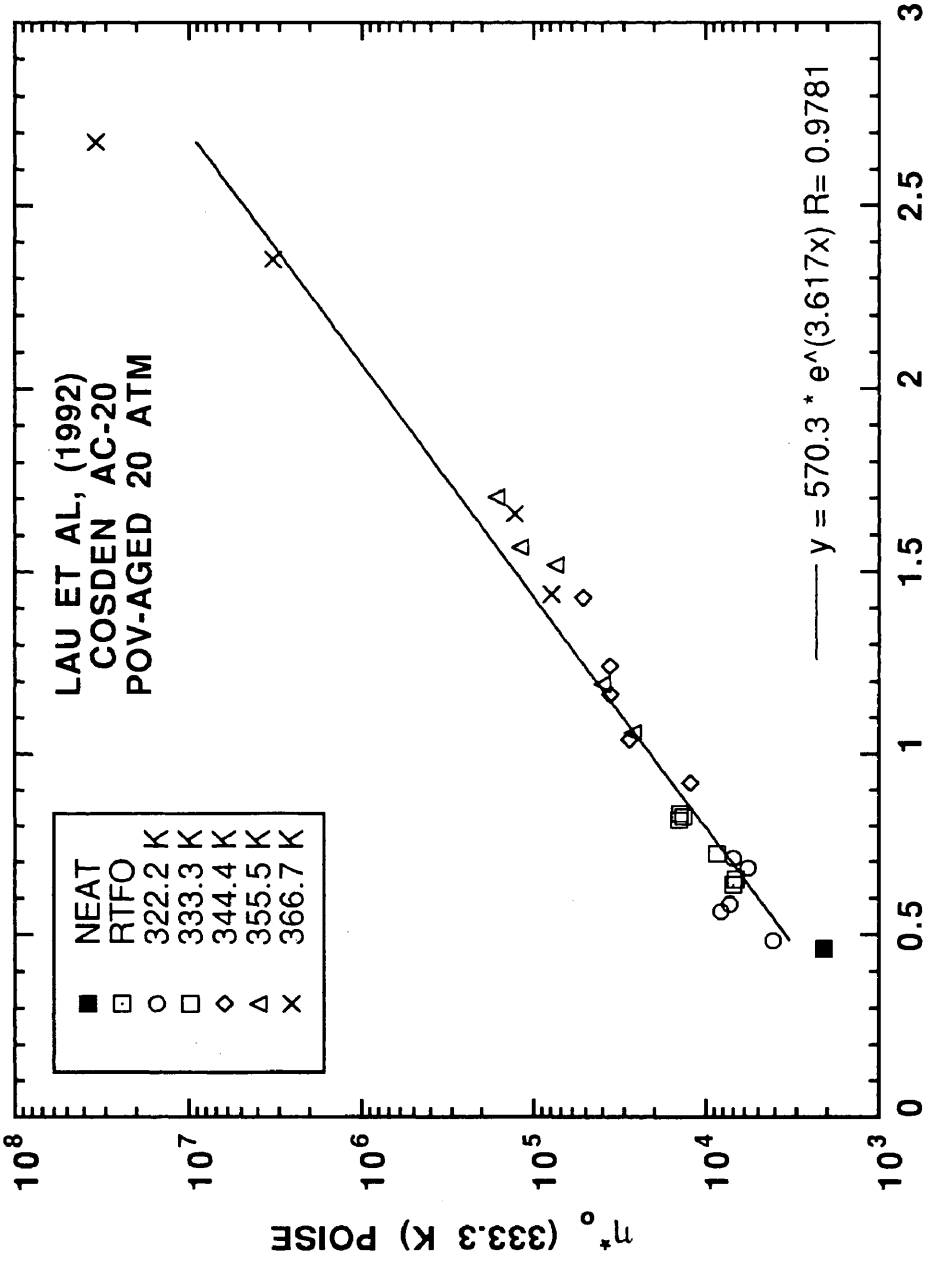

Figure VII-8. η_o^* at 333.3 K and CA of neat, RTFO, and all short term POV-aging conditions studied for Lau *et al.*, (1992) Cosden AC-20.

Table VII-4. *HS* and exp(m) at 333.3 K for All *ST* Aging Studies

Group	Asphalt	*HS*(333.3 K) 1 / *CA*	exp(m) 333.3 K P
Lau *et al.*, (1992)			
	Ampet AC-20	3.45	659
	Coastal AC-20	4.73	373
	Cosden AC-20	3.62	570
	Exxon AC-20	2.70	1300
	Texaco AC-20	4.56	484
Jemison *et al.*, (1992b)			
	Coastal AC-20	6.23	202
	Fina AC-20	3.24	978
	Texaco AC-20	4.59	580
Davison *et al.*, (1987)			
	Dickens D.S.[b]	3.32	832
SHRP (1990)			
	AAA-1	5.27	79.9
	AAC-1	3.48	233
	AAD-1	3.73	141
	AAG-1	0.968	1950
	AAK-2	2.97	312
	AAM-1	3.69	710

[a] Model: $\eta_o^*(333.3\text{ K}) = \exp(HS \cdot CA + m)$
[b] D.S. represents Diamond Shamrock

Lau *et al.*, (1992), Davison *et al.*, (1987) Dickens Diamond Shamrock AC-20, and Jemison *et al.*, (1992b) asphalts were used to compare *ST* and *LT* physicochemical parameters, *HS* and exp(m). Table VII-5 gives *ST* and *LT* *HS* and exp(m) and the percent difference between *ST* and *LT* for both parameters. *HS* from *ST* aging is always greater than *HS* from *LT* aging for Lau *et al.*, (1992) asphalts. The difference in the *HS* is almost 30% for Texaco AC-20. Only Exxon AC-20 with a percent difference of 2.7 shows good agreement between *LT* and *ST* aging *HS* for Lau *et al.*, (1992) asphalts. Exp(m) for *ST* aging is less relative to exp(m) for *LT* aging for Lau *et al.*, (1992) asphalts. The comparison for Davison *et al.*, (1987) Dickens Diamond

Table VII-5. Comparisons between *HS* and exp(m) for *LT* and *ST* Aging of Different Asphalts

Group	Asphalt	*HS*			exp(m)		
		HS_{LT} 1 / *CA*	HS_{ST} 1 / *CA*	% Diff[a]	$\exp(m)_{LT}$ P	$\exp(m)_{ST}$ P	% Diff
Lau *et al.*, (1992)							
	Ampet AC-20	3.03	3.45	13.8	1126	659	-41.5
	Coastal AC-20	3.97	4.73	19.1	655	373	-43.0
	Cosden AC-20	2.95	3.62	22.7	1032	570	-44.8
	Exxon AC-20	2.63	2.70	2.66	1377	1300	-5.59
	Texaco AC-20	3.39	4.56	34.5	687	484	-29.6
Davison *et al.*, (1989)							
	Dickens D.S.[b]	3.64	3.32	-8.79	447	832	86.1
Jemison *et al.*, (1992b)							
	Coastal AC-20	6.20	6.23	0.48	82.3	202	-145
	Fina AC-20	3.25	3.24	-0.31	713	978	-37.2
	Texaco AC-20	3.58	4.59	28.2	1164	580	50.2

[a] % Diff $= 100 \times \left(\frac{x_{LT} - x_{ST}}{x_{LT}}\right)$

[b] D.S. represents Diamond Shamrock.

Shamrock AC-20 shows much closer agreement with *HS*. In fact, *HS* for *ST* aging is lower relative to *HS* for *LT* aging. The percent difference in exp(m) is large, 80%, partially because of the definition of the percent difference in the table. For Jemison *et al.*, (1992b) asphalts, Coastal AC-20 and Fina AC-20 show excellent agreement in *HS* but significant differences in exp(m). Agreement between the *HS* for *ST* and *LT* aging for Jemison (1992) Coastal AC-20 and Fina AC-20 is within 1%. Exp(m) has a 100% difference comparing *ST* and *LT* parameters. Agreement for Jemison *et al.*, (1992b) Texaco AC-20 *HS* is not very good with 30% percent difference.

There are three reasons accounting for higher *HS* from *ST* aging relative to *HS* from *LT* aging for the Lau *et al.*, (1992) asphalts. First, extremely high η_o^* from aging at 366.7 K was included in the parameter estimation. At high η_o^* and *CA*, the rate of change of log η_o^* with respect to *CA* increases, and *HS* increases. Second, Lau *et al.*, (1992) did not use time-temperature superposition to determine η_o^* at high viscosity. Reported η_o^*s are at a frequency of 0.001 rad/s, and the values may be lower than true η_o^*. Lower η_o^* would result in a lower *HS*. Finally, small differences in the ATR prism for measuring *CA* also affect *HS* estimation. Even though *HS* differ, the relative rankings of most of the asphalts based on *HS* remain the same. Only Lau *et al.*, (1992), Ampet AC-20 and Cosden AC-20 exchange places from *LT* to *ST* aging.

For equal data set ranges, the estimated parameters for *ST* and *LT* aging should be in closer agreement. The effect of the ATR prism and measured versus calculated η_o^* should also be considered when comparing the current data sets. This suggests that a standard procedure be developed for data collection and analysis.

(1 / J″)-CA relationships

(1 / J'') at 333.3 K and 10 rad/s was measured for the SHRP (1990) asphalts studied. A unique relationship between the (1 / J'') and CA was discovered for LT POV and field aging. RS or rutting susceptibility is defined by equation VI – 1.

$$(1 / J'') = (1 / J'')_o \exp\left\{ RS \cdot CA \right\} \qquad \text{(VI – 1)}$$

Figure VII-9 illustrates the relationship for SHRP (1990) AAC-1 ST aging. For this asphalt, the simple linear model sufficiently describes the data. However, not all asphalts studied could be accurately described by this simple linear model. Figure VII-10 shows the data and estimated parameters for AAA-1. The simple linear model is not sufficient for this asphalt. Figures G-28 through G-31 show (1 / J'') and CA for the other SHRP (1990) asphalts studied. The linear model describes the data except for AAA-1, AAD-1 and AAK-2. These asphalts show a decreasing rate of change of log (1 / J'') with CA at high CA.

Table VII-6 gives equation VI–1 model parameters for the SHRP (1990) asphalts studied. RS ranges from 3.08 to 0.916 $1/CA$. AAG-1 has the lowest RS. Asphalt AAG-1 is probably very prone to rut because of its low RS. RS are lower than HS for the same asphalt. RS and HS comparisons in Tables VII-4 and VII-6 yield no correlation. For example, AAC-1 has a HS of 3.48 $1/CA$ and RS of 2.75 $1/CA$. AAD-1 has a higher HS and a lower RS relative to AAC-1.

η_o^*-% A relationships

η_o^* at 333.3 K and % A were measured at all aging conditions for the Lau *et al.*, (1992) asphalts. A modified Pal-Rhodes model was used to analyze the data (Lin *et*

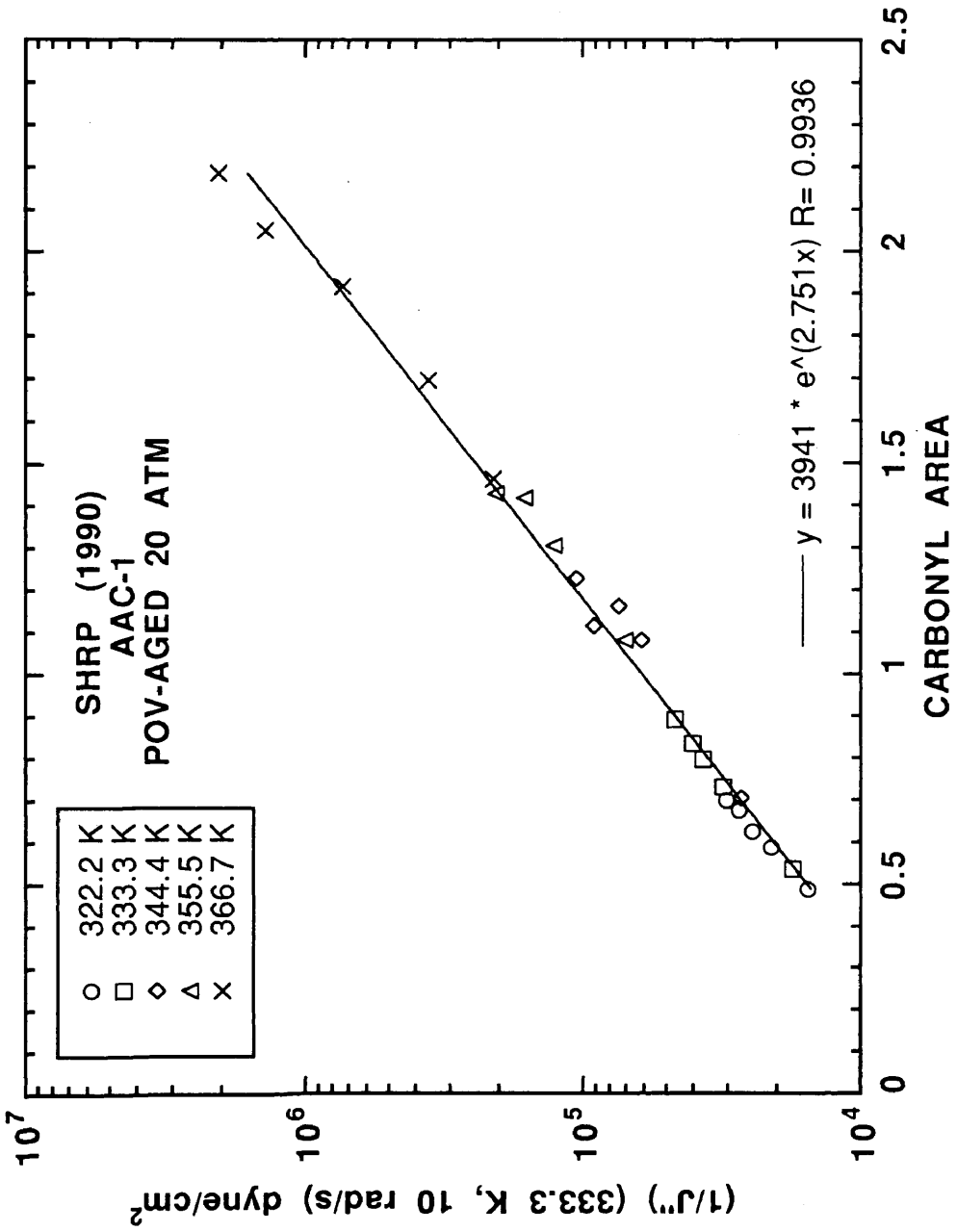

Figure VII-9. $(1 / J'')$ at 333.3 K, 10 rad/s and CA of all short term POV-aging conditions studied for SHRP AAC-1.

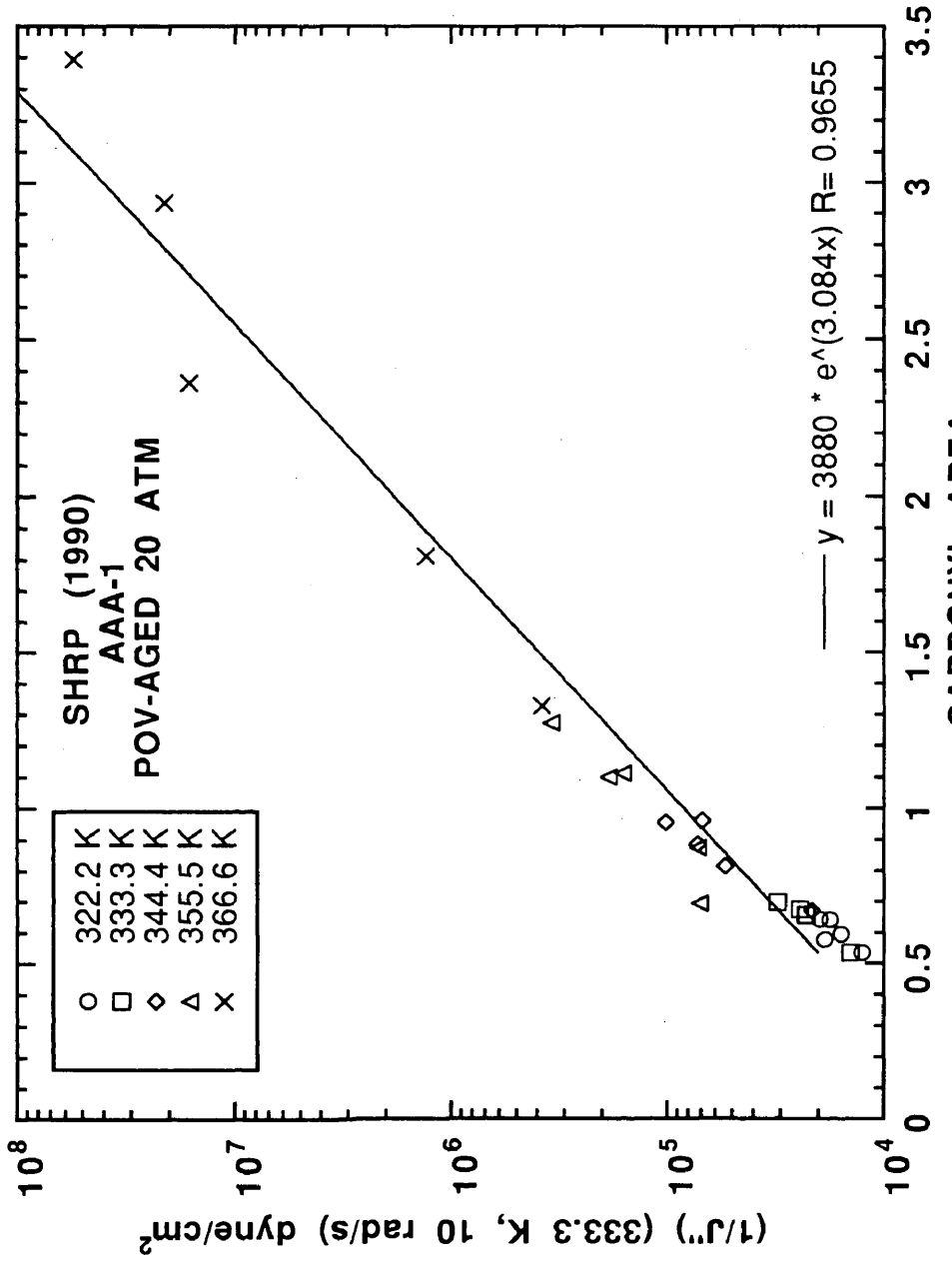

Figure VII-10. $(1 / J'')$ at 333.3 K, 10 rad/s and CA of all short term POV-aging conditions studied for SHRP AAA-1.

Table VII-6. RS and $(1 / J'')_o$ at 333.3 K and 10 rad/s for ST Aging Studies of SHRP Asphalts[a]

Group	Asphalt	RS(333.3 K) $1 / CA$	$(1 / J'')_o$ 333.3 K dyne / cm^2
SHRP (1990)			
	AAA-1	3.08	3880
	AAC-1	2.75	3940
	AAD-1	2.72	3163
	AAG-1	0.916	20800
	AAK-2	2.06	5540
	AAM-1	2.42	14800

[a] Model: $(1 / J'')(333.3\ \text{K}, 10\ \text{rad} / \text{s}) = (1 / J'')_o \exp(RS \cdot CA)$

al., 1993). The model is given in equation I – 7.

$$\eta_o^* = \eta_M (1 - K' \cdot \%\ A)^{-\nu} \qquad \text{(I – 7)}$$

η_M, K', and ν are estimated free parameters. Actually, η_M could be measured but, in this study, was not.

Figure VII-11 shows data and the model for Lau *et al.*, (1992) Ampet AC-20. The model predicts upward curvature of η_o^* with % A at high % A. Neat and RTFO data were not used in the parameter estimation. The model extrapolates back to the neat datum with amazing accuracy. Further extrapolation back to zero % A must be confirmed by measuring η_o^* of the hexane maltene. Figures G-32 through G-35 show the η_o^*-% A relationship for Lau *et al.*, (1992) Coastal AC-20, Cosden AC-20, Exxon AC-20, and Texaco AC-20, respectively.

The Pal-Rhodes model parameters are given in Table VII-7. Each asphalt gives a unique set of model parameters relating to the maltene viscosity, η_M, solvation shell, K', and intrinsic viscosity, ν. These parameters describe the asphalt's resistance to hardening with % A due to oxidative aging. From a more fundamental viewpoint,

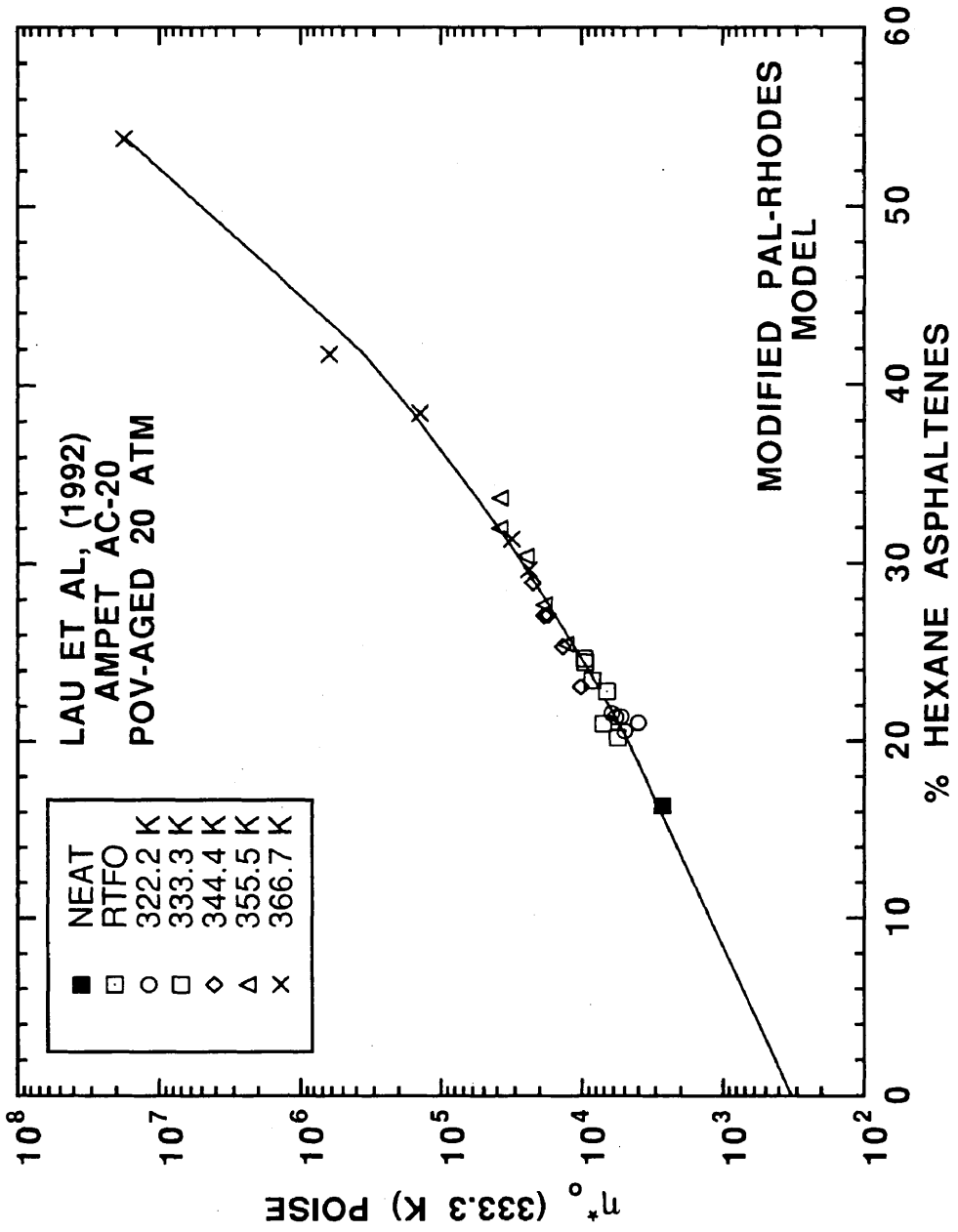

Figure VII-11. η_o^* at 333.3 K and % hexane asphaltenes of neat, RTFO, and all short term POV-aging conditions studied for Lau *et al.*, (1992) Ampet AC-20.

these parameters relate to the structure of the asphaltene molecules and the ability of the particular maltene phase to solvate the asphaltene particles (Lin *et al.*, 1993). If it is possible to relate these parameters to compositional and structural properties of an asphalt, asphalts with known resistance to hardening with % A production due to oxidative aging could be designed.

Table VII-7. Modified Pal-Rhodes Parameters for ST Aging of Lau *et al.*, (1992) Asphalts

Asphalt	Parameters[a]		
	K'	ν	η_M Poise
Ampet AC-20	1.33	8.64	327
Coastal AC-20	1.73	6.09	116
Cosden AC-20	1.15	12.24	189
Exxon AC-20	1.37	12.00	255
Texaco AC-20	1.08	16.21	68

[a] Model: $\eta_0^*(333.3\ \mathrm{K}) = \eta_M(1 - K' \cdot \%\ A)^{-\nu}$

Summary

A comparison between ST and LT aging produced the following in terms of r_{CA} and physicochemical relationships. ST and LT aging kinetic parameters did not appear to be correlated. A more sophisticated aging model (Nicholas and Dickinson, 1949) accounting for the small population of highly reactive compounds in the asphalt is necessary to obtain meaningful comparisons between ST and LT aging. ST aging was an efficient way to generate data for physicochemical relationships. The physicochemical model parameters for ST and LT aging did not agree as well as expected for most of the asphalts studied. However, some of the asphalts showed excellent

agreement in *HS*. The difference in the model parameters is thought to result from the following reasons. First, high η_o^* data were included for *ST* aging resulting in higher *HS* relative to *HS* from *LT* data. Second, there were inconsistent methods of data collection and analysis. Comparing the data sets at equal *CA* ranges should result in better agreement between *LT* and *ST* physicochemical model parameters. $(1 / J'')$ at 333.3 K and 10 rad/s was correlated with *CA* . Finally, η_o^* at 333.3 K and % *A* was correlated with a modified Pal-Rhodes model (Lin *et al.*, 1993). Each asphalt showed unique model parameters describing the asphalts ability to resist hardening with asphaltene production from oxidative aging. *ST* aging experiments can be extremely useful to determine these physicochemical parameters for an unknown asphalt. Once the physicochemical parameters are determined and certain undesirable asphalts screened, more complete kinetic information can be obtained by *LT* aging experiments.

CHAPTER VIII

CONCLUSIONS

Two models describing asphalt aging were developed. The first is the asphalt-aging model accounting for both carbonyl formation, equation II – 1, and unsteady variable $\mathcal{D}_{O_2}$ oxygen diffusion and reaction, equation II – 40, in an asphalt film of finite thickness.

$$\left(\frac{\partial CA}{\partial t}\right) = r_{CA} \tag{II – 1}$$

$$\left(\frac{\partial P}{\partial t}\right) = \left(\frac{\partial \mathcal{D}_{O_2}}{\partial P}\right)\left(\frac{\partial P}{\partial x}\right)^2 + \mathcal{D}_{O_2}\left(\frac{\partial^2 P}{\partial x^2}\right) - \left(\frac{cRT}{h}\right) r_{CA} \tag{II – 40}$$

The second is the highway-pavement aging model that relates fundamental quantities in the asphalt-aging model, P and L, to measurable core properties such as percent voids, % V, and percent asphalt, % Asp, equations II – 41 and II – 42.

$$P_{\text{eff}} = f(\%\ V, t) \tag{II – 41}$$

$$L_{\text{eff}} = f(\%\ Asp, \%\ V) \tag{II – 42}$$

These models can not only be used to simulate field aging but also predict field aging.

Carbonyl content, CA, was used to monitor asphalt aging for two reasons. First, previous research has shown that CA due to oxidative aging correlates with physical and rheological properties. Second, CA can be measured at known locations in a film. Using the ATR technique, CA at the exposed surface, ES, practically eliminated oxygen diffusion problems for low-pressure experiments. To estimate r_{CA} at a known thickness in the film, CA at the substrate interface SI was measured. These measurements of r_{CA} in the film include oxygen diffusion effects. Other methods of monitoring asphalt aging such as viscosity, penetration, GPC, and Corbett fractionation require

bulk samples, and oxygen diffusion and reaction effects cannot be separated. This work is the first to design experiments that separate oxygen diffusion and reaction effects in an asphalt film.

A kinetic equation including both effects of temperature and oxygen pressure on CA in asphalt was formulated, equation II – 7.

$$r_{CA} = A \exp\left(\frac{-E_A}{RT}\right) P^{\alpha} \qquad \text{(II – 7)}$$

The Arrhenius parameters, A and E_A, were dependent on asphalt composition. Asphalt E_A for oxidation ranged from 66.7 to 80.5 kJ/gmol and compared favorably with literature values. The order of reaction in terms of oxygen pressure, α, was 0.270 and independent of asphalt composition for the five asphalts studied. r_{CA} estimated at a single high oxygen pressure can be reliably extrapolated to highway conditions. The initial jump or CA_o was a function of aging pressure. An empirical model was used to represent the data, equation IV – 2.

$$CA_o = sP^{\beta} \qquad \text{(IV – 2)}$$

The parameters, β and s, were approximately 0.7 and 0.08, respectively, and dependent on asphalt composition. From this discovery, at least one of the aging pressures in a laboratory test must be at the highway condition to reliably determine CA_o.

The oxygen diffusivity, $\mathcal{D}_{O_2}$, in asphalt was estimated. A theoretical model accounting for transport and reaction of oxygen in the asphalt film was developed from first principles. In this model, $\mathcal{D}_{O_2}$ was allowed to change in the film as a result of CA. Before $\mathcal{D}_{O_2}$ was estimated, supplementary relationships were required. A model relating r_{CA} to r_{O_2} was formulated, and a model relating η_o^* to both CA and T was developed.

With a limited data set, a relationship between r_{CA} and r_{O_2} in asphalt was developed, equation II – 10.

$$r_{O_2} = c r_{CA} \qquad (II - 10)$$

For one asphalt studied, c was 6.56×10^{-4} gmol O_2 / mL CA. The data included the neat sample. Sulfoxide appears to account for only a small portion of reacted oxygen even though the sulfoxide IR absorbance is much larger than carbonyl absorbance. This relationship was assumed to hold for all asphalts studied.

Models relating η_o^* to CA and T were developed and given in equations I – 6, II – 14, and II – 15.

$$\eta_o^* = \exp\left\{ HS \cdot CA + m \right\} \qquad (I - 6)$$

$$E_V = \gamma CA + \delta \qquad (II - 14)$$

$$\begin{aligned} HS(T) &= HS(T_o) + \gamma\left(\frac{1}{T} - \frac{1}{T_o}\right) \\ m(T) &= m(T_o) + \delta\left(\frac{1}{T} - \frac{1}{T_o}\right) \end{aligned} \qquad (II - 15)$$

The parameters, γ, δ, $HS(T_o)$, and $m(T_o)$, were dependent on asphalt composition. γ ranges from 1000 to 2560 K/ CA. δ ranges from 19000 to 20600 K. Because of the small value of γ relative to δ, HS is relatively insensitive to temperature.

In order to estimate $\mathcal{D}_{O_2}$, another boundary condition had to be specified. The oxygen pressure at the substrate interface, P_{SI}, provided the additional constraint in this study. P_{SI} was estimated from r_{CA} at the SI assuming a steady-state long-term aging model and the known kinetic parameters in equation II – 7. Estimated P_{SI} was generally lower than P_{ES} suggesting an oxygen pressure gradient in the asphalt film. However, some of the estimates were physically inconsistent, and an error analysis showed that small errors in r_{CA} transform to larger variability in P_{SI} due to the small value of α.

With a steady-state constant $\mathcal{D}_{O_2}$ oxygen diffusion and reaction model and all of the required constraints, oxygen diffusivities were estimated. Estimated $\mathcal{D}_{O_2}$ values were within the range of the two reported literature values. In the data set there were several questionable data points that were eliminated. The remaining data suggested that $\mathcal{D}_{O_2}$ and η_o^* were related by equation II – 34.

$$\mathcal{D}_{O_2} = D_o(\eta_o^*)^B \qquad \text{(II – 34)}$$

This model is supported in the literature and the value of B was -0.84. B was also in the range of literature values. D_o was 4.04×10^{-9} mm/s^2. Furthermore, the model parameters were independent of asphalt composition for the five asphalts studied and independent of temperature. The effect of η_o^* completely masks the effect of T of $\mathcal{D}_{O_2}$.

With an estimation of $\mathcal{D}_{O_2}$, the Thiele modulus, ϕ, was calculated for the experimental aging conditions. Values of ϕ were less than unity and indicated that a diffusion controlled regime may not have been established. Experiments with thicker films increase ϕ and insure a diffusion controlled regime.

Using a steady-state variable $\mathcal{D}_{O_2}$ oxygen diffusion and reaction model, oxygen pressure profiles were calculated for one of the asphalts studied. In this case P_{SI} was estimated for discrete aging times. The profiles showed decreasing P_{SI} with increasing time. The range of P_{SI} estimated from steady-state variable $\mathcal{D}_{O_2}$ oxygen diffusion and reaction and P_{SI} estimated from r_{CA} were compared. The data removed from the parameter estimation of equation II – 34 did not show very good agreement. However, the other data compared favorably. Even at 20 atm oxygen pressure and 333.3 K with a 1 mm thick film, the calculations showed that diffusion resistance was not entirely eliminated for some of the asphalts. The relative magnitudes of $\left(\frac{d\mathcal{D}_{O_2}}{dP}\right)\left(\frac{dP}{dx}\right)^2$ and

$\mathcal{D}_{O_2}\left(\frac{d^2P}{dx^2}\right)$ were defined by a dimensionless variable, ξ, in equation V – 24.

$$\xi = \left| \frac{\left(\frac{d\mathcal{D}_{O_2}}{dP}\right)\left(\frac{dP}{dx}\right)^2}{\mathcal{D}_{O_2}\left(\frac{d^2P}{dx^2}\right)} \right| \qquad (V-24)$$

ξ is a measure of the oxygen transport limitation from variable $\mathcal{D}_{O_2}$. For one asphalt studied, ξ increased with time, temperature, and position from the *SI* holding all other variables constant. The maximum value of ξ at the *ES* was approximately 0.2.

The unsteady-state, variable $\mathcal{D}_{O_2}$, oxygen diffusion and reaction equation was numerically solved. Calculated *CA* at the *ES* and *SI* were compared to measured *CA*. There were significant differences in *CA*; however, the r_{CA} appeared to compare more favorably. The error in *CA* resulted from the empirical model, equation IV – 2, estimating the integration constant, CA_o. Oxygen pressure, *CA*, $\log \eta_o^*$, and $\log \mathcal{D}_{O_2}$ profiles were calculated for one of the asphalts studied. The oxygen pressure profile showed that initially oxygen transport rates exceed oxygen consumption rates. However, with time, oxygen transport rates decrease as a result of decreasing $\mathcal{D}_{O_2}$ at the *ES* from increasing η_o^* due to *CA*. Preliminary calculations for an aging test showed that not including oxygen diffusion effects may lead to faulty conclusions about an asphalt's ability to resist oxidative aging.

Field- and POV-aged asphalts were compared using physicochemical relationships and the asphalt-aging model. Three test sections, Dickens, Pineland and Bryan, were located, and ten different asphalts were compared. The field-aged material ranged from 2 to 11 years. Several different asphalts were used at the Dickens and Pineland test sections. One asphalt was used at the Bryan test section. Neat asphalts were POV aged, and physicochemical relationships were determined. Field-aged cores were extracted, and the changes in physical and chemical properties as a result of

field aging were compared to those developed from POV aging. The physicochemical relationships are given in equations I – 6, VI – 1, and VI – 2.

$$\eta_o^* = \exp\Big\{ HS \cdot CA + m \Big\} \qquad \text{(I – 6)}$$

$$(1 \,/\, J'') = (1 \,/\, J'')_o \exp\Big\{ RS \cdot CA \Big\} \qquad \text{(VI – 1)}$$

$$\eta_o^* = v(MW)^N \qquad \text{(VI – 2)}$$

In all but two cases, which were discovered to be contaminated, agreement between field and POV aging was very good based on η_o^*-CA and $(1 \,/\, J'')$-CA relationships. From the Bryan test section, the extraction and recovery procedure probably accounts for the scatter in the data. Comparisons based on η_o^*-MW were not very good. Careful analysis of the GPC and IR spectra indicated that the extracted road core was chemically different; however, it was never determined if the difference resulted from the extraction and recovery procedure or from field aging.

Using the asphalt-aging model and climatic data from the test section sites, a theoretical minimum time, t_{theor}, to reach the measured core properties was calculated assuming no diffusion resistance. These calculations showed that without diffusion resistance, changes that normally take 10 years only take one to two years. This indicates that actual field aging is oxygen-diffusion limited. Therefore only models that account for both oxygen diffusion and reaction can accurately simulate and predict field aging.

Before the asphalt-aging model is used to simulate and predict field aging, a set of relationships between measurable core properties, % V and % Asp, and fundamental quantities in the asphalt-aging model, L_{eff} and P_{eff}, were developed. These relationships form the highway-pavement aging model. L_{eff} was estimated by comparing measured properties to those calculated from the asphalt-aging model.

Field locations with low % V did not yield realistic L_{eff} assuming a constant P_{eff} of 0.2 atm. Equations VI – 3 and VI – 4 are hypothesized models.

$$P_{\text{eff}} = (P_{\text{eff}})_o \exp(-\lambda t) \qquad \text{(VI – 3)}$$

$$\lambda = \lambda_o (\% V)^l \qquad \text{(VI – 4)}$$

The parameters $(P_{\text{eff}})_o$, λ_o, and l were assumed to have values of 0.2 atm, 0.154 1/day, and -2.41, respectively. With variable P_{eff} as a function of t and % V, estimated L_{eff} ranged from 1.93 to 0.76 mm. Based on very limited data, a crude linear model between L_{eff} and % Asp was hypothesized.

$$L_{\text{eff}} = a(\% \ Asp) + e \qquad \text{(VI – 5)}$$

The model parameters, a and e, were 1.822 mm/% Asp and -9.95 mm, respectively. However, this model can only be used for pavements with % Asp greater than 5.21. Although these models are crude, they represent the initial development of a model relating measurable core properties to fundamental quantities in the asphalt-aging model.

Data from short-term and long-term POV aging experiments were compared. There appeared to be no correlation between the kinetic parameters. The physicochemical properties compared much better. However, historical comparisons are difficult due to inconsistent data collection and analysis. Standardized procedures should be developed.

CHAPTER IX

RECOMMENDATIONS

Based on the conclusions and discussion in this work, the following recommendations are given to extend and refine the understanding of oxidation in asphalt materials.

Apparatus

More precise temperature and oxygen pressure control and measurement are required, since more sophisticated models relating aging temperature and oxygen pressure to carbonyl formation in asphalt are to be developed. Currently, on/off temperature controls are used. A control system using a PID controller is recommended. Although P may have very little effect on r_{CA} and the current gauges may be sufficient, to further study the effect of P on CA_o may require more precise gauges.

Carbonyl Formation Kinetics

The model parameters for r_{CA} were separated into two categories, parameters that were dependent on asphalt composition, and parameters that were independent of asphalt composition for the five asphalts studied. The fact that the order of reaction, α, is truly independent of asphalt composition needs to be confirmed. This is done by comparing calculated r_{CA} for different asphalts at low pressure to measured r_{CA} at low pressure. The Arrhenius parameters determined at high temperature of 366.7 K and above may not by valid for estimating low temperature r_{CA}. In fact, there may be a slight curvature in r_{CA} versus $(1 \ / \ T)$ at constant P. Since the model is used to extrapolate to road conditions, using higher temperature laboratory

data for extrapolation may introduce greater errors. Furthermore, at field aging conditions, long-term r_{CA} for different asphalts may be surprisingly similar. This has not been studied and may have a profound effect on the required experimental data for an asphalt-aging test. Finally, all of the data collected in this work was for neat asphalt. Since highways have modifiers such as recycling agents and tire rubber, the kinetic parameters for these mixtures may be different compared to neat asphalt. The effect of composition on the Arrhenius parameters and order of reaction have yet to be determined. Finally, aging experiments using air instead of oxygen need to be performed. This studies the effect of the nitrogen film and transport effects on the r_{CA} at the surface of the asphalt film.

Oxygen Consumption Rates and Carbonyl Formation Rates

In Chapter IV, one asphalt was used to relate r_{O_2} to r_{CA}. This relationship was assumed to be independent of the asphalts studied. Obviously, this needs to be confirmed by studying different asphalts and mixtures of asphalts and additives.

Carbonyl-Viscosity Relationships at Different Temperatures

A model relating η_o^* to CA and T was presented in Chapters II and IV. With limited data, this was confirmed; however, some of the data were questionable at best. More asphalts and rheological properties including such low temperature properties as stress relaxation and shear modulus should be compared with CA to understand more about the physicochemical relationships. Relating CA to the entire rheological spectrum would allow researchers to monitor the rheological behavior of pavements solely by IR analysis.

Oxygen Diffusion and Reaction in an Asphalt Film

In this study, five asphalts, three temperatures, two oxygen pressures, and one film thickness were used to formulate an expression between $\mathcal{D}_{O_2}$ and η_o^*. The parameters were independent of temperature and asphalt composition. Another study that uses thicker films should provide better data to estimate r_{CA} at the *SI* and $\mathcal{D}_{O_2}$. Using the equations developed, a systematic study of the maximum oxygen penetration depth as a function of T and P should be conducted. Such tests as the PAV use film thicknesses of 3.18 mm (1/8 inch) and 6.35 mm (1/4 inch). These tests should be analyzed with the asphalt-aging model to determine if the experiments are valid for the specified times. Since many additives are in asphalts today, a systematic study of the effect of additives on $\mathcal{D}_{O_2}$ in asphalt should be done. With tire rubber and recycling agents, the parameters relating $\mathcal{D}_{O_2}$ and η_o^* may depend on composition and temperature.

Comparison of Laboratory Aging and Field Aging-Properties

In the comparison of POV- and field-aged asphalts there was considerable scatter in the property relationships for the field-aged material. All of the extractions in this study used a specific solvent mixture. The effect of other extraction solvents on these properties has not been studied and may decrease the scatter when compared with laboratory aging. Extracted asphalt from hot-mix and field-aged cores should also be POV aged. This determines if the same physicochemical relationships exist or if the extraction process irreversibly alters or sensitizes the asphalt to oxidation. Other methods of *in situ* property measurement should also be explored. Currently, IR methods of analysis can be used to analyze asphalts in a pavement core without extraction procedures. Other compositional properties such asphaltene formation,

rheological properties at other temperatures and elemental analysis should be used to confirm that POV aging is truly simulating field aging.

Comparison of Laboratory Aging and Field Aging-Kinetics

There were very limited data relating field and laboratory aging with the asphalt-aging model. A crude estimation of the annual periodic temperature cycle was used. A better approach would be to measure the temperature in the pavement as a function of depth. The data are then integrated over the time period in the asphalt-aging model. A more systematic approach to study the effect of % V and % Asp on P_{eff} and L_{eff} in the highway-pavement aging model should be devised. This study did not have control over those variables. To simplify the study, laboratory constructed cores and controlled aging should be used initially. Using both the controlled- and field-aging data, a better estimate of the core properties on P_{eff} and L_{eff} will be made. More core properties need to be studied such as air permeability and aggregate gradation.

Short-Term Aging

To make an aging test both operational and valuable in terms of yielding the correct kinetic information, the aging times need to be decreased. Obviously, aging for 80 days is necessary for a research effort. A practical evaluation of an asphalt, asphalt/rubber mixture, or asphalt/recycling mixture should require less time. Short-term aging produced physicochemical relationships in a short period of time. However, the relationship between the short-term and long-term aging kinetics was not apparent from the data collected.

Perhaps researchers should evaluate which characteristic, kinetics or physicochemical properties, truly discriminate asphalts with regard to oxidative aging at field conditions. More often than not, the differences in the physicochemical properties such as the Hardening Susceptibility are more apparent than differences in the kinetic parameters describing r_{CA} for different asphalts. If the differences in the kinetic parameters for different asphalts are small, it may be assumed that all asphalts have roughly the same kinetic parameters based on already published research. Then, the aging test only evaluates the physicochemical properties for an unknown asphalt. This would be a remarkably simple aging test. The only requirement is that the temperature of the test be such that the same products are formed as in field aging. This test would not have to be conducted under isothermal conditions either, since the physicochemical relationships are independent of the kinetics. This simple test could potentially yield enough information to predict the aging of the asphalt.

Overall

The overall objective of this work was to develop models describing the oxidative characteristics of asphalts. Several sets of experimental data were collected. From these data, parameters were estimated based on the models. For more detailed model analysis, data from experiments with more precise temperature and pressure control need to be analyzed. Finally more emphasis needs to be placed on statistical and error analysis in model development and parameter estimation for asphalt oxidation.

NOTATION

A = Arrhenius constant, CA / day atm$^{\alpha}$

B = model parameter in equation II – 34

C = concentration, gmol / mL

CA = carbonyl content or area

$\mathcal{D}$ = diffusivity, m^2 / s

D_o = model parameter in equation I – 8 or II – 34, m^2 / s

E = energy per unit gram mol, J / gmol

ES = exposed surface

G' = shear storage modulus, dyne / cm^2

G'' = shear loss modulus, dyne / cm^2

G_o = model parameter in equation I – 8

HS = hardening susceptibility in equation I – 6, 1 / CA

J'' = loss compliance, cm^2 / dyne

$(1 / J'')_o$ = model parameter in equation VI – 1, dyne / cm^2

K' = model parameter in equation I – 7

L = film thickness, m

LT = long term

MW = molecular weight

N = model parameter in equation VI – 2

P = pressure, atm

P^* = transformation variable for pressure in equation V – 13

R = universal gas constant

RS = rutting susceptibility in equation VI – 1, 1 / CA

SI = substrate interface

ST = short term

T = temperature, K

X = transformation variable for position in equation V – 13

$\%\ A$ = percent hexane asphaltenes

$\%\ Asp$ = percent asphalt

$\%\ V$ = percent air voids

a = time-temperature superposition horizontal shift factor or model parameter in equation I – 1, I – 2, I – 5, or VI – 5

b = model parameter in equation I – 1, I – 2, or I – 5

c = model parameter in equation II – 10, gmol O_2 / mL CA

ϵ = model parameter in equation VI – 5, mm

g = model parameter in equation I – 8

h = Henry's law constant

j = nodes in finite difference equations

k = reaction rate constant

l = model parameter in equation VI – 4

m = model parameter in equation I – 6, ln(Poise)

n = stoichiometric coefficients in equation II – 9

r = rate of formation or consumption

s = model parameter in equation IV – 2, CA / atm$^{\beta}$

t = time

v = model parameter in equation VI – 2

x = spatial variable

x_f = point of variable transformation in equation V – 14

y = any measurable or log of the measurable asphalt property

$\mathbf{N}$ = molar flux, gmol / m^2 s

∇ = vector operator

Greek letters

Δ = change in

Π = dimensionless pressure

α = order of reaction

β = model parameter in equation IV – 2

γ = model parameter in equation II – 14, K / CA

δ = model parameter in equation II – 14, K

η = viscosity, Poise

θ = dummy variable of integration

λ = time constant in equation VI – 3, 1/day

λ_o = model parameter in equation VI – 4

ν = model parameter in equation I – 7

ξ = ratio of $\left(\frac{d\mathcal{D}_{O_2}}{dP}\right)\left(\frac{dP}{dx}\right)^2$ to $\mathcal{D}_{O_2}\left(\frac{d^2P}{dx^2}\right)$

ρ = density, g / mL

ϕ = Thiele modulus for diffusion and reaction in equation V – 21

ψ = latitude in equation I – 9

ω = frequency

Subscripts

A = activation for chemical reaction

$A+$ = asphalt active sites

C = concentration

CA = carbonyl content or area

ES = exposed surface

LT = long term

M = maltene, equation I – 7

N = number of nodes

O_2 = oxygen

P = pressure

SI = substrate interface

ST = short term

T = temperature

V = viscosity

h = the hyperbolic model, equation I – 1

l = the linear model, equation I – 2

n = the Dickinson and Nicholas (1949) model, equation I – 5

o = initial condition, reference, zero-shear limiting, or intercept

act = actual

avg = average

cal = calculated

dif = diffusion

eff = effective

ima = imaginary

max = maximum

mea = measured

min = minimum

rea = reaction

sur = surface

theor = theoretical

Superscripts

* = complex rheological property

LITERATURE CITED

Adams, C.K., and R.J. Holmgreen, *Asphalt Properties and Pavement Performance*, Report FHWA-TX-86/287-4. Texas Transportation Institute, College Station, TX (1986).

Anderson A.P., F.H. Stross, and A. Ellings, "Measurement of Oxidation Stability of Road Asphalts," *Ind. and Eng. Chem. Anal. Ed.*, **14**, 45 (1942).

Anderson, A.P., and K.A. Wright, "Permeability and Absorption Properties of Bituminous Coatings," *Ind. and Eng. Chem.*, **33**, 992 (1941).

Andrade, E.N., "The Viscosity of Liquids," *Nature*, **125**, 309 (1930).

ASTM, *Annual Book of ASTM Standards Road and Paving Materials; Traveled Surface Characteristics*, ASTM, Vol 4.03, Philadelphia, PA (1984).

Baldwin R.R., and S.G. Daniel, "The Solubility of Gases in Lubricating Oils and Fuels," *Institute of Petroleum Journal*, **39**, 105 (1953).

Bateman, L., "Olefin Oxidation," *Quart. Rev.*, **8**, 147 (1954).

Bird, R.B., W.E. Stewart, and E.N. Lightfoot, *Transport Phenomena*, Wiley, New York, NY (1960).

Blokker, P.C. and H. van Hoorn, "Durability of Bitumen in Theory and Practice," *5th World Petroleum Congress*, 417 (1959).

Bolland, J.L., "Kinetics of Olefin Oxidation," *Quart. Rev.*, **3**, 1 (1949).

Brown A.B., J.W. Sparks, and O. Larsen, "Rate of Change of Softening Point, Penetration, and Ductility of Asphalt in Bituminous Pavement," *Proc. AAPT*, **26**, 66 (1957).

Burr B.L., "Improved Methods for Extracting and Recovering Asphalts from Pavement Samples," PhD Dissertation, Texas A&M University, College Station, TX (1993).

Burr, B.L., R.R. Davison, C.J. Glover, and J.A. Bullin, "Solvent Removal from Asphalt," *Trans. Res. Rec.*, **1269**, 1 (1990).

Burr, B.L., R.R. Davison, H.B. Jemison, C.J. Glover, and J.A. Bullin, "Asphalt Hardening in Extraction Solvents," *Trans. Res. Rec.*, **1323**, 70 (1991).

Button, J.W., M. Jawle, V. Jagadam, and D.N. Little, "Evaluation and Development of a Pressure Aging Vessel for Asphalt," *Trans. Res. Rec.*, **1391**, 11 (1993).

Campen, W.H., J.R. Smith, L.G. Erickson, and L.R. Mertz, "The Relationships between Voids, Surface Area, Film Thickness and Stability in Bituminous Paving Mixtures," *Proc. AAPT*, **28**, 149 (1959).

Chipperfield, E.H., J.L. Duthie, and R.B. Girdler, "Asphalt Characteristics in Relation to Road Performance," *Proc. AAPT*, **39**, 575 (1970).

Davison, R.R., J.A. Bullin, C.J. Glover, B.L. Burr Jr., H.B. Jemison, A.L.G. Kyle, and C.A. Cipione, *Development of Gel Permeation Chromatography, Infrared and Other Tests to Characterize Asphalt Cements and Correlate with Field Performance*, Report FHWA-TX-90/458-1F. Texas Transportation Institute, College Station, TX (1989).

Davison, R.R., J.A. Bullin, C.J. Glover, H.B. Jemison, C.K. Lau, K.M. Lunsford, and P.L. Bartnicki, *Design and Use of Superior Asphalt Binders*, Report FHWA-TX-92/1249-1F. Texas Transportation Institute, College Station, TX (1992).

Dickinson E.J., and J.H. Nicholas, "The Reaction of Oxygen with Tar Oils," *Road Research Technical Paper No 16.*, 1 (1949).

Dickinson E.J., J.H. Nicholas, and S. Boas-Traube, "Physical Factors Affecting the Absorption of Oxygen by Thin Films of Bituminous Road Binders," *J. Appl. Chem.*, **8**, 673 (1958).

Ebberts A.R., "Oxidation of Asphalt in Thin Films," *Ind. and Eng. Chem.*, **34**, 1048 (1942).

Edler, A.C., M.M. Hattingh, V.P. Servas, and C.P. Marais, "Use of Aging Tests to Determine the Efficacy of Hydrated Lime Additions to Asphalt in Retarding its Oxidative Hardening," *Proc. AAPT*, **54**, 118 (1985).

Ferry J., *Viscoelastic Properties of Polymers*, John Wiley and Sons, 4th ed., New York, NY (1985).

Froment, G.F, and K.B. Bischoff, *Chemical Reactor Analysis and Design*, John Wiley and Sons, New York, NY (1979).

Glover, C.J., J.A. Bullin, J.W. Button, R.R. Davison, G.R. Donaldson, M.W. Hlavinka, and C.V. Philip, *Characterization of Asphalt Using Gel Permeation Chromatography and Other Methods*, Report FHWA-TX-87/419-1F. Texas Transportation Institute, College Station, TX (1987).

Goode, J.A., and L.A. Lufsey, "Voids, Permeability, Film Thickness vs. Asphalt Hardening," *Proc. AAPT*, **34**, 430 (1965).

Griffin, R.L., T.K. Miles, and C.J. Penther, "Microfilm Durability Test for Asphalt," *Proc. AAPT*, **24**, 31 (1955).

Halstead W.J., "The Relation of Asphalt Ductility to Pavement Performance," *Proc. AAPT*, **32**, 247 (1963).

Heithaus, J.J., and R.W. Johnson, "A Microviscometer Study of Road Asphalt Hardening in the Field and Laboratory," *Proc. AAPT*, **27**, 17 (1958).

Jamieson I.L. and M.M. Hattingh, "The Correlation of Chemical and Physical Properties of Bitumens with Their Road Performance," *Proc. ARRB*, **5**, 293 (1970).

Jemison H.B., "Supercritical Refining of Asphalts," PhD Dissertation, Texas A&M University, College Station, TX (1992).

Jemison, H.B., B.L. Burr, R.R. Davison, J.A. Bullin, and C.J. Glover, "Application and Use of the ATR, FT-IR Method to Asphalt Aging Studies," *Fuel Science and Technology*, **10**, 795 (1992a).

Jemison, H.B., R.R. Davison, C.J. Glover, and J.A. Bullin, "Evaluation of Standard Oven Tests for Hot-Mix Plant Aging," *Trans. Res. Rec.*, **1323**, 77 (1991).

Jemison, H.B., K.M. Lunsford, R.R. Davison, C.J. Glover, and J.A. Bullin, "Properties of Asphalt Fraction Obtained by Supercritical Extraction with Pentane and Cyclohexane," *ACS Preprints*, **37**, 1490 (1992b).

Kandhal, P.S., and W.C. Koehler, "Significant Studies on Asphalt Durability: Pennsylvania Experience," *Trans. Res. Rec.*, **999**, 41 (1984).

Kemp, G.R. and N. H. Predoehl, "A Comparison of Field and Laboratory Environments on Asphalt Durability," *Proc. AAPT*, **50**, 492 (1981).

Kim, O.K., C.A. Bell, J.E. Wilson, and G. Boyle, "Development of Laboratory Oxidative Aging Procedures for Asphalt Cements and Asphalt Mixtures," *Trans. Res. Rec.*, **1115**, 101 (1984).

Knoterus, J., "Bitumen Durability-Measurement by Oxygen Absorption," *Ind. and Eng. Chem. Prod. Res. Dev.*, **11**, 411 (1972).

Krchma, L.C., D.E. Allison, C.E. Quiring, and T. Groening, "A Laboratory Exposure for Study of Asphalt Hardening," *Proc. AAPT*, **29**, 362 (1960).

Krchma, L.C. and T. Groening, "Influence of Pavement Voids, Asphalt Content and Asphalt Grade on Asphalt Performance," *Proc. AAPT*, **28**, 34 (1959).

Kumar, A., and W.H. Goetz, "Asphalt Hardening as Affected by Film Thickness, Voids, and Permeability in Asphaltic Mixtures," *Proc. AAPT*, **46**, 571 (1977).

Lau C.K., "Photo- and Moderate-Temperature Oxidation Reactions and Their Impacts on the Properties and Performance on Asphalt as a Pavement Binder," MS Thesis, Texas A&M University, College Station, TX (1991).

Lau, C.K., K.M. Lunsford, C.G. Glover, R.R. Davison, and J.A. Bullin, "Reaction Rates and Hardening Susceptibilities as Determined from POV Aging of Asphalts," *Trans. Res. Rec.*, **1342**, 50 (1992).

Lee, A.R., and E.J. Dickinson, "The Durability of Road Tar," *Road Research Technical Paper No 31.*, 1 (1954).

Lee, A.R., and E.J. Dickinson, "The Weathering of Bituminous Materials," in *Bituminous Materials in Road Construction*, W.H. Glanville, ed., Her Majesty's Stationery Office, London, p.176 (1962).

Lee, D.Y., "Development of a Laboratory Durability Test for Asphalt," *Hwy. Res. Board Bulletin*, **231**, 34 (1968).

Lee, D.Y., "Asphalt Durability Correlation in Iowa," *Hwy. Res. Rec.*, **468**, 43 (1973).

Lee, D.Y. and R.J. Huang, "Weathering of Asphalts as Characterized by Infrared Multiple Internal Reflection Spectra," *Anal. Chem.*, **46**, 2242 (1973).

Lin, M.S., K.M. Lunsford, C.J. Glover, R.R. Davison, and J.A. Bullin, "The Effects of Asphaltenes on the Chemical and Physical Characteristics of Asphalts," *The Fine Particle Society*, Preprints at 24th Annual Meeting (1993).

Martin, K.L., R.R. Davison, C.J. Glover, and J.A. Bullin, "Asphalt Aging in Texas Roads and Test Sections," *Trans. Res. Rec.*, **1269**, 9 (1990).

NOAA, "Local Climatological Data, Annual Summary with Comparative Data," National Oceanic and Atmospheric Administration, Asheville, NC (1988).

Pauls, J.T. and W.J. Halstead, "Progressive Alteration of Sheet Asphalt Pavement Over a Long Period of Service," *Proc. AAPT*, **58**, 123 (1958).

Pearson, C.D., G.S. Huff, and S.G. Gharfeh, "Technique for the Determination of Asphaltenes in Crude Oil Residues," *Anal. Chem.*, **58**, 3266 (1986).

Petersen, J.C., "Chemical Composition of Asphalt as Related to Asphalt Durability: State of the Art," *Trans. Res. Rec.*, **999**, 13 (1984).

Petersen, J.C., "A Thin Film Accelerated Aging Test for Evaluating Asphalt Oxidative Aging," *Proc. AAPT*, **58**, 220 (1989).

Petersen, J.C., F.A. Barbour, and S.M. Dorrence, "Catalysis of Asphalt Oxidation by Mineral Aggregate Surfaces and Asphalt Components," *Proc. AAPT*, **43**, 162 (1974).

Petersen, J.C., J.F. Branthaver, R.E. Robertson, P.M. Harnsberger, J.J. Duvall, and E.E. Ensley, "Effects of Physicochemical Factors on Asphalt Oxidation Kinetics," *Trans. Res. Rec.*, **1391**, 1 (1993).

Plancher, H., E.L. Green, and J.C. Petersen, "Reduction of Oxidative Hardening of Asphalts by Treatment with Hydrated Lime-A Mechanistic Study," *Proc. AAPT*, **45**, 1 (1976).

Reid, R.C., J.M. Prausnitz, and T.K. Sherwood, *The Properties of Gases and Liquids*, McGraw-Hill, 4th, ed., New York, NY (1983).

Rosen, S.L., *Fundamental Principles of Polymeric Materials*, John Wiley and Sons, New York, NY (1982).

Ruede, J.E., "Ageing of Low-Temperature Coal-Tar Pitch. 1.Influence of Weather and U.V. Light," *Fuel*, **58**, 595 (1979).

SHRP, "Properties of Materials Reference Library Asphalt Cements," National Research Council, Washington, DC (1990).

SHRP, "SHRP Binder Specification, Draft No. 7G," Federal Highway Administration, Washington, DC (1992).

Solaimanian M., and T.W. Kennedy, "Predicting Maximum Pavement Surface Temperature Using Maximum Air Temperature and Hourly Solar Radiation," *Trans. Res. Rec.*, Preprint #930671 at 72nd Annual Meeting (1993).

Strieter O.G. and H.R. Snoke, "A Modified Accelerated Weathering Test Asphalts and Other Materials," *Journal of Research of the National Bureau of Standards*, **16**, 481 (1936).

Vallerga, B.A., and W.J. Halstead, "Effects of Field Aging on Fundamental Properties of Paving Asphalts," *High. Res. Rec.*, **361**, 71 (1971).

Van Oort, W.P., "Durability of Asphalt, Its Aging in the Dark," *Ind. and Eng. Chem.*, **48**, 1196 (1956).

Verhasselt, A.F. and F.S. Choquet, "A New Approach to Studying the Kinetics of Bitumen Ageing," *Proceedings of the International Symposium Chemistry of Bitumens, Vol II.*, 686 (1991).

Verhasselt, A.F. and F.S. Choquet, "Comparing Field and Laboratory Aging of Bitumens on a Kinetic Basis," *Trans. Res. Rec.*, **1391**, 30 (1993).

Way, P.J., H.I. Fuller, T. Les, and A. Winward, "Road and Laboratory Experiments on Bitumens from Western Hemisphere and Middle East Crudes," *5th World Petroleum Conference*, 433 (1959).